

MINERALOGICAL AND CHEMICAL CHARACTERISTICS
OF HYDROTHERMAL ALTERATION ASSOCIATED WITH
THE PROTEROZOIC VAMP LAKE CU-ZN SULFIDE
DEPOSIT, FLIN FLON AREA

by

Rita Wadien

A thesis
Submitted to the Faculty of Graduate Studies
in Partial Fulfillment of the Requirements
for the Degree of

MASTER OF SCIENCE

Department of Geological Sciences
University of Manitoba
Winnipeg, Manitoba

(c) May, 1993



National Library
of Canada

Acquisitions and
Bibliographic Services Branch

395 Wellington Street
Ottawa, Ontario
K1A 0N4

Bibliothèque nationale
du Canada

Direction des acquisitions et
des services bibliographiques

395, rue Wellington
Ottawa (Ontario)
K1A 0N4

Your file *Votre référence*

Our file *Notre référence*

The author has granted an irrevocable non-exclusive licence allowing the National Library of Canada to reproduce, loan, distribute or sell copies of his/her thesis by any means and in any form or format, making this thesis available to interested persons.

L'auteur a accordé une licence irrévocable et non exclusive permettant à la Bibliothèque nationale du Canada de reproduire, prêter, distribuer ou vendre des copies de sa thèse de quelque manière et sous quelque forme que ce soit pour mettre des exemplaires de cette thèse à la disposition des personnes intéressées.

The author retains ownership of the copyright in his/her thesis. Neither the thesis nor substantial extracts from it may be printed or otherwise reproduced without his/her permission.

L'auteur conserve la propriété du droit d'auteur qui protège sa thèse. Ni la thèse ni des extraits substantiels de celle-ci ne doivent être imprimés ou autrement reproduits sans son autorisation.

ISBN 0-315-86147-9

Canada

MINERALOGICAL AND CHEMICAL CHARACTERISTICS
OF HYDROTHERMAL ALTERATION ASSOCIATED WITH
THE PROTEROZOIC VAMP LAKE CU-ZN SULFIDE
DEPOSIT, FLIN FLON AREA

BY

RITA WADIEN

A Thesis submitted to the Faculty of Graduate Studies of the University of Manitoba in partial fulfillment of the requirements for the degree of

MASTER OF SCIENCE

© 1993

Permission has been granted to the LIBRARY OF THE UNIVERSITY OF MANITOBA to lend or sell copies of this thesis, to the NATIONAL LIBRARY OF CANADA to microfilm this thesis and to lend or sell copies of the film, and UNIVERSITY MICROFILMS to publish an abstract of this thesis.

The author reserves other publications rights, and neither the thesis nor extensive extracts from it may be printed or otherwise reproduced without the author's permission.

Abstract

The Vamp Lake deposit is a stratiform, metamorphosed Cu-Zn massive sulfide deposit in the Proterozoic Flin Flon-Snow Lake greenstone belt of northern Manitoba. The deposit occurs at the contact between underlying mafic flows and overlying intermediate to felsic volcanoclastic rocks and flows in a 500 m thick and overturned supracrustal sequence. The host rocks and the deposit have been metamorphosed to middle amphibolite grade. Metamorphism and deformation of the deposit are supported by the elongation of the ore zone, and ore textures such as: euhedral pyrite crystals with inclusions and caries type embayments; cracked, shattered, and brecciated pyrite grains; rounded pyrite grains and gangue material; exsolution of chalcopyrite in sphalerite; and the interstitial nature of sphalerite, chalcopyrite, and pyrrhotite which also rim and fill fractures in pyrite crystals.

The deposit consists of two separate ore zones that occur at the same stratigraphic level but are about 400 m apart and in different fault blocks. The sulfide assemblages in each zone are mineralogically simple, consisting of pyrite, pyrrhotite, sphalerite and chalcopyrite. Combined tonnage and grade of the two ore zones is 422,400 tonnes of 1.3% Cu, 1.9% Zn, and 0.116 oz./T Au. Metal zonation is present in one zone, which contains a gold-rich Cu-Zn zone, overlain by a more laterally extensive Zn-rich ore.

Each ore zone is associated with alteration that is both in direct contact with the mineralization (proximal), and underlies, but is separated from, the ore by relatively unaltered rocks

but is separated from, the ore by relatively unaltered rocks (distal). Proximal alteration is well developed in a thin zone below one ore zone, and poorly developed above it; the other zone has a well developed proximal alteration envelope. Alteration beneath the ore zones has been superimposed on mafic rocks and local intercalated intermediate flows or tuff. Proximal alteration has also locally affected overlying felsic rocks. The alteration zones are characterized by the phyllosilicate minerals chlorite, biotite, and muscovite that display a well developed schistosity parallel to regional foliation, and local axial planar and crenulation cleavage, demonstrating that the alteration zones have been deformed and metamorphosed. In the largest distal alteration zone, the central part of the zone consists of chlorite-biotite-quartz-amphibole and lesser quartz-biotite-garnet assemblages; this grades upward to quartz-biotite, quartz-muscovite+/-biotite, and chlorite-quartz-biotite assemblages. Outer margins of the zone consist of chlorite-quartz-sericite-amphibole and/or sericite-epidote-chlorite-biotite assemblages. The assemblages appear to occur in stratigraphically controlled sub-zones possibly indicative of different precursor rocks. Proximal zones are dominated by tremolite-quartz-biotite-chlorite, quartz-muscovite, and quartz-chlorite assemblages, and rocks containing amphibole-biotite-sulfide clusters.

Chemical changes associated with the development of both distal and proximal alteration zones are gains in K, and for those assemblages where trace element data are available, Ni, Cr, Ba and

Au. Although somewhat variable in behavior, Rb, Mg, Mn, P, Fe, and Si are gained in most assemblages. Ca is consistently depleted in the distal alteration zones, but is gained in the tremolitic proximal alteration assemblage which is characterized by anomalously high Mg, Cr, and Ni relative to all other rocks in the Vamp Lake area. Na, Sr, and Nb are depleted in most assemblages.

TABLE OF CONTENTS

Abstract.....	i
List of Figures.....	vii
List of Tables.....	xi
1. Introduction	
1.1 Sulfide deposits of the Flin Flon-Snow Lake Greenstone Belt.....	1
1.2 History of Exploration.....	6
1.3 Purpose of Investigation.....	6
1.4 Acknowledgments.....	8
1.5 Methodology	
1.5.1 Field Work.....	8
1.5.2 Laboratory Techniques.....	9
1.5.3 Analytical Methods.....	11
1.6 Previous Geological Studies.....	12
1.7 Regional Setting.....	13
1.7.1 Structural and Deformational Regime.....	17
1.7.2 Metamorphic Regime.....	18
2. Geology of the Vamp Lake Area	
2.1 Lithology.....	20
2.2 Younging Direction.....	22
2.3 Stratigraphic Correlation.....	23
2.4 Metamorphism.....	23
2.5 Structural Geology and Deformation.....	26
3. Stratigraphy Near the Vamp Lake Ore Zones.....	27
3.1 Stratigraphy of the Island Fault Block.....	28
3.1.1 Island Ore Zone.....	29
3.1.2 Alteration Zones.....	37
3.2 Stratigraphy of the Mainland Fault Block.....	37
3.2.1 Lake Ore Zone.....	40
3.2.2 Alteration Zones.....	40
4. Rock Types.....	41
4.1 Mafic Volcanic Rocks and Intrusions.....	41
4.1.1 Mafic Flows	
4.1.1.1 Massive Flows.....	42
4.1.1.2 Pillowed Mafic Flows.....	43
4.1.2 Mafic Breccias.....	44
4.1.3 Layered Mafic Units.....	49
4.1.4 Mafic Intrusions.....	50
4.2 Intermediate and Felsic Volcanic Rocks and Intrusions... ..	50
4.2.1 Felsic and Intermediate Flows	
4.2.1.1 Felsic Flows.....	51
4.2.1.2 Quartz-Plagioclase-Phyric Felsic Flow.....	52
4.2.1.3 Intermediate Plagioclase-Phyric Flow.....	52
4.2.2 Fragmental Rocks	
4.2.2.1 Felsic Tuff.....	54

4.2.2.2 Felsic Crystal-Bearing Tuff.....	55
4.2.2.3 Intermediate Tuff.....	55
4.2.2.4 Intermediate Tuff-Breccia.....	59
4.2.2.5 Felsic Tuff-Breccia.....	62
4.2.3 Felsic Intrusions	64
4.3 Possible Sedimentary Rocks.....	66
5. Structure of the Vamp Lake Area.....	68
5.1 Foliation and Lineation.....	68
5.2 Isoclinal Folding.....	68
5.3 Faults.....	69
5.4 Schistose Zones.....	71
5.5 Conjugate Fracture System.....	71
6. Physical Features of the Alteration Zones	
6.1 Introduction.....	73
6.2 Distal Alteration Zones.....	76
6.2.1 Characteristics of Distal Alteration.....	76
6.2.1.1 Chlorite-Biotite-Quartz-Amphibole Assemblage.....	78
6.2.1.2 Quartz-Biotite-Garnet Assemblage.....	86
6.2.1.3 Quartz-Biotite Assemblage.....	87
6.2.1.4 Quartz-Muscovite+/-Biotite Assemblage.....	89
6.2.1.5 Chlorite-Quartz-Biotite Assemblage.....	90
6.2.1.6 Sericite-Epidote-Chlorite-Biotite Assemblage.....	92
6.2.1.7 Chlorite-Quartz-Sericite-Amphibole Assemblage.....	94
6.3 Proximal Alteration Zones.....	95
6.3.1 Characteristics of Proximal Alteration	
6.3.1.1 Tremolite-Quartz-Biotite-Chlorite Assemblage.....	96
6.3.1.2 Quartz-Muscovite Assemblage.....	98
6.3.1.3 Amphibole-Biotite-Sulfide Assemblage.....	100
6.3.1.4 Quartz-chlorite Assemblage.....	101
6.4 Peripheral Alteration.....	101
6.4.1 Chloritization.....	101
6.4.2 Silicification.....	103
6.4.3 Amphibole-Biotite Clusters.....	103
6.4.4 Epidotization.....	104
6.4.5 Chlorite-Epidote+/-Calcite-Quartz Veining.....	106
6.5 Late Stage Alteration.....	107
7. Geochemistry	
7.1 Composition of Major Rock Types.....	109
7.2 Discrimination Diagrams.....	116
7.2.1 Magma Types.....	117
7.2.2 Possible Sedimentary Rocks.....	122
7.2.3 Tectonic Environment.....	122
Chemical Changes Associated with Alteration	
7.3 Determining Changes in Whole Rock Chemistry.....	128

7.4	Changes in Whole Rock Chemistry - Results	
7.4.1	Distal Alteration Zones.....	159
7.4.2	Proximal Alteration Zones.....	161
7.4.3	Peripheral Alteration.....	163
7.5	Summary of the Chemical Features of Alteration.....	163
7.6	Mineral Chemistry	
7.6.1	Chemical Variations of Chlorite.....	164
7.6.2	Biotite-Chlorite Intergrowths.....	170
8.	Mineralization.....	172
8.1	Characteristics of the Island Ore Zone.....	174
8.1.1	Cu-Zn Ore	
8.1.1.1	Sulfide Mineralogy.....	180
8.1.1.2	Gold Content.....	185
8.1.2	Zn-Rich Ore	
8.1.2.1	Sulfide Mineralogy.....	186
8.1.3	Disseminated (non-economic) Sulfide Zones.....	190
8.1.4	Gangue Mineralogy.....	194
8.2	Characteristics of the Lake Ore Zone.....	198
8.2.1	Sulfide Mineralogy.....	199
8.2.2	Gangue Mineralogy.....	202
9.	Discussion	
9.1	Introduction.....	203
9.2	Type of Deposit - Classification.....	203
9.2.1	External Characteristics of the Ore Zones.....	204
9.2.2	Internal Characteristics of the Vamp Lake Deposit.	205
9.2.3	Deformation and Metamorphism of Ores.....	206
9.3	Spatial Association of Alteration Zones with Mineralization	
9.3.1	Distal Alteration Zones.....	207
9.3.2	Proximal Alteration Zones.....	208
9.4	Genesis of Alteration.....	209
9.4.1	Distal Zones.....	210
9.4.1.1	Island Fault Block.....	211
9.4.1.2	Mainland Fault Block.....	215
9.4.2	Proximal Alteration Zones.....	215
9.4.2.1	Island Fault Block.....	216
9.4.2.2	Mainland Fault Block.....	217
9.5	Genesis of Mineralization.....	219
9.5.1	Island Ore Zone	
9.5.1.1	Economic to Sub-Economic Ore.....	219
9.5.1.2	Disseminated Sulfide Zone.....	220
9.5.1.3	Gold Mineralization.....	221
9.5.2	Lake Ore Zone.....	223
9.6	Timing of Mineralization and Alteration.....	224
	Conclusions.....	226
	References.....	100
	Appendix A - Petrographic Data Table	
	Appendix B - Electron Microprobe Results	
	Appendix C - Whole Rock Analyses	

LIST OF FIGURES

Figure 1:	Geology and Sulfide Deposits of the Flin Flon-Snow Lake Greenstone Belt.....	3
Figure 2:	Regional Geology of the Vamp Lake Area.....	14
Figure 3:	Geology of the Vamp Lake Area.....	21
Figure 4:	Schematic stratigraphic sections of the Two Main Fault Blocks in the Vicinity of the Vamp Lake Ore Zones.....	25
Figure 5:	Plan Sections of the Area around the Ore Zones at depths of 30, 200, & 300 m.....	Back Enclosure
Figure 6:	Geology of the Ore Discovery Island.....	30
Figure 7:	Location Map showing Position of Cross-sections (Figures 8-12).....	31
Figure 8:	Cross-section A-A'.....	32
Figure 9:	Cross-section B-B'.....	33
Figure 10:	Cross-section C-C'.....	34
Figure 11:	Cross-section D-D'.....	35
Figure 12:	Cross-section E-E'.....	36
Figure 13:	Composite Cross-section of the Lake Ore Zone.....	39
Figure 14:	Megapillows on mainland (photograph).....	45
Figure 15:	Pillowed mafic flow (photograph).....	46
Figure 16:	Mafic breccia (photograph).....	47
Figure 17:	Mafic breccia (photograph).....	48
Figure 18:	Quartz-plagioclase-phyric felsic flow (photograph).....	53
Figure 19:	Intermediate tuff (photograph).....	57
Figure 20:	Mineralized fragments within intermediate tuff (photograph).....	58
Figure 21:	Intermediate tuff-breccia (photograph).....	60
Figure 22:	Intermediate tuff-breccia (photograph).....	61
Figure 23:	Felsic tuff-breccia (photograph).....	63
Figure 24:	Felsic dike (photomicrograph).....	65
Figure 25:	Small scale isoclinal folding (photomicrograph)....	70
Figure 26:	Location map showing the distribution of various alteration types.....	74
Figure 27:	Chlorite-biotite-quartz-amphibole alteration assemblage (photomicrograph).....	80
Figure 28:	Chlorite-biotite-quartz-amphibole alteration assemblage (photomicrograph).....	81
Figure 29:	Chlorite-biotite-quartz-amphibole assemblage (photomicrograph).....	82
Figure 30:	Kinked chlorite crystals (photomicrograph).....	83
Figure 31:	Deformed chlorite-biotite-quartz-amphibole alteration assemblage (photomicrograph).....	84
Figure 32:	Chlorite-biotite-quartz-amphibole assemblage (photomicrograph).....	85
Figure 33:	Quartz-biotite-garnet alteration assemblage (photomicrograph).....	88

Figure 34:	Chlorite-quartz-biotite alteration assemblage (photomicrograph).....	91
Figure 35:	Accessory gahnite and garnet in chlorite-quartz-biotite alteration assemblage (photomicrograph).....	93
Figure 36:	Tremolite-quartz-biotite-chlorite alteration assemblage (photomicrograph).....	97
Figure 37:	Biotite-chlorite intergrowths (photomicrograph)...	99
Figure 38:	Amphibole-biotite-sulfide clusters in felsic rocks (photomicrograph).....	102
Figure 39:	Amphibole-biotite clusters (photomicrograph).....	105
Figure 40:	Al ₂ O ₃ - TiO ₂ binary plot.....	112
Figure 41:	Zr/TiO ₂ versus Nb/Y magmatic differentiation plot..	118
Figure 42:	SiO ₂ versus Nb/Y magmatic differentiation plot....	119
Figure 43:	SiO ₂ versus Zr/TiO ₂ magmatic differentiation plot..	121
Figure 44:	AFM diagram (Na ₂ O+K ₂ O-Fe ₂ O ₃ -MgO ternary plot).....	123
Figure 45:	Zr-Ti/100-Sr/2 tectonic environment ternary discrimination diagram.....	124
Figure 46:	Ti - Zr binary plot showing the trace element signatures of mafic volcanic rocks from massive sulfide deposits from various tectonic setting; comparison to Vamp Lake.....	125
Figure 47:	TiO ₂ - Zr binary tectonic discrimination diagram..	126
Figure 48:	Ti/Cr versus Ni tectonic setting discrimination diagram.....	127
Figure 49:	Hughes magmatic discrimination diagram (Na ₂ O+K ₂ O versus K ₂ Ox100/Na ₂ O+K ₂ O.....	130
Figure 50:	Na ₂ O - CaO binary discrimination diagram for unaltered rocks.....	131
Figure 51:	Jensen cation diagram (Al-Fe+Ti-Mg ternary plot)..	132
Figure 52:	TiO ₂ - Zr magmatic discrimination diagram for unaltered and altered Vamp Lake area rocks.....	136
Figure 53:	Comparison of altered Vamp Lake samples to defined mafic sub-groups on a Al ₂ O ₃ - TiO ₂ binary diagram.	138
Figure 54:	Isocon diagrams Chlorite-biotite-quartz-amphibole assemblage of the distal alteration zone (island fault block) compared to: a) Low TiO ₂ mafic flows (mainland fault block)....	141
	b) TiO ₂ mafic flows moderate TiO ₂ mafic flows (mainland fault block).....	143
	c) High TiO ₂ mafic flows (mainland fault block)...	143
	d) Plagioclase-phyric intermediate flow (island fault block).....	144
Figure 55:	Isocon diagram Quartz-biotite-garnet assemblage of the distal alteration zone (island fault block) compared to low TiO ₂ mafic flows (mainland fault block).....	145
Figure 56:	Isocon diagrams Quartz-biotite assemblage of the distal alteration zone (island fault block) compared to plagioclase-phyric flow (island fault block).....	146

Figure 57:	Isocon diagrams Chlorite-quartz-biotite assemblage of the distal alteration zone (Island Fault Block) compared to:	
	a) Moderate TiO ₂ mafic flow (mainland fault block).....	147
	b) Moderate TiO ₂ mafic flows (island fault block).....	147
Figure 58:	Isocon diagrams Quartz-muscovite assemblage of the distal alteration zone (island fault block) compared to:	
	a) Moderate TiO ₂ mafic flows (island fault block).....	148
	b) Moderate TiO ₂ mafic flow (mainland fault block).....	148
	c) Plagioclase-phyric intermediate flow (island fault block).....	149
Figure 59:	Isocon diagrams Sericite-epidote-chlorite-biotite assemblage of the distal alteration zone (island fault block) compared to:	
	a) Moderate TiO ₂ mafic flows (island fault block).....	150
	b) Moderate TiO ₂ mafic flow (mainland fault block).....	150
	c) Low TiO ₂ mafic flows (mainland fault block).....	151
Figure 60:	Isocon diagrams Chlorite-quartz-feldspar assemblage of the distal alteration zone (mainland fault block) compared to low TiO ₂ mafic flows (mainland fault block).....	152
Figure 61:	Isocon diagram Tremolite-quartz-biotite-chlorite assemblages of the proximal alteration zone (mainland fault block) compared to low TiO ₂ mafic flows (mainland fault block).....	153
Figure 62:	Isocon diagrams Tremolite-quartz-biotite-chlorite assemblage of the proximal alteration zone (island fault block) compared to:	
	a) Moderate TiO ₂ mafic flow (mainland (Fault block).....	154
	b) Moderate TiO ₂ mafic flows (island fault block).....	154
Figure 63:	Isocon diagram Sample containing amphibole-biotite clusters (island fault block) compared to low TiO ₂ mafic flows (mainland fault block).....	155
Figure 64:	Classification of chlorites.....	166
Figure 65:	Composition of chlorite; relationship to observed interference color.....	167
Figure 66:	Relationship between alteration assemblage type and chlorite composition within distal alteration zones.....	168
Figure 67:	Composition of chlorite from the tremolite-quartz-biotite-chlorite alteration assemblage of proximal alteration zones.....	169
Figure 68:	Stratigraphic section through island ore zone (Diamond drill hole intersection CON 7).....	175

Figure 69:	Stratigraphic section through island ore zone (Diamond drill hole intersection CON 57).....	176
Figure 70:	Stratigraphic section through island ore zone (Diamond drill hole intersection CON 44W2).....	177
Figure 71:	Stratigraphic section through island ore zone (Diamond drill hole intersection CON 5).....	178
Figure 72:	Stratigraphic section through island ore zone (Diamond drill hole intersection CON 39).....	179
Figure 73:	Cu-Zn ore (photomicrograph).....	182
Figure 74:	Cu-Zn ore (photomicrograph).....	183
Figure 75:	Cu-Zn ore (photomicrograph).....	184
Figure 76:	Zn-rich ore, island ore zone (photomicrograph)....	187
Figure 77:	Zn-rich ore, island ore zone (photomicrograph)....	188
Figure 78:	Zn-rich ore, island ore zone (photomicrograph)....	189
Figure 79:	Zn-rich ore, island ore zone (photomicrograph)....	191
Figure 80:	Zn-rich ore, island ore zone (photomicrograph)....	192
Figure 81:	Zn-rich ore, island ore zone (photomicrograph)....	193
Figure 82:	Cu- and Zn-poor, high sulfide minerals lens in disseminated sulfide zone (photomicrograph).....	195
Figure 83:	Cu- and Zn-poor, high sulfide mineral lens in disseminated sulfide zone (photomicrograph).....	196
Figure 84:	Lake Ore Zone (photomicrograph).....	200
Figure 85:	Lake Ore Zone (photomicrograph).....	201

TABLES

Table 1:	Selected Massive Sulfide Deposits within the Flin Flon-Snow Lake Greenstone Belt.....	2
Table 2:	History of Discovery and Exploration of the Vamp Lake Deposit.....	7
Table 3:	Lithologic Subdivisions of the Flin Flon-Snow Lake Greenstone Belt, Flin Flon Area.....	16
Table 4:	Generalized Stratigraphy of the Vamp Lake Area.....	24
Table 5:	Geochemistry of Mafic Volcanic Rocks.....	110
Table 6:	Geochemistry of Intermediate and Felsic Volcanic Rocks.....	113
Table 7:	Geochemistry of Altered Rocks.....	114
Table 8:	Measure of the coincidence of isocons independently based on constant Zr, TiO_2 , and Zr.....	157
Table 9:	Summary of the Various Alteration Types, and the Chemical Changes Involved in the Formation of the Assemblages.....	158

CHAPTER 1

Introduction

1.1 SULFIDE DEPOSITS OF THE FLIN FLON-SNOW LAKE GREENSTONE BELT

The Flin Flon-Snow Lake Proterozoic greenstone belt is well known for its base metal production from numerous massive sulfide deposits that range widely in tonnage and grade (Table 1), and are at various stages of production. The sulfide deposits are unevenly distributed within the belt; most of the ore bodies are concentrated near Flin Flon and Snow Lake (Figure 1). The volcanogenic massive sulfide deposits of the Flin Flon-Snow Lake belt characteristically consist of either a concordant sulfide lens or series of lenses. The deposits appear to be restricted to certain, relatively thin, stratigraphic intervals that are referred to as "favorable horizons" (Gale, 1983).

The massive sulfide deposits in the Flin Flon-Snow Lake greenstone belt have traditionally been subdivided into proximal and distal types (Syme et al, 1982,; Bailes et al, 1987). Proximal deposits are those that are closely associated with alteration zones, whereas distal massive sulfide deposits lack this association. In proximal massive sulfide deposits, the upper ore-wallrock contact is typically sharp, but the lower contact is usually gradational into a large stringer ore zone. Metal zonation is commonly present, resulting in Cu-rich foot walls and Zn-rich hanging walls (Syme et al, 1982). Characteristically, there appears to be a close spatial association between proximal massive sulfide

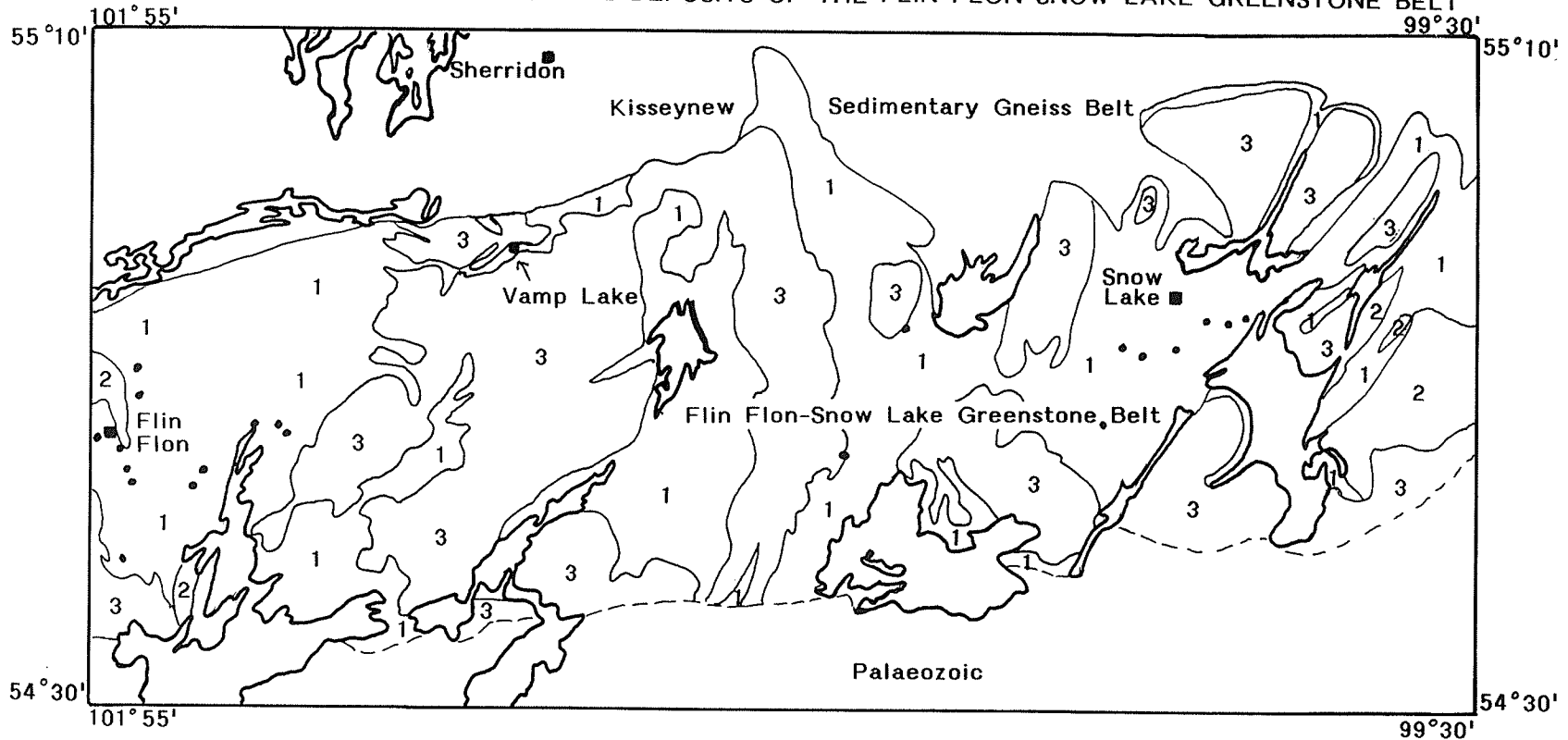
TABLE 1: SELECTED MASSIVE SULFIDE DEPOSITS WITHIN THE FLIN FLON-SNOW LAKE GREENSTONE BELT. THE DEPOSITS ARE LISTED IN ORDER OF DECREASING SIZE

DEPOSIT NAME	TONNES	⁴ Au (oz/T)	Cu (%)	Zn (%)
Flin Flon	64,000,000	0.090	2.2	4.4
Trout Lake ²	5,707,000	0.044	2.0	5.4
Chisel Lake	5,500,000	0.053	0.5	11.7
Stall Lake	5,000,000		4.8	0.6
Embury Lake	3,600,000		2.6	4.3
Anderson Lake	3,000,000	0.014	3.8	0.1
Callinan ³	2,377,000		1.5	4.1
Schist Lake	2,000,000	0.044	4.2	7.0
Reed Lake	1,350,000		2.1	
Pine Bay	1,350,000		1.3	
Centennial	1,200,000	0.044	2.6	2.6
Dickstone	1,000,000	0.015	2.6	3.1
West Arm	700,000		4.6	0.6
Rod	680,000		5.4	2.5
Cuprus	500,000	0.044	3.3	6.4
Joannie	500,000		1.3	
Ghost Lake	490,000	0.048	1.8	12.6
Vamp Lake	422,000	0.116	1.3	1.9
White Lake	400,000	0.020	2.1	4.5
Rail Lake	300,000		3.0	0.7
North Star	250,000	0.011	6.1	
Mandy	150,000	0.099	8.0	15.0
Copperman	143,000		2.8	4.5
Pot Lake ¹	112,000	0.012	1.4	4.5
Don Jon	80,000	0.027	3.1	

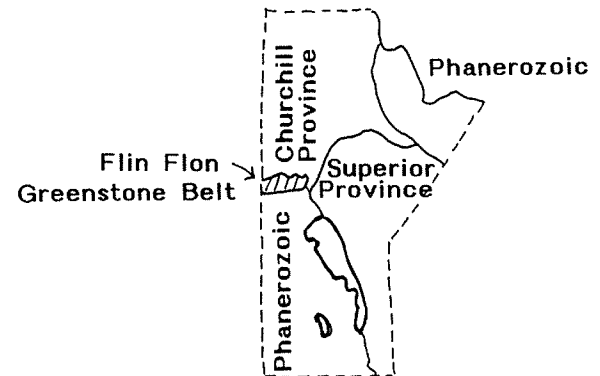
- References:
- ¹ Syme et al., 1982
 - ² Canadian Mines Handbook 1989-1990
 - ³ Prouse & Esposito, 1989
 - ⁴ Franklin & Thorpe, 1982

Remaining (unspecified) data from
Gale et al., 1982

FIGURE 1: GEOLOGY AND SULFIDE DEPOSITS OF THE FLIN FLON-SNOW LAKE GREENSTONE BELT



- 3 Intrusive Rocks
- 2 Missi Group Metasedimentary Rocks
- 1 Amisk Group Metavolcanic Rocks
- Massive Sulfide Deposit



(After Bailes, 1970)

ores and the presence of coarse volcanoclastic rocks (Syme et al, 1982; Bailes et al, 1987). These fragmental units are typically tuff-breccia or pyroclastic breccia based on the classification system of Fisher (1966). Such coarse fragmental rocks that host and underlie the massive sulfide bodies are historically known as 'millrock' (Sangster, 1972). Another commonly recognized association is the apparent affinity between massive sulfide deposits and felsic volcanic rocks. Distal deposits in the belt occur in basin structures and are typically hosted by fine-grained graphitic mudstone and minor chert.

It is generally accepted that volcanogenic massive sulfide deposits were formed on the seafloor by the discharge of submarine hydrothermal fluids, and they are thought to be ancient analogues of the seafloor mound chimney deposits presently being formed on the seafloor in the East Pacific Rise and other mid-ocean ridge areas (Lydon, 1984; Franklin et al, 1981). The stockwork alteration and associated stringer ore zones of the Proterozoic deposits are thought to represent the near-surface conduits of a hydrothermal system. As the focussed flow of the hydrothermal fluid was expelled from the vent into a coarse fragmental sequence at the seafloor, the flow became diffusive, enhancing the precipitation of sulfides from solution within the breccia mound and onto the seafloor above and around the discharge vent (Lydon, 1988). The relatively narrow stratigraphic intervals in which the deposits occur are possibly indicative of the relatively short periods of time within which such deposits are formed (Gale, 1983). The discharge sites of

hydrothermal fluids may be influenced by tectonic controls such as faults or fractures that could have provided an avenue for the discharge of the ore-bearing fluids onto the seafloor (Gair & Vokes, 1984). The origin of the metal bearing fluids is more controversial. Suggestions include the leaching of metal from footwall rocks by seawater or connate water, or the generation of ore-bearing fluids during the crystallization of fractionating magmas (Franklin et al, 1981; Gale, 1983). The heat produced by a synvolcanic intrusive body could also have been the mechanism for generating a hydrothermal system (Campbell et al, 1982).

The Vamp Lake deposit, the focus of this study, has both proximal and distal characteristics. The deposit is outside the two main areas where most sulfide deposits in the belt occur (Figure 1), making it difficult to ascertain whether the deposit occurs within a comparable time interval. The metallogeny of the Cu-Zn deposit is similar to that of other ore bodies in the region, although it is more gold-rich. The deposit is otherwise unexceptional in terms of size and ore grades (Table 1). Located about 48 km northeast of Flin Flon, Vamp Lake was, until recently, accessible only by float plane. Today, a branch road off the Kississing Lake road leads directly to the property.

1.2 HISTORY OF EXPLORATION

The Vamp Lake sulfide deposit was discovered about 1926 by a prospector named Paton, who staked the original claims on the property and initiated trenching of pyrrhotite-pyrite-chalcopyrite- and sphalerite showings on a large island in the northern part of the lake. In the years subsequent to the initial discovery, the property changed hands several times; an outline of the exploration history of the deposit is given in Table 2. The outline is not complete, but represents the best compilation that can be constructed from the sketchy existing company files and government records. To date, 197 drill holes amounting to 34,000 m have been drilled on the property. These drill holes are concentrated within a 1 km strike distance; most are less than 350 m deep.

1.3 PURPOSE OF INVESTIGATION

Prior to this research project, work on the Vamp Lake sulfide deposit had been concentrated on delineating the extent of mineralization; little data were available on the host rocks to the deposit, and the nature and genesis of the mineralization and associated alteration were virtually unknown. In this project the unaltered and altered host rocks have been studied in order to:

1. determine the nature of the host rocks to the deposit,

TABLE 2: HISTORY OF DISCOVERY AND EXPLORATION OF THE VAMP LAKE DEPOSIT. OWNERSHIP AND DESCRIPTION OF WORK IS BASED ON AVAILABLE DATA AND MAY NOT BE COMPLETE

DATE	OWNER/OPERATOR	DESCRIPTION OF WORK
1926-1928	Mr. Patton (prospector)	Staked original claims; trenched main showing
1928-1929	Nipissing Mines Ltd.	7 diamond drill holes (total length 488m)
1929-1949		Inactive, although claims changed hands several times
1949-1957	Lee Gordan Mines Ltd.	40 diamond drill holes (total length 4,128 m); magnetic survey; 2 electro magnetic surveys
1957-1958	Mining Corporation of Canada	First major geological mapping program; magnetic & electromagnetic surveys
1958-1963	Lee Gordan Mines Ltd.	Inactive?
1963-1965	Marcon Mines Ltd	54 diamond drill holes (total length 7,284 m); electromagnetic survey; geological mapping of entire 915 hectare property
1965-1968	Mr. John Noble	Consultant's report (1966) consisting of a compilation of previous work
1968-1972	Hudson Bay Exploration & Development Co. Ltd. and Conmar Mines Ltd.	32 diamond drill holes (total length 6,663 m)
1972-1987	Hudvam Mines Ltd. (formed by previous owners)	64 diamond drill holes drilled between 1981 and 1985 (total length 11,756 m)
1987-1990	Mingold Resources Inc. and Golden Range Resources Inc.	13 diamond drill holes (total length 5,079 m); 244 m of decline completed in 1988 (indefinitely closed in July, 1988)
1990-1992	Rayrock Yellowknife Resources	Maxiprobe EM survey; 16 diamond drill holes (total length 1,837 m)

2. study the petrology and geochemistry of the host rocks,
3. evaluate the wall rock alteration associated with the mineralization,
4. provide an interpretation of the geologic setting of the deposit, and
5. interpret the genesis of the deposit.

1.4 ACKNOWLEDGEMENTS

The author is deeply indebted to Dr. Ayres for his invaluable guidance and for always making time available whenever it was needed. Dr. Gale and Dr. Laznicka are thanked for their assistance in the early stages of the study. Access to the study site and to the drill core was freely given by Hudson Bay Exploration and Development Co. Ltd. Field support was provided by the Manitoba Mines Branch. This project was funded the Canada-Manitoba Mineral Development Agreement.

1.5 METHODOLOGY

1.5.1 Field work

Work on the project commenced in the summer of 1985 with three months of field work that concentrated on geological mapping and sampling of the ore zones and host rocks. This included an investigation of the local geology of a 2.1 km by 3.9 km area of the northern part of Vamp Lake mapped at a scale of 1:5000, and

detailed geological mapping, at a scale of 1:240, of a 260 m X 210 m island that hosts the main ore zone. Surface exposures on the island are not extensive, and in many areas, moss stripping and cleaning with the use of a Wajax water pump were required to obtain adequate surface exposure. Diamond drill core from some of the 197 drill holes (and wedges) that had been drilled by various companies between 1928 and 1989 was also examined to determine the rock types and extent of alteration in unexposed areas. Host rocks to the deposit were sampled in outcrop exposures and in drill core for petrologic and geochemical investigations. Several ore specimens were also collected for petrographic examination. Field work was continued for three weeks in the 1986 field season when core from 23 additional drill holes was examined and sampled.

1.5.2 Laboratory techniques

Due to the lack of outcrop exposures in key areas, particularly the main alteration zone, data collected from drill core examination were a critical part of the study; drill holes provided the only access to the main alteration zone. Thus, the construction of individual drill hole cross-sections and composite cross-sections incorporating several drill holes were important steps in establishing both the stratigraphy of the area, and the relationship of the alteration zone to the mineralization.

In wall rock units exposed in outcrop, megascopic primary structures and textures are not easily recognized on fresh or

weathered surfaces; this severely limited the collection of genetic data from field observations. To minimize this problem, representative samples of rock units were cut into slabs and etched with hydrofluoric acid in order to enhance primary textural and structural features that otherwise would not be visible.

Petrographic studies were done on 257 normal thin sections to establish the mineralogy and paragenesis of host rocks and ores. In addition, 29 polished thin sections were examined under both reflected and transmitted light to establish the relationship between the ore minerals and gangue.

Geochemical data were obtained from 78 rock samples. Major and trace element analyses, plus metal assays for 63 samples were done by X-Ray Assay Laboratories Ltd. Bondar-Clegg provided major element analyses for 15 additional samples, and carried out CO₂ and S determinations on all 78 samples. Examination of the trace element data revealed a wide scatter of Y, Nb, and Zr values with many samples reported to contain abundances unusual for the type of rocks involved. Consequently, 29 random samples were reanalyzed at the University of Manitoba. Both sets of data are given in Appendix C for comparison. Only the University of Manitoba analyses have been used in geochemical plots utilizing the elements in question.

Electron microprobe analyses were carried out on selected chlorite and biotite samples to examine the possibility of correlation between chemical zonation in the alteration zones and variations in mineral compositions. The analyses are provided in Appendix B.

1.5.3 Analytical Methods

Samples used for geochemical analysis were collected from a 0.5 by 2.2 km area during the 1985 field season. For host rocks that were not visibly altered, chip samples were taken from outcrop exposures within the map area. In addition, representative altered and unaltered wall rocks were carefully selected from drill core. The chip samples and core specimens were processed through a jaw crusher. The semi-prepared samples were then sent to X-Ray Assay Laboratories Ltd. where they were pulverized into powders with the use of an agate mill, a process that may have slightly increased the silica values obtained. Analysis of major element oxides and the trace elements Ba, Zr, Y, Nb, Sr and Rb were done by X-ray fluorescence spectroscopy; the reported detection limit was 0.01% and 2 ppm for the major oxides and trace elements respectively. Metal assays were done by plasma emission spectrometry; gold was determined through a combined fire assay and plasma emission spectrometry process. The detection limits were 0.500 ppm for Ag and Cu, 2.0 ppb for Au, 1.0 ppm for Co, Ni, Mo and Cd, and 2.0 ppm for Mn, Fe, and Pb. X-ray fluorescence spectroscopy was repeated on selected samples at the University of Manitoba with an A.R.L. 8420 X-ray fluorescence spectrometer to recheck the initial trace element values. The precision of the repeat samples was 2 ppm for Y, Zr, Sr, Rb and Rh, and 5 ppm for Nb. Major element analyses of the 15 additional samples sent to Bondar-Clegg were done by plasma emission spectrometry; detection limits were reported to be 0.01%. S and CO₂ analyses were carried out by Bondar-Clegg on 80 of the 81

samples for which whole rock analyses had been completed. CO₂ and S values were determined gravimetrically. Analyses of chlorite and biotite were carried out using an MAC-5 electron microprobe at the University of Manitoba.

1.6 PREVIOUS GEOLOGICAL STUDIES

Little published data is available on the local geology of Vamp Lake, or on the regional framework of the area. Regional mapping has been done by J.C. McGlynn at a scale of 1:50000. A very brief description of the property was given in McGlynn's (1959) report on the Elbow Lake and Heming Lake areas, but most information on the property is in the form of unpublished company files and reports.

The uncertain genesis of the deposit is evident from distinctly different mineralization and alteration processes mentioned in various unpublished summary reports on the property. Early work quickly established an association between mineralization and host rocks that had been altered to chlorite schist. In many of these reports, it was concluded that these altered rocks were the product of faulting and shearing (Walker, 1982). Parliment (1966) further suggested that faults were the dominant factor responsible for the localization of the sulfide mineralization with folds and contacts between mafic metavolcanic and pyroclastic rocks being contributing factors. In an alternative

interpretation, Walker (1982) proposed that the altered rocks represent the location of a hydrothermal alteration pipe related to the deposition of the massive sulfide body, a proposal based on the model outlined by Sangster (1972).

Previous petrographic work was restricted to a study of selected mineralized core samples by the Institute of Mineral Research, Michigan Technological University. Twenty-one polished thin sections were prepared, described, and examined with a scanning electron microscope in an effort to determine the precious metal phases (Hwang, 1984). This study was inconclusive because Au- and Ag-bearing phases were not detected.

1.7 REGIONAL SETTING

Vamp Lake is in a narrow arm of the Flin Flon-Snow Lake greenstone belt about 4.4 km south of the Kisseynew gneissic complex (Figures 1, 2). The greenstone belt consists of a sequence of early Proterozoic, isoclinally folded, mafic to felsic metavolcanic and metasedimentary rocks intruded by plutons of various compositions (Bailes, 1971; Gale et al, 1982; Bailes et al, 1987). The most common units in the Flin Flon area are mafic flows and related breccias that are interpreted to be subaqueous deposits, forming parts of major shield volcanoes (Syme et al, 1982; Bailes & Syme, 1989). Intermediate pyroclastic rocks and heterolithic breccias were deposited in intervalcanic basins from

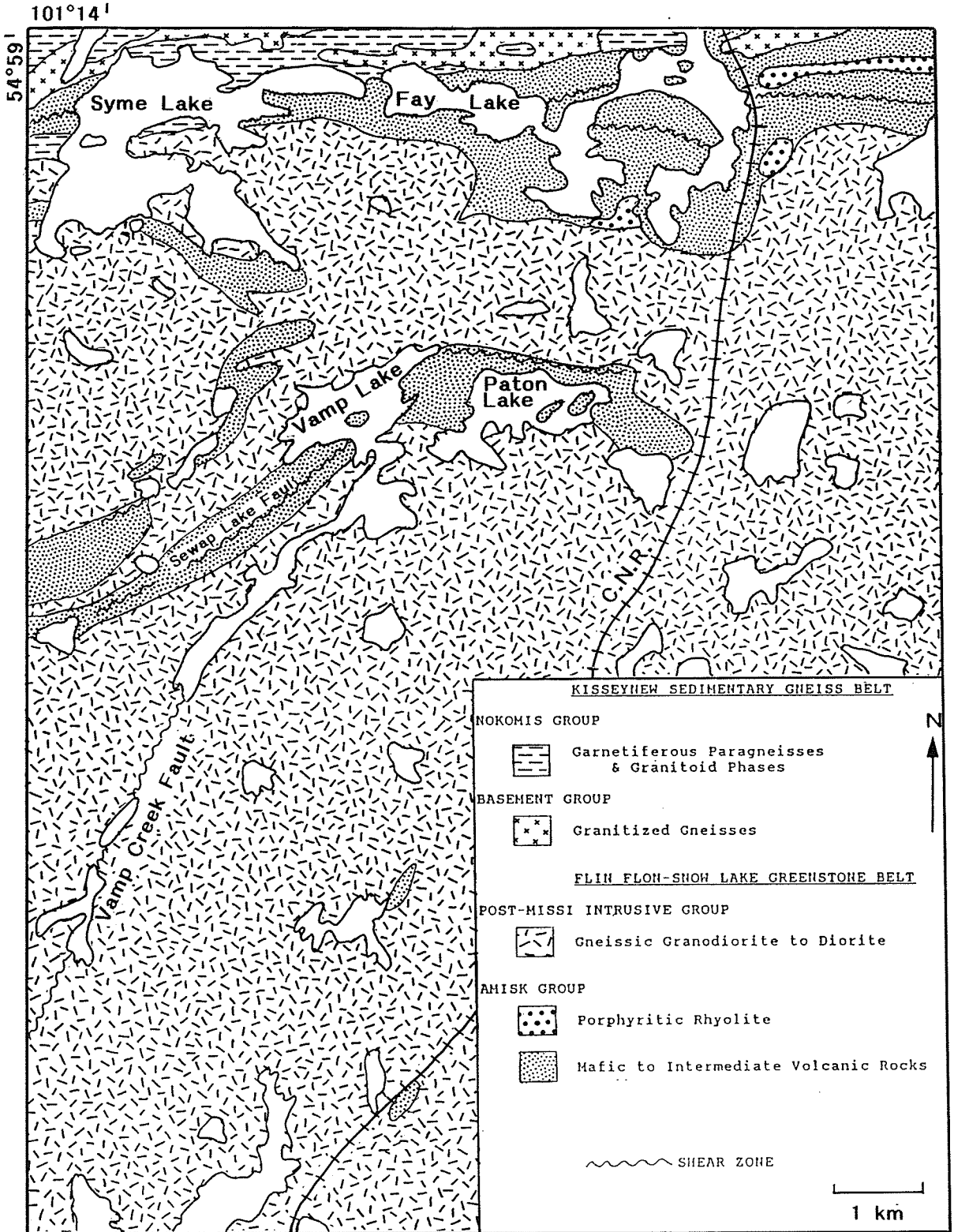


FIGURE 2: REGIONAL GEOLOGY OF THE VAMP LAKE AREA

Geology after McGlynn (1959), nomenclature of geological subdivisions after Bruce (1918)

subaqueous flows. Fine-grained sedimentary rocks cap some of these thick pyroclastic sequences. Rhyolite complexes occur at several different stratigraphic positions, and may be subaqueous lava flows. In general, intermediate and felsic units are much less abundant than mafic units overall, and tend to be more common in upper stratigraphic levels. In the Snow Lake area, the abundance of felsic volcanic rocks is equal to that of mafic volcanic rocks, with the felsic units concentrated in the lower part of the section (Syme et al, 1982). In general, all volcanic and sedimentary rocks of the belt have been metamorphosed with metamorphic grade ranging from subgreenschist to amphibolite facies, and increasing northward (McGlynn, 1959; Bailes & Syme, 1989). All volcanic and sedimentary rocks in the belt thus have metamorphic overprints, but for convenience, the terminology used in the following discussion ignores this aspect; references to primary rock types imply the metamorphic equivalents.

The greenstone belt comprises four lithologic groups (Table 3) described by Bailes (1971). The Amisk Group, which forms the lower part of the sequence, is characterized by volcanic rocks ranging in composition from basalt to rhyolite. In the Flin Flon area, the lower part of the group is dominated by mafic flows, many of which are pillowed, and intercalated mafic to intermediate pyroclastic rocks; comagmatic mafic intrusions are associated with these rocks. Upper units of the Amisk Group in the Flin Flon area are dominantly intermediate to felsic flows, pyroclastic rocks, and subvolcanic intrusions. Volcaniclastic sedimentary rocks, many of which are

TABLE 3: LITHOLOGICAL SUBDIVISION OF THE
FLIN FLON-SNOW LAKE GREENSTONE BELT,
FLIN FLON AREA

POST-MISSI INTRUSIVE GROUP

Intrusive rocks of variable composition:

Quartz monzodiorite, quartz diorite, diorite, gabbro,
meladiorite and pyroxenite

INTRUSIVE CONTACT

MISSI GROUP

Metamorphosed sedimentary rocks

Sandstone, pebbly sandstone and conglomerate

UNCONFORMITY

PRE-MISSI INTRUSIVE GROUP

Zoned, differentiated intrusions

Gabbro, ferrogabbro, tonalite

Mafic intrusions with ultramafic components

Peridotite, pyroxenite, gabbro, quartz diorite

Zoned, differentiated tholeiitic intrusions

Gabbro, gabbronorite, ferrogabbro, quartz ferrodiorite
ferrotonalite, leucotonalite

Mafic intrusions that vary widely in size, shape, texture,
composition and age

Gabbro, diorite, quartz diorite, and tonalite

High level felsic intrusions

Tonalite, leocogranite, quartz+/- plagioclase porphyry,
rhyolite intrusions

INTRUSIVE CONTACT

AMISK GROUP

Sedimentary rocks

Felsic volcanoclastic rocks, volcanic conglomerate, oxide
facies iron formation, greywacke-siltstone-mudstone, and
carbonate-rich sedimentary rocks

Felsic volcanic rocks

Rhyolite flows, possibly with aprons of reworked felsic tuff

Mafic to intermediate volcanic rocks

basalt and basaltic andesite sheet and pillowed lava flows;
highly variable volcanoclastic rocks, mainly deposited from
subaqueous density currents

(After Bailes & Syme, 1989)

turbidites, are intercalated with the volcanic units. The Amisk Group is unconformably overlain by sedimentary rocks of the Missi Group, a sequence of arkose, greywacke, quartzite, and conglomerate. Intrusive rocks have been divided into 2 groups on the basis of their relationship to the Missi Group. The Post-Missi Intrusive Group, which includes most of the intrusions within, and marginal to, the greenstone belt, is composed of gneissic granodioritic plutons and nonfoliated felsic to mafic plutons. The four groups comprising the Flin Flon-Snow Lake greenstone belt have been interpreted as an evolving island arc sequence (Bailes, 1971; Bailes & Syme, 1989).

1.7.1 Structural and Deformational Regime

The Flin Flon part of the greenstone belt is structurally complex as a result of multiple deformational events during the Hudsonian Orogeny (Stauffer and Mukherjee, 1971; Bailes & Syme, 1989). The pre-Missi period was characterized by tight folding of the Amisk Group, followed by uplift and erosion. In the post-Missi period, there were four phases of deformation: 1) open to tight east-trending pre-metamorphic folds in the Missi Group that have steeply dipping axial surfaces but lack axial planar foliation; 2) tight north and northeast-trending isoclinal folds in the Amisk Group characterized by a penetrative lineation; 3) north-trending open folds in the Missi Group with a strong associated axial planar schistosity and lineation; and 4) formation of a large open

northeast-trending antiform near Flin Flon, and the generation of several northwest-trending, oblique-slip faults. Block-bounding faults of uncertain age were originally described by Stauffer & Mukherjee (1971) in the Flin Flon area. The faults are commonly subparallel to stratigraphy, and possibly represent thrust surfaces. More recently, Bailes & Symes (1989) have identified previously unknown faults which divide the stratigraphy into blocks, each of which contains a unique stratigraphic sequence not duplicated in the other blocks.

Two folding events have been recognized in the Snow Lake area (Froese & Moore, 1980). In the earlier phase, tight to nearly isoclinal structures with prominent axial planar schistosity were generated. The second phase produced northeast-trending open flexures represented by the Threehouse synform, Southeast Bay antiform and the Whitefish Bay synform, and development of axial planar schistosity and penetrative lineation.

1.7.2 Metamorphic Regime

Rocks in the Flin Flon area have been subjected to low to middle greenschist facies metamorphism, with grade increasing to the north and northeast, reaching almandine-amphibolite facies in the Kisseynew complex, and in the Snow Lake area (Syme et al, 1982; Froese & Moore, 1980). In the Flin Flon area, the metamorphic peak corresponded to the second post-Missi folding event, whereas in the

Snow Lake area metamorphism began during the first folding event, and reached a peak after the culmination of the second phase of deformation (Syme et al, 1982). In spite of the metamorphic overprint, primary textures of the rocks are well preserved in low metamorphic grade areas, and locally preserved in other places.

Chapter 2

GEOLOGY OF THE VAMP LAKE AREA

2.1 LITHOLOGY

At Vamp Lake, the rock units can be broadly subdivided into three associations: a supracrustal sequence consisting of mafic to felsic flows and pyroclastic rocks of the Amisk Group; a comagmatic gabbroic intrusion; and large gneissic granodioritic stocks (Figures 2 and 3).

In the map area, the supracrustal sequence forms a 500 to 1000 m wide, northeasterly-trending belt that crosses the northern part of the lake; rock units dip 75 to 85 degrees to the southeast and host the Vamp Lake sulfide deposit. Mafic to intermediate volcanic rocks, dominantly flows, comprise about 70% of the supracrustal sequence forming 3 separate stratigraphic formations; these alternate with 2 felsic to intermediate formations. Although each of the 5 lithologic formations is dominated by a single lithology, some units contain interlayers of other rock types, and some unit boundaries are arbitrary.

A large gabbroic body is exposed on the mainland and on an island in the northeast part of the lake; it was also intersected by several drill holes beneath the lake. The gabbro is interpreted to be an intrusion because (1) the contact between gabbro and fine-grained mafic volcanic units, where exposed in outcrop, is

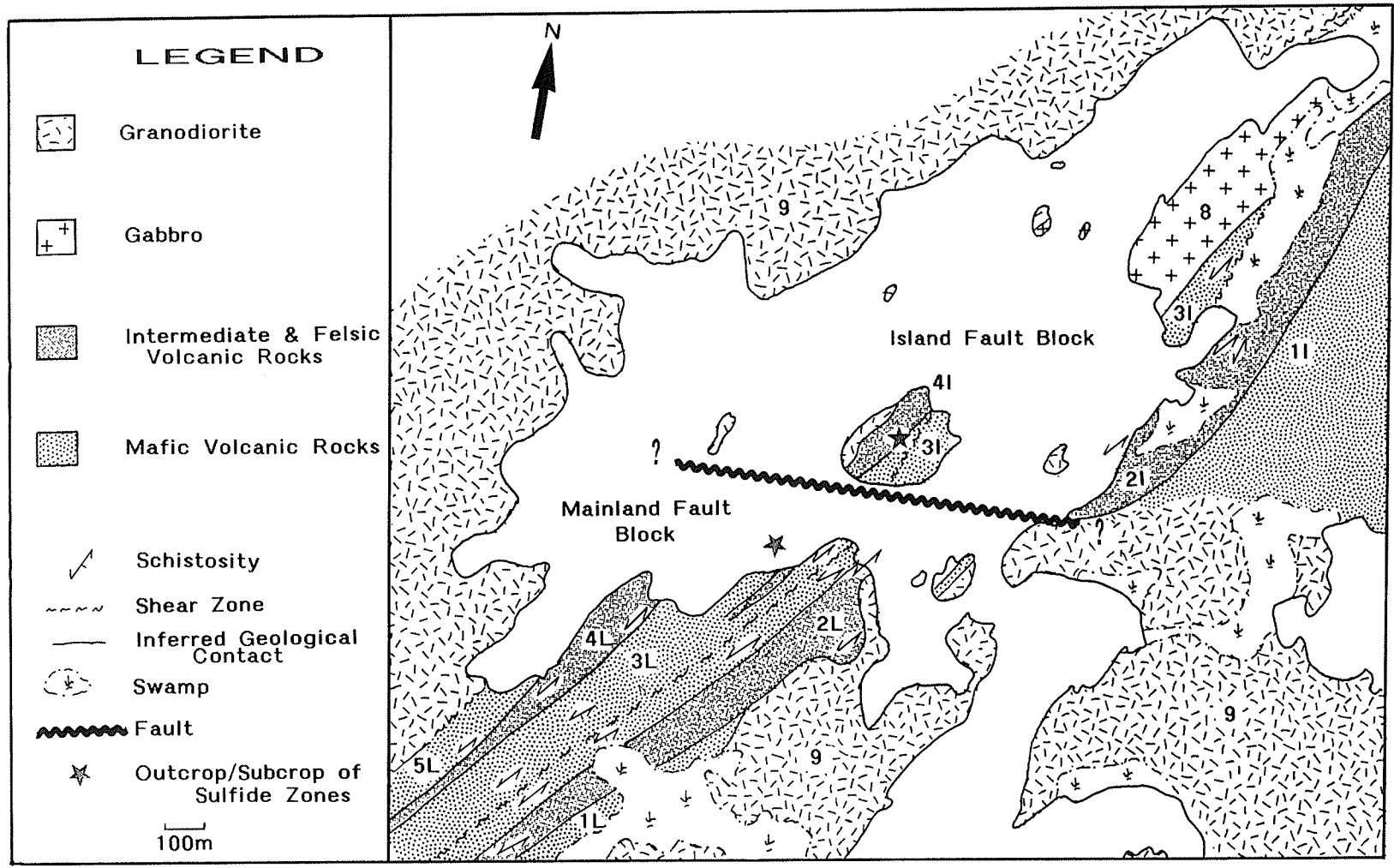


FIGURE 3: GEOLOGY OF THE VAMP LAKE AREA

Note: see text for explanation of sequence numbers
 Mapping completed by author as part of the present study

relatively sharp and well defined, although the gabbro lacks an obvious chilled zone, (2) in drill core, the gabbro contains xenoliths of the volcanic host rocks, and 3) compositional layering is present.

The volcanic-sedimentary belt is bounded on the northwest and southeast by large, semi-concordant, generally gneissic biotite and hornblende-biotite granodiorite stocks. Based on work by Bruce (1918), these intrusions are assigned to the Post-Missi Intrusive Group.

2.2 YOUNGING DIRECTION

Determination of stratigraphic younging direction is difficult at Vamp Lake because of poor outcrop exposure, lake cover, high metamorphic grade and deformation. Most of the evidence is based on primary structures found on a few outcrops on the large island that was the main focus of the investigation. Deformed pillowed flows, a poorly exposed scour channel in tuffaceous rocks, and a possible rip-up feature in a mafic unit all suggest a northwesterly-younging stratigraphy. This younging direction is also supported by (1) the asymmetrical distribution of highly altered rocks, which may represent alteration feeder pipes, relative to mineralized zones; alteration is mostly on the southeast sides of the mineralized zones, and (2) the occurrence of sulfide-rich clasts in rock units on the northwest side of the mineralized zone. Thus, although

evidence is limited, the consistent indication is that the stratigraphic sequence youngs northwest, and because units dip southward, the sequence is apparently overturned.

2.3 STRATIGRAPHIC CORRELATION

The generalized stratigraphy of the Vamp Lake area is provided in Table 4. There is some uncertainty in correlation of stratigraphic units across the east-trending fault south of the large island (Figure 3). Therefore, stratigraphy of each fault block is indicated separately on a schematic stratigraphic section (Figure 4). Units in the mainland fault block are designated with the code 'L', whereas those in the island fault block have been coded 'I'. The correlation between the two blocks is based on the comparable sequence of formations, and the similarity of formation lithologies and thicknesses in each fault block. This interpretation requires minimal movement along the fault, and both ore zones occur at the same stratigraphic level, indirectly supporting this correlation.

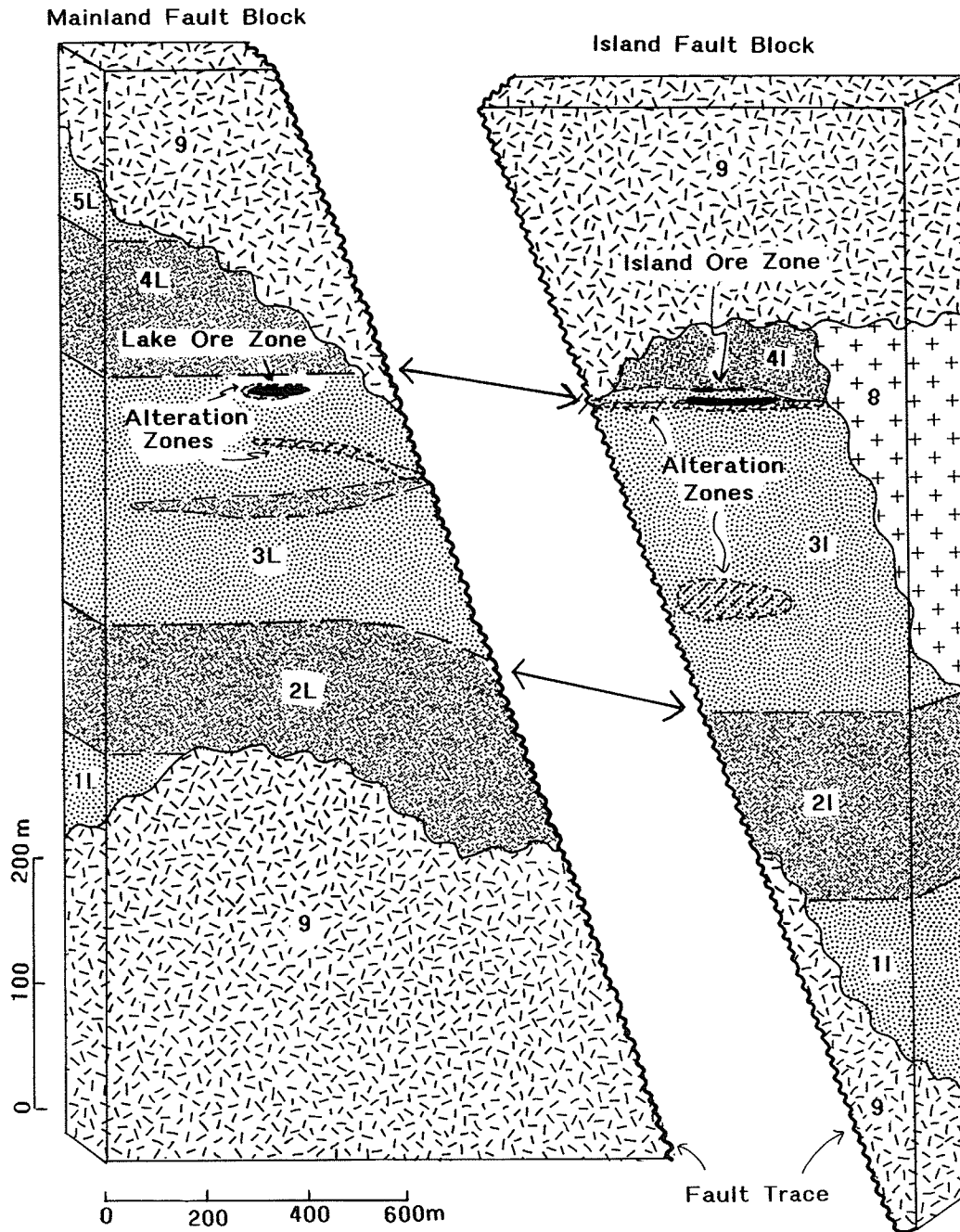
2.4 METAMORPHISM

Hornblende, oligoclase-andesine and quartz are the dominant mineralogical components of mafic volcanic rocks in the area, and varying proportions of epidote are present in most specimens. Such a mineralogical assemblage suggests that regional metamorphic grade

FORMATION	ROCK TYPES		
9	GRANODIORITE		
8	GABBRO/DIORITE		
5	MAFIC VOLCANIC ROCKS, GENERALLY FLOWS		
4	INTERMEDIATE AND FELSIC VOLCANICLASTIC ROCKS, AND INTERCALATED MAFIC FLOWS	7 Feldspar Porphyritic Felsic Dikes	6 Mafic Dikes
3	MAFIC TO INTERMEDIATE FLOWS AND TUFFS, INTERCALATED WITH FELSIC TUFFS		
2	FELSIC TO INTERMEDIATE VOLCANIC ROCKS, GENERALLY FLOWS		
1	MAFIC VOLCANIC ROCKS, GENERALLY FLOWS		

TABLE 4 : GENERALIZED STRATIGRAPHY OF THE VAMP LAKE AREA

FIGURE 4: SCHEMATIC STRATIGRAPHIC SECTIONS OF THE TWO MAIN FAULT BLOCKS IN THE VICINITY OF THE VAMP LAKE ORE ZONES



Numbers and patterns used match those of Figure 3 and Table 4. Thicknesses indicated are the present dimensions of the formations and may not reflect the original thicknesses.

is low to medium amphibolite facies. This is substantiated by the presence of poikiloblastic garnets and gahnite in intermediate to mafic units, and rare staurolite in a more aluminous unit. The metamorphic grade is largely a reflection of the narrowness of the supracrustal sequence in relation to the surrounding granodioritic bodies, although the proximity of the high metamorphic grade Kisseynew Complex, 4.5 km to the north, may also be a factor.

2.5 STRUCTURAL GEOLOGY AND DEFORMATION

The supracrustal sequence displays evidence of several distinct types of deformation, apparently the result of multiple deformation events. The northerly younging, southward dipping units indicate that the stratigraphy is slightly overturned. This, in conjunction with stratiform foliation, indicates that the supracrustal sequence has been isoclinally folded. Small scale isoclinal folds and boudinaged units have also been observed in outcrop. Later deformation includes the development of schistose zones, a conjugate fracture set, and faults.

No structural studies have been done in the area, and thus the number and types of deformation phases and their timing cannot be established. Therefore, the various deformational features are described in Chapter 5, but no attempt is made to subdivide them into distinct phases.

Chapter 3

STRATIGRAPHY NEAR THE VAMP LAKE ORE ZONES

There are two main ore zones in the Vamp Lake area, both of which are concordant with stratigraphy. The largest zone is partly exposed on the largest island in the lake; the second smaller zone subcrops beneath the lake, 250 m west of the island (Figure 3). The two ore zones will be referred to as the island zone and lake zone respectively.

The main ore zones are on opposite sides of the east-trending fault. The lake ore zone is in the mainland fault block; the island ore zone is in the island fault block. Based on the tentative correlation of formations across the fault, a separation of 35 m has occurred. Due to small-scale differences between blocks, the stratigraphy of each fault block is described separately.

Figure 5A is a surface map of the area near the ore zones based on surface mapping, supplemented by diamond drill hole data in unexposed and water-covered areas. Figures 5B, 5C, and 5D show level plan sections of the same area at depths of 30, 200, and 300 m respectively. There is an apparent lack of lithologic correlation among some drill holes. This is interpreted to reflect rapid facies changes, although small-scale folds and faults produced by deformation may have contributed to the rapid vertical and horizontal changes.

3.1 STRATIGRAPHY OF THE ISLAND FAULT BLOCK

The stratigraphic sequence hosting the island ore zone is outlined in Table 4 and Figure 4. Mapping has indicated that the supracrustal sequence has a minimum thickness of 450 m and comprises 5 formations (Figure 3).

The lowest stratigraphic formation (1I) is a series of mafic flows that outcrop on the the eastern mainland (Figure 3). Although terminated by granodiorite to the southeast, mapping by McGlynn (1959) east of the area shown in Figure 3 suggests a maximum exposed thickness of 2 km. This is overlain by a 150 m thick felsic to intermediate formation (2I) of interlayered tuffs and flows, followed in turn by a 245 m thick middle formation (3I) of mafic flows and breccias. The middle mafic formation (3I) is overlain by a 60 m thick formation (4I) of intermediate and felsic, locally garnetiferous, tuff and breccia, that is characterized by rapid lateral and vertical changes, and contains intercalated mafic flows. At surface and on the 30 m level, the boundary between these two formations is a zone of interlayered mafic and intermediate-felsic lithologies (Figure 5); at depth, however, the interlayering is absent. In the Island Fault Block, granodiorite is in contact with the upper felsic to intermediate formation (4I) and the upper mafic formation is missing.

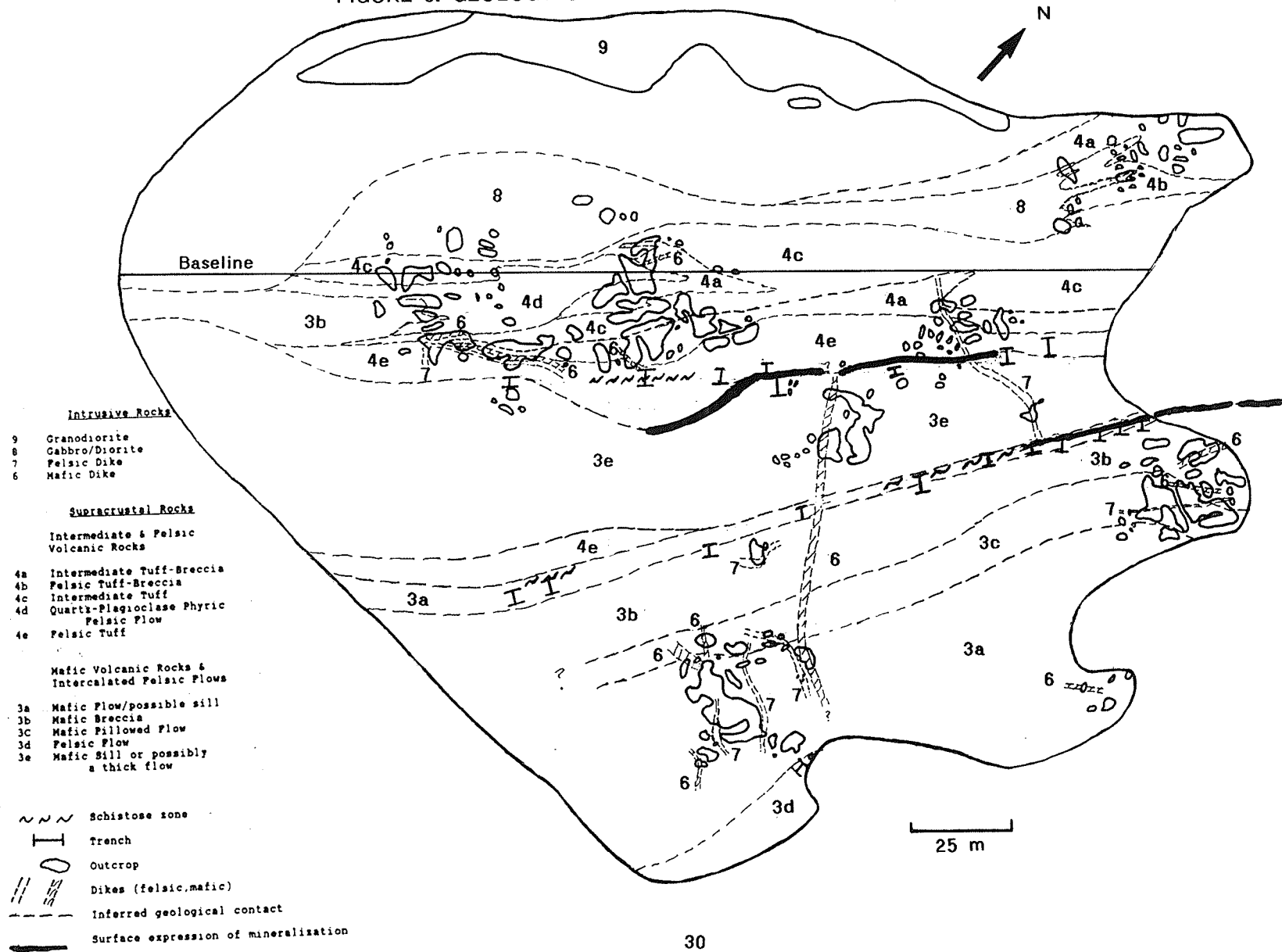
The island ore zone is exposed on a large island, termed the ore discovery island. This is the only locality where wall rocks to the mineralized zone can be observed and described in outcrop. The island has been a focal point of the research and a detailed map of

the island is provided in Figure 6. Because the main zone of alteration can be observed only in drill core, cross-sections and level plans generated from drill hole data in conjunction with surface mapping are the best means of showing the spatial relationship of ore zones, wall rocks and alteration. Figure 7 shows the approximate position of 5 cross-sections through the island ore zone.

3.1.1 Island Ore Zone

The Island Ore Zone is a 1.5-18 m thick stratiform zone at the contact between altered mafic flows (formation 3) and overlying intermediate to felsic volcanoclastic rocks (formation 4). The mineralization is exposed on surface and has been traced to a depth of 350 m; the lower limit has not been determined, although ore grades and thicknesses decrease below 275 m. Most of the economic grade mineralization occurs between 200 and 275 m depth (Figures 10-12) where it has been traced for a strike length of 190 m. At the present erosion surface, a second sulfide zone occurs 20 m above the main mineralization zone. The upper zone has a maximum thickness of 13 m, and has been traced for a strike length of 60 m. The felsic dominated 4I formation overlies the upper zone, and a mafic sill or flow separates the two ore zones (Figure 8). The distance between the upper and lower zones decreases with depth, and the 2 mineralized zones appear to merge as the mafic unit pinches out at a depth of 90 m (Figures 8 & 9).

FIGURE 6: GEOLOGY OF THE ORE DISCOVERY ISLAND



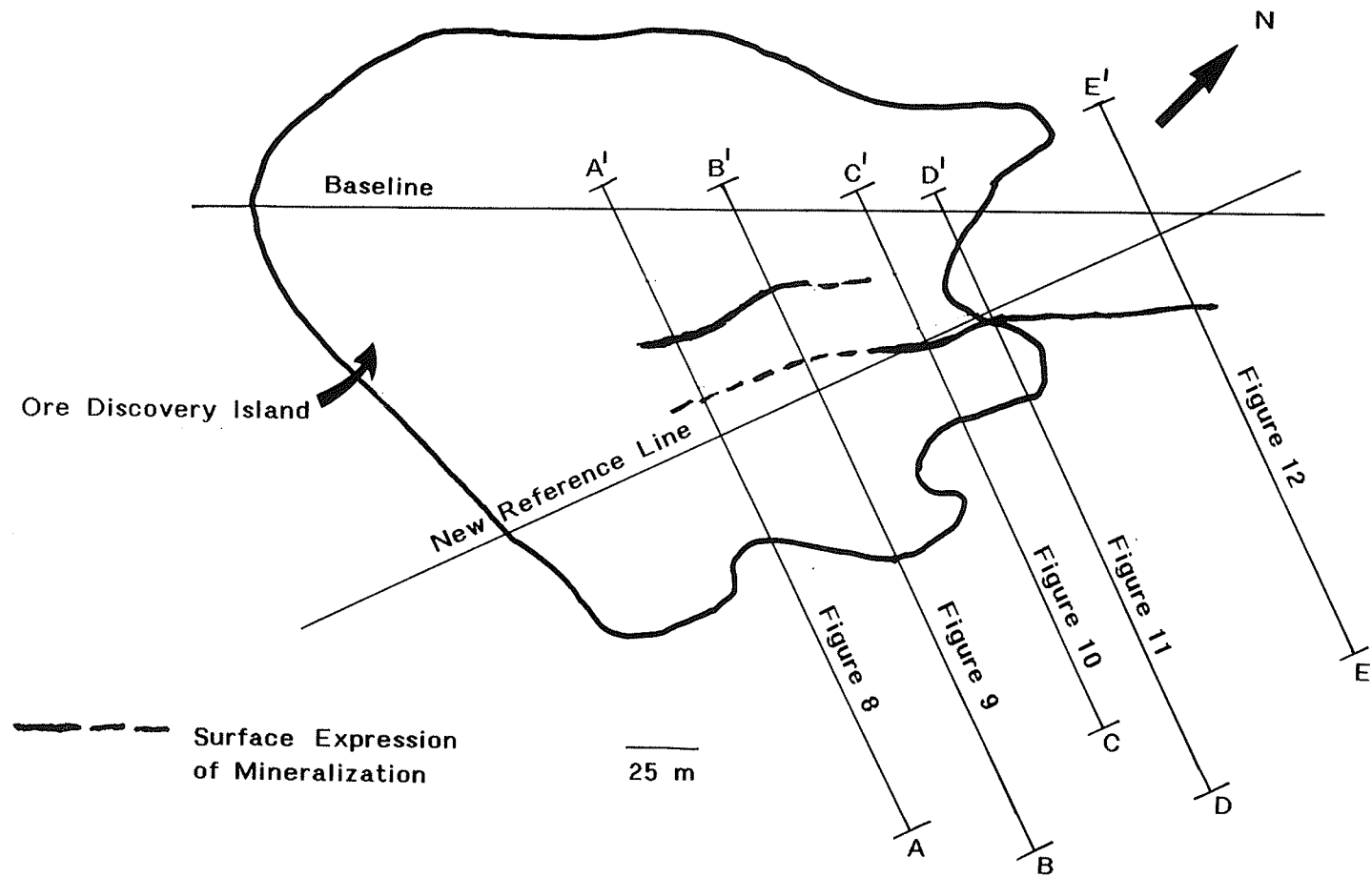
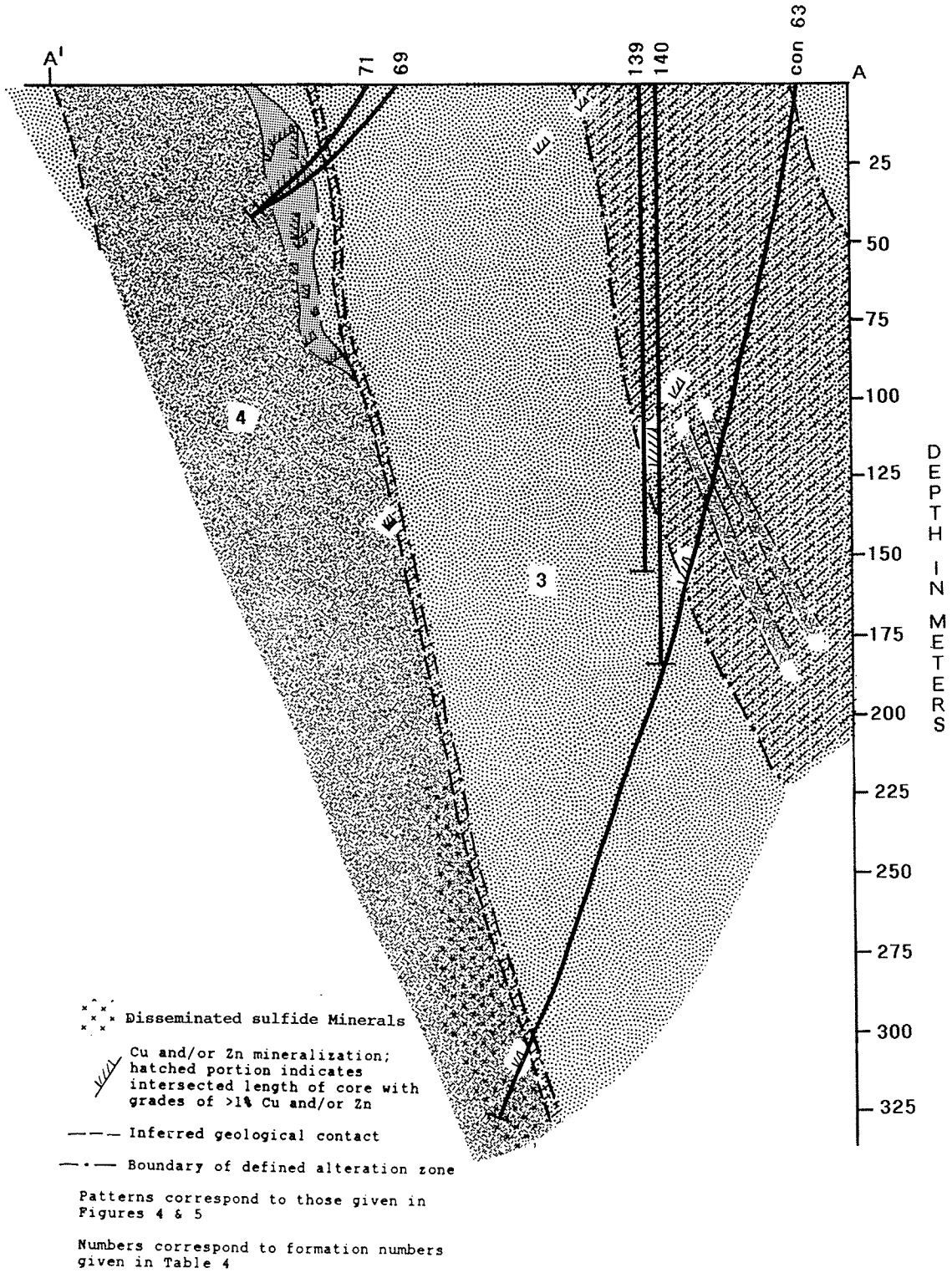


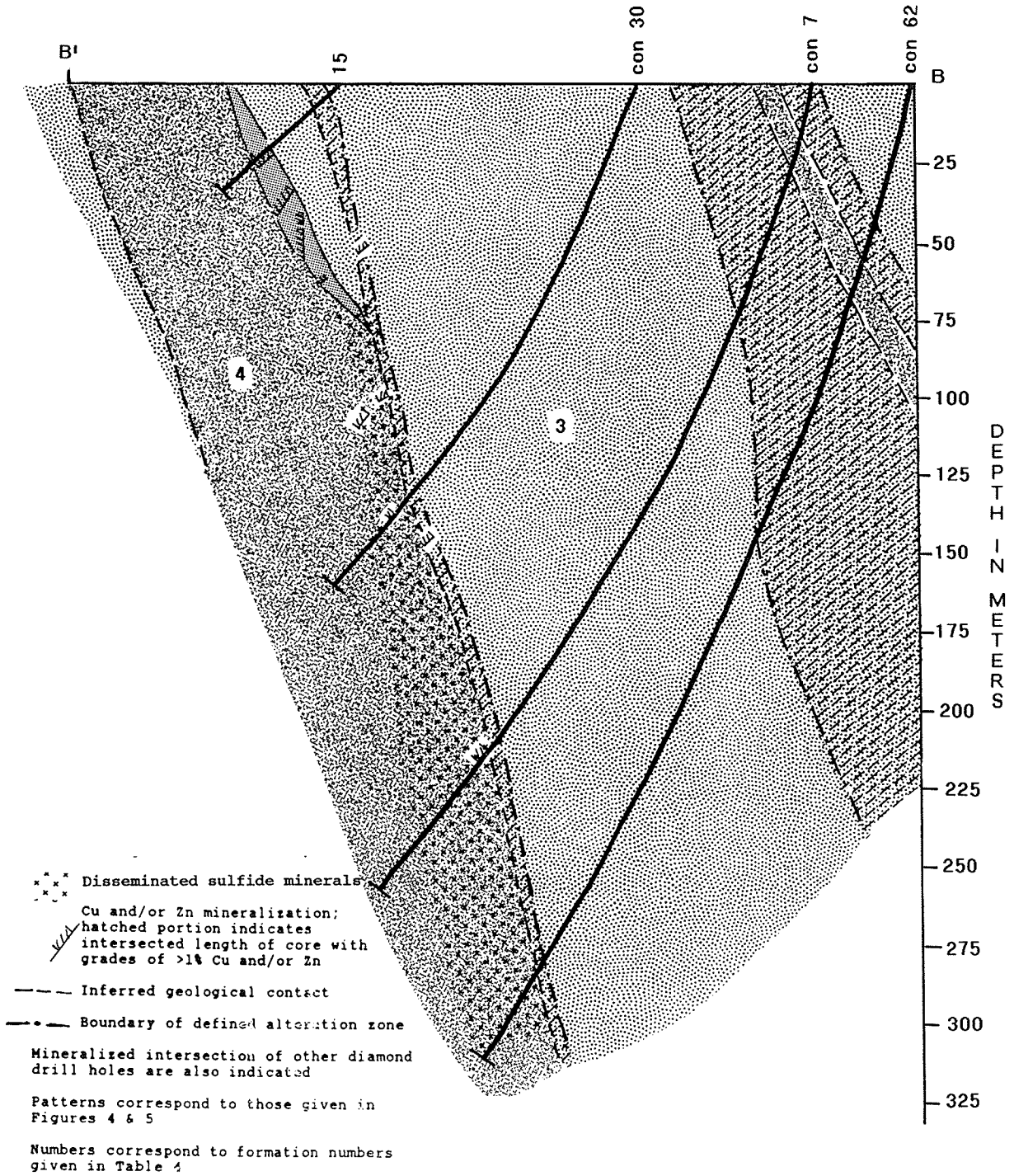
FIGURE 7: LOCATION MAP SHOWING THE POSITION OF CROSS-SECTIONS FIGURES 8-12

FIGURE 8: CROSS-SECTION (A-A') OF THE ISLAND ORE ZONE



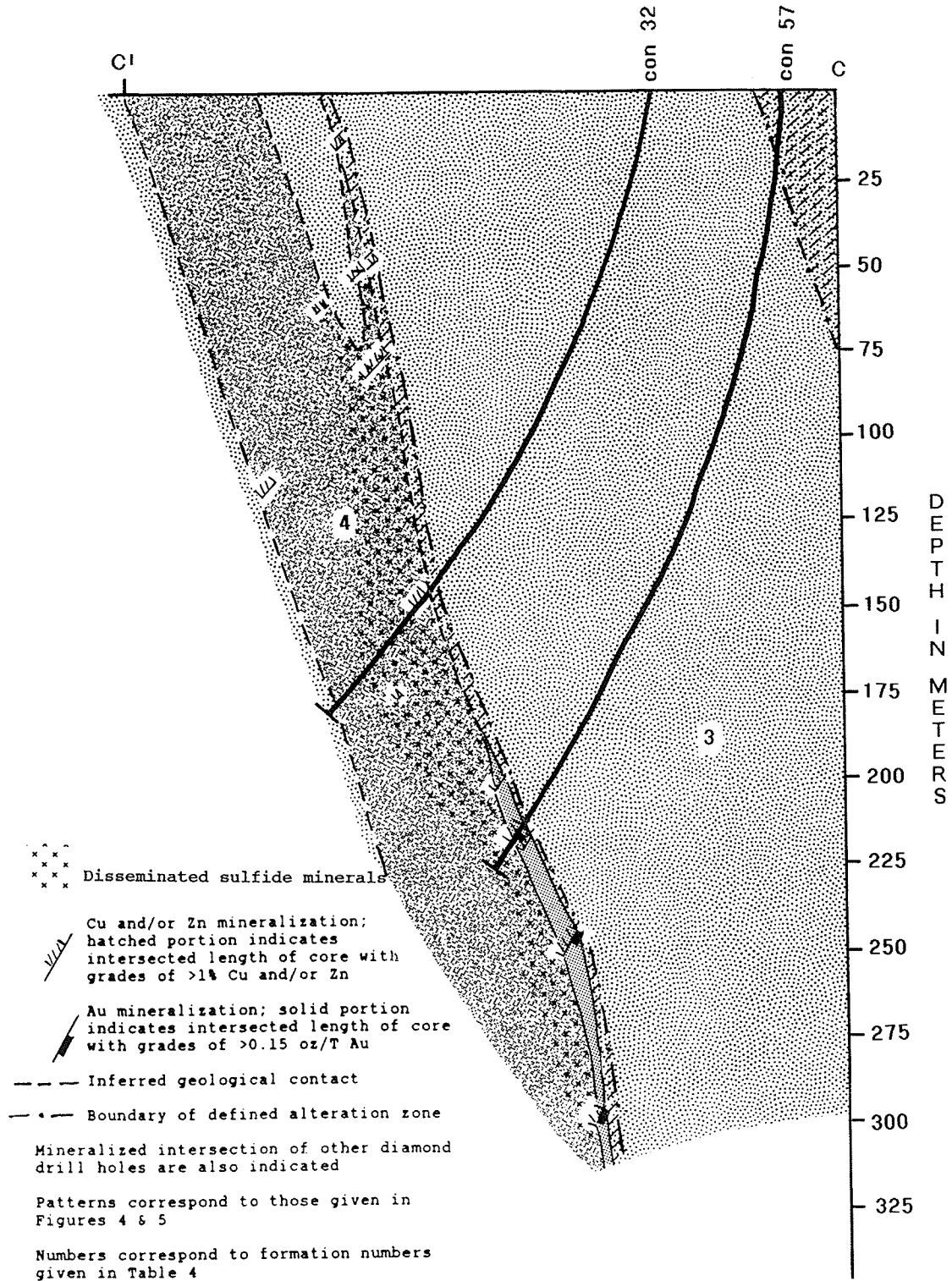
See Figure 7 for location of cross-section

FIGURE 9: CROSS-SECTION (B-B') OF THE ISLAND ORE ZONE



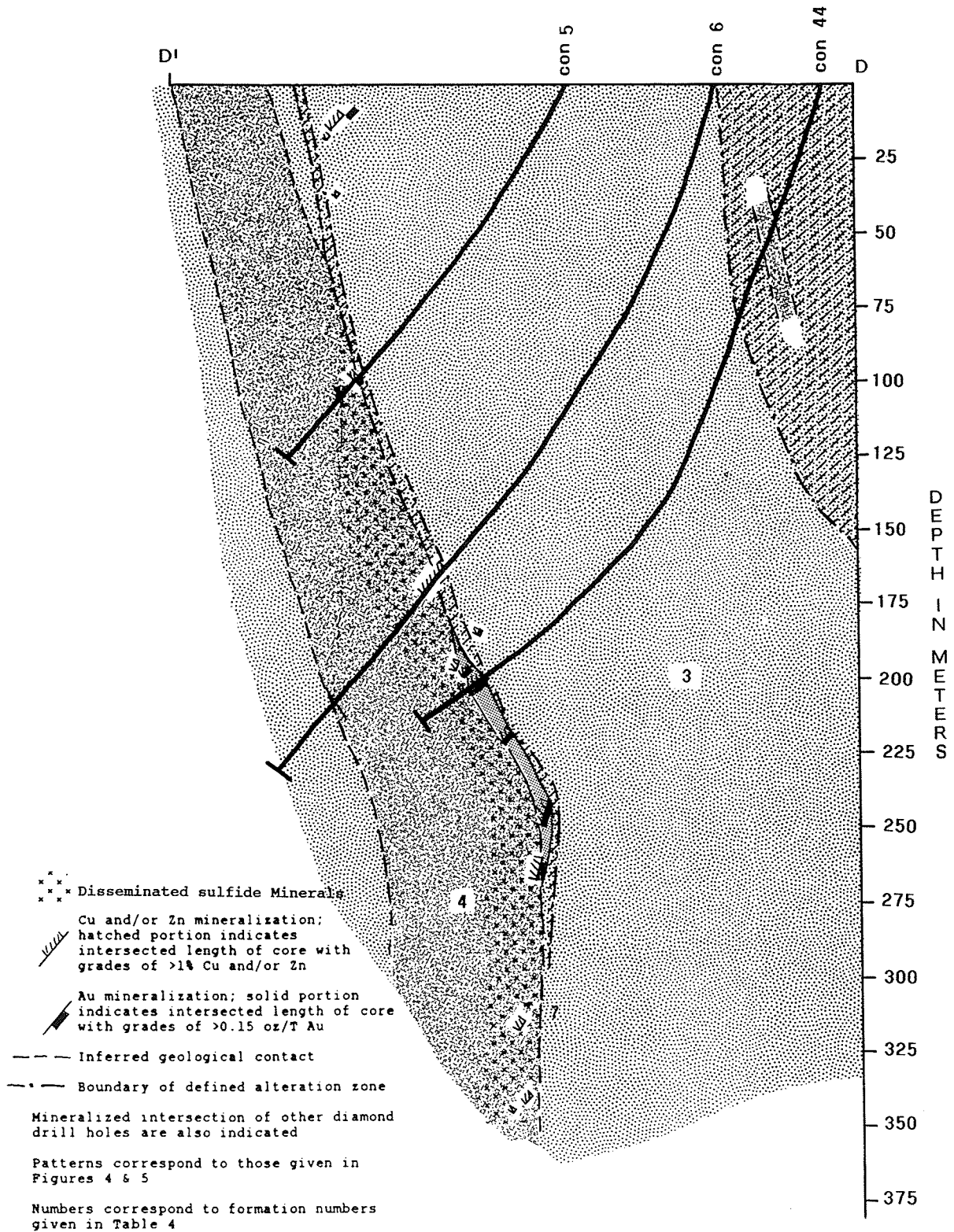
See Figure 7 for location of cross-section

FIGURE 10: CROSS-SECTION (C-C') OF THE ISLAND ORE ZONE



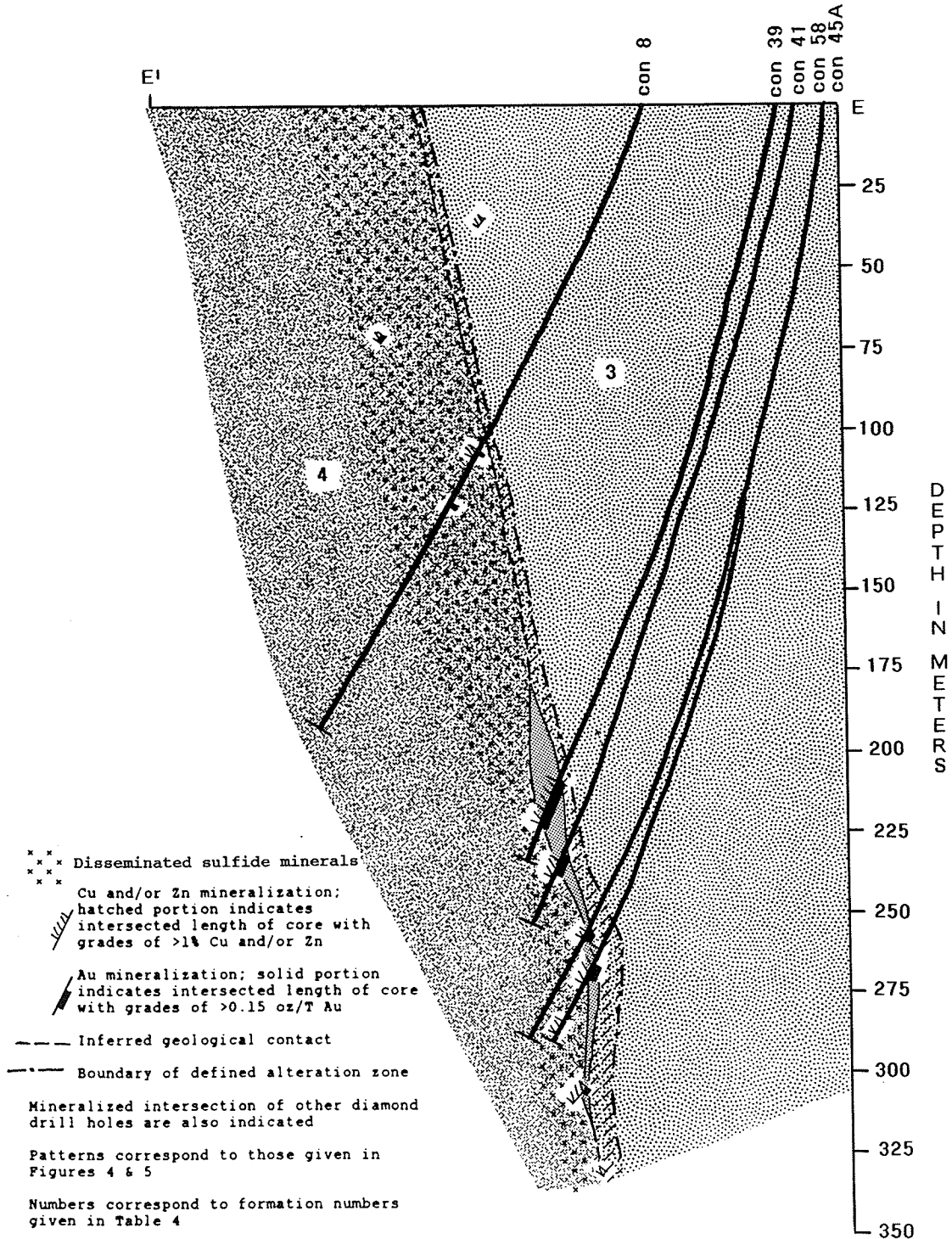
See Figure 7 for location of cross-section

FIGURE 11: CROSS-SECTION (D-D') OF THE ISLAND ORE ZONE



See Figure 7 for location of cross-section

FIGURE 12: CROSS-SECTION (E-E') OF THE ISLAND FAULT BLOCK



See Figure 7 for location of cross-section

Mineralization also occurs as numerous thin lenses within the overlying felsic to intermediate units, and the underlying mafic units; most of the lenses are close to the mafic (3I)-felsic (4I) contact (Figures 9-12).

3.1.2 Alteration Zones

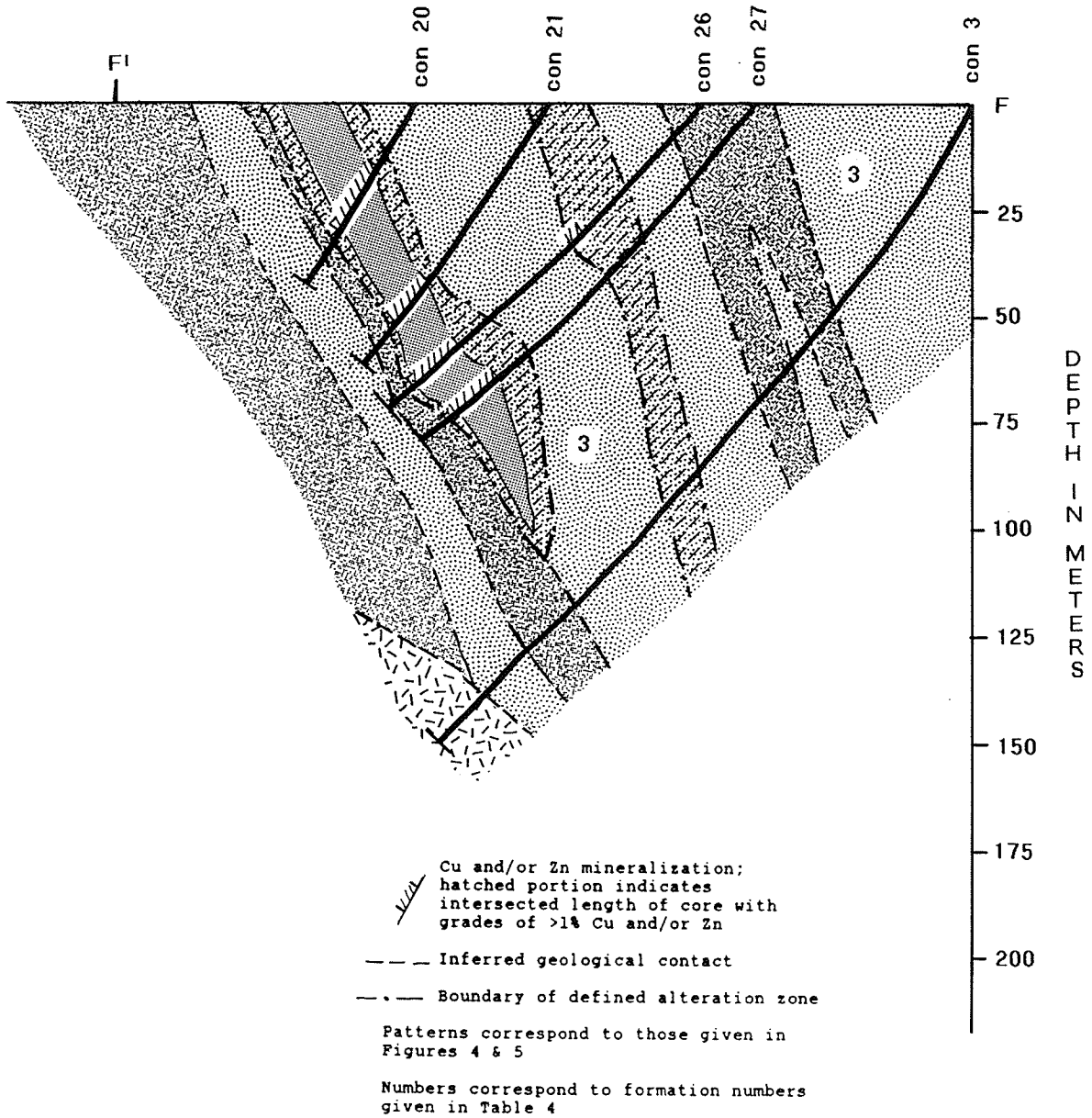
There are two alteration zones. The main alteration zone, which is largely characterized by a chlorite-biotite-quartz-amphibole mineralogical assemblage, is confined mainly to the middle mafic formation south of the ore discovery island. In surface exposures on the ore discovery island and in the vertical interval tested by diamond drilling, the top of the alteration zone is about 140 m below the ore zone. The alteration zone has a maximum thickness of 73 m, and a maximum length of 244 m. These dimensions decrease with depth (Figures 5A-5D). The altered units are dominantly mafic with minor altered intermediate flows at the northeast corner of the alteration zone; several apparently unaltered felsic units also occur in the zone (Figure 8). A second, thin alteration zone occurs immediately below the main mineralized zone (Figures 8-12) and appear to be developed in mafic volcanic precursor lithologies. No alteration was observed in the mafic flow or sill that occurs beneath the upper mineralized zone.

3.2 STRATIGRAPHY OF THE MAINLAND FAULT BLOCK

The stratigraphic sequence hosting the lake ore zone is

summarized in Table 4 and Figure 4. From surface mapping and diamond drill hole data, the stratigraphy of the supracrustal sequence of this fault block has been defined over a 435 m thick stratigraphic interval beginning 365 m below the ore zone. The basal formation of the supracrustal sequence of the mainland fault block comprises mafic flows that are exposed in the western margin of the map area (Figure 3); these are assigned to the 1L formation. Total exposed thickness of the formation is 55 m. This is overlain by intermediate to felsic tuffs and/or flows of the 2L formation, which varies in thickness between 100 and 180 m, and then by a 180-215 m thick mafic volcanic formation (3L) composed of massive to foliated, locally garnetiferous and/or amygdaloidal flows and minor mafic tuff. Minor discontinuous felsic tuff members are intercalated with the mafic flows and the mineralized zone occurs near the top of the formation (Figures 3 & 5). A series of intermediate to felsic pyroclastic rocks (4L) overlies the mafic sequence and ranges in thickness from 10 to 110 m because of truncation by granodiorite; the intermediate to felsic formation is only 10 m thick above the lake ore zone. In the western margin of the map area, the 4L formation is overlain by a 90 m thick formation of massive mafic flows (5L) that are bounded to the north by the granodiorite. Figure 13 is a cross-section of the lake ore zone and associated wall rocks.

FIGURE 13: CROSS-SECTION OF THE LAKE ORE ZONE



Refer to Figure 5A for location of cross-section

3.2.1 Lake Ore Zone

The ore body occurs in mafic rocks near the top of the 3L formation, but, in places, the ore zone is overlain by a thin felsic to intermediate intercalation (Figures 5B, 13). Mineralization in the mainland fault block occurs as a single concordant, massive sulfide lens that intersects the lake bottom and extends to a depth of 95 m. The zone has a strike length of 134 m and a maximum thickness of 12 m.

3.2.2 Alteration Zones

As in the island fault block, there are two alteration zones (Figure 5). The lower zone is a 17 m thick, sub-concordant zone that is mostly within mafic units of formation 3L, but also intersects an intercalated layered felsic unit. The alteration zone is 35 m below the ore zone, is entirely under the lake, has a strike length of 415 m, and is apparently truncated by the east-trending fault. A second alteration zone is a 2-11 m thick alteration envelope that almost completely surrounds the ore body.

Chapter 4

ROCK TYPES

Because similar lithologic units occur at several stratigraphic positions, and because most primary textures and structures have been obscured by metamorphism and deformation, rock units will be described lithologically, in order of decreasing abundance, rather than stratigraphically. This will avoid considerable repetition in the descriptions. Where appropriate, stratigraphic position will be noted in reference to Figures 3 and 4 and Table 4.

4.1 MAFIC VOLCANIC ROCKS AND INTRUSIONS

Mafic volcanic rocks are the dominant supracrustal lithology in the Vamp Lake area comprising most of stratigraphic formations 1, 3 and 5. Mafic rocks are mostly massive, non-amygdaloidal to slightly amygdaloidal apparently aphyric flows. Pillowed flows and associated breccias have a restricted distribution and were observed in outcrop at approximately the same stratigraphic level of formation 3 in both the island and mainland fault blocks; this restricted distribution however, may be more apparent than real, and could be the result of limited outcrop exposure and the difficulty of identifying these rocks in drill core.

Mafic dikes (unit 6) are common. They are compositionally and texturally similar to the flows, and can only be recognized by field relations. In drill core, the dikes are more difficult to

recognize, although in most places sharp discordant contacts, relatively narrow widths, and homogeneous appearance facilitate identification. Local mafic sills are also present.

Geochemical data on the various mafic lithologies are provided in Chapter 7.

4.1.1 Mafic Flows

4.1.1.1 Massive Flows

Massive mafic flows are the main lithology. They are homogeneous and are generally greenish-blue to grey-black on weathered surfaces; fresh surfaces are dark grey-black. The flows are generally foliated, and are locally gneissic.

The flows are composed of 35-55%, <0.1-0.45 mm subhedral amphibole; 10-44%, <0.1 mm plagioclase; 3-32%, <0.1 mm quartz; 1-5%, <0.1-0.3 mm opaque oxide minerals; and trace-3%, <0.1-0.2 mm biotite. Locally present are 4-12%, 0.45-1.35 mm well rounded quartz-filled amygdules. In most specimens, the amphibole is lineated and in some samples, it is concentrated in 0.2-1.0 cm laminae that contain up to 90% amphibole.

Less common are more mafic massive flows that comprise 75-80%, <0.1-0.3 mm anhedral to subhedral amphibole; 12-17%, <0.1 mm anhedral plagioclase; 3-6%, <0.1 mm anhedral quartz; and trace-2%, <0.1 mm opaque oxide minerals. These flows are more texturally variable than the less mafic flows; many contain hornblende porphyroblasts. The hornblende porphyroblasts, which form 12-30% of

many amphibole-rich units are 0.4-2.5 mm rounded anhedral or subhedral grains that occur as single grains or 2-4 mm rounded clusters. These porphyroblasts are poikilitic, with straight inclusion trains that are discordant to foliation. In clusters, inclusion train orientations differs among grains. The porphyroblasts deflect the foliation of the finer grained amphibole, a feature typical of metablastic growth (Barker, 1990). One distinctive porphyroblastic unit occurs in formation 3 in both fault blocks; in the island fault block, the unit has been traced laterally for 130 m. This unit is distinguished by the presence of 7-13%, 0.8-3.5 mm round to irregular brownish patches comprising a plagioclase core, surrounded by a central zone of fine-grained amphibole and epidote, and an outer zone of medium-grained quartz; these patches could be relict phenocrysts or amydules, or they could be the result of alteration.

In mafic flows amphibole content and grain size increase with increasing proximity to the gabbroic body east of the island ore zone. These rocks are characterized by 72-80%, 0.4-2.25 mm anhedral, randomly oriented poikilitic amphibole crystals; 14-15%, <0.1 mm plagioclase; 2-6%, <0.1 mm quartz; trace-8%, <0.1-0.22 mm epidote; and trace-2%, <0.1 mm opaque oxide minerals.

4.1.1.2 Pillowed mafic flows

Pillowed flows have been identified in outcrops of formation

3 on both the island and mainland fault blocks, where they occur at approximately the same stratigraphic level. On the mainland, elongated megapillows up to 4 m long (Figure 14) occur in a flow unit that is between 5 and 20 m thick. On the ore discovery island a single pillowed flow unit about 10 m thick was observed. Pillows here are not as stretched, and are smaller than those on the mainland; pillow margins are accentuated by epidote (see Figure 15). The pillows are mineralogically similar to the massive mafic flows.

4.1.2 Mafic Breccias

Mafic breccias are well exposed on the ore discovery island where they overlie the pillowed flow unit. On outcrop surfaces the breccias are characterized by 5-15 cm angular to lenticular, generally deformed, commonly amygdaloidal fragments; amygdule abundance, which range from 5 to 20%, is variable between and within fragments (Figures 16-17). The fragments, which form 80% of the breccia, are composed of: 35-50%, 0.14-0.45 mm subhedral amphibole; 33-37%, <0.1 mm plagioclase; 17-18%, <0.1 mm quartz; trace-5%, <0.1 mm epidote; and trace-3%, locally up to 15%, 0.1-4.0 mm sulfide minerals. The fragments occur in an amphibole-poor matrix composed of 60%, <0.1 mm plagioclase; 20%, <0.1 mm quartz; and 20%, <0.1-0.23 mm amphibole. Rounded to oval shaped amygdules



Figure 14: Highly stretched and elongated megapillows on the western mainland (sequence 3L), 300 m west along strike from the Lake Ore Zone. Pillow margins are intensely schistose. Hammer is 14 cm long.



Figure 15: Pillowed mafic flow (unit 3c in Figure 6), 20 m below the surface expression of the lower Island Ore Zone. Pillow margins are accentuated by epidote. Pillow shapes indicate stratigraphic younging is north (towards the top of the photograph). Hammer is 14 cm long.



Figure 16: Mafic breccia (unit 3b on Figure 6) approximately 12 m below the surface expression of the lower Island Ore Zone. Note the mixture of highly amygdaloidal fragments, and weakly amygdaloidal or non-amygdaloidal fragments. The amygdules are quartz. Diameter of lens cap is 5.6 cm.



Figure 17: Mafic breccia (unit 3b in Figure 6) in which fragments have been deformed. The dark colored margins surrounding the fragments may be chill margins, or possibly the result of alteration. Diameter of lens cap is 5.6 cm.

are locally concentrated within the fragments. These 0.45-1.7 mm features are composed dominantly of <0.1-0.6 mm quartz crystals, and less abundant <0.1-0.3 mm plagioclase crystals.

4.1.3 Layered Mafic Units

Layered mafic units that may be tuffs are intercalated with mafic flows of formation 3, and with felsic tuffs and flows of formations 4 and 2L. Overall, these units, which range in thickness from 20 cm to 13 m are much less common than the adjacent rock types. Individual layers within the units are defined by mineralogic and/or grain size differences, range in thickness from 0.03-4.00 cm, and may represent relict beds.

Overall, the layered mafic units are composed of: 30-55%, <0.1-0.27 mm amphibole; 13-52%, <0.1 mm quartz; 7-42%, <0.1 mm plagioclase; and trace-6% (and rarely up to 17%), <0.1-0.125 mm biotite. Minor epidote and sulfide minerals are also present in some samples. The amphibole content of individual layers varies between 15 and 80%; that of plagioclase and quartz varies between 7-82%, and 3-52% respectively. In some layers there are up to 10%, larger plagioclase grains that range in size from 0.34-2.0 mm; these grains are inferred to be relict plagioclase pyrogenic crystals.

4.1.4 Mafic Intrusions

Mafic dikes and local sills are common in the Vamp Lake area, but due to the more detailed examination of rocks on the ore discovery island, all petrographic information on these rocks is from this area. The intrusions are mineralogically similar to the massive mafic flows described earlier. Also present are fine-grained diorite dikes that are virtually indistinguishable from the mafic flows and dikes, except by petrographic examination; diorite typically contains euhedral, twinned plagioclase crystals, and quartz is absent. As seen in Figure 6, most dikes are approximately perpendicular to stratigraphy, and 1-2 m thick. The exception is a thicker concordant unit that is interpreted to be a sill. This unit outcrops on the island, is 40 m thick at its widest point, and pinches out rapidly downward and to the northeast. This unit is interpreted to be a sill on the basis of its homogeneous nature, and occurrence between and apparently dissecting the ore zone. However, since it is mineralogically similar to the mafic flows of the area and contact relations are not exposed, it is also possible that the unit is a thick lava flow.

4.2 INTERMEDIATE AND FELSIC VOLCANIC ROCKS AND INTRUSIONS

Intermediate and felsic rocks occur at two stratigraphic

levels in the supracrustal sequence and locally elsewhere. Felsic and intermediate flows dominate in formation 2, whereas intermediate and felsic pyroclastic rocks dominate in formation 4. Minor intermediate and felsic units are intercalated with the mafic units of formation 3.

Chemical compositions of the various lithologic types are provided in Chapter 7.

4.2.1 Felsic and Intermediate Flows

4.2.1.1 Felsic Flows

Felsic flows are the dominant rock type in formation 2, but they also occur as minor units in the 4L and 3L formations. In most places, outcrop surfaces are homogeneous, with randomly distributed biotite-amphibole flecks and streaks. Weathered surfaces are generally orange-brown to pinkish-orange in color, fresh surfaces are light grey. The felsic flows are composed of 35-66%, <0.1 mm anhedral quartz; 15-46%, <0.1 mm anhedral plagioclase; trace-15%, <0.1-0.45 mm shreddy amphibole; trace-12%, <0.1-0.25 mm subhedral biotite; trace-10%, <0.1-0.34 mm epidote; trace-10%, <0.1-0.45 mm sulfide minerals; trace-5%, 0.5-1.35 mm poikilitic garnet; and minor (<3%) calcite, muscovite and retrograde chlorite. No phenocrysts were recognized, and, if originally present, have been destroyed by recrystallization.

4.2.1.2 Quartz-Plagioclase-Phyric Felsic Flow

A 12 m thick quartz-plagioclase-phyric unit in formation 4I is probably a flow. It is distinguished in the field by abundant plagioclase phenocrysts and oval to ellipsoidal quartz eyes that stand out in relief on weathered surfaces (Figure 18). Weathered surfaces are pale-brown to orange-pink in color; fresh surfaces are grey. The unit is composed of 32-68%, <0.1 mm quartz; 10-37%, <0.1 mm plagioclase; trace-12%, 0.11 mm shreddy amphibole; trace-8%, <0.1-0.22 mm muscovite; trace-7%, <0.1-0.22 mm sulfide minerals; trace-6%, <0.1-0.115 mm biotite; trace-5%, locally up to 10%, <0.1-0.3 mm epidote; and rarely, up to 5% retrograde chlorite and 2% calcite patches. The remainder of the unit is composed of 6-17%, 1.2-5.4 mm, oval to elongate aggregates of <0.1-0.9 mm quartz that represent recrystallized quartz phenocrysts; and 3-15%, 0.34-1.0 mm recrystallized plagioclase phenocrysts. This rock type is interpreted as a flow, because of its homogeneous, massive nature.

4.2.1.3 Intermediate Plagioclase-Phyric Flow

Minor intermediate plagioclase-phyric flows, about 15 m thick, occur in the 2L formation. The groundmass of the flows is composed of 15-30%, 0.2-0.25 mm anhedral amphibole; 33-35%, <0.1 mm plagioclase; 29-35%, <0.1-0.23 mm quartz; 4-8%, <0.1-0.125 mm biotite; trace-7%, <0.1-0.12 mm epidote; and 1-5%, <0.1-0.2 mm sulfide minerals. The remainder of the unit consists of 1-8%, 0.3-1.5 mm rounded, augen-like altered plagioclase phenocrysts



Figure 18: Slab of quartz-plagioclase-phyric felsic flow that has been etched with hydrofluoric acid. The abundant creamy, oval to elongate features are recrystallized quartz crystals. The small white spots are recrystallized feldspar crystals, composed of epidote, clinozoisite, carbonate, zoisite, and local remnants of plagioclase.

overgrown by zoisite and epidote.

4.2.2 Fragmental Rocks

4.2.2.1 Felsic Tuff

Felsic tuff units, 15-30 m thick, were found mostly in formation 4, but are also intercalated with felsic flows in formation 2. Minor units were observed in formation 3. In outcrop, these units are extremely fine-grained and dense, with few megascopic textural features. The units are locally layered with 0.25-2.0 cm laminae defined by variations in grain size and amphibole and biotite contents. Weathered surfaces are cream to orange-brown, whereas fresh surfaces are variable in color, with layers varying from purplish blue-grey, to green, to very pale purplish grey-white.

The felsic units are composed of: 20-70%, <0.1 mm anhedral plagioclase; 14-50%, <0.1 mm quartz; trace-15%, <0.1-0.4 mm anhedral to subhedral epidote; trace-14%, <0.1-0.45 mm anhedral to subhedral amphibole; trace-12%, <0.1-0.22 mm biotite; trace-5%, <0.1-0.23 mm sulfide minerals; trace-4%, <0.1 mm epidote; and trace-2%, <0.1 mm calcite and retrograde chlorite.

The felsic tuff units are mineralogically similar to the felsic flows described in section 4.2.1.1, although tuff units contain slightly more plagioclase and less quartz.

4.2.2.2 Felsic Crystal-bearing tuff

Felsic crystal-bearing tuff units, 4-13 m thick, were found mostly in formation 4, although minor units were observed in the 3I and 2I formations. These units are texturally and mineralogically similar to the felsic tuff units described above, although they also contain the following constituents: 3-17%, 0.45-4.5 mm elongate aggregates of <0.1-0.9 mm polycrystalline quartz grains; trace-9%, 0.7-1.9 mm poikilitic garnet; trace-2%, 0.36-1.7 mm plagioclase crystals overgrown by fine-grained epidote, calcite, and clinozoisite; and black, opaque, elongate fragments, up to 7 mm long, whose mineralogy could not be identified. The elongated quartz aggregates have wispy, drawn-out ends, and the individual crystals in the aggregates have sutured contacts. These aggregates are interpreted to be recrystallized quartz crystals.

4.2.2.3 Intermediate Tuff

An intermediate crystal tuff unit outcrops on the Ore Discovery Island in the 4I formation. This unit varies in thickness from 4-20 m. On fresh surfaces this unit is a fine-grained, uniformly dark grey rock; weathered exposures are various shades of blue-grey. Well defined bedding was identified only in one area where beds are 10 cm thick, have sharp contacts and are distinguished by markedly different colours (pale blue-green versus dark blue-grey) and differences in abundances of quartz eyes and

white spots that may be recrystallized plagioclase crystals.

In general the matrix of the intermediate tuff unit contains 25-35%, <0.1-0.15 mm anhedral to subhedral amphibole; 22-40%, <0.1 mm plagioclase; 20-32%, <0.1 mm quartz; trace-4%, <0.1-0.23 mm sulfide minerals; trace-4%, <0.1 mm epidote; trace <0.1-0.13 mm anhedral biotite; and minor garnet associated with epidote and sulfide minerals. The amphibole is not evenly distributed but is concentrated in lineated aggregates, or rounded to oval clusters up to 4 mm long. On weathered outcrop surfaces these porphyroblastic clusters stand out in relief (Figure 19).

The larger, remaining constituents of the unit consist of 3-10%, 0.45-4.5 mm lenticular quartz aggregates composed of <0.1-0.5 mm crystals; and trace-5%, 0.45-1.35 mm, well rounded patches consisting of fine-grained aggregates of chlorite, sericite, clinozoisite, and quartz. The shape and mineralogy of the quartz aggregates suggest that they are recrystallized pyrogenic quartz crystals. Locally, there are larger aggregates that are up to 2.5 cm long and contain some amphibole and stringers of pyrrhotite and pyrite (Figure 20). These larger aggregates are interpreted to be fragments.

The chlorite-sericite-clinozoisite-quartz patches observed in thin section are probably recrystallized plagioclase crystals. This is supported by the remnant large twinned plagioclase grains within some patches.

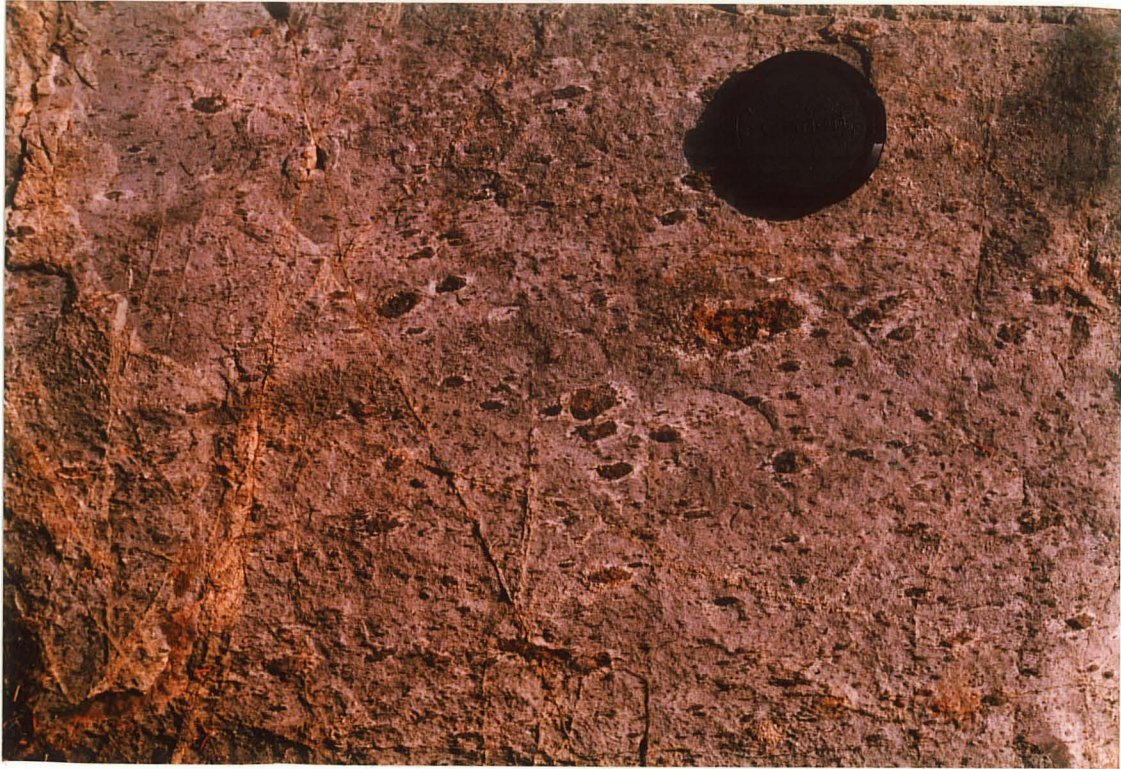


Figure 19: Weathered surface of an intermediate tuff (unit 4c in Figure 6). Dark "clots" are composed dominantly of amphibole. Some clots are rusty, due to the weathering of enclosed sulfide minerals. Figure 20 shows these sulfide-bearing aggregates on a fresh, etched surface. Diameter of lens cap is 5.6 cm.



Figure 20: Slab of intermediate tuff (unit 4c in Figure 6) which has been etched by hydrofluoric acid. Large, 0.5-2.0 cm fragments (upper right and center) are composed of quartz, amphibole, and pyrite stringers; comparable pyrite stringers are not found in the matrix. The abundant white spots are aggregates of chlorite, sericite, clinozoisite and quartz, possibly replacing plagioclase crystals. A set of conjugate fractures cross-cuts the sample; these are infilled by an aggregate of calcite, epidote and possibly prehnite.

4.2.2.4 Intermediate Tuff-Breccia

Intermediate tuff-breccia units, 1.6 to 16 m thick, commonly alternate with intermediate tuff units on the ore discovery island. On weathered surface, pale grey-blue fragments occur in a darker blue-grey matrix. Locally, fragments have a positive relief on weathered surfaces (Figure 21). On fresh surfaces the matrix is dark greenish grey-black whereas the fragments are grey-blue. The fragment to matrix ratio varies from 4:1 to 2:1. Fragments are commonly elongate and range in length from 5 to 30 cm, and in width from 2 to 5 cm; many fragments have irregular, jagged edges (Figures 21 and 22).

The fragments consist of 23-63%, <0.1-0.45 mm quartz; 12-53%, <0.1 mm plagioclase; 10-17%, <0.1-0.15 mm subhedral to anhedral, non-poikilitic amphibole; 7-16%, 0.45-5.1 mm oval to flattened ellipsoidal "eyes" composed of <0.1-0.7 mm grains of quartz; and 1-7%, <0.1-0.15 mm biotite. The quartz eyes are probably phenocrysts.

The matrix contains 25-45%, and rarely up to 65%, <0.1-0.5 mm and rarely, 1.8 mm anhedral amphibole; 16-50%, <0.1 mm plagioclase; 5-44%, <0.1 mm quartz; 1-7%, 0.23-4.5 mm poikilitic garnet; trace-8%, 0.4-5.0 mm aggregates of 0.1-0.45 mm quartz, probably recrystallized pyrogenic crystals; trace-3%, 0.36-1.7 mm relict plagioclase crystals; trace-3%, <0.1-0.15 mm opaque minerals; trace, <0.1 mm biotite; and locally, up to 6% retrograde chlorite.

The petrographic characteristics of the matrix are relatively uniform but those of the fragments are more variable. Mineralogically the matrix and the fragments are not significantly



Figure 21: Highly weathered outcrop surface of intermediate tuff-breccia (unit 4a in Figure 6). Fragments are more quartz rich than the matrix, and therefore, as shown in the photograph, tend to be more resistant to weathering. Diameter of lens cap is 5.6 cm.



Figure 22: Intermediate tuff-breccia (center of photograph) intercalated with intermediate tuff on the Ore Discovery Island. The breccia unit (4a on Figure 6) is characterized by elongate intermediate fragments within a darker, more mafic matrix. Both units have been cross-cut by a conjugate set of fractures which have weathered orange-pink in color.

different, although garnet is restricted to the matrix which is also distinguished by more abundant, coarser-grained amphibole, less abundant quartz aggregates and biotite, and the presence of minor plagioclase crystals.

4.2.2.5 Felsic Tuff-Breccia

Poorly exposed felsic tuff-breccia occurs in formation 4I at the top of the stratigraphic section on the ore discovery island. This unit is 1.5 to 6.5 m thick. Most weathered surfaces are cream to buff; fresh surfaces are grey-blue in outcrop exposures. Outcrop surfaces have a vaguely inhomogeneous appearance produced by uneven distribution of 0.3-7.0 mm oval shaped blebs or clots composed dominantly of amphibole. Distinct fragment outlines were only rarely observed on outcrop exposures (Figure 23), but where clasts can be distinguished, the mafic blebs are mostly within 7-30 cm rounded to slightly elongate fragments. The matrix is compositionally more felsic, contains only sparse mafic blebs, and on weathered surfaces is bleached white in color. Because fragments are difficult to define, the fragment to matrix ratio is poorly constrained but appears to range from 3:1 to 1:2.

The fragments generally consist of 29%, <0.1 mm plagioclase; 44%, <0.1 mm quartz; 25%, 0.1-0.2 mm, anhedral amphibole which tends to be concentrated in 0.3-7.0 mm elongate lenses or aggregates; 10%, 4.5-7.0 mm oval to rounded, quartz eyes composed of 0.4-0.9 mm grains; and 2%, <0.1 mm biotite shreds. Aside from

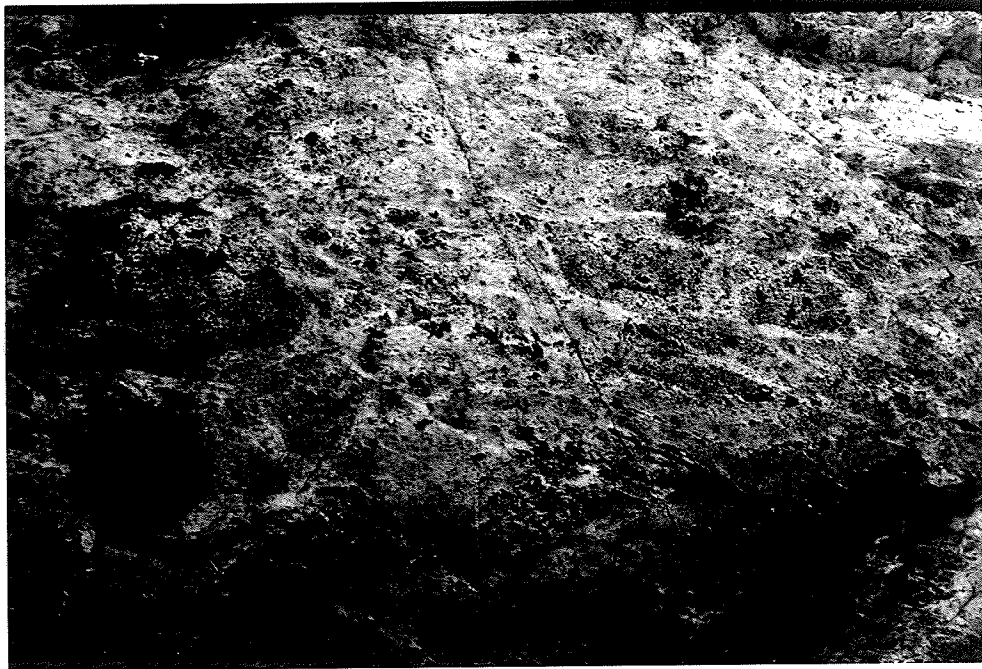


Figure 23: Felsic tuff-breccia exposed at the top of the supracrustal sequence on the Ore Discovery Island. The large fragments (the darker colored areas) are mineralogically similar to the intermediate tuffs that underlie this unit. The matrix is more felsic in composition, and weathers to a creamy white color. Diameter of lens cap is 5.6 cm.

the slightly larger and more rounded nature of the quartz aggregates, the fragments are compositionally and texturally similar to fragments in the intermediate tuff-breccia unit.

The felsic matrix is composed of 39%, <0.1 mm plagioclase; 34%, <0.1 mm quartz; 10%, 0.17 mm subhedral to euhedral biotite; 10%, 0.9-5.1 mm irregular quartz aggregates composed of 0.15-0.45 and rarely up to 1.2 mm grains; and 7%, <0.1 mm epidote in 0.2 mm patches. The matrix is texturally and mineralogically similar to the felsic tuff unit described in section 4.2.2.1.

4.2.3 Felsic Intrusions

Felsic dikes intruded both the 3I and 4I formations on the ore discovery island. The dikes are pale creamy-brown on weathered surfaces; fresh surfaces are dark grey. Abundant plagioclase phenocrysts are ubiquitous in the dikes (Figure 24).

The felsic dikes are composed of 28-39%, <0.1 mm quartz; 22-40%, <0.1 mm plagioclase; 12-17%, 0.4-1.5 mm euhedral, twinned and zoned plagioclase phenocrysts; 6-12%, <0.1-0.4 mm biotite that is generally concentrated in lineated aggregates up to 3.0 mm long; and minor epidote, muscovite and retrograde chlorite. Locally present are 7%, 0.36-0.6 mm aggregates of 0.11-0.45 mm quartz that are interpreted to represent recrystallized quartz phenocrysts.

The plagioclase phenocrysts are commonly overgrown by fine-grained sericite, epidote, clinozoisite or zoisite. Some of the

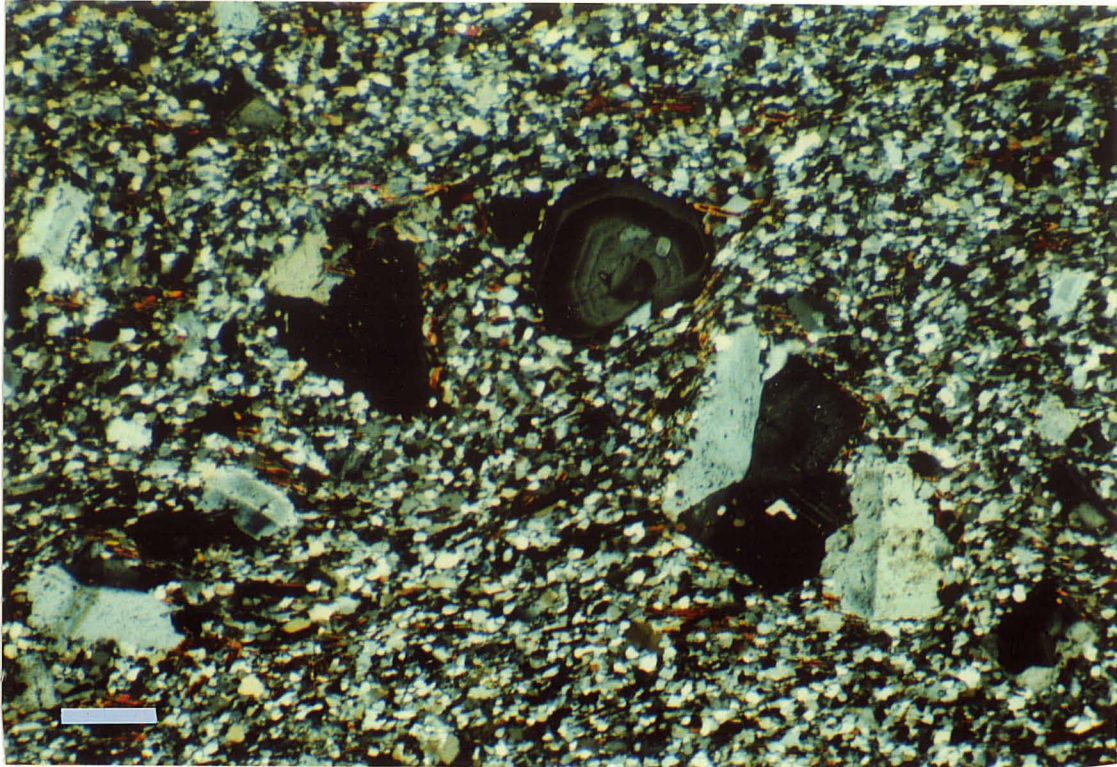


Figure 24: Photomicrograph of a typical felsic dike that intruded the supracrustal sequence on the Ore Discovery Island. Zoned and twinned plagioclase phenocrysts are the most characteristic feature of this rock type. Sample number CON 63-590. Scale bar 0.5 mm.

phenocrysts have been partly to completely replaced by pseudomorphs of very fine-grained non-pleochroic grey-brown to dark brown material of uncertain mineralogy and intergrown zoisite.

Mineralogically, the felsic dikes are similar to the felsic quartz-feldspar phyric flow described in section 4.2.1.2 although the dikes contain slightly more biotite, and they have been subjected to a lower grade of metamorphism than the flow (Figure 24).

4.3 POSSIBLE SEDIMENTARY ROCKS

Fine-grained, felsic appearing rocks that are petrographically and chemically distinct from other felsic units were encountered in drill core at two different stratigraphic levels in the island fault block. Based on chemical characteristics to be discussed in Chapter 7, it is tentatively concluded that these units are sedimentary, although the homogeneous nature of these units and the chemical and petrographic similarity among samples from different stratigraphic levels, would be compatible with the units being felsic sills. This rock type was not found in outcrop although outcrop occurrences may have been overlooked because of the megascopic similarity to other felsic units. The units encountered in drill core are 0.6 and 2.4 m thick; the concordant contacts are sharp. The rocks are typically light grey in color, and extremely massive and homogeneous in appearance. The lateral extent of these

units is not known.

Petrographically, the units contain 32-50%, <0.1-0.4 mm anhedral to subhedral plagioclase; 13-29%, <0.1-0.23 mm anhedral quartz; 14-16%, <0.1-0.2 mm shreddy biotite; 9-13%, <0.1-0.25 mm epidote; 3-11%, <0.1-0.8 mm sulfide minerals; 1-2%, <0.1 mm shreddy chlorite characterized by green-brown interference colors; and trace, <0.1 mm zoisite, calcite, and apatite. Locally present are 5%, 0.45-1.8 mm aggregates composed of 52-57% biotite; 38% epidote; 5%, sulfide minerals; and trace-5%, <0.1-0.18 mm retrograde chlorite. The grains within the aggregates are larger than the average grain size outside the aggregates.

Chapter 5

STRUCTURE OF THE VAMP LAKE AREA

The supracrustal sequence displays evidence of several distinct types of deformation, apparently the result of multiple deformation events. These structures include a well developed foliation and lineation, isoclinal folding, faulting, a conjugate fracture set, and schistose zones. No structural studies have been done in the area, and thus the number and types of deformational phases and their timing cannot be established. The deformational structures, either inferred or observed, are described below.

5.1 Foliation and Lineation

Most rock units are foliated. Foliation has a mean orientation of 45 degrees/80 degrees southeast, coincident with regional stratigraphy. Lineations were locally observed and plunge 75 degrees northeast. Although information on the alteration zones is restricted to diamond drill core, core angle measurements indicate that the alteration zones are also foliated with foliation orientation consistent with the regional foliation.

5.2 Isoclinal Folding

Evidence suggests that the area is part of a northerly

younging limb of an isoclinal fold. This evidence includes the overturned stratigraphy with stratiform foliation, and small-scale isoclinal folds observed in various thin sections of the wall rocks to the deposit (eg. Figure 25), wall rock fragments that had been incorporated into the ore zones, and in outcrops of various lithologic units

5.3 Faults

A wide, east-trending fault zone has been inferred from drill hole data near the ore zones at Vamp Lake. The presence of the fault is supported by an apparent displacement of magnetic trends defined by magnetometer surveys completed in 1969 and 1984 by Hudson Bay Exploration and Hudvam Mines respectively.

The fault was intersected in diamond drill holes 53 and Con 64. It is marked by a highly brecciated and blocky zone with a minimum true width of 36 m. The fault is interpreted to have a strike azimuth of 095 degrees and a dip of 62 degrees south. Based on correlation of lithologic units and mineralization on either side of the fault, there has been 35 m of right lateral horizontal offset along the fault.

Other 3 to 32 m wide brecciated zones that may be faults were encountered in several other drill holes in the area. These breccia zones are partly cemented by carbonate.



Figure 25: Photomicrograph displaying isoclinal folding in an altered mafic flow immediately overlying the Lake Ore Zone. Sample number CON 24-158 (altered unit 3L). Scale bar 1.0 mm.

5.4 Schistose Zones

Three schistose zones have been identified in the area examined. These include the Sewap Lake fault (Figure 2), a concordant schistose zone in the 3L volcanic formation, and two minor sub-parallel zones on the ore discovery island (Figure 6). The zones are characterized by highly schistose rocks and thus differ from the faults described above which are characterized by breccia zones. The schistose zones may be the product of one or more deformational events.

Other locally developed schistose, chloritic and/or sericitic zones, which earlier workers referred to as shear zones, have been identified from drill core. These zones are relatively wide in relation to limited strike length, and are spatially associated with the ore zones. As a result, the author believes that these zones are primarily a function of alteration rather than deformation. These areas will be discussed in Chapter 6.

5.5 Conjugate fracture system

A conjugate fracture system was observed in the intermediate to felsic pyroclastic units exposed on the ore discovery island. These <0.1-2 mm wide fractures are spaced about 0.05-10 cm apart and cross-cut lithologic contacts; they have been infilled by epidote and/or prehnite (Figures 20 and 22). The orientation of

these fractures indicates that the direction of principal stress responsible for their development was perpendicular to the stratiform foliation. The fractures are not deformed suggesting that the fracture-producing phase of deformation was a relatively late event in the deformation history.

Chapter 6

PHYSICAL FEATURES OF THE ALTERATION ZONES

6.1 INTRODUCTION

Four types of alteration have been defined in the Vamp Lake area on the basis of present stratigraphic position relative to the ore zones: distal, proximal, peripheral, and late stage (Figure 26). Each type is examined independently to determine possible relationships to the ore zones. Each of these alteration types is dominated by minerals such as chlorite, quartz, biotite, amphibole, and muscovite, which differ in abundances, textures, form, or compositions from surrounding unaltered rocks. Mineralogical assemblages and textural data indicate that in distal, proximal and peripheral alteration types, the present alteration mineralogy is the result of metamorphism of pre-existing but unidentifiable alteration assemblages.

Although metamorphism hampers the recognition of the precursor lithology of an altered rock, the problem can be mitigated by the use of geochemistry (section 7.3). In the following discussion, where the term precursor is used in reference to a specific lithology, this refers to the pre-metamorphic rock; the use of the term precursor component in the descriptions of partly altered rocks refers to the metamorphosed minerals of the unaltered portion of the rock.

Distal alteration zones are large altered areas that are

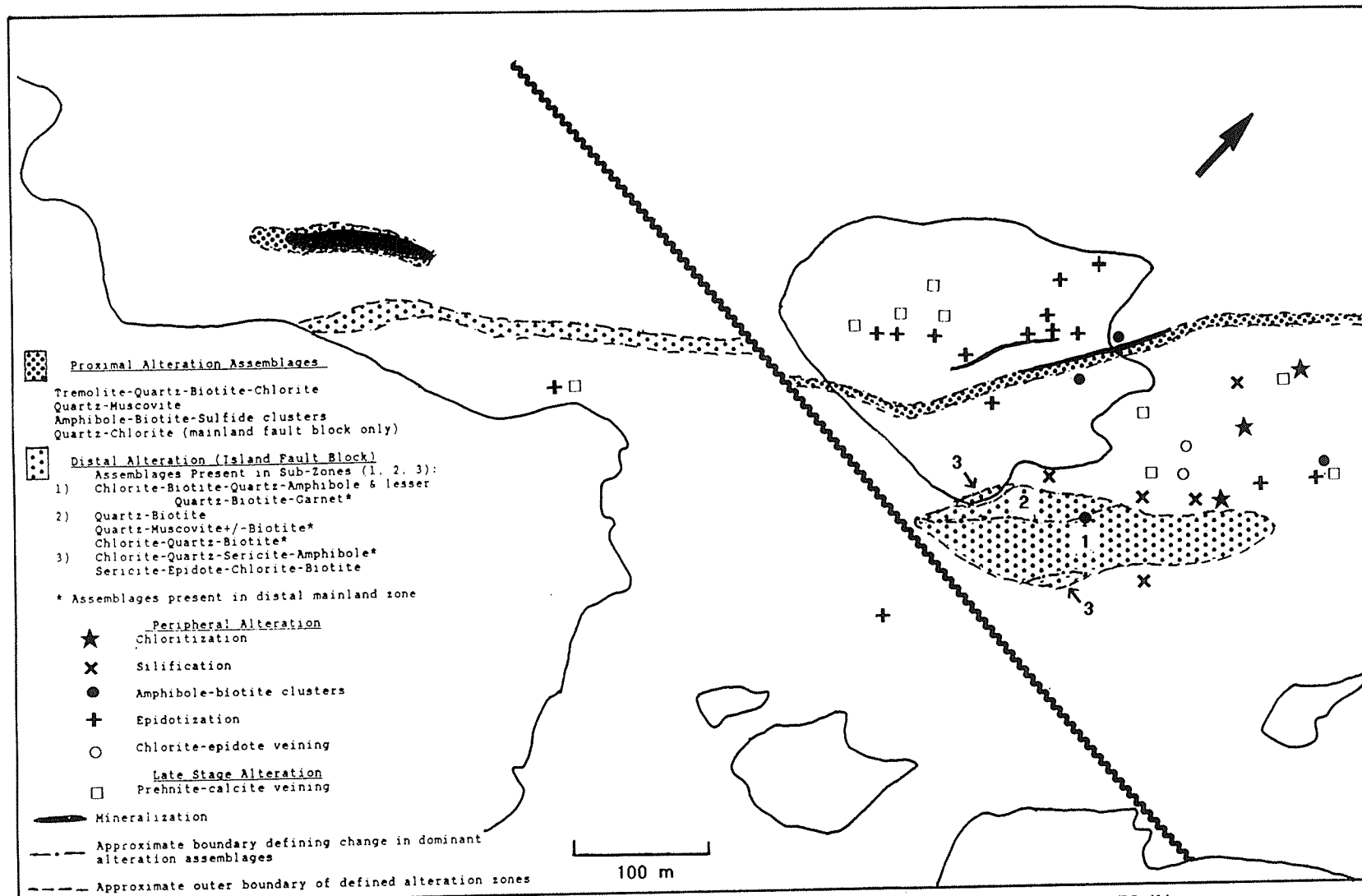


Figure 26: LOCATION MAP SHOWING THE DISTRIBUTION OF VARIOUS ALTERATION TYPES IN THE VAMP LAKE AREA

separated from the mineralization by relatively unaltered rock units. They are the largest alteration zones and underlie both the lake and island ore zones. These ovoid to elongate shaped zones are concordant with stratigraphy, but are of limited lateral extent, grading along strike into unaltered rocks.

Proximal alteration is defined as alteration that occurs adjacent to and in contact with the ore zones. Proximal alteration is associated with both ore zones, but it is more laterally extensive beneath the island ore zone, extending beyond the mineralization along an apparently stratigraphically controlled boundary. Proximal alteration zones are much thinner than distal alteration zones. The precursors to both distal and proximal alteration zones appear to have been dominantly mafic volcanic rocks, with lesser amounts of intermediate to felsic volcanic rocks. In addition to the different spatial positions, proximal and distal alteration zones differ in alteration mineralogy. A tremolitic assemblage is dominant in proximal alteration zones, whereas chlorite, quartz, biotite and muscovite are the dominant alteration minerals in distal zones. In each of these types of alteration, there are textural and mineralogical changes in the characteristics of the alteration as a function of the degree of alteration and/or different precursors.

Peripheral alteration comprises localized occurrences of veins or patches of alteration minerals in virtually unaltered host rocks. In most places, this type of alteration can only be identified in thin section.

Late-stage alteration is largely restricted to areas near the island ore zone and is defined by the occurrence of low temperature minerals in fractures that cross-cut stratigraphy and regional foliation. The fractures appear to be unrelated to and younger than the other types of alteration.

6.2 DISTAL ALTERATION ZONES

The volumetrically largest, distal alteration zone in the Vamp Lake area is 125 m south of, and below the island ore zone (Figure 5). The alteration zone has been traced for a strike length of about 244 m, but the eastward extent of the alteration is uncertain due to the lack of diamond drill hole data in that direction; the zone narrows downward, but the bottom has not been defined. On plan section the zone is ovoid shaped and approximately 73 m thick at the widest point. The second distal alteration zone is a minimum of 25 m south of, and below, the lake ore zone. This alteration zone has a maximum thickness of 17 m, and extends to a vertical depth of at least 105 m below present surface. Maximum strike length of the zone at surface is 415 m; the zone is apparently terminated by the east-trending fault.

6.2.1 Characteristics of Distal Alteration

The main alteration assemblages found in distal alteration

zones are: chlorite-biotite-quartz-amphibole, quartz-biotite, quartz-biotite-garnet, quartz-muscovite+/-biotite, chlorite-quartz-biotite, sericite-epidote-chlorite-biotite, and chlorite-quartz-sericite-amphibole. In the distal alteration zone underlying the island ore zone, there is a distinct spatial distribution of the various alteration assemblages (Figure 26). This spatial distribution appears to be consistent at all depths. One sub-zone represents the alteration of a different precursor lithology, and the distribution of the zone reflects the original stratigraphic position of this lithology. Minor sections of unaltered rock occur inside the boundaries of the defined alteration zone; in the central part, unaltered rocks appear to be dominantly mafic in composition. The boundaries between unaltered units and the completely altered assemblages are gradational. The nature of the transition is uncertain; however, based on megascopic examination of drill intersections, there appears to be some intercalation of assemblages near sub-zone contacts, and thus boundaries between sub-zones 1 to 3 are approximate.

The central part of the alteration zone is dominated by a chlorite-biotite-quartz-amphibole assemblage with locally developed quartz-biotite-garnet assemblages. Alteration assemblages are more variable in the outer part of the alteration zone and sub-zone 2 consists of a mixture of quartz-muscovite+/-biotite, quartz-biotite, and chlorite-quartz-biotite assemblages. Sub-zone 3, which occurs in both north and south marginal parts of the zone is dominated by a chlorite-quartz-sericite-amphibole assemblage, and

the local presence of a sericite-epidote-chlorite-biotite assemblage. The most noteworthy mineralogical differences between the upper and lower parts of the distal alteration zone relative to the centre are: less chlorite and amphibole, and in many samples, absence of chlorite or amphibole; and local presence of muscovite, garnet, staurolite, apatite, and Fe-Ti-oxide. The distal alteration zone in the mainland fault block contains the assemblages chlorite-quartz-biotite, quartz-biotite-garnet, quartz-muscovite+/-biotite and chlorite-quartz-sericite-amphibole. Although these are similar to some assemblages found in the upper and lower parts of the island alteration zone, the spatial distribution of these assemblages in the mainland distal alteration zone is unknown due to a limited data base. Full descriptions of all assemblages are given below.

6.2.1.1 Chlorite-Biotite-Quartz-Amphibole Assemblage

The chlorite-biotite-quartz-amphibole assemblage is generally restricted to the central part of the island distal alteration zone and represents the largest volume of altered rock. The most intensely altered rocks characterized by this assemblage are composed of: 15-65%, <0.1-2.0 mm intergrown chlorite laths forming an anastomosing network of veins <0.1-9.0 mm thick, that, in places, merge to form solid monomineralic masses; 5-25%, 0.1-1.35 mm (most commonly 0.25-0.5 mm) biotite as euhedral crystals or as felted masses of subhedral crystals within massive chlorite; 14-

35%, 0.2-0.4 mm, and rarely up to 1.5 mm, interstitial quartz in 0.72-3.00 mm aggregates and 0.45-2.0 mm wide irregular veinlets; 4-31% amphibole that most commonly forms <0.1 mm anhedral crystals and 0.9-1.8 mm long, needle-like laths; and 1-7%, <0.1-1.0 mm pyrite grains that are most common in quartz veinlets and lenses, or concentrated in laminae, parallel to the foliation defined by biotite and chlorite. A strong schistose fabric that is parallel to regional foliation is ubiquitous to these assemblages. These characteristics are displayed in Figures 27, 28 and 29.

The chlorite typically has grey interference colors characteristic of a Mg-rich variety (Kranidiotis & MacLean, 1987; Wynne & Strong, 1984). Large crystals are kinked (Figure 30), demonstrating that they pre-date the last tectonic event (Barker, 1990), and locally the chlorite schistosity is folded with subsequent development of axial planar cleavage (Figure 31). Biotite is most common as patches within chlorite, or as laminae up to 1.0 mm thick, parallel to the schistosity defined by the chlorite veining. Occasionally, biotite crystals within such laminae are speckled with fine-grained (<0.1 mm) inclusions of undetermined mineralogy. Amphibole is spatially associated with both chlorite and biotite, but particularly with biotite. The long, thin, needle-like amphibole crystals are commonly randomly oriented, possibly suggesting post-tectonic growth. In addition, the rare occurrence of large, skeletal amphibole crystals suggest metablastic growth during metamorphism (Figure 32).

Some rocks of this assemblage are not as intensely altered and

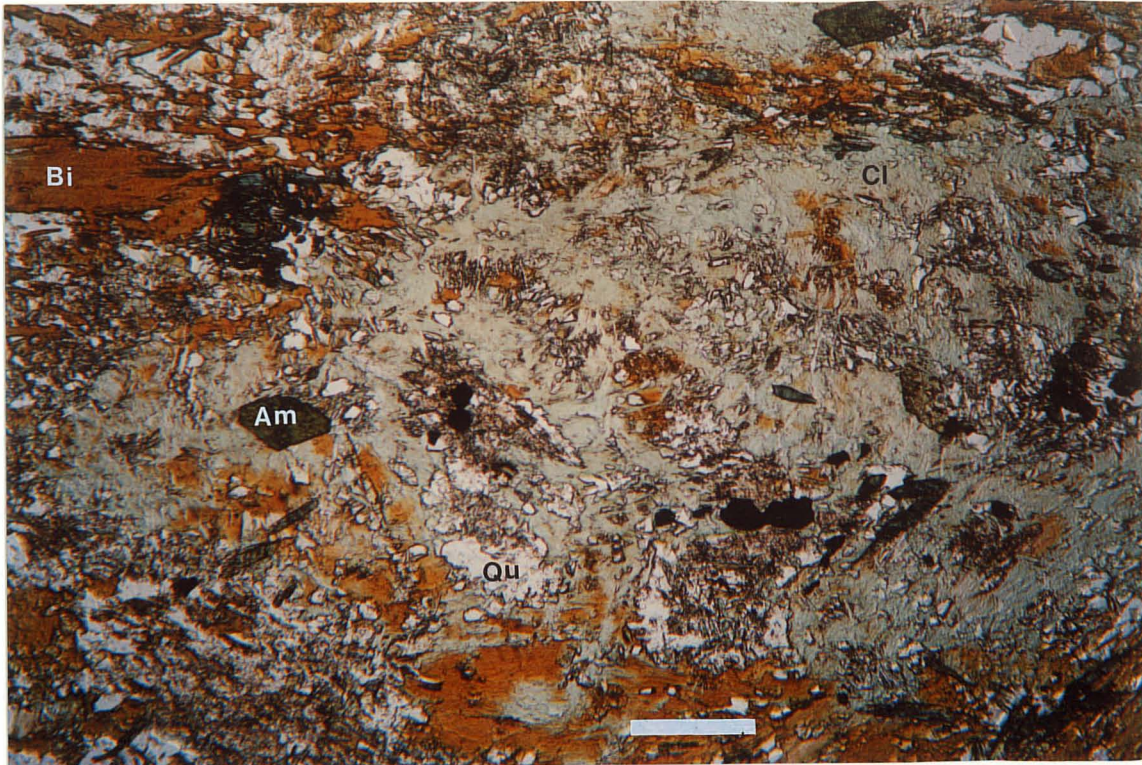


Figure 27: Sample CON 44-248; Distal alteration zone; Island fault block; chlorite-biotite-quartz-amphibole assemblage, typical of the central part of the alteration zone.

In Figures 27 to 39, sample numbers correspond to diamond drill hole number and depth in feet. Abbreviations used are as follows: St=staurolite; Qu=quartz; Cl=chlorite; Bi=biotite; Am=amphibole; Gar=garnet; and Gah=gahnite. Scale bar is 0.5 mm in length, unless otherwise specified.

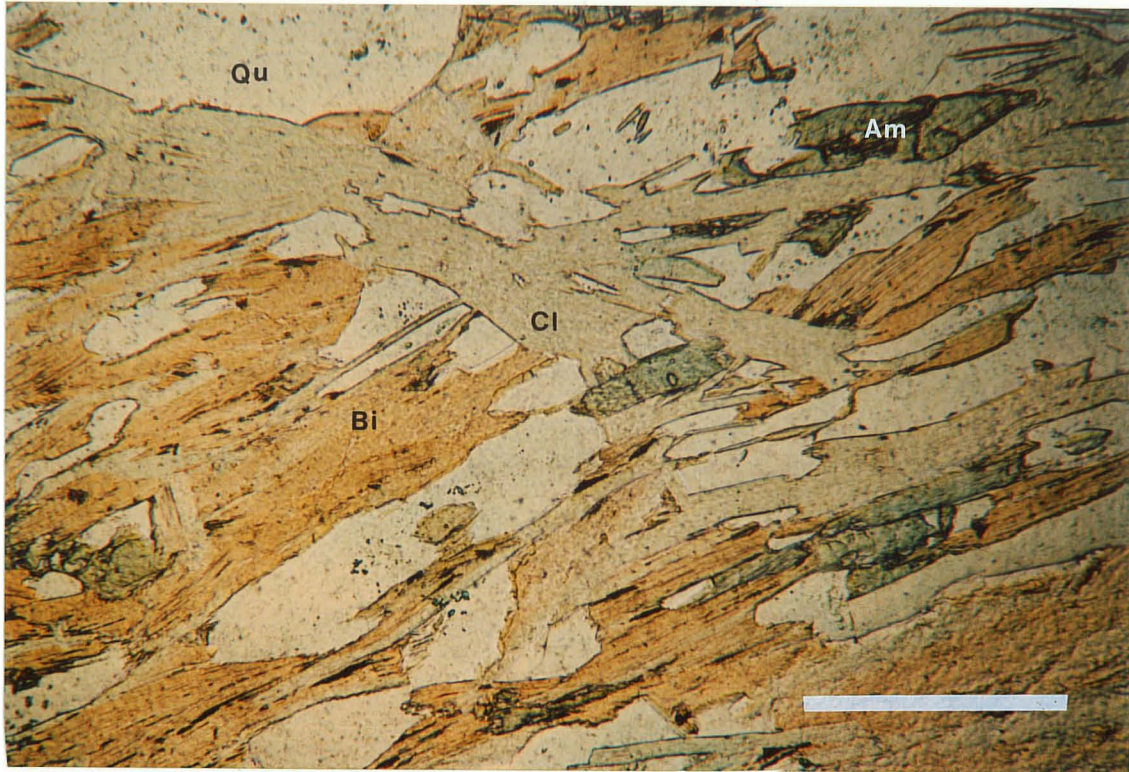


Figure 28: Sample CON 63-188.5; Distal alteration zone; Island fault block; typical example of the chlorite-biotite-quartz-amphibole assemblage most common in the central part of the alteration zone.

Refer to Figure 27 for explanation of location, abbreviations, and scale.

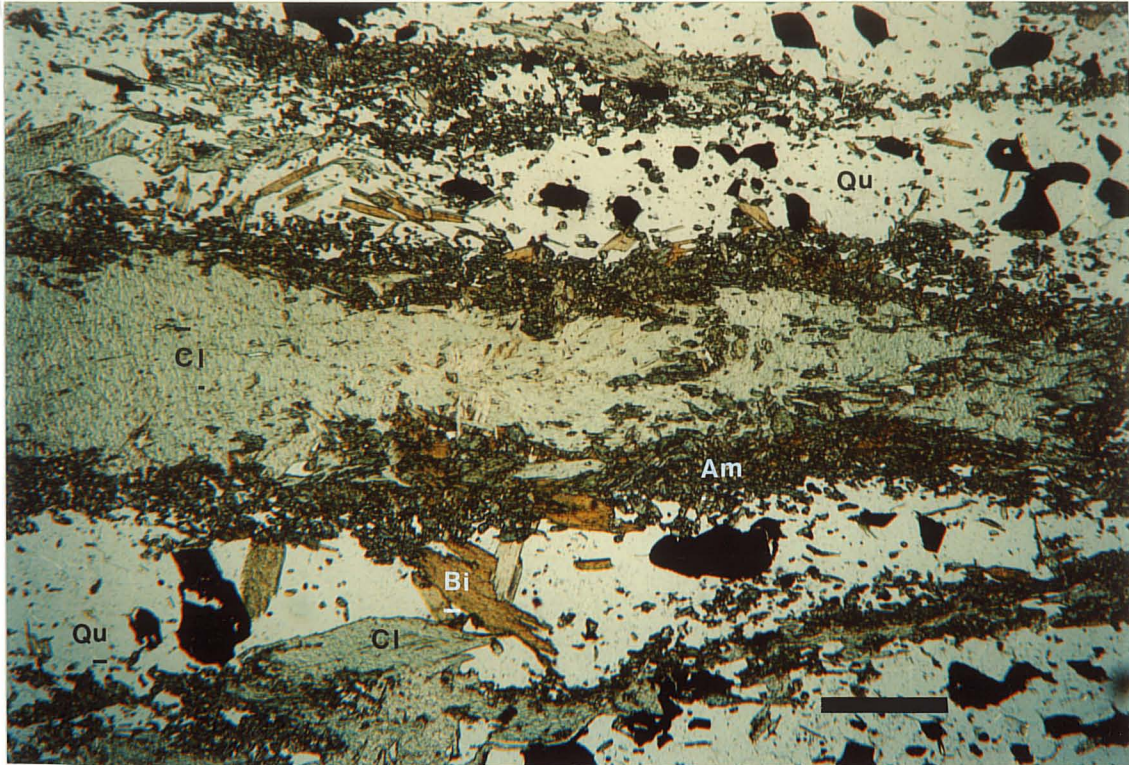


Figure 29: Sample CON 62-367.5; Distal alteration zone; Island fault block; chlorite-biotite-quartz-amphibole assemblage. Chlorite veins have amphibole selvages. Black grains are pyrite and are mostly in quartz veins that parallel the chlorite veins.

Refer to Figure 27 for explanation of location, abbreviations, and scale.

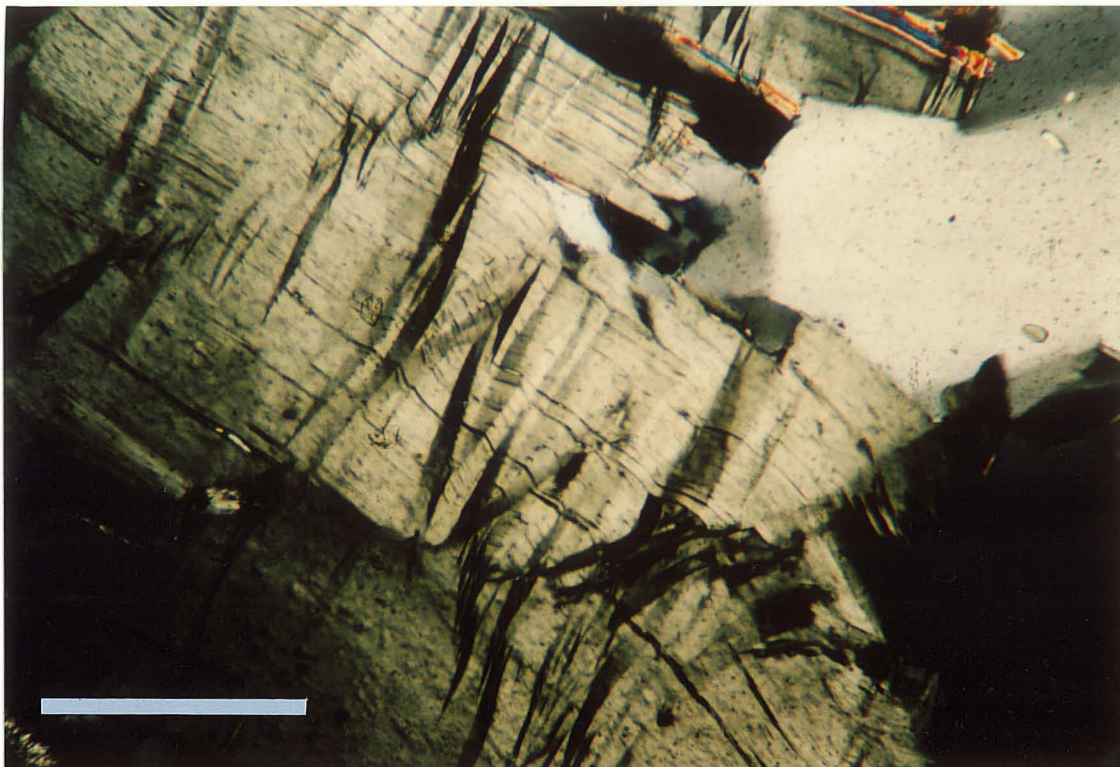


Figure 30: Sample CON 63-188.5; Distal alteration zone; Island fault block; kinked chlorite laths in a chlorite-biotite-quartz-amphibole assemblage. Such a microtexture suggests that these crystals pre-date the last tectonic event. (X polars).

Refer to Figure 27 for explanation of location, abbreviations, and scale. Scale bar = 0.1 mm.

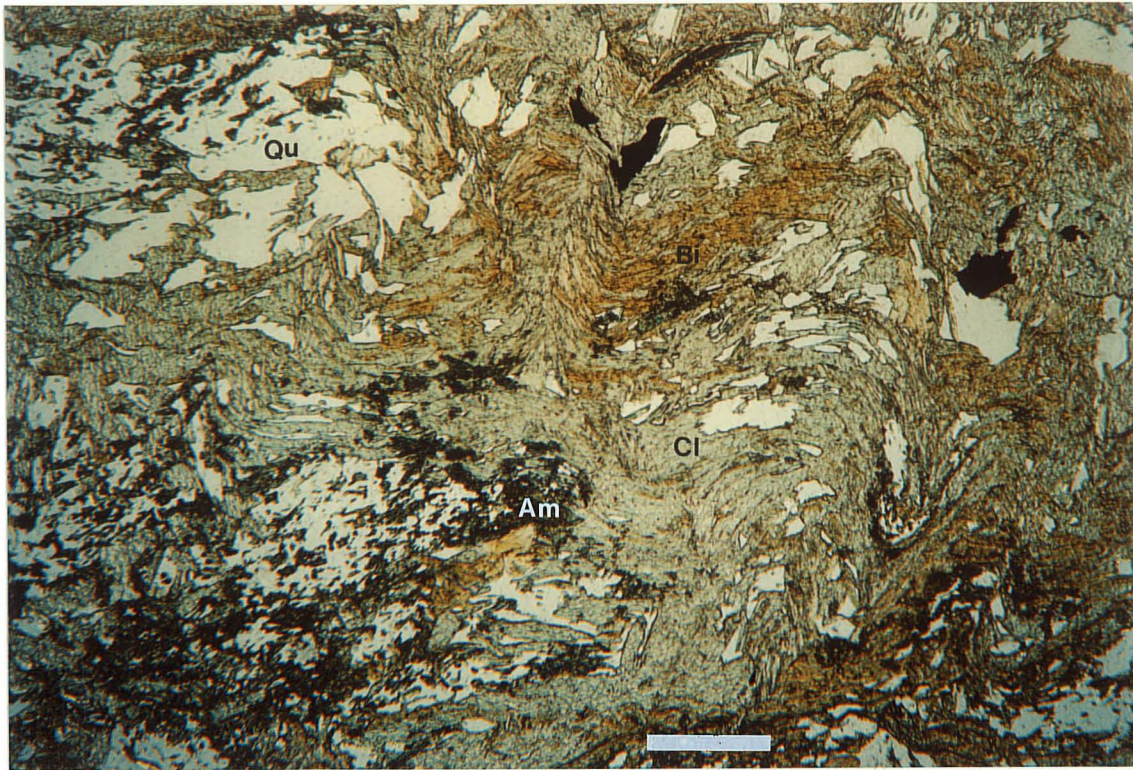


Figure 31: Sample CON 7-165; Distal alteration zone; Island fault block; chlorite-biotite-quartz-amphibole assemblage. Highly deformed (folded) alteration assemblage, with the local development of axial planar cleavage.

Refer to Figure 27 for explanation of location, abbreviations, and scale.

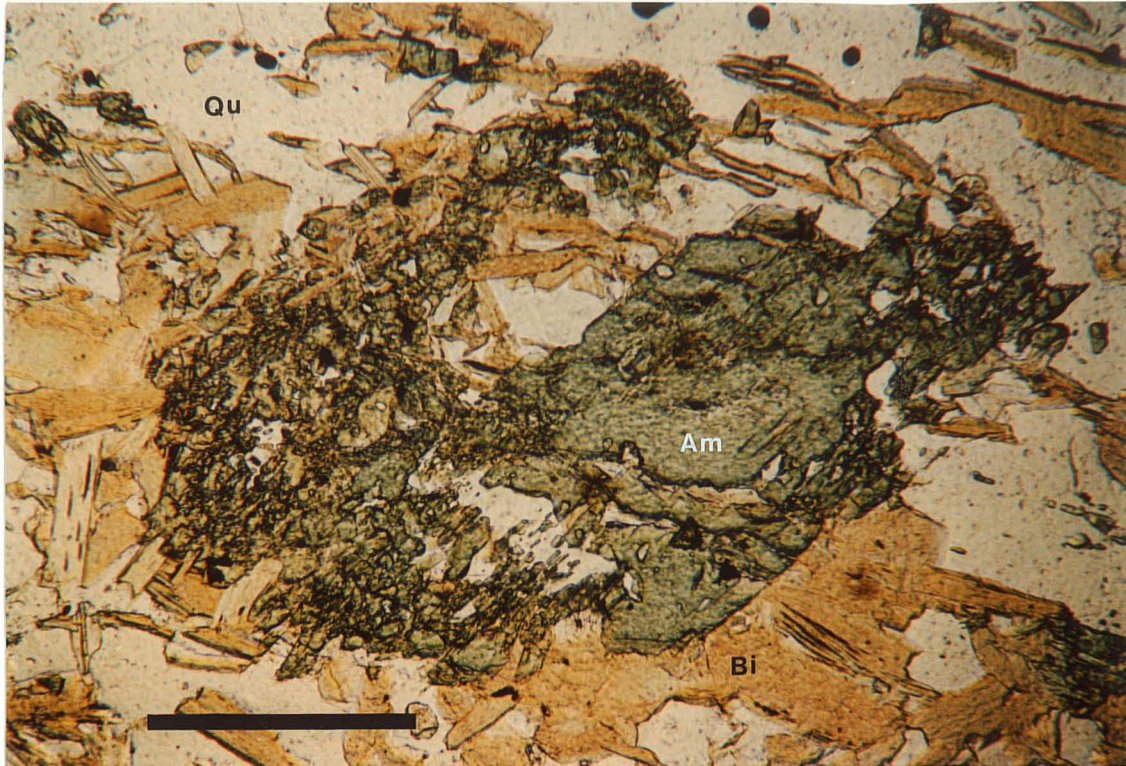


Figure 32: Sample CON 44-248; Distal alteration zone; Island fault block; chlorite-biotite-quartz-amphibole assemblage. Rarely, amphibole crystals are larger than normal and are skeletal in appearance, suggesting metablastic growth during metamorphism.

Refer to Figure 27 for explanation of location, abbreviations, and scale.

precursor components can be identified. The precursor components consist of plagioclase, quartz, and amphibole that have similar proportions, sizes, and habits as unaltered mafic flows described in Chapter 4. Partial alteration is shown by the presence of 0.45 mm chlorite shreds which are uniformly distributed throughout the specimens, 0.33-3.4 mm irregular sulfide grains and elongate blebs, and minor <0.1-0.2 mm biotite laths. Rarely, 1.2-4.5 mm wide, concordant chlorite-quartz-sulfide veins are present; vein components have the same characteristics as similar assemblages in intensely altered samples of the distal alteration zone. Both vein and disseminated forms of chlorite are characterized by the same grey and green-grey interference colors observed in the intensely altered chlorite-biotite-quartz-amphibole assemblage. With increasing alteration the amphibole acquires the long needle-like habits of the amphibole in completely altered samples; the plagioclase becomes sericitized, and biotite content increases.

6.2.1.2 Quartz-Biotite-Garnet Assemblage

A quartz-biotite-garnet assemblage occurs in the mainland distal alteration zone, and in sub-zone 1 of the distal island zone. The mainland occurrence is based on megascopic identification; petrographic data on the assemblage is limited to one sample from the island fault block. The sample is composed of 55%, 0.115-0.51 mm euhedral garnet characterized by opaque cores produced by inclusions of opaque minerals, possibly sulfide

minerals (Figure 33); 32% 0.15-0.2 mm quartz crystals, commonly in 0.42-1.26 mm thick veins; 10%, 0.125 mm biotite laths; and 3%, 0.6-1.4 mm sulfides, typically associated with quartz veins. This assemblage represents a complete alteration product; no precursor components remain.

6.2.1.3 Quartz-Biotite Assemblage

Chlorite-biotite-quartz-amphibole and quartz-biotite-garnet assemblages of sub-zone 1 grade northward into the quartz-biotite assemblage of sub-zone 2. The data are insufficient to determine the nature of the transition. Quartz-biotite assemblages are composed of 10-25%, 0.15-3.4 mm quartz forming 1.0-5.1 mm wide veins; 10-19%, 0.3-0.42 mm biotite as irregularly distributed anhedral masses or euhedral laths; 3-20% pyrite, typically associated with quartz veins; and 5%, 1.5 mm long amphibole crystals that are commonly associated with biotite and are similar to those in the more intensely altered chlorite-biotite-quartz-amphibole assemblage. Precursor components which consist of equal proportions of fine-grained interstitial plagioclase and quartz, and the local presence of 0.72-1.34 mm relict plagioclase phenocrysts. These precursor components are similar to those in unaltered intermediate flow and tuff units.

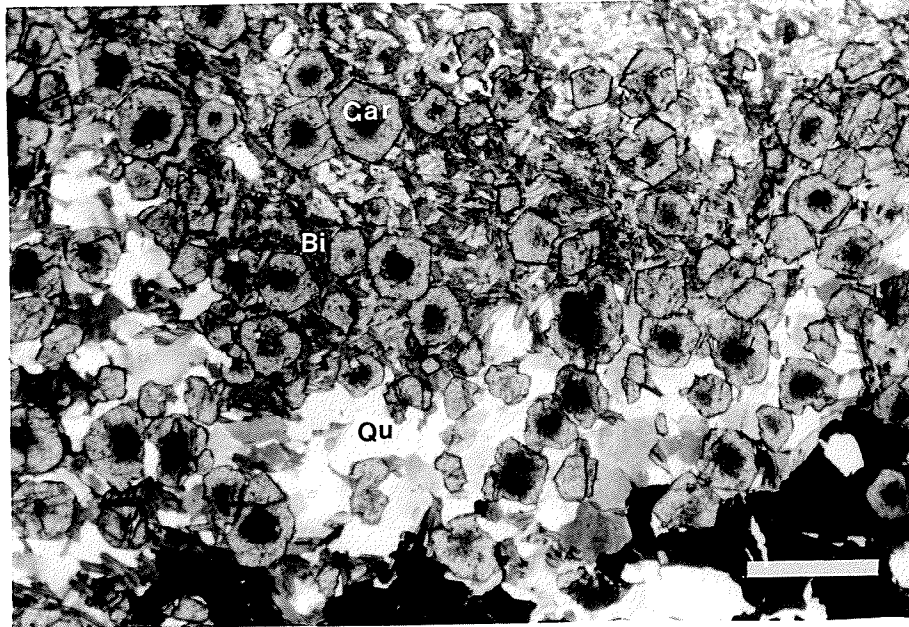


Figure 33: Sample CON 62-477; Distal alteration zone; Island fault block; quartz-biotite-garnet assemblage. This assemblage is found locally in the central part of the distal alteration zone, in a sulfide-rich area. The dark central parts of the garnet crystals may consist of sulfide inclusions.

Refer to Figure 27 for explanation of location, abbreviations, and scale.

6.2.1.4 Quartz-Muscovite+/-Biotite Assemblage

In the distal alteration zone of the island fault block, quartz-biotite assemblages grade northward into quartz-muscovite-biotite assemblages. The transition occurs within a 10 m distance but no data are available on the precise nature of the transition. The quartz-muscovite-biotite assemblages occur in a stratiform zone, approximately 6 m wide. All samples from this zone are partly altered, with the alteration assemblage comprising 35-55% of the rock. The alteration component of these samples is 8-15%, 0.115-0.45 mm quartz in 0.6-1.2 mm aggregates and 0.45-1.8 mm wide veins; 10-24%, <0.1-0.125 mm evenly disseminated muscovite laths; up to 9%, <0.1-1.35 mm sulfide grains, most commonly associated with quartz veins; 8%, <0.1-0.3 mm biotite shreds and euhedral laths; and 1-2%, <0.1-0.6 mm garnet. The precursor components are 0.1-0.15 mm grains of quartz and partly sericitized plagioclase; the quartz content varies from equal to nearly double the amount of plagioclase. These particular components may indicate an intermediate or felsic precursor. The alteration and precursor components are relatively well interspersed and evenly distributed.

In the distal alteration zone that underlies the lake ore zone, there is a somewhat similar assemblage, but no precursor components remain, and the assemblage lacks biotite, has a higher quartz and sulfide content (up to 69% and 22% respectively), and contains larger (0.2-0.45 mm) muscovite laths.

6.2.1.5 Chlorite-Quartz-Biotite Assemblage

In the distal alteration zone of the island fault block, all samples of the chlorite-quartz-biotite alteration assemblage were obtained from a single 25 m drill intersection in sub-zone 2; as a result, lateral continuity of the assemblage is uncertain and relationship of this assemblage to the other two assemblages of this sub-zone is unknown. All specimens examined from this locality represent complete replacement products that are composed of 58-67%, <0.1-1.0 mm chlorite laths forming anastomosing vein networks or near massive aggregates; 12-25%, <0.1-0.45 mm quartz; 3-18%, <0.1-2.0 mm anhedral to subhedral biotite; and 6-8%, <0.1-1.1 mm sulfide minerals. Additional constituents, which are present in some samples, include: 1%, <0.1 mm apatite in 0.6-1.7 mm masses; <4%, 0.18-0.4 mm plagioclase; <2%, 0.23-0.72 mm staurolite; <1%, 0.115-0.8 mm garnet; and <3%, <0.1 mm crystals of Fe-Ti-oxide in 0.2-0.6 mm masses. Occasionally, large euhedral biotite laths cross-cut the chlorite and the foliation defined by the chlorite. The chlorite has the green-grey interference colors typical of chlorite in the chlorite-biotite-quartz-amphibole assemblage in the central part of the alteration zone. The assemblage is similar to the chlorite-biotite-quartz-amphibole assemblage, but lacks the amphibole. Figure 34 is a typical example of this type of alteration.

In the distal zone beneath the lake ore zone this assemblage also locally contains up to 12%, 0.72-1.0 mm euhedral, non-poikilitic garnet crystals, as well as 8%, 0.15-0.6 mm subhedral to

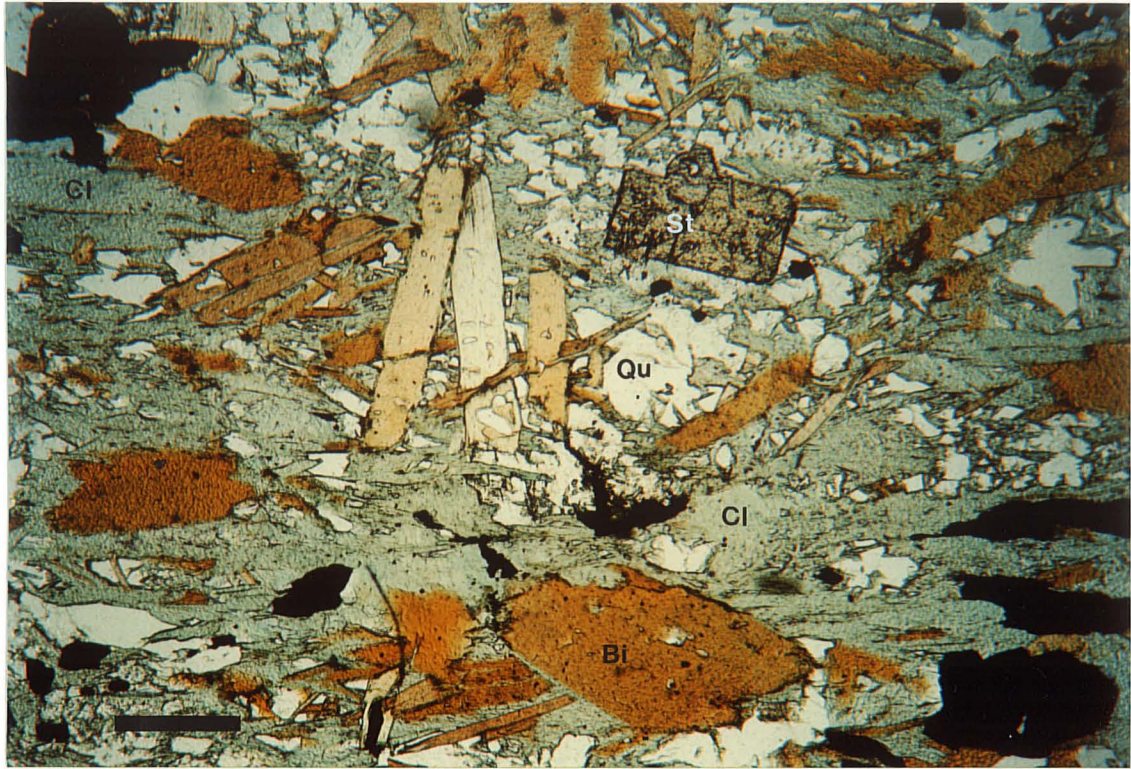


Figure 34: Sample 139-280.5; Distal alteration zone; Island fault block; chlorite-quartz-biotite assemblage found in upper part of the zone. This alteration type may also contain staurolite (as shown), sphene, and garnet.

Refer to Figure 27 for explanation of location, abbreviations, and scale.

ehedral dark green spinel crystals that may be gahnite (Figure 35). The chlorite has green-brown and rarely violet or berlin blue interference colors rather than grey-green colors. Cores of the garnet crystals contain abundant opaque inclusions, possibly a sulfide mineral, giving the crystals a zoned appearance. Garnet overgrowths on spinel suggest that the garnet is a later phase than spinel.

6.2.1.6 Sericite-Epidote-Chlorite-Biotite Assemblage

An alteration assemblage consisting of sericite-epidote-chlorite-biotite occurs locally at the extreme southeastern tip of the ore discovery island. Based on subsurface drill hole data, this area is the uppermost part of the distal alteration zone of the island fault block. All samples of this mineralogical alteration type represent partly altered rocks. Alteration components comprise 36 to 75% of the samples examined. The alteration component is composed of 10-26% fine-grained sericite replacement of plagioclase; 8-17%, <0.1-0.25 mm anhedral to subhedral epidote; 5-13%, <0.1-0.45 mm biotite as anhedral shreds to euhedral laths; 3-11%, <0.1-0.45 mm chlorite laths and irregular anhedral masses; and 8-10%, <0.1-0.23 mm pyrite. The chlorite is characterized by green-brown interference colors, and is commonly associated with the biotite. Many of the larger, more euhedral phyllosilicate laths are crystals of biotite with lesser amounts of chlorite intergrown into the lattice structure of the individual biotite crystals. The result is a crystal composed of alternating biotite and chlorite



Figure 35: Sample CON 26-137; Distal alteration zone; Mainland fault block; chlorite-quartz-biotite assemblage. Subhedral gahnite crystals and zoned garnet crystals are part of the alteration assemblage in this particular area.

Refer to Figure 27 for explanation of location, abbreviations, and scale.

layers that can be observed in crystal sections normal to (010); the overall appearance of these grains is broadly similar to albite twins in plagioclase feldspars.

The precursor component consists of highly variable amounts of <0.1-0.23 mm quartz and <0.1-0.45 mm partly replaced plagioclase crystals; trace <0.1 mm apatite; and up to 15%, <0.1-2.0 mm amphibole crystals. The crystal habit of the amphibole is similar to that of unaltered mafic and intermediate units, and as such, is interpreted to be a precursor component. The variability of the quartz content may indicate that some of the quartz is also an alteration product; however, there are no obvious features such as quartz veins that would differentiate between precursor and secondary quartz. The high content of precursor amphibole would suggest a mafic or possibly an intermediate precursor lithology.

6.2.1.7 Chlorite-Quartz-Sericite-Amphibole Assemblage

Chlorite-quartz-sericite-amphibole is a minor part of the distal alteration zones. In the island fault block, this assemblage is restricted to the uppermost and lowermost part of the alteration zone; it also occurs in the distal alteration zone of the mainland fault block. All samples examined appear to represent partial alteration. The alteration components that are present are 31-33%, <0.1-1.3 mm quartz grains commonly in 1.7-3.2 mm wide veins parallel to schistosity; 25%, 0.34-1.44 mm laths of chlorite characterized by greenish-grey to greenish-brown interference colors; 8-10%, <0.1-1.5 mm pyrite grains that are commonly in

quartz veins; trace-7%, <0.1 mm sericite; trace-7%, <0.1-0.45 mm anhedral biotite shreds; and 3%, 0.23-1.35 mm pale green, non-pleochroic, skeletal amphibole crystals. The precursor component consists of 24-25%, <0.1-0.7 mm anhedral plagioclase. Some of the quartz may be a precursor component, but this is not texturally distinguishable. There is nothing definitive in the precursor components to suggest parental lithology.

6.3 PROXIMAL ALTERATION ZONES

Proximal alteration in the island fault block forms a 0.5-2.0 m thick, laterally extensive, stratigraphically controlled zone at the contact between mafic formation 3 and felsic formation 4, and generally immediately beneath the lower mineralization zone. This alteration is dominantly a tremolite-quartz-biotite-chlorite assemblage. Minor alteration overlies both the upper mineralization zone, as well as the main ore lens at depth where the upper mineralization is absent. The hangingwall alteration is generally characterized by the presence of amphibole-biotite-sulfide clusters in felsic volcanic rocks, or a quartz-muscovite assemblage.

In the mainland fault block, proximal alteration is also a relatively thin zone adjacent to mineralization, but differs from the island proximal alteration zone in 2 aspects: 1) it is well developed in both hangingwall and footwall to the lake ore zone,

and 2) it has a limited lateral extent, generally terminating within meters of the ore zone extremities. Quartz-muscovite and quartz-chlorite assemblages are the dominant alteration assemblages in the proximal mainland alteration zone; amphibole-biotite-sulfide clusters are locally present, and tremolite-quartz-biotite-chlorite assemblages are restricted to the southwestern margin of the ore body, both above and below the mineralization.

6.3.1 Characteristics of Proximal Alteration

6.3.1.1 Tremolite-Quartz-Biotite-Chlorite Assemblage

The most intensely altered samples are characterized by: 36-96% (averaging 70%), 0.1-0.45 mm (average 0.25 mm) subhedral to euhedral amphibole laths forming near massive granular aggregates; 1-36% (average 12%), 0.11-0.45 mm anhedral, interstitial quartz grains; trace-20% (average 7%), 0.12-0.5 mm euhedral biotite laths that locally form 0.25-0.45 mm thick veins concordant with foliation; trace-16% (average 3%), 0.34-2.6 mm chlorite laths in clumps up to 0.72 mm in size, and locally forming anastomosing veins up to 0.8 mm thick; and trace-12% (average 5%), <0.1-1.8 mm sulfide disseminations that are generally interstitial to amphibole or biotite. The amphibole is pale green and non-pleochroic. Based on optical properties the amphibole is most likely tremolite. Figure 36 is a typical example of this alteration type. Based on electron microprobe data presented in Chapter 7, biotite and

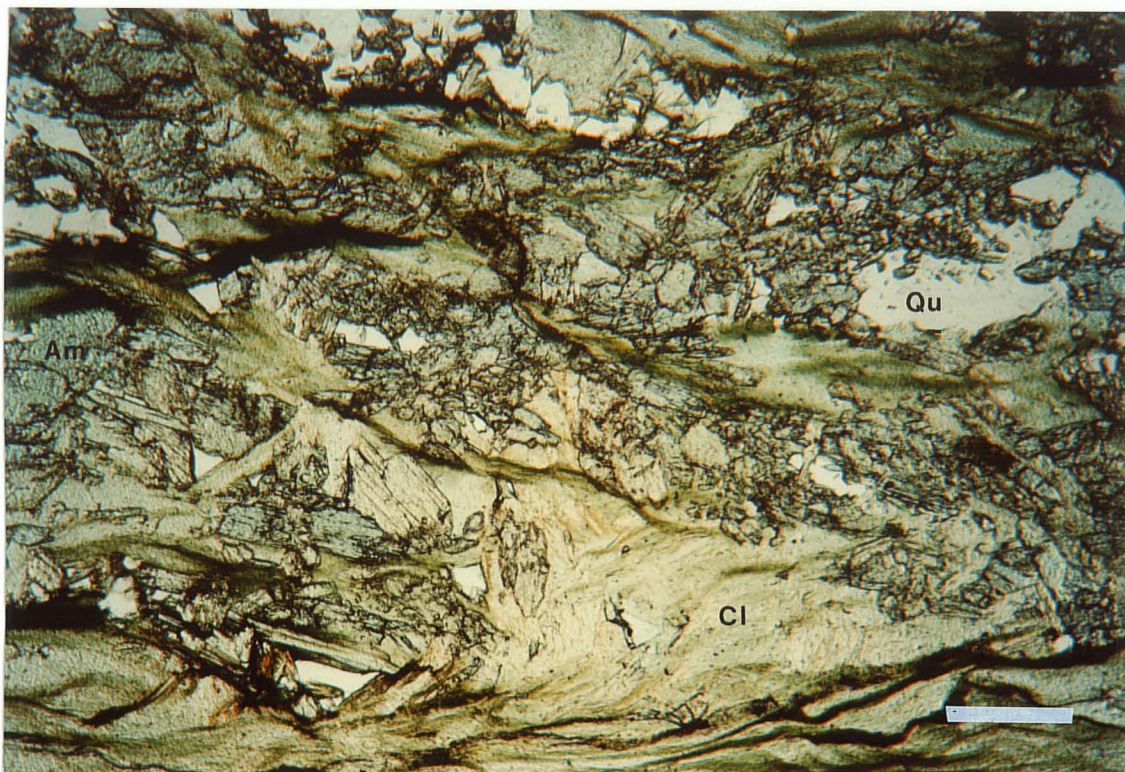


Figure 36: Sample CON 21-201; Proximal alteration; Mainland fault Block; tremolite-quartz-biotite-chlorite assemblage; stratigraphic hangingwall to the ore zone. Chlorite veins define a crude foliation.

Refer to Figure 27 for explanation of location, abbreviations, and scale.

chlorite are locally combined on a molecular scale producing crystals that petrographically resemble green biotite (Figure 37). These green intergrowths are 0.2-0.3 mm euhedral laths that form either 0.46-0.9 mm thick layers or veins, or <0.1-0.9 mm masses interstitial to amphibole. Biotite-chlorite intergrowths are more abundant in samples with higher sulfide mineral contents.

Mafic rocks underlying the intensely altered tremolite-quartz-biotite-chlorite assemblage described above, are locally partly altered for as much as 85 m below the defined proximal alteration zone. Partial alteration is defined by the presence of up to 35%, 0.7-3.5 mm round patches of pale amphibole optically identical to that in the completely altered assemblage described above. These patches occur within a rock that is otherwise similar petrographically to unaltered mafic flow units of formation 3I.

6.3.1.2 Quartz-Muscovite Assemblage

A less widespread form of proximal alteration is characterized by a quartz-muscovite assemblage. This alteration assemblage occurs beneath the lake ore zone, and is also found overlying the main ore lens of the island zone. This assemblage is typically characterized by: 28-33%, <0.1 mm muscovite shreds that are intergrown to form a massive anastomosing network of veins; 20-33%, <0.1-1.12 mm sulfide minerals; and 11-33%, 0.23-1.35 mm quartz in 1.15-1.7 mm wide veins. Although most samples are completely altered with no remaining precursor components, rarely there is highly sericitized precursor plagioclase. This assemblage differs from the quartz-

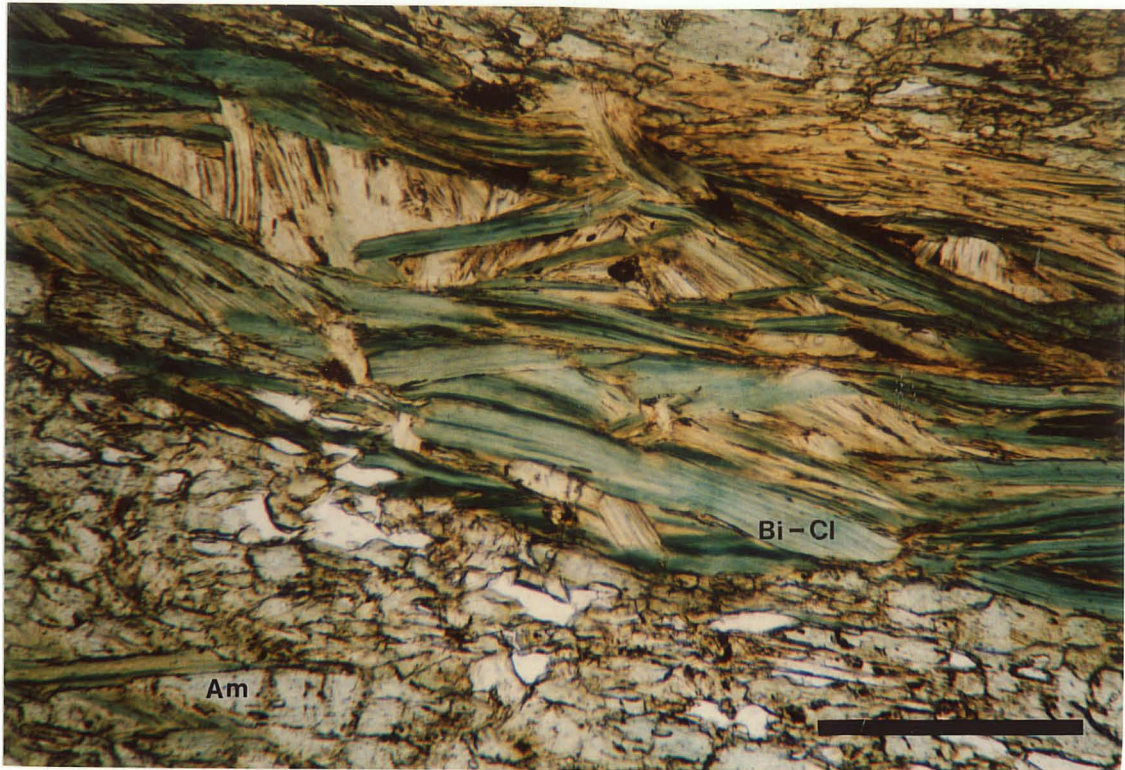


Figure 37: Sample CON 24-167.5; Proximal alteration; Mainland fault block; tremolite-quartz-biotite-chlorite assemblage; stratigraphic hangingwall to ore zone. Biotite-chlorite intergrowths (that resemble green biotite in thin section) form parallel to regional foliation. Remainder of rock is pale green, non-pleochroic amphibole, and minor quartz.

Refer to Figure 27 for explanation of location, abbreviations, and scale.

muscovite assemblage of the distal alteration zones in having higher sulfide and lower quartz contents. In the island fault block the muscovite is finer grained than in the mainland fault block and biotite may be present.

6.3.1.3 Amphibole-Biotite-Sulfide Assemblage

In felsic units above both the island and lake ore zones there is locally developed alteration in the form of 10-15%, <0.1-0.45 mm randomly disseminated, pale green, non-pleochroic amphibole; 5-10%, 0.56-3.0 mm round to irregular amphibole-biotite-sulfide clusters; and trace to 6%, 0.4-0.72 mm dark green amphibole needles similar to those in the distal alteration zone. The disseminated pale green amphibole is similar to that in the tremolite-quartz-biotite-chlorite assemblage described earlier. In the mainland fault block, the amphibole-biotite-sulfide clusters change characteristics as a function of proximity to the Lake Ore Zone. With increasing distance from the ore zone, the amphibole changes from a pale green nonpleochroic variety to a dark green pleochroic variety; there is a corresponding increase in sulfide mineral abundance. The alteration assemblages comprise 20-25% of the samples containing this type of alteration. The unaltered component of the rock is composed of 21-55%, <0.1-1.2 mm plagioclase; 18-41%, <0.1-0.31 mm quartz; trace-9% (locally up to 25%), <0.1-0.72 mm biotite; 1-12%, <0.1-1.36 mm sulfide minerals; 2%, <0.1 mm epidote, and 1%, <0.1-0.23 mm chlorite. Based on the precursor components, this form of alteration appears to be superimposed on a felsic lithology. Figure

38 is an example of this alteration assemblage.

6.3.1.4 Quartz-Chlorite Assemblage

Quartz-chlorite assemblages appear to be restricted to the proximal alteration of the mainland fault block, where they both underlie and overlie the ore zone. This apparent spatial distribution is based mainly on megascopic identification; petrographic data is available from one sample above the ore zone. This sample is composed of 46%, 0.2-1.35 mm chlorite laths; 46%, 0.1-0.4 mm quartz; and 8%, 0.12-0.4 mm sulfide grains as inclusions within chlorite laths. No precursor components remain.

6.4 PERIPHERAL ALTERATION

Minor alteration was observed locally in both mafic and felsic units outside of the distal and proximal alteration zones delineated in Figure 26. This alteration is in the form of minor chloritization, silicification, amphibole-biotite clusters, epidotization, and chlorite-epidote+/-calcite-quartz veins and associated minor sericitization. Figure 26 shows all locations where this type of alteration was observed in outcrop or drill core.

6.4.1 Chloritization

Peripheral chlorite alteration is manifest by the presence of

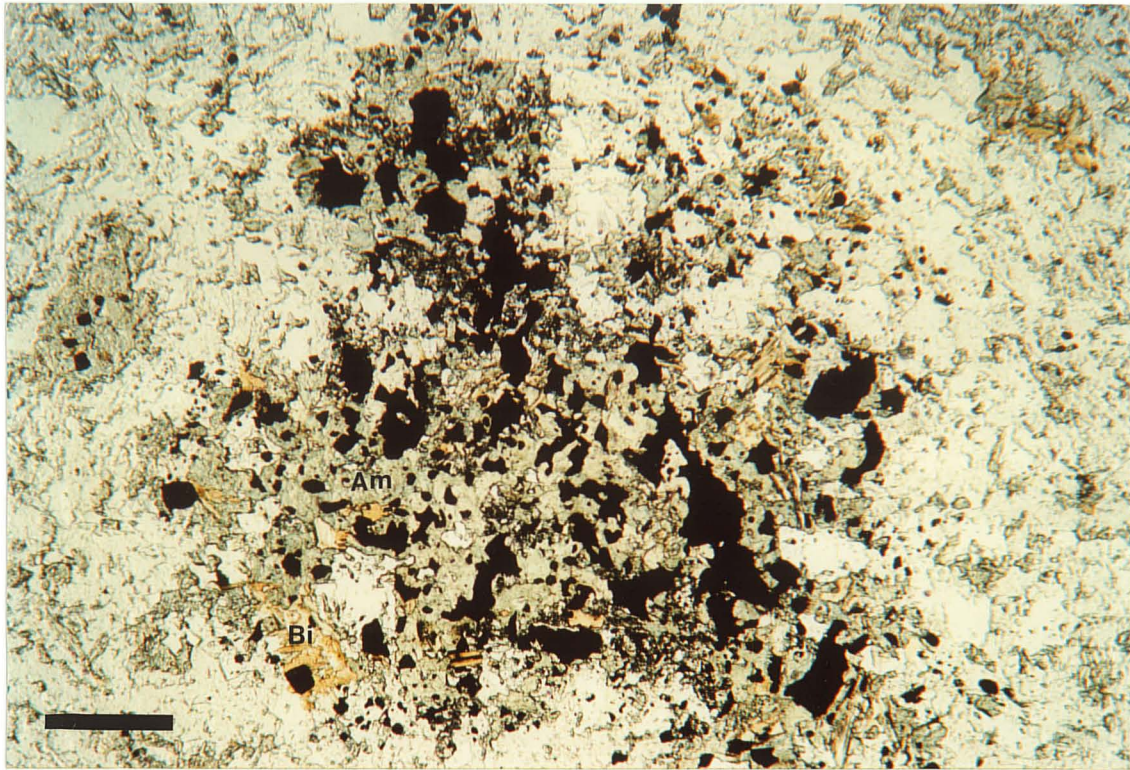


Figure 38: Sample CON 39-753; Proximal alteration of felsic volcanic rocks; amphibole-biotite-sulfide clusters; stratigraphic hangingwall to the Island Ore Zone. Alteration is defined by irregular clusters of pale, non-pleochroic amphibole, sulfide minerals and biotite.

Refer to Figure 27 for explanation of location, abbreviations, and scale.

2-7%, <0.1-0.45 mm (and rarely up to 0.6 mm) chlorite laths that occur as either isolated crystals or as irregular 0.115-0.5 mm (less commonly up to 3.4 mm in size) aggregates or patches paralleling regional foliation. This chlorite typically has brown to green-brown interference colors indicative of a more Fe-rich variety than the Mg-rich type that characterizes most distal and proximal alteration assemblages. Abundances and textures of the remaining mineral components are comparable to those of unaltered equivalents.

6.4.2 Silicification

Silicification within peripheral areas is characterized by 8-13%, 0.115-1.35 mm quartz forming 0.23-3.3 mm irregular patches, or 0.115-1.8 mm wide veins. The veins are generally concordant with foliation. Other textures and mineral assemblages are identical to those in unaltered precursors. The mafic volcanic rocks described in sections 4.1.1 to 4.1.3 contain an abnormally high quartz content for rocks of this type, and this is possibly indicative of pervasive silification. Therefore the alteration presently described must represent a more focused form of silification.

6.4.3 Amphibole-Biotite Clusters

Amphibole-biotite clusters mainly occur in areas peripheral to distal alteration, and less commonly, within proximal and distal alteration zones. These clusters are 1.35-10 mm in size, and rounded to elongated subparallel to foliation; they form up to 37%

of individual samples (Figure 39). The clusters are composed of 46-55%, <0.1-0.3 mm biotite, and 40-54%, 0.11-0.8 mm euhedral dark green amphibole that is evenly distributed within the biotite. Trace-4%, <2.0 mm garnets are also present. The garnets commonly contain opaque inclusions that are concentrated in the core, a feature similar to that noted in the underlying, more intensely altered quartz-biotite-garnet assemblage of the island distal alteration zone. Locally, the garnets are partly replaced by chlorite. These clusters are similar to those found within proximal alteration zones, but lack sulfide blebs and the amphibole is not the tremolitic variety characteristic of proximal alteration. Rocks containing amphibole-biotite clusters may also contain one or more of the other types of peripheral alteration such as: a sericitized groundmass or matrix; abnormal abundances of epidote; and chlorite veins.

6.4.4 Epidotization

Epidotization is the most widely distributed form of peripheral alteration in the Vamp Lake area. Epidotization occurs in four forms: (1) epidote-quartz-sulfide lenses concordant with regional foliation; (2) irregular aggregates of epidote +/- sulfide minerals that increase in abundance with increasing proximity to the ore bodies; (3) large, isolated, generally rounded, epidote patches that are an order of magnitude larger than type 2 aggregates; and (4) local epidotization of pillow selvages in flows underlying the island ore zone.

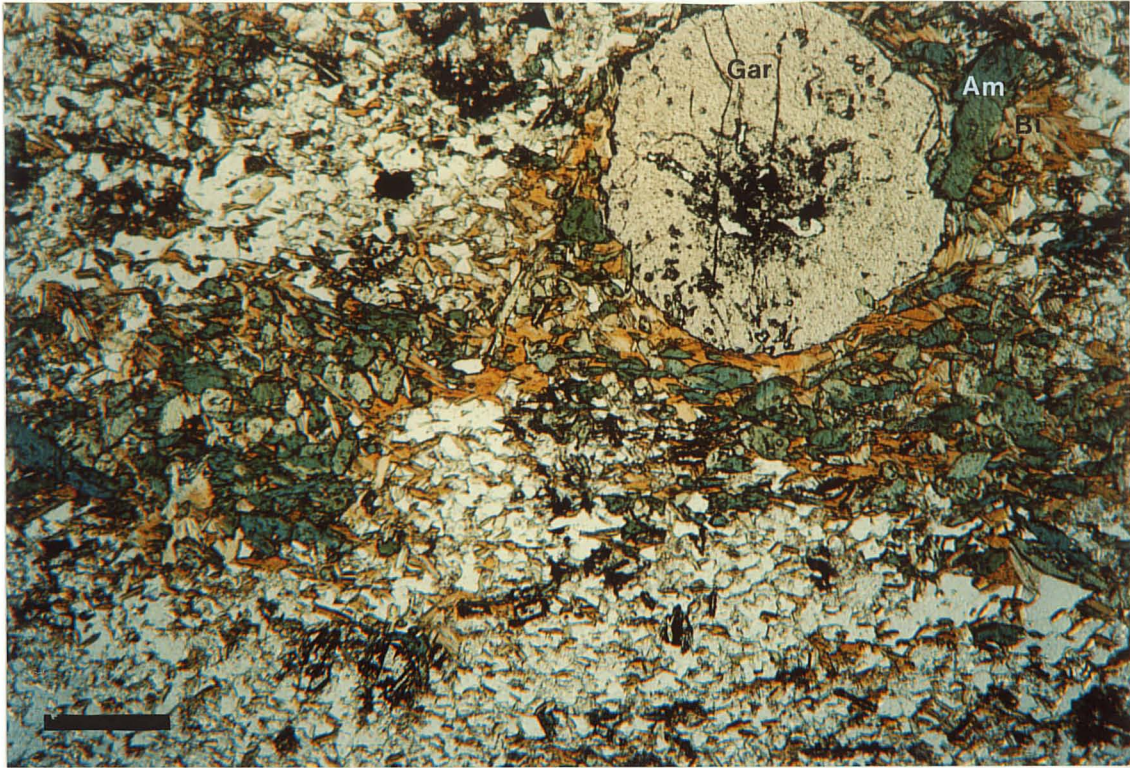


Figure 39: Sample CON 62-522; Island fault block; amphibole-biotite clusters. This alteration type is typically found in areas peripheral to the distal alteration zone of the Island fault block. This form of alteration emphasizes the affinity between biotite and amphibole noted in the chlorite-biotite-quartz-amphibole assemblage of the central part of the distal alteration zone of the island fault block. Opaque inclusions are concentrated in the core of garnet crystals, as noted in other localities.

Refer to Figure 27 for explanation of location, abbreviations, and scale.

Type 1 lenses occur in both mafic and felsic rocks; they typically pinch and swell, ranging in thickness from 0.45 to 5.1 mm. These lenses are composed of 50%, <0.1-0.8 mm epidote; 10-50%, <0.1-0.9 mm quartz; tr-20%, <0.1-0.3 mm sulfide minerals; and tr-20%, <0.1 mm plagioclase. Type 2 aggregates are 0.3-2.26 mm in size and are composed of <0.1-0.23 mm epidote, with 0 to 25%, <0.1-0.78 mm sulfide grains. The irregularly shaped epidote aggregates are evenly distributed, forming 7-12% of most samples; aggregate abundance increases to 20-35% in felsic units adjacent to proximal alteration zones. Type 3 patches are less widespread than type 2 aggregates. These patches are 7-15 mm in size, and are composed of 37-98%, <0.1-0.6 mm epidote; tr-52%, <0.1-0.8 mm quartz; and tr-10%, <0.1-0.36 mm sulfide minerals; in some samples with type 3 patches, sulfide grains are found only in the epidote patches, and not elsewhere in the host rock. Plagioclase, amphibole and calcite also occur in some epidote patches, but abundance of each of these minerals is less than 6%. Type 4 epidotization was megascopically identified in outcrop (Figure 15), and no data are available on the petrographic characteristics.

6.4.5 Chlorite-Epidote +/- Calcite-Quartz Veins

Another form of peripheral alteration is the local presence of chlorite-epidote+/-calcite-quartz veins. These veins are 0.1-0.5 mm thick, and are 70-90 degrees discordant to foliation. Where multiple veins are present, they are spaced 0.9-2.55 mm apart. Adjacent to some veins, the plagioclase in the host rock is

sericitized in a 0.45-0.67 mm thick boundary zone. Adjacent to other veins, particularly thicker veins, the host rock is epidotized and chloritized in a 1.35-3.4 mm wide boundary zone. Within this second type of boundary zone, 0.2-0.45 mm aggregates of <0.1 mm epidote grains are evenly distributed, and comprise 7-15% of these zones. The chlorite is also uniformly distributed, with <0.1 mm irregular shreds comprising 20-55% of the altered boundary zones. The chlorite is characterized by brown to purple-brown and occasionally blue interference colors. Cross-cutting relationships indicate that the veins are younger than the large epidote patches described in section 6.4.4.

6.5 LATE STAGE ALTERATION

A second type of alteration has been identified in formation 4I on the ore discovery island. Within this localized area the alteration is pervasively developed. Due to cross-cutting relations, it is not considered to be part of the alteration described in the previous sections. The alteration is characterized by <0.1-2.00 mm thick veins that are greenish-white on fresh surfaces, weather pinkish-white, and are composed of a combination of epidote, prehnite, and calcite (Figures 20, 22). Based on cross-cutting relationships, there were at least 2 periods of late vein development. The earlier period is an infilling of a conjugate set of fractures that are 0.05-10.00 cm apart. These veins are composed

of fine-grained (<0.1 mm) epidote and/or prehnite. These fracture filling veins are cross-cut by more infrequent, <0.1-0.15 mm thick epidote or prehnite +/- calcite veins.

Chapter 7

GEOCHEMISTRY

7.1 COMPOSITIONS OF MAJOR ROCK TYPES

The chemical composition of both primary rock types and altered equivalents has been determined for selected units in the Vamp Lake area. Compositions of the various mafic units described in chapter 4 are given in Table 5. The mafic flows have been subdivided into 3 geochemically distinct groups defined primarily by differences in TiO_2 content (Figure 40). Slight variations in the abundances of various other elements (MgO , P_2O_5 , Fe_2O_3 , Cr , Ni) correspond with variations in TiO_2 contents (Table 5). Chemical analyses of representative felsic and intermediate rock types are listed in Table 6. Chemical analyses for representative samples of the various alteration assemblages described in Chapter 6 are given in Table 7. The fault block and formation in which each sample occurs is also indicated in the Tables. Compositional comparison of primary and altered samples provides an evaluation of the chemical changes that occurred during alteration, thereby providing a means of identifying alteration in samples less intensely altered. All geochemical sample sites are plotted on plan sections (Figures 5A-D); core samples were projected along dip onto the plan section that corresponds closest in depth to the sample site. The mineralogical components of each analyzed sample are listed in Appendix A.

Table 5: Geochemistry of Mafic Volcanic Rocks

Mafic Flows																				
Low TiO2										Moderate TiO2										
										Hornblende Porphyroblastic Units										
Sample #	GR 14	59	67	Con 24	GR 36	GR 49	Con 9	Con 63	52	Con 45A	Con 45A	Con 63	Con 57	Con 51	Con 57	67	Con 44	Con 44	Con 57	GR 33
Formation	L-3	L-3	L-3	L-3	I-3	I-3	I-3	I-3	I-4	I-3	I-3	I-3	I-3	L-3	I-3	L-3	I-3	I-3	I-3	L-5
Wt. %																				
SiO2	55.20	53.03	52.30	59.90	60.75	56.40	56.90	56.40	59.20	53.30	52.40	52.40	54.10	53.50	50.38	54.90	56.90	56.60	55.80	55.30
TiO2	0.39	0.47	0.36	0.38	0.33	0.31	0.26	0.29	0.33	0.33	0.29	0.32	0.35	0.19	0.32	0.52	0.59	0.55	0.56	0.64
Al2O3	13.90	15.93	15.80	13.10	12.10	13.40	12.50	11.00	11.60	10.90	10.80	12.00	12.50	8.53	12.20	13.50	15.00	14.70	14.80	15.40
Fe2O3	11.90	9.76	11.70	10.30	11.00	11.60	11.10	11.90	11.10	12.70	13.60	12.70	12.00	12.20	12.60	13.00	13.05	12.80	12.60	11.60
MnO	0.22	0.18	0.22	0.18	0.18	0.19	0.18	0.16	0.20	0.27	0.24	0.27	0.21	0.23	0.26	0.23	0.20	0.19	0.18	0.18
MgO	4.95	6.65	6.42	4.26	4.52	5.08	6.77	8.27	5.65	10.30	10.10	10.20	6.99	11.30	10.70	4.73	4.10	3.62	3.66	4.69
CaO	9.99	11.07	8.84	6.15	8.51	9.69	7.81	9.24	7.94	11.00	11.50	11.80	10.80	11.10	11.80	7.96	7.86	8.54	8.38	8.57
Na2O	1.25	1.97	2.26	2.75	1.48	1.32	1.65	0.81	1.65	1.17	0.93	1.15	0.76	0.95	1.13	2.76	1.59	1.76	2.00	2.08
K2O	0.48	0.54	0.91	0.56	0.35	0.37	0.69	0.27	0.72	0.29	0.27	0.33	0.32	0.24	0.51	0.71	0.55	0.64	0.82	0.53
P2O5	0.06	0.21	0.07	0.07	0.04	0.05	0.06	0.05	0.14	0.32	0.27	0.31	0.05	0.04	0.37	0.12	0.11	0.13	0.14	0.11
LOI	0.85	0.67	1.08	1.62	0.76	0.77	1.54	1.16	1.62	0.80	0.70	0.50	1.08	0.93	0.60	1.00	0.57	0.70	1.23	0.47
S	0.03	0.02	0.10	0.73	0.28	0.06	0.61		1.46	<0.01	0.05	0.09	0.51	<0.01	0.16	0.11	0.10	<0.01	0.33	<0.01
CO2	0.10	0.02	0.01	0.03	<0.01	<0.01	0.03		0.60	0.09	0.12	0.03	0.02	0.04	0.07	0.02	0.02	0.02	0.01	0.01
PPM																				
Ba	160	90	240	220	170	140	180	80	170				120	70		210	370	270	420	180
Cr	70	40	40	90	50	30	280	160	340				290	710		50		<10	10	20
Ni	10	14	16	27	18	10	21	29	90				42	8		12	9	7	11	10
PPB																				
Au	6	3	<2	110	3	<2	12	14	50				3	<2		<2	5	5	5	<2
PPM																				
Y	16.73				14.84	14.67			15.59				13.85							22.45
Zr	17.71				15.75	17.01			20.31				16.12							37.02
Nb	6.03				3.60	2.61			3.02				5.16							4.93
Rb	9.43				6.50	4.95			13.06				6.42							18.53
Sr	117.31				120.34	103.19			88.46				124.27							229.61

Table 5 continued									
	High TiO2 Mafic Flows					Mafic Tuff			Diorite
Sample #	59 47	Con 51 171	GR 3	GR 7	GR 26	GR 13	Con 51 682	140 176	GR 40
Formation	L-3	L-3	L-3	L-3	L-3	L-3	L-3	L-3	I-4
Wt. %									
SiO2	58.90	59.70	56.80	54.70	54.70	59.00	57.80	55.60	55.93
TiO2	0.95	0.89	1.05	1.14	0.89	0.82	0.28	0.55	0.72
Al2O3	13.90	14.00	13.80	14.00	14.50	13.80	12.80	14.90	15.77
Fe2O3	12.20	11.90	13.30	14.20	13.10	11.50	11.90	11.90	10.83
MnO	0.24	0.18	0.22	0.24	0.23	0.29	0.20	0.21	0.19
MgO	3.38	2.84	3.62	3.49	4.30	3.16	4.99	4.49	4.53
CaO	5.32	6.86	8.37	8.99	9.28	7.41	9.00	8.02	8.94
Na2O	3.01	2.58	2.43	2.25	1.73	2.48	1.27	1.50	2.14
K2O	0.80	0.67	0.58	0.56	0.36	0.87	0.36	1.01	0.53
P2O5	0.34	0.17	0.28	0.46	0.12	0.15	0.05	0.12	0.26
LOI	1.45	0.01	0.60	0.40	0.62	0.70	0.54	1.16	0.43
S	0.41	0.04	<0.01	<0.01	<0.01	<0.01	<0.01	1.02	0.25
CO2	0.08	0.01	0.18	0.12	0.07	0.01	0.07	0.01	0.04
PPM									
Ba		240			120	160	150	930	190
Cr		10			10	10	50	10	20
Ni		4			8	8	6	11	14
PPB									
Au		4			9	3	<2	49	<2
PPM									
Y		32.92			26.61	30.64	13.22		
Zr		55.31			39.16	51.20	13.64		
Nb		7.75			7.87	4.83	3.16		
Rb		16.89			5.68	15.86	5.71		
Sr		152.59			145.88	157.75	117.75		

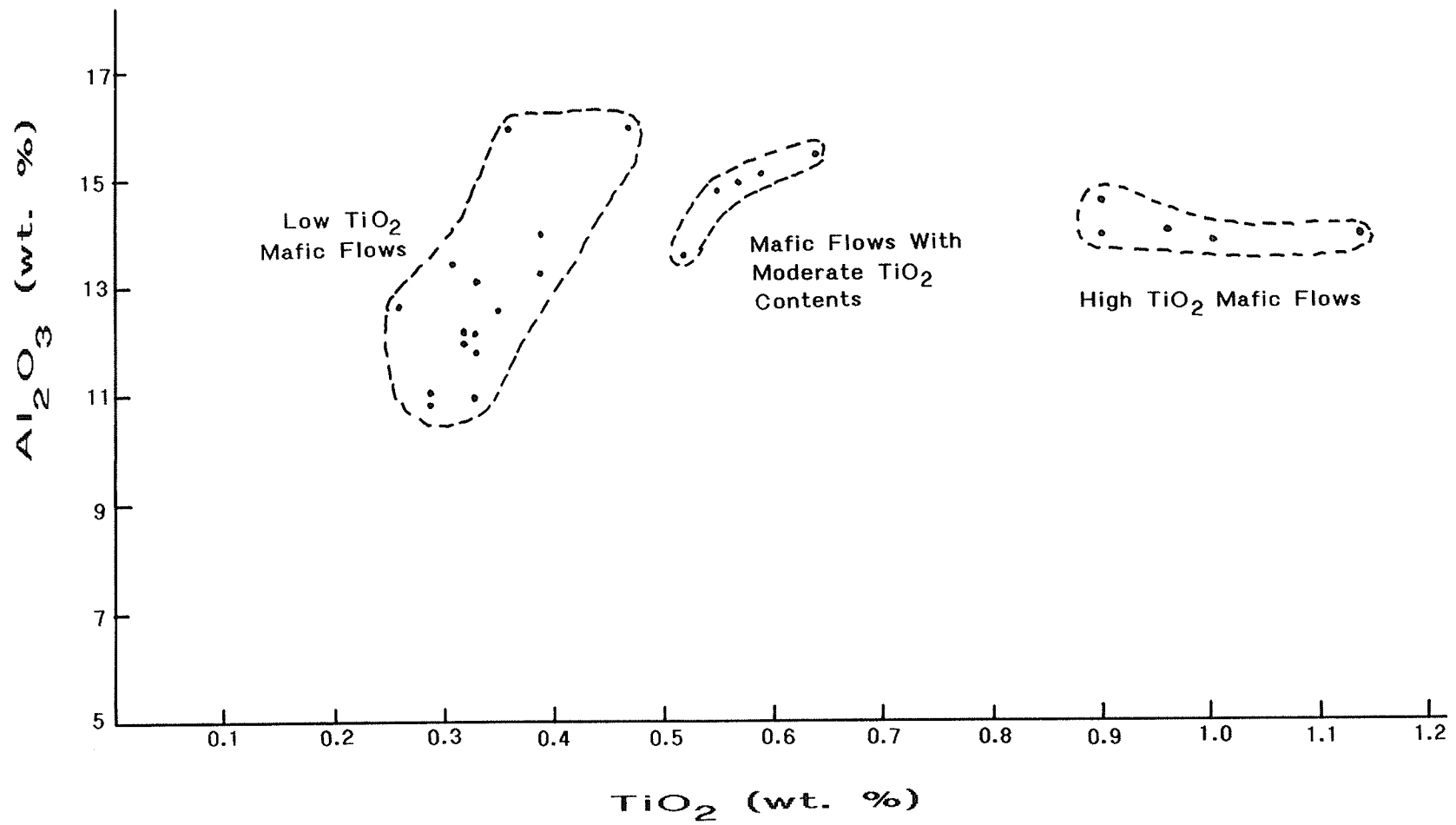


FIGURE 40: COMPARISON OF TiO_2 AND Al_2O_3 CONTENTS OF THE VARIOUS MAFIC FLOWS IN THE VAMP LAKE AREA

Table 6 – Geochemistry of Intermediate and Felsic Volcanic Rocks

	Felsic Flow				Quartz – Plagioclase – phyric felsic flow			Intermediate Plagioclase –phyric Flow		Felsic Tuff							Felsic Crystal-bearing Tuff		Intermediate Tuff			Felsic Dikes			Possible Sediments	
Sample #	GR 8	Con 52 614.5	Con 64 122	GR 25	GR 39	Con 57 779	Con 63 1118	Con 45A 835.5	Con 52 96.5	GR 45	GR52	GR 6	GR 32	67 787	Con 20 124	52 474	GR 12	GR 19	GR 48	GR 59	GR 35	67 889	Con 63 590	52 350	Con 63 171	
Formation	L-2	L-2	L-2	L-4	I-4	I-4	I-4	I-3	L-2	I-2	I-2	L-3	L-4	L-4	L-4	I-4	L-4	L-4	I-4	I-4	I-7	L-7	I-7	I-4	I-4	
Wt. %																										
SiO ₂	71.00	73.00	67.80	72.50	70.60	68.90	68.30	62.70	58.80	71.90	68.40	70.90	65.50	67.10	68.10	66.30	73.00	72.00	62.50	62.30	71.3	68.40	69.20	60.70	61.30	
TiO ₂	0.36	0.31	0.53	0.31	0.37	0.37	0.37	0.40	0.32	0.26	0.36	0.40	0.60	0.51	0.64	0.42	0.25	0.25	0.62	0.52	0.3	0.33	0.30	1.09	1.11	
Al ₂ O ₃	11.90	11.80	13.00	12.10	14.10	12.40	14.20	13.90	15.10	11.40	11.30	12.25	12.80	10.50	13.80	13.40	12.50	12.50	14.75	12.90	15.2	15.30	16.10	15.60	15.70	
Fe ₂ O ₃	5.72	5.37	7.06	5.59	3.51	6.88	6.37	8.84	9.60	4.92	7.35	5.54	6.33	10.60	6.67	8.35	4.85	5.45	8.26	11.60	2.85	3.11	2.66	6.62	6.73	
MnO	0.10	0.11	0.10	0.10	0.07	0.09	0.05	0.11	0.18	0.11	0.24	0.12	0.18	0.18	0.12	0.16	0.12	0.10	0.16	0.20	0.05	0.08	0.06	0.09	0.08	
MgO	0.48	0.76	1.00	0.66	0.58	0.68	0.54	2.43	3.37	0.58	2.60	0.77	1.86	1.53	1.33	1.28	0.48	0.67	1.75	1.13	0.9	1.11	0.96	2.56	2.90	
CaO	4.31	3.22	3.91	3.49	4.88	4.49	4.21	7.01	8.08	4.57	3.04	4.50	5.51	5.64	6.32	6.17	3.27	3.93	7.81	6.09	3.51	3.24	4.24	5.35	4.90	
Na ₂ O	3.55	3.88	3.66	2.60	3.54	2.81	2.96	1.69	1.80	2.29	1.34	2.56	3.10	1.64	2.70	2.41	3.63	3.08	2.14	2.42	4.46	4.62	4.28	3.20	3.44	
K ₂ O	0.74	0.86	1.17	1.80	0.68	1.22	1.43	0.74	1.38	1.15	1.74	1.31	0.70	1.18	0.60	0.65	1.07	1.09	0.38	0.73	1.27	1.40	1.01	2.11	2.01	
P ₂ O ₅	0.10	0.07	0.16	0.07	0.14	0.21	0.14	0.13	0.13	0.21	0.49	0.24	0.14	0.20	0.16	0.17	0.06	0.06	0.18	0.38	0.09	0.11	0.10	0.57	0.58	
LOI	0.47	0.62	0.70	0.77	0.47	1.70	1.39	1.16	0.85	0.75	1.50	0.82	0.54	1.00	1.16	0.85	0.39	0.54	0.32	0.85	0.31	1.39	0.85	1.16	1.08	
S	<0.01	0.03	0.04	0.06	<0.01	2.26	1.97	0.28	<0.01	0.06	0.31	0.23	<0.01	0.04	0.31	0.52	0.02	<0.01	<0.01	1.17	0.01	0.01	<0.01	0.05	0.05	
CO ₂	0.18	0.16	0.16	0.08	0.18	0.19	0.07	0.05	0.03	0.33	0.04	0.05	0.02	0.25	0.02	0.09	0.05	0.09	0.04	<0.01	0.09	0.04	<0.01	0.18	0.03	
PPM																										
Ba	290	450	530	470	290	390	660	360	320			390	200	220	170	200	380	330	160	350	620	390	530	1150	1170	
Cr	10	10		10	10	10	10	10	30			10	10	10	10	10	10	10	10	<10	10	10	10	20	30	
Ni	3	3	6	5	4	31	45	7	9			4	5	3	6	4	3	3	4	13	6	6	4	17	19	
PPB																										
Au	<2	2	<2	<2	3	74	67	4	4			<2	<2	<2	29	24	<2	<2	<2	27	4	<2	6	<2	<2	
PPM																										
Y		45.72	39.07		22.27			21.10	17.95						36.21		34.15				11.15			24.74	24.50	
Zr		107.36	90.89		47.21			42.10	25.56						80.53		80.45				123.60			243.46	240.55	
Nb		7.72	10.35		3.10			3.82	5.01						4.24		8.51				4.40			17.63	16.49	
Rb		12.15	18.43		11.53			19.80	22.71						10.06		14.85				25.22			38.21	41.66	
Sr		143.53	174.49		145.28			263.25	334.21						273.75		114.36				353.17			966.25	855.84	

Table 7: Geochemistry of Altered Rocks

Distal Alteration																
Sample #	Chlorite - Biotite - Quartz - Amphibole				Quartz - Biotite					Quartz - Biotite Garnet	Quartz - Muscovite	Chlorite - Quartz - Biotite			Sericite - Epidote - Chlorite - Biotite	Chlorite - Quartz - Sericite - Amphibole
	Con 9 312	Con 44 154	Con 44 248	Con 63 188.5	139 - 442.5	139 - 481	139 - 502	140 - 264	Con 63 446.5	Con 62 447	140 298	139 - 280.5	139 - 325	139 - 365	TR 21	59 214.5
Formation	I-3	I-3	I-3	I-3	I-3	I-3	I-3	I-3	I-3	I-3	I-3	I-3	I-3	I-3	I-3	L-3
Wt. %																
SiO2	56.90	60.90	52.30	53.80	62.84	64.12	63.60	59.10	56.00	49.10	57.50	45.20	46.80	42.50	50.00	50.17
TiO2	0.30	0.32	0.33	0.25	0.41	0.31	0.35	0.36	0.24	0.38	0.35	0.56	0.42	0.60	0.57	0.35
Al2O3	12.50	12.52	13.80	11.50	12.30	9.68	15.30	14.40	7.49	16.90	12.40	14.50	14.40	16.00	18.40	11.00
Fe2O3	10.00	9.29	12.80	12.90	12.80	11.30	7.09	10.10	19.80	16.10	14.30	18.80	15.60	19.90	11.90	20.07
MnO	0.11	0.11	0.08	0.16	0.14	0.46	0.16	0.07	0.07	5.14	0.11	0.21	0.28	0.28	0.14	0.09
MgO	10.50	8.93	9.85	12.10	1.32	5.19	2.33	3.94	6.05	4.21	1.46	11.50	13.50	11.12	3.83	7.92
CaO	2.24	0.96	1.53	1.84	5.28	5.46	4.22	5.17	0.38	3.97	1.32	1.02	0.74	1.83	6.81	0.55
Na2O	0.33	0.73	0.63	0.11	1.73	0.87	2.93	1.06	0.11	0.95	0.28	0.55	0.03	0.29	2.07	0.44
K2O	2.72	2.49	2.62	0.44	0.44	0.33	1.71	2.07	1.67	1.77	3.42	1.72	0.33	0.67	1.98	1.43
P2O5	0.04	0.14	0.05	0.05	0.39	0.19	0.07	0.06	0.03	0.43	0.05	0.33	0.10	0.34	0.40	0.17
LOI	3.31	3.94	5.39	6.00	2.30	2.80	1.70	2.85	7.77	1.35	7.85	5.55	6.93	6.20	3.95	8.17
S	0.46	0.54	2.03	1.33	4.55	3.51	1.28	2.17	7.55	3.27	6.66	2.63	0.41	1.05	4.26	5.16
CO2	0.03	0.02	0.01	0.01	0.01	0.04	0.02	0.01	0.02	0.05	<0.01	0.13	0.04	0.02	0.02	<0.01
PPM																
Ba	530	440	490	180			850	640	370		3520					500
Cr	210	70	90	320			20	70	210		260					100
Ni	27	27	33	33			16	22	57		60					56
PPB																
Au	7	5	7	6			13900	120	24							12
PPM																
Y		8.98		13.73	16	13				21	11	20		15	22	8.90
Zr		11.67		10.93	28	26				27	27	33		29	35	13.14
Nb				3.38	2	3				<2	<2	<2		<2	<2	3.51
Rb		46.47		12.37	8	6				39	39	28		13	60	33.34
Sr		63.62		11.04	116	52				98	25	38		28	158	55.18

Table 7 continued							
	Proximal Alteration				Peripheral Alteration		
	Tremolite – Quartz – Biotite – Chlorite				Biotite – Amphibole Clusters	Peripheral Chl–Ep Alteration	
Sample #	Con 24 158	Con 45A 860	Con 57 753	Con 63 1035	Con 62 522	Maf. Flow Con 57 343.5	Maf. Tuff Con 57 551.5
Formation	L-3	I-3	I-3	I-3	I-3	I-3	I-3
Wt. %							
SiO ₂	57.95	48.50	48.90	47.80	51.40	53.70	58.00
TiO ₂	0.11	0.36	0.35	0.36	0.42	0.34	0.33
Al ₂ O ₃	6.89	9.70	9.67	9.95	18.20	14.30	14.00
Fe ₂ O ₃	12.70	11.00	11.10	10.90	9.95	11.80	12.70
MnO	0.17	0.18	0.24	0.19	0.77	0.20	0.19
MgO	13.15	15.70	15.80	16.00	6.10	5.75	3.32
CaO	5.66	9.30	9.22	8.93	7.64	9.03	9.29
Na ₂ O	0.40	0.76	0.72	0.73	0.79	1.71	1.15
K ₂ O	0.42	1.27	1.40	1.80	2.51	0.49	0.52
P ₂ O ₅	0.04	0.16	0.16	0.17	0.27	0.05	0.12
LOI	3.12	2.23	1.62	1.93	1.60	1.62	0.47
S	0.91	0.07	0.38	0.06	0.57	0.08	0.05
CO ₂	0.08	0.03	0.02	0.02	0.03	0.84	0.03
PPM							
Ba	120	280	320	350		160	270
Cr	1320	1160	1190	1180		30	20
Ni	82	240	360	260		17	5
PPB							
Au	24	<2	3	<2		3	3
PPM							
Y	8.44			12.75	16		15.06
Zr	4.65			24.65	30		23.30
Nb	3.09			1.88	4		1.32
Rb	16.80			47.59	51		6.52
Sr	20.80			44.01	142		226.68

7.2 DISCRIMINATION DIAGRAMS

Rocks in the Vamp Lake area have been subjected to both alteration and medium grade metamorphism. Under such conditions all major elements become mobile, and geochemical plots using major element abundances for classifying rock types on the basis of magmatic differentiation are of limited use. There are, however, several trace element discrimination diagrams that can be used to mitigate this problem. These discrimination diagrams are based on the premise that different magma types are characterized by specific abundances of particular relatively immobile trace elements. Similar types of discrimination diagrams can be used to infer the tectonic setting in which the rocks were emplaced, because magmas generated in different tectonic settings are also characterized by particular abundances or ratios of these trace elements.

To establish the different magmatic rock types in the Vamp Lake area and the tectonic environment of their emplacement, geochemical plots have been chosen that utilize relatively immobile elements such as Zr, Ti, Nb, and Y. Of these particular elements, Zr and Ti are relatively immobile even during intense hydrothermal alteration whereas Y and Nb may be extremely mobile (Finlow-Bates & Stumpfl, 1981). Therefore only Zr and Ti can be used with any reliability in hydrothermally altered rocks. Despite these

problems, various studies have determined the usefulness of all of these particular elements in discrimination diagrams (Roberts & Reardon, 1978; Riverin & Hodgson, 1980; Finlow-Bates & Stumpfl, 1981; Gibson et al, 1983).

7.2.1 Magma types

The various discrimination diagrams used in this study make use of different combinations of the immobile elements to identify the degree of magmatic differentiation (Figures 41, 42); the use of several different diagrams is useful in verifying results and in cross-checking the apparent immobility of various elements and the subsequent reliability of a particular plot. For all primary rock types, only the trace element analyses determined at the University of Manitoba were used because these are believed to be more accurate. For all diagrams using major element oxides, the analyses have been recalculated on a volatile-free basis.

Using only trace element ratios (Figure 41), a complete range of data is indicated. Mafic and intermediate rocks plot in the same fields, although the two groups are characterized by different Zr/TiO₂ ratios; felsic rocks plot in separate fields. The mafic rocks plot in the sub-alkaline basalt and andesite/basalt fields, intermediate rocks fall in the andesite/basalt field, and felsic rocks in the andesite and dacite fields. On diagrams where SiO₂ is one of the discriminants, mafic and intermediate rocks plot in the

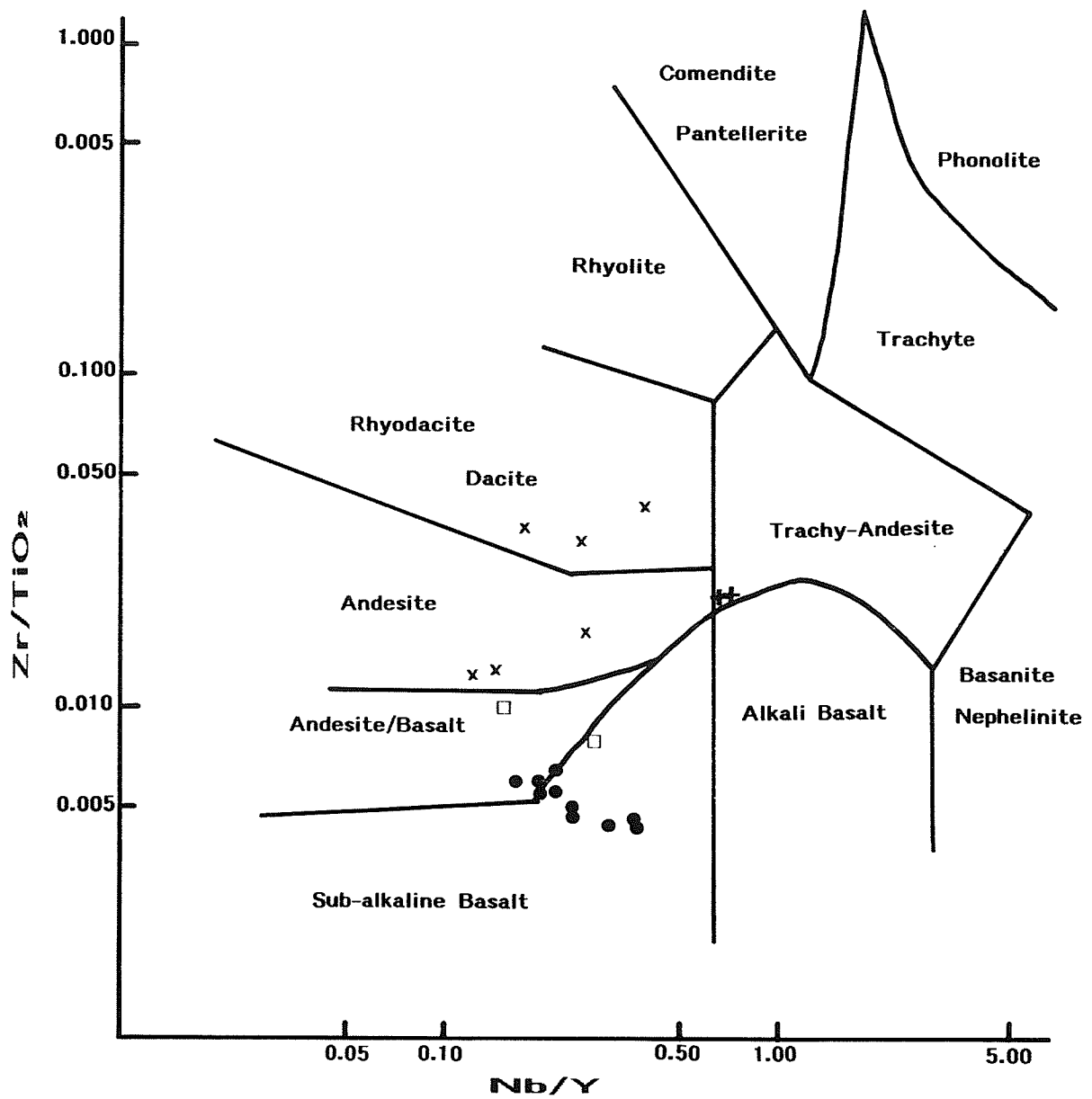


Figure 41: Magmatic Discrimination Diagram

Symbols used are as follows: ● = mafic volcanic rocks; x = felsic volcanic rocks; □ = intermediate volcanic rocks; ⊕ = possible sedimentary rocks
 Only those samples with University of Manitoba trace element data have been plotted.

(After Winchester & Floyd, 1977)

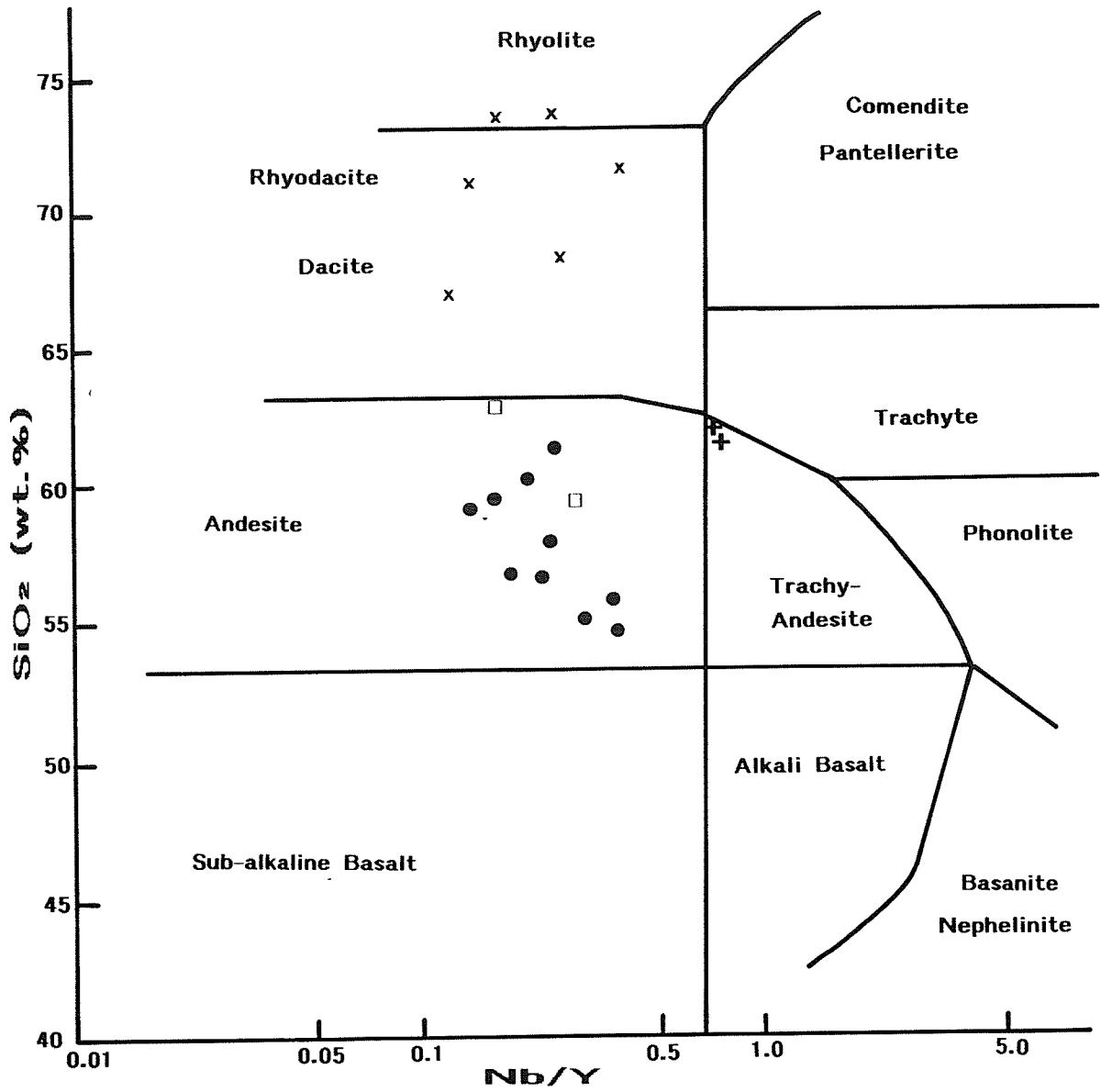


Figure 42: Magmatic Discrimination Diagram
 Refer to Figure 41 for explanation of symbols

(After Winchester & Floyd, 1977)

andesitic field, whereas the felsic rock types are in the dacite and rhyolite fields (Figures 42, 43). The discrepancy in rock types between those defined from Figure 41 and those from Figures 42 and 43 suggests that silica has been enriched in most samples. Silica enrichment is supported by the unusually high quartz content of mafic flows described in Chapter 4, and possibly reflects some degree of regional silicification. Because of the possibility of silicification, Figure 40 provides the best measure of primary composition. Rocks classified in the field as intermediate to felsic are thus andesitic, or possibly basaltic, to dacitic in composition, mafic rocks are basaltic to possibly andesitic.

Perusal of mafic rock data in Table 5 shows that there is a wide variation in TiO_2 contents; high TiO_2 values correspond with higher P_2O_5 and possibly Zr contents. The variation in TiO_2 is shown diagrammatically in Figure 40 as a function of Al_2O_3 . Although Al_2O_3 does not differ substantially among samples, TiO_2 shows considerable variation, with the samples clustering in three groups. The TiO_2 differences appear to be primary rather than the result of Ti mobility because P_2O_5 and Zr show comparable differences. Because the separation between low TiO_2 and moderate TiO_2 flows on Figure 43 is not pronounced, the gap between these two sub-groups may be the result of limited sampling rather than a true boundary between chemically distinct groups. High TiO_2 flows, however, form a distinct field far removed from the other flows. High TiO_2 mafic flows occur exclusively in the mainland fault block. The low TiO_2 and moderate TiO_2 flows occur in both fault blocks.

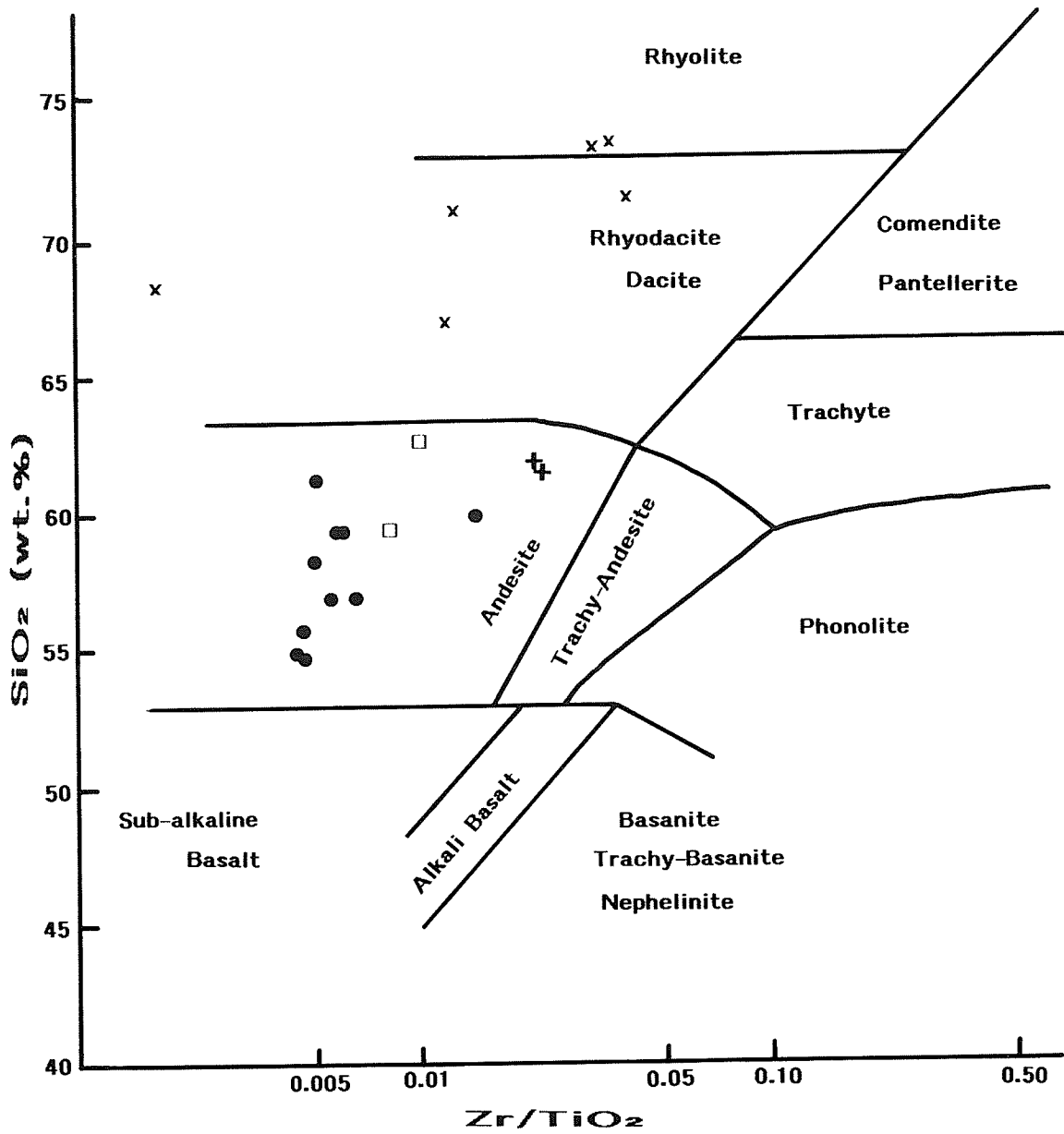


Figure 43: Magmatic Discrimination Diagram
 Refer to Figure 41 for explanation of symbols

(After Winchester & Floyd, 1977)

7.2.2 Possible Sedimentary Rocks

There are several, thin rock units at Vamp Lake that are chemically distinct from all other units, and are distinguished by high Ba (1150-1170 ppm), Zr (240.55-243.46 ppm), and Sr (855.64-966.25 ppm) contents, when compared to other units (see Tables 5 and 6). These samples plot in distinctly different positions than other rock types on discrimination diagrams (Figures 41, 42, 43), and are also petrographically different from other unaltered lithologies; the plagioclase is coarser grained in the possible sedimentary rocks, and biotite-epidote clusters are present (see section 4.3). These units are also chemically and petrographically distinct from the alteration rock types, although they occur within or near the alteration zones. As such, the unique chemical and petrographic characteristics are interpreted to reflect a different primary rock type.

7.2.3 Tectonic environment

The mafic Vamp Lake rocks have been plotted on five discrimination diagrams (Figures 44-48) that have been devised for mafic rocks exclusively. These plots consistently suggest that the Vamp Lake mafic volcanism represents a tholeiitic island arc setting. This conclusion is in agreement with the tectonic setting proposed for the Flin Flon greenstone belt (Bailes & Syme, 1989;

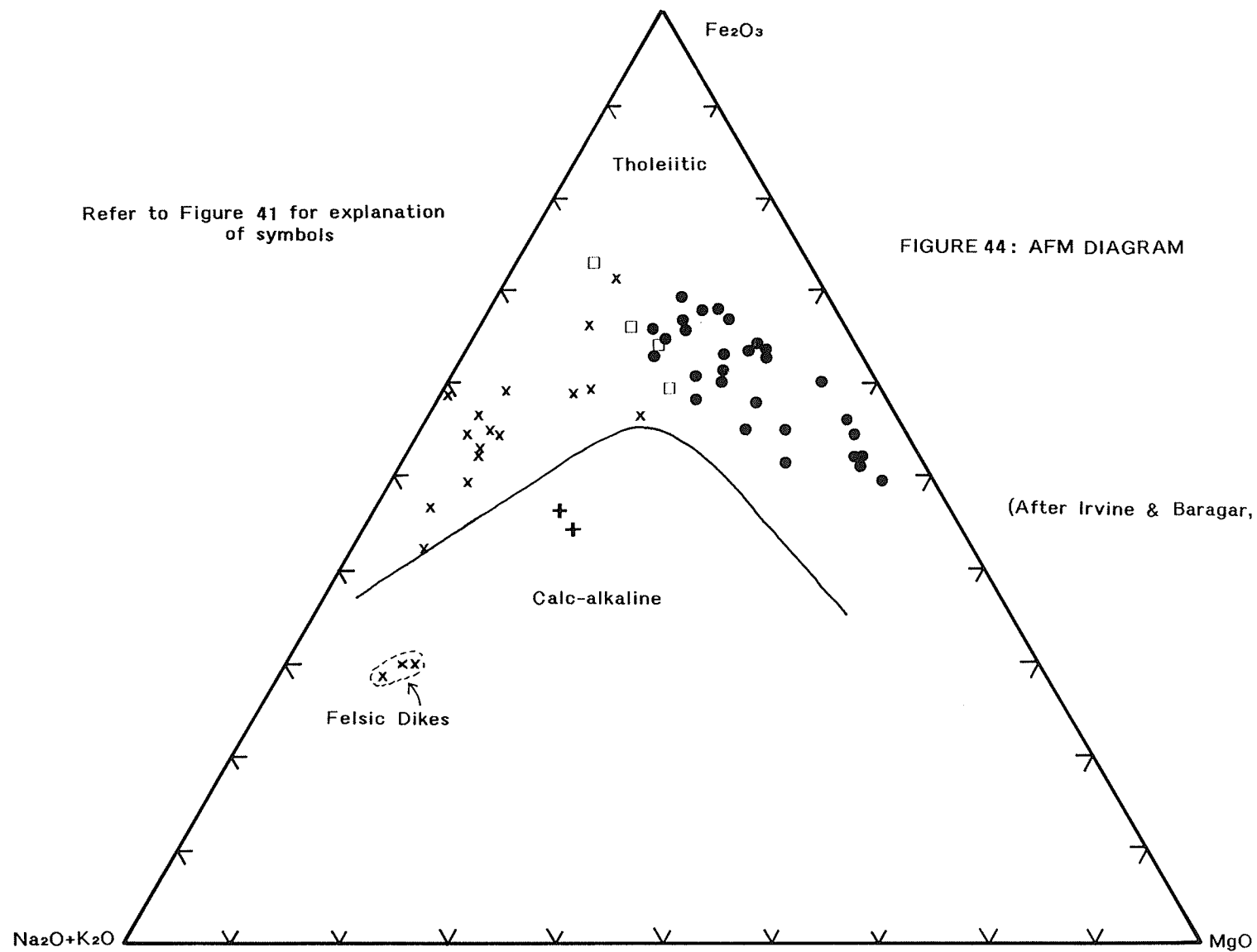
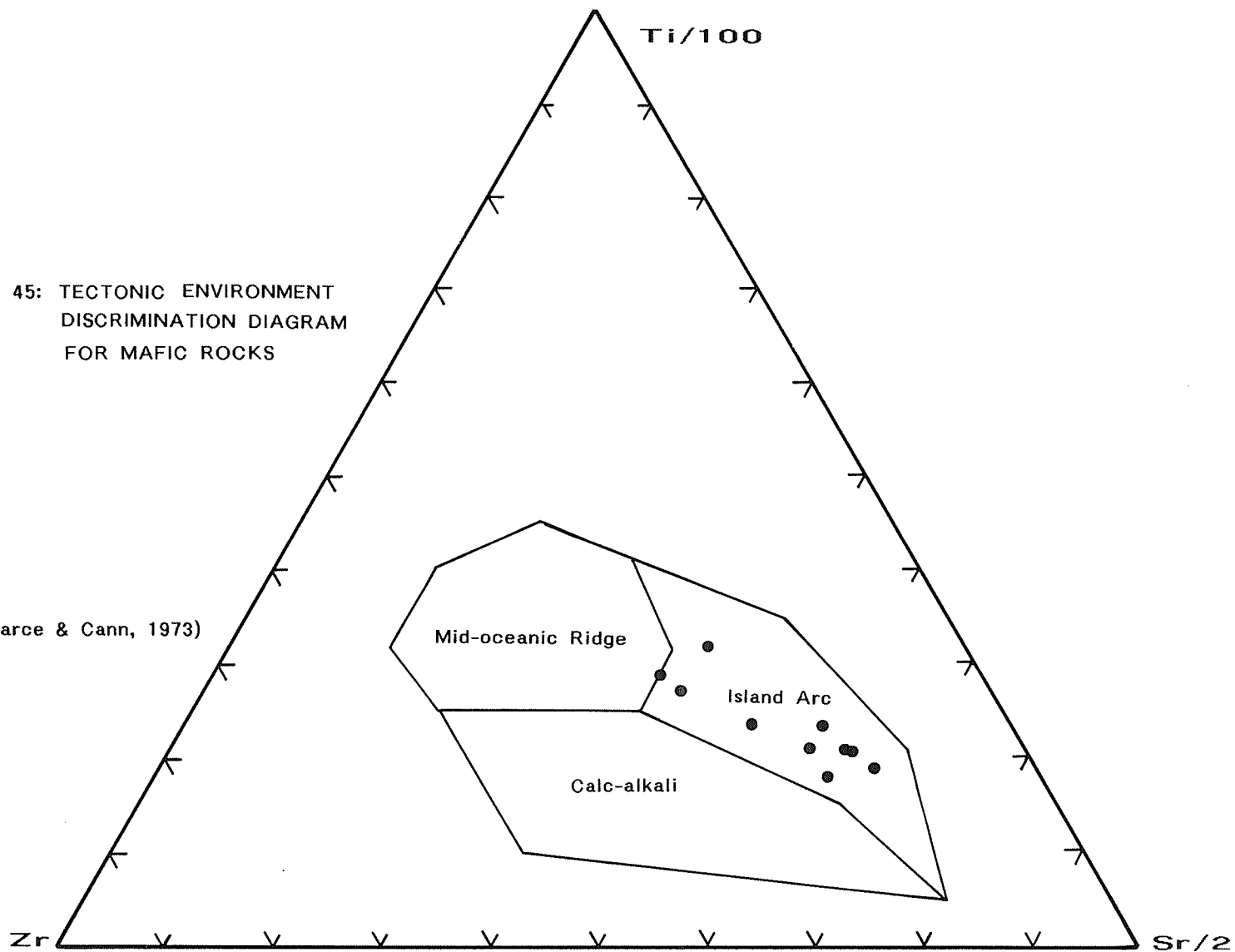


FIGURE 45: TECTONIC ENVIRONMENT
DISCRIMINATION DIAGRAM
FOR MAFIC ROCKS

(After Pearce & Cann, 1973)



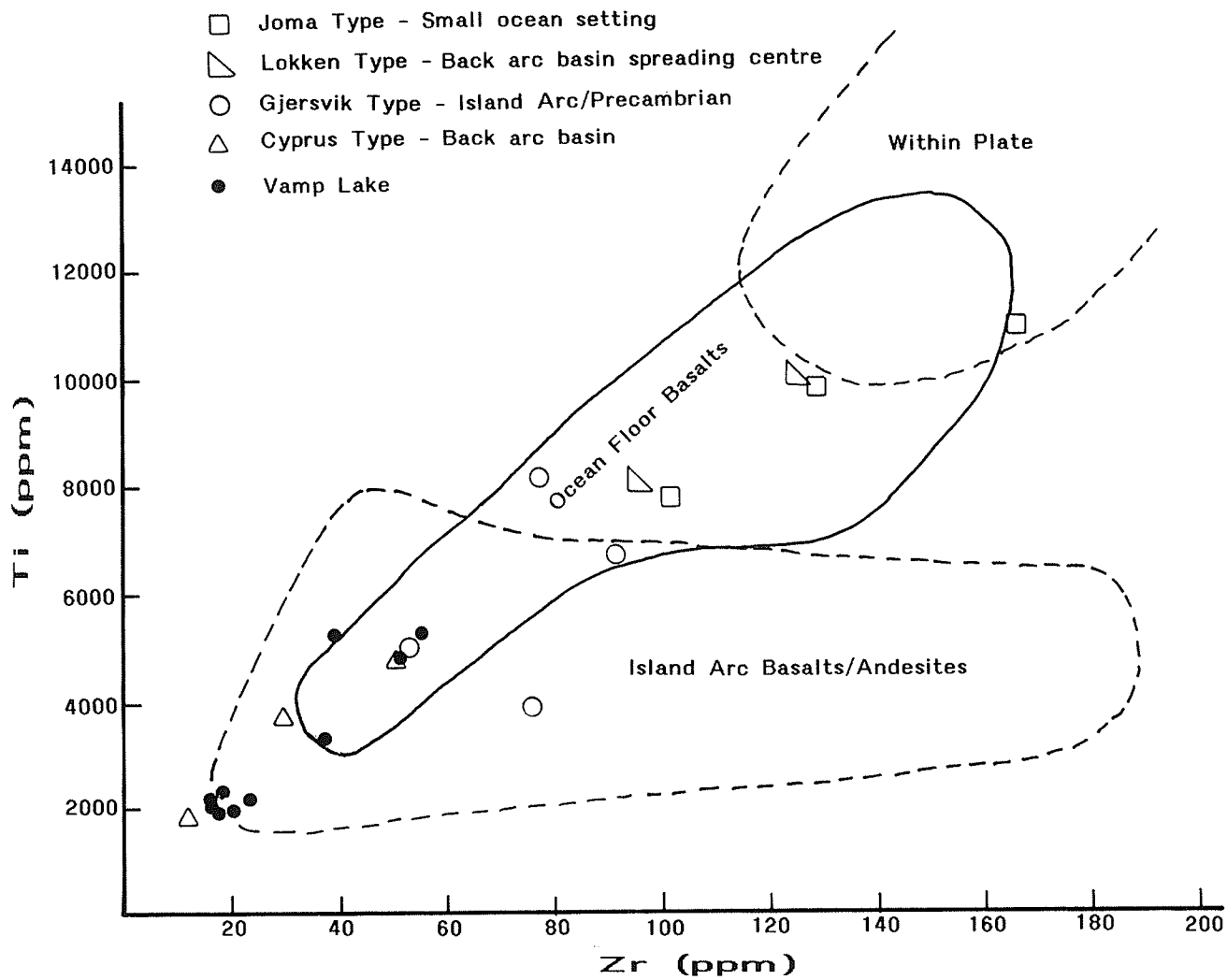


FIGURE 46: TRACE ELEMENT SIGNATURES OF MAFIC VOLCANIC ROCKS FROM MASSIVE SULFIDE DEPOSITS FROM VARIOUS TECTONIC SETTINGS; COMPARISON TO VAMP LAKE

(After Pearce & Gale, 1977)

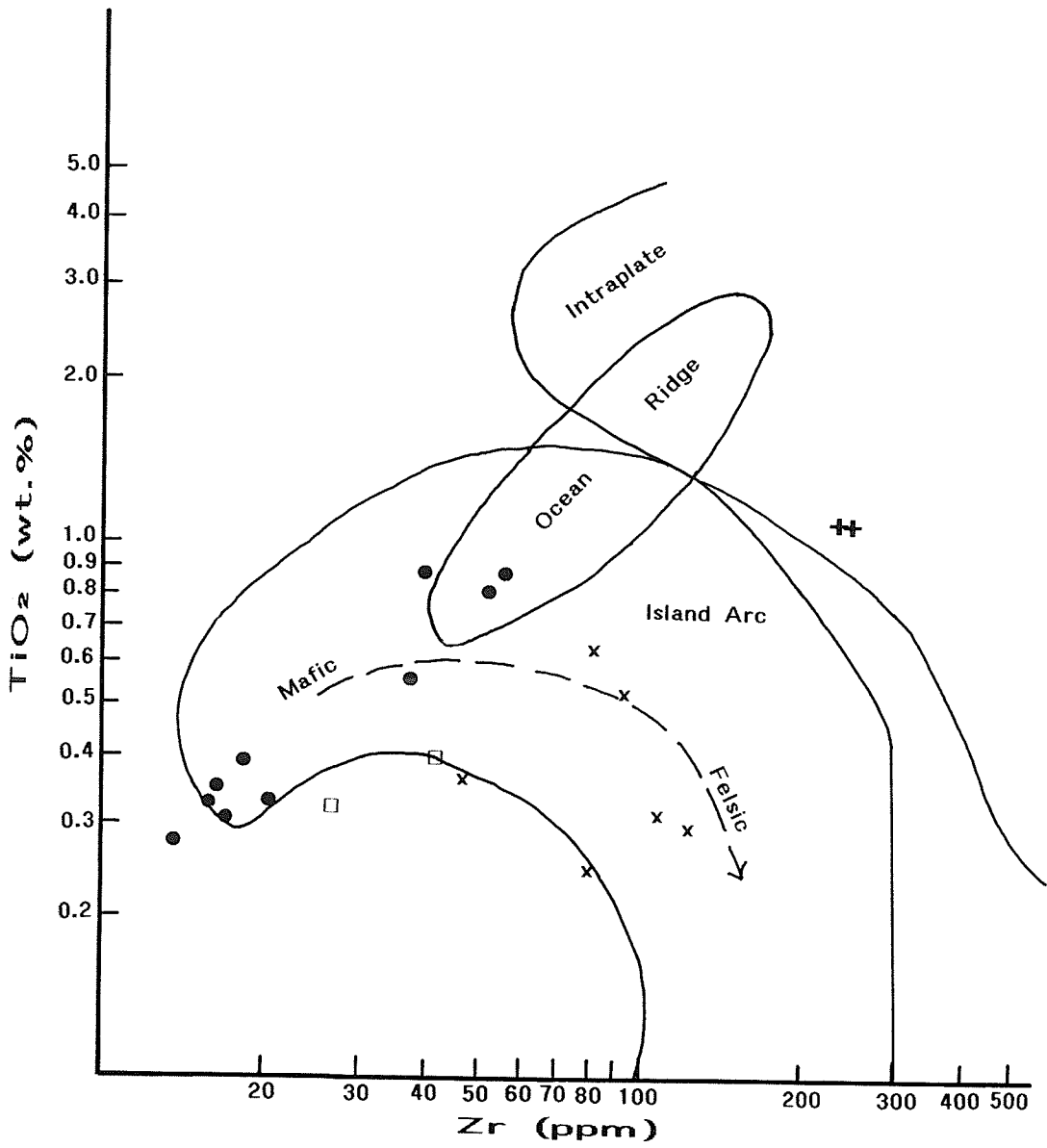


FIGURE 47: TECTONIC DISCRIMINATION DIAGRAM

Refer to Figure 41 for explanation of symbols

(After Gass, 1982)

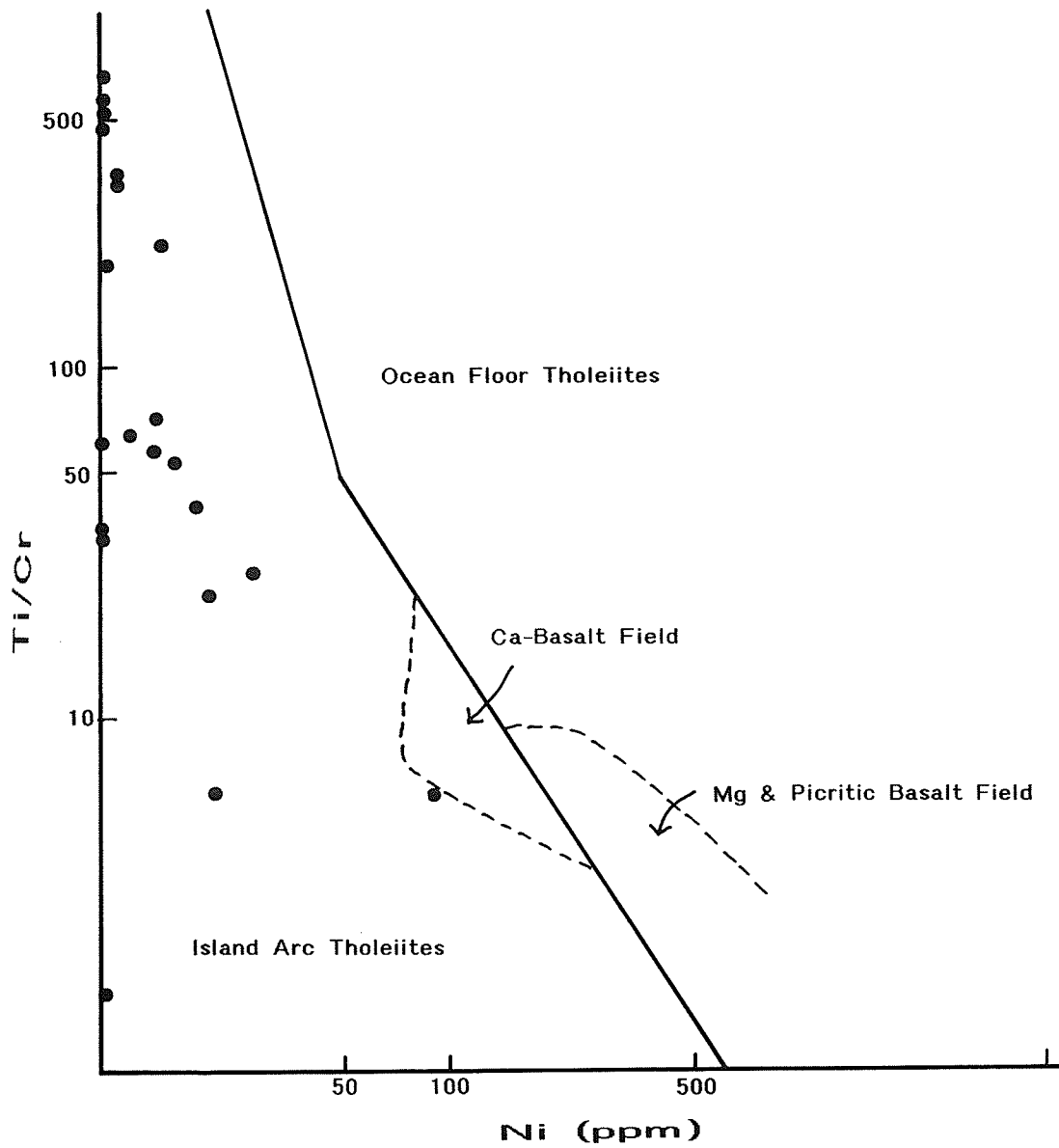


FIGURE 48: TECTONIC SETTING OF THE MAFIC VOLCANIC ROCKS AT VAMP LAKE, BASED ON Ti, Cr, AND Ni CONTENTS

(After Beccaluva et al., 1979)

Stauffer et al, 1975, Koo & Mossman, 1975).

The tholeiitic nature of the volcanic rocks at Vamp Lake is clearly indicated on an AFM diagram where all samples except felsic dikes and possible sedimentary rocks plot in the tholeiitic field (Figure 44). The apparent island arc affinities of the mafic volcanic rocks at Vamp Lake are demonstrated in Figures 45-48, although there is some overlap with the ocean floor basalt field in Figure 46, and the ocean ridge field in Figure 47. In Figure 46, data from the mafic host rocks of several sulfide deposits developed in various known or inferred tectonic settings have also been plotted. Host rocks of the Cyprus deposits are characterized by low concentrations of small ion lithophile elements and therefore plot in the tholeiitic island arc field on geochemical discrimination diagrams such as Figure 46. The main host rocks to the Cyprus deposits, however, are ophiolites that apparently formed in back arc basins. Although Vamp Lake compares well with Cyprus deposits in Figure 46, the presence of extensive pyroclastic rocks precludes a setting similar to that of Cyprus deposits.

CHEMICAL CHANGES ASSOCIATED WITH ALTERATION

7.3 DETERMINING CHANGES IN WHOLE ROCK CHEMISTRY

On geochemical plots that use the more mobile major elements

K_2O , CaO , and Na_2O (Figures 49, 50), some of the visibly altered samples overlap the field of apparently unaltered precursor lithologies, but most of the altered samples plot in distinctly different areas. The altered samples define a trend away from the unaltered precursors suggesting that, in general, consistent chemical changes occurred during the alteration process. On the Hughes diagram (Figure 49), the primary mafic rocks define two fields with some of the mainland samples having higher total alkalis than island fault block samples. The altered samples define a trend parallel to the X-axis, indicating K enrichment and/or Na depletion and plot closest to the mafic samples of the island fault block. In a CaO - Na_2O binary plot (Figure 50), few felsic samples and none of the mafic samples plot in the unaltered fields defined by Stephen et al. (1984), and mafic and felsic samples overlap; as in Figure 49, altered samples plot closest to mafic rocks of the island fault block. Thus all samples have been affected by a certain amount of Ca and Na mobility. The presence of pervasive alteration is not unexpected; pervasive silification was indicated by petrographic data (section 6.4.2). Whether the mobility of Ca, Na, and Si is the result of metamorphism or more widespread hydrothermal alteration is not clear.

More evidence of pervasive alteration in the island fault block is evident in Figure 51. On this diagram both altered and apparently unaltered mafic samples show a wide compositional variation and plot in both tholeiitic and komatiitic basalt fields, with altered samples showing greater scatter than unaltered

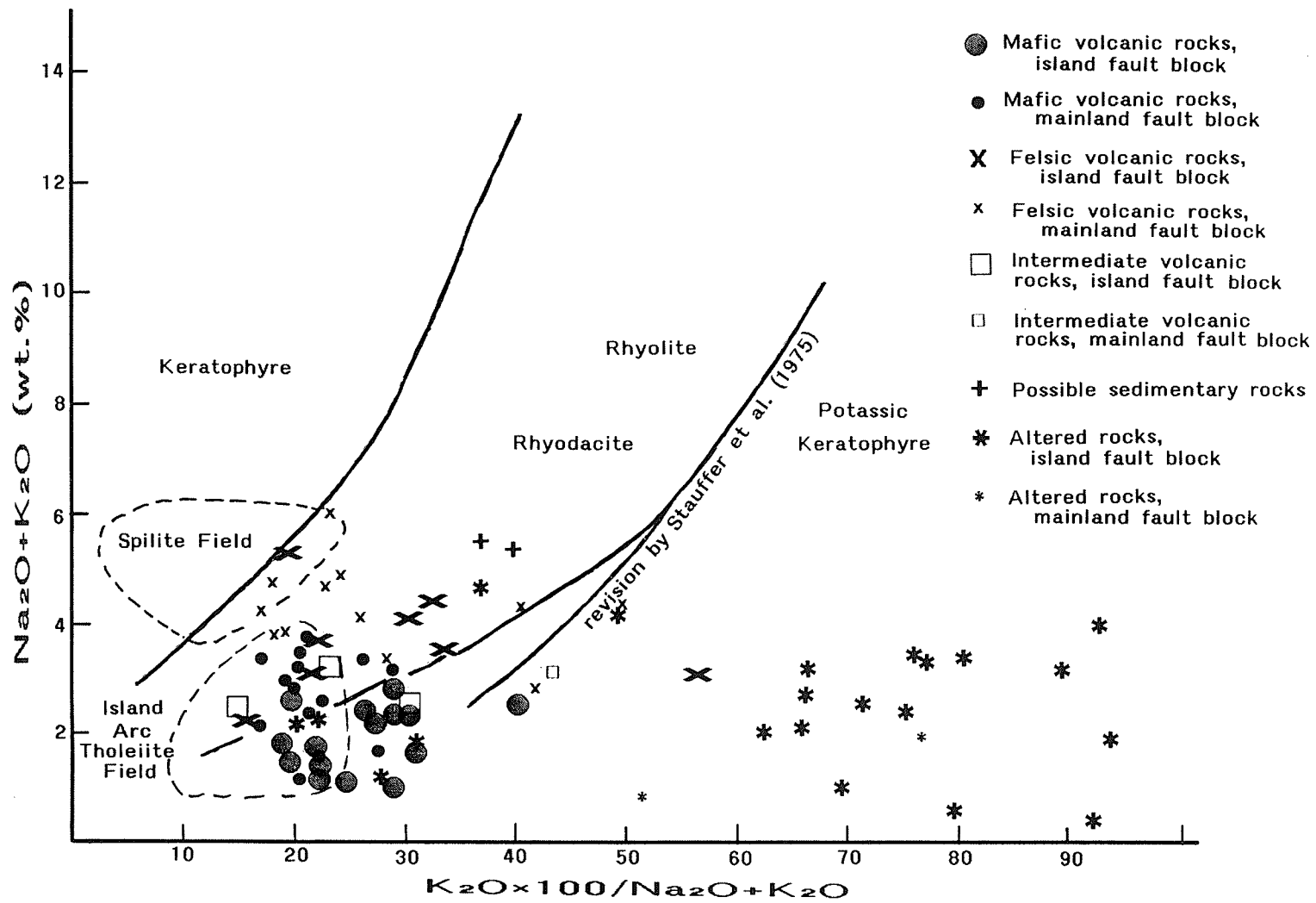


FIGURE 49: HUGHES MAGMATIC DISCRIMINATION DIAGRAM

(After Hughes, 1973)

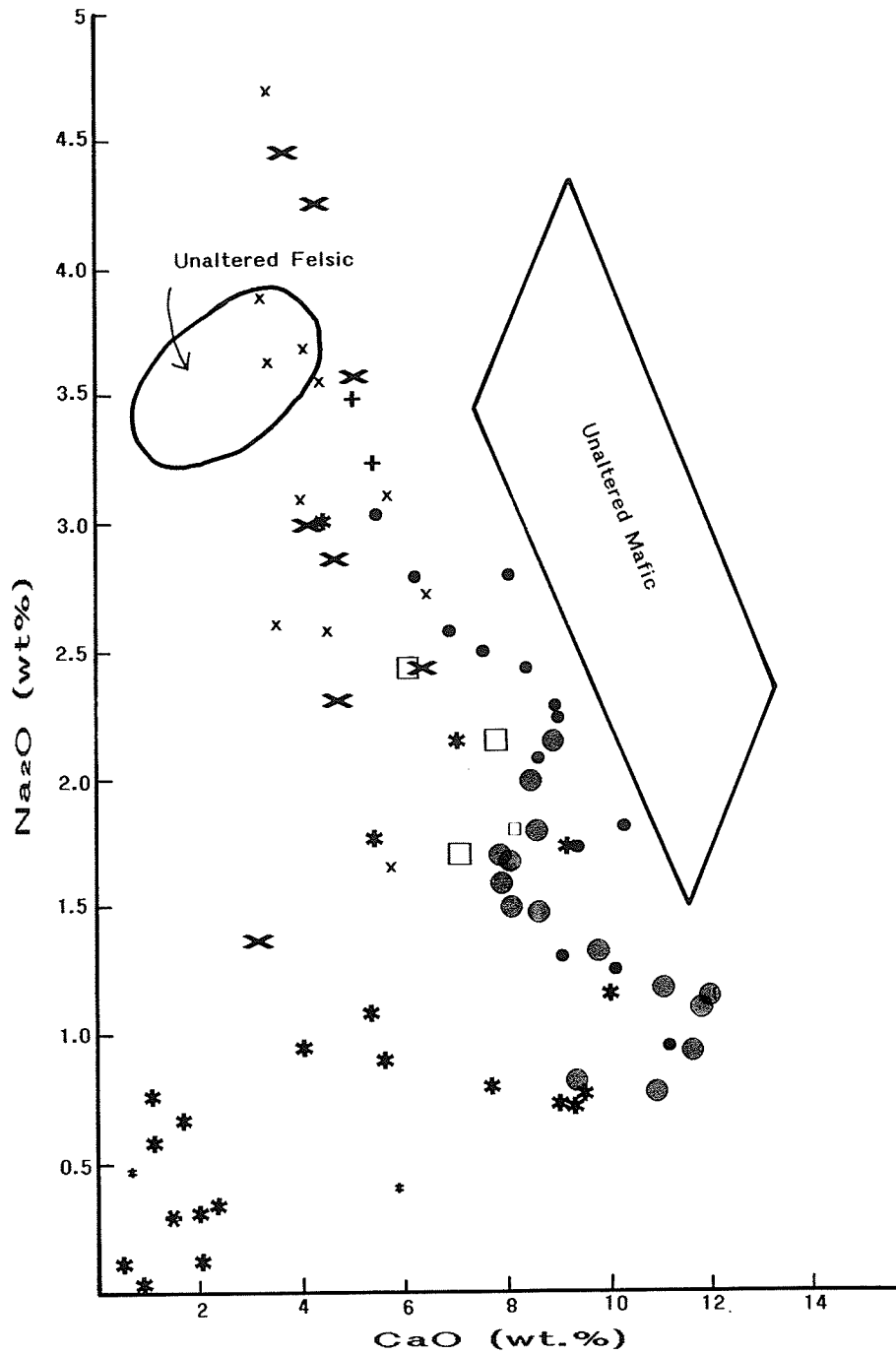
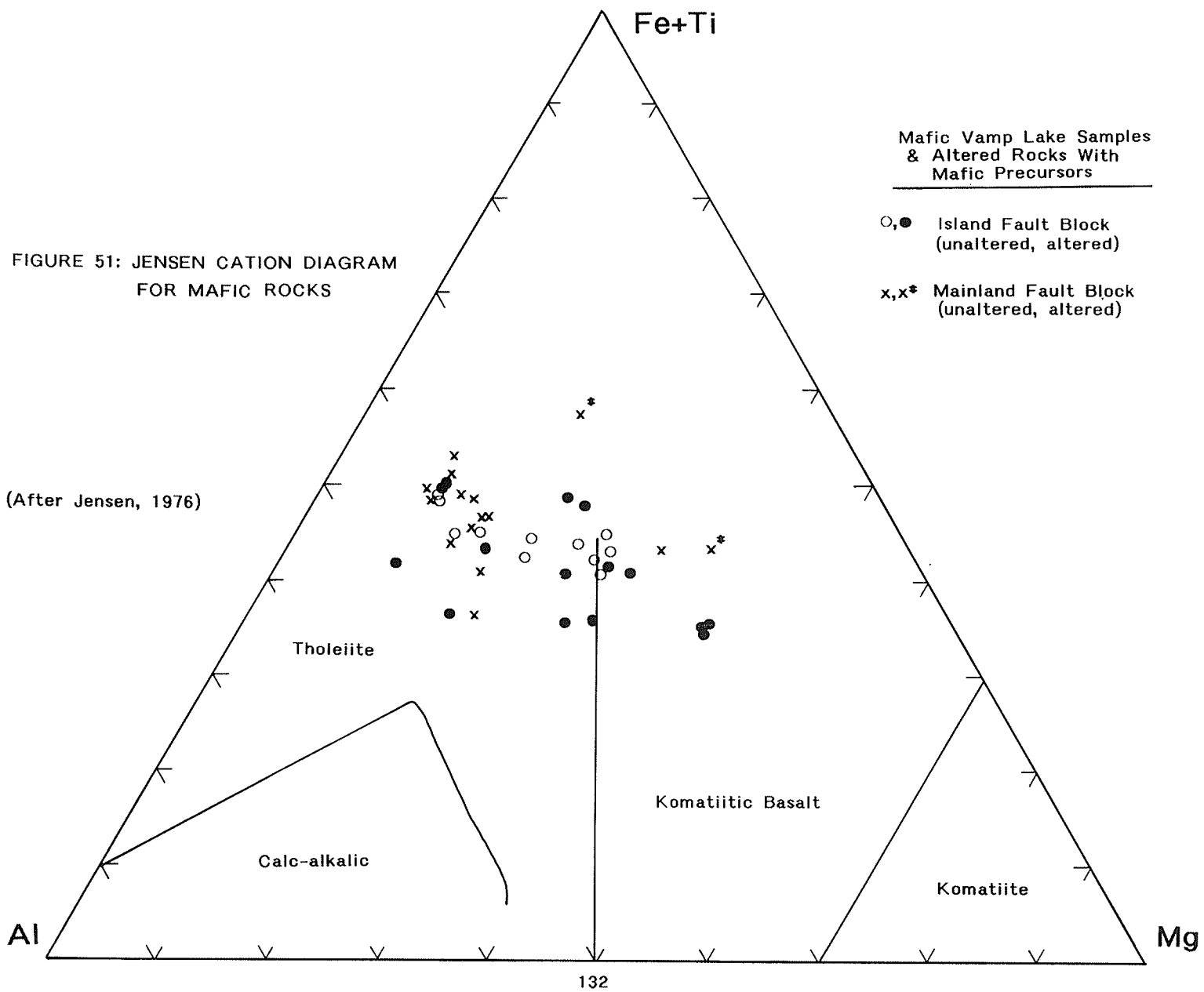


FIGURE 50: Na₂O - CaO BINARY DISCRIMINATION DIAGRAM FOR UNALTERED ROCKS

Refer to Figure 49 for explanation of symbols
(After Stephen et al., 1984)



samples. This suggests that Mg may have been mobile in all samples, and Fe may have been mobile during alteration, accounting for the greater vertical scatter of altered samples.

In order to determine the chemical effects of the alteration more quantitatively, the whole rock analyses of visibly altered rocks must be compared to unaltered samples of the same rock type. Choosing unaltered equivalents with which to compare altered samples is a problem because of the difficulty of recognizing primary rock types in highly altered regions, and no totally unaltered precursor can be found among the Vamp Lake samples because of the pervasive alteration. The choice of unaltered equivalents is based on stratigraphic position of the alteration zones, identifiable precursor components in partly altered samples, apparently unaltered units within the defined boundaries and at the margins of the alteration zones, and chemical evidence.

Alteration zones, both distal and proximal are developed within formation 3, which is composed mostly of mafic units with some intercalated intermediate and felsic units; thus mafic units should be the most common precursor, but with the possibility of some intermediate and felsic precursors. Unaltered parts of partly altered chlorite-biotite-quartz-amphibole rocks from the central part of the distal alteration zone in the island fault block are petrographically and mineralogically similar to mafic flows, and mafic flows are the most probable precursor of this particular alteration assemblage. This is consistent with the apparently unaltered dominantly mafic units identified within the central part

of the alteration zone. No petrographic evidence for original rock type was found for the quartz-biotite-garnet assemblage although the spatial association of the assemblage with the chlorite-biotite-quartz-amphibole assemblage may indicate a similar mafic precursor although minor unaltered felsic units are also present in this part of the zone. The large precursor amphibole component of the sericite-epidote-chlorite-biotite assemblage may indicate a mafic precursor. The tremolite-quartz-biotite-chlorite samples of the proximal alteration zones are interpreted to be altered mafic flows based on stratigraphic position, and precursor phases in partly altered samples.

The quartz-biotite assemblage contains relict plagioclase phenocrysts and groundmass components comparable to that of plagioclase-phyric intermediate flows and/or tuff; thus an intermediate unit is the most likely precursor. The quartz-muscovite+/-biotite assemblage in the distal island zone is confined to a thin, laterally continuous zone that is conformable with regional stratigraphy, suggesting a stratigraphic control for this particular assemblage. Precursor plagioclase and quartz suggest a felsic to intermediate parentage; the spatial relationship of the quartz-muscovite+/-biotite assemblage with the quartz-biotite assemblage may indicate a similar precursor, supporting an intermediate parentage. The quartz-muscovite assemblage and amphibole-biotite clusters in the proximal alteration zone above the island ore zone contain precursor components which suggests felsic precursors.

No definitive evidence was found for the precursor of the chlorite-quartz-sericite-amphibole assemblage because plagioclase was the only precursor mineral distinguishable; because plagioclase is an integral mineral of all rock types, the solitary presence of plagioclase cannot help determine precursor lithologies. The precursor composition of the chlorite-quartz-biotite assemblages is unknown because these samples were complete alteration products. The host rocks for the amphibole-biotite clusters may vary depending upon locality.

Because mafic and felsic rocks are characterized by different TiO_2 and Zr contents, all unaltered and altered rocks from the Vamp Lake area have been plotted on a TiO_2 versus Zr diagram (Figure 52) where unaltered samples define distinct compositional fields. Altered samples have been divided into three groups based on stratigraphic and petrographic evidence of precursor lithology: mafic precursor, intermediate precursor, and samples for which a precursor could not be determined. From this figure it would appear that all alteration assemblages that were interpreted to be altered mafic rocks plot along the linear trend defined by unaltered Vamp Lake mafic volcanic flows and tuffs. Altered samples of possible intermediate precursors generally straddle the boundary between unaltered mafic and intermediate rock types. Altered samples of uncertain precursors tend to be coincident with altered mafic samples. No samples of known or inferred felsic precursors were analyzed.

Based on all evidence listed above, mafic rocks are the

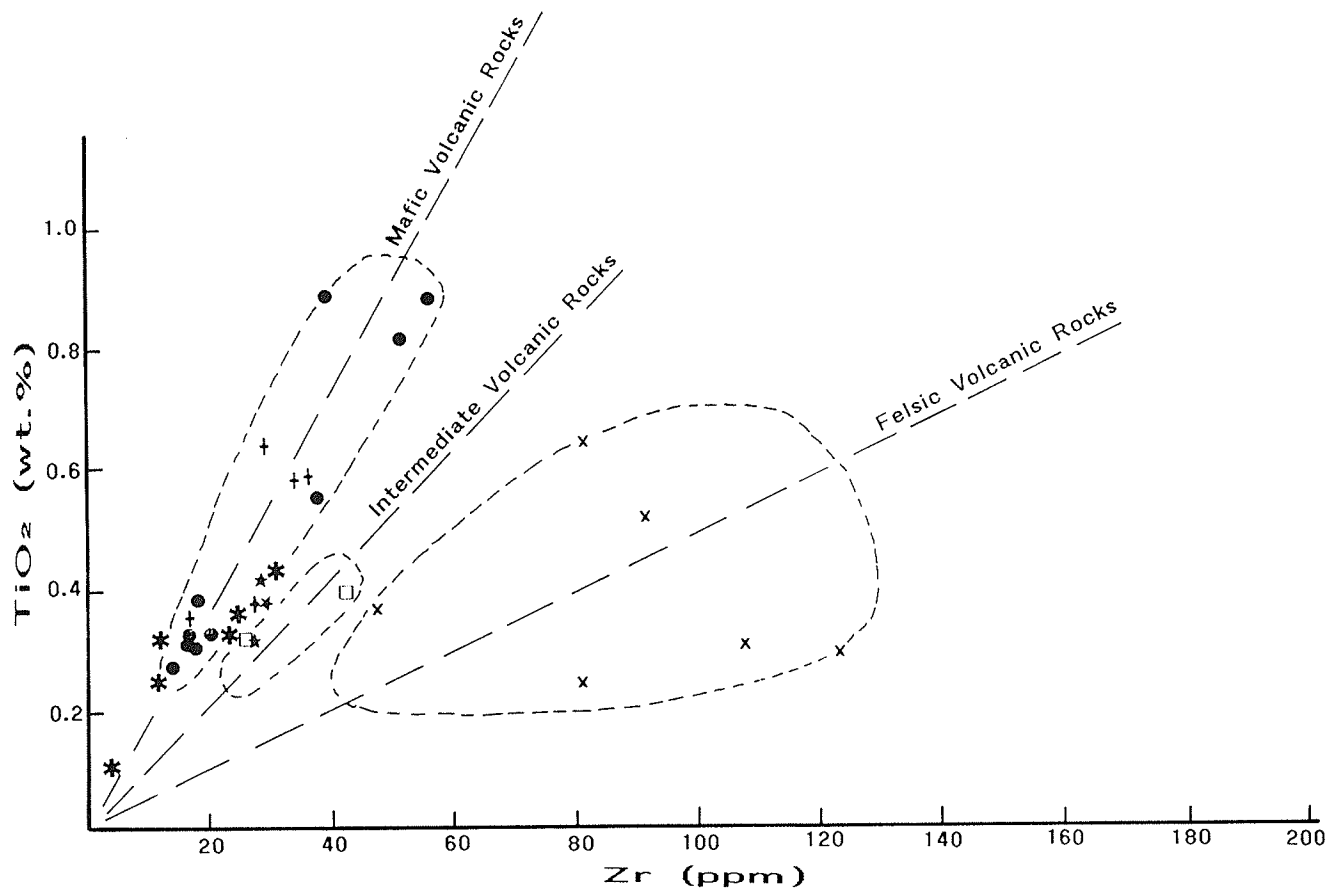


FIGURE 52: MAGMATIC DISCRIMINATION DIAGRAM

Symbols used are as follows: ● = mafic volcanic rocks; x = felsic volcanic rocks; □ = intermediate volcanic rocks; + = possible sedimentary rocks; * = altered mafic rocks; ★ = altered intermediate rocks; † = uncertain precursor. Proposed precursor rock types are based on field relations and petrography. Defined fields and trend lines are based on Vamp Lake data.

(After Pearce, 1975)

probable precursor for most alteration assemblages, with the exception of the quartz-muscovite+/-biotite and quartz-biotite assemblages from Sub-zone 2 of the distal alteration zone of the island fault block where petrography and spatial relations suggest a possible intermediate precursor.

In order to determine the chemical fluxes involved with the alteration process responsible for producing altered rocks which have been subsequently metamorphosed to produce the various assemblages described in Chapter 6, a precursor lithology and composition must be known. As indicated in Figure 40, there appears to be three different types of mafic flows at Vamp Lake, each with a particular composition. The specific mafic precursor sub-group must be determined in order to make a valid comparison for mass balance calculations. Assuming TiO_2 and Al_2O_3 were immobile during alteration, comparing the $\text{TiO}_2/\text{Al}_2\text{O}_3$ ratios of altered assemblages, known or suspected of having mafic parentage, to the $\text{TiO}_2/\text{Al}_2\text{O}_3$ ratios characteristic of the various sub-groups will help establish the appropriate mafic precursor. For all assemblages of probable and possible mafic precursors, the $\text{TiO}_2/\text{Al}_2\text{O}_3$ values of altered samples were compared to fields defined for low, moderate, and high TiO_2 mafic flows to better constrain the probable precursor composition (Figure 53). The alteration assemblages that fit best to the low TiO_2 mafic flows are chlorite-biotite-quartz-amphibole, quartz-biotite-garnet, sericite-epidote-chlorite-biotite, and the sample containing amphibole-biotite clusters. Lithologic parentage of the chlorite-quartz-biotite assemblage is less definitive;

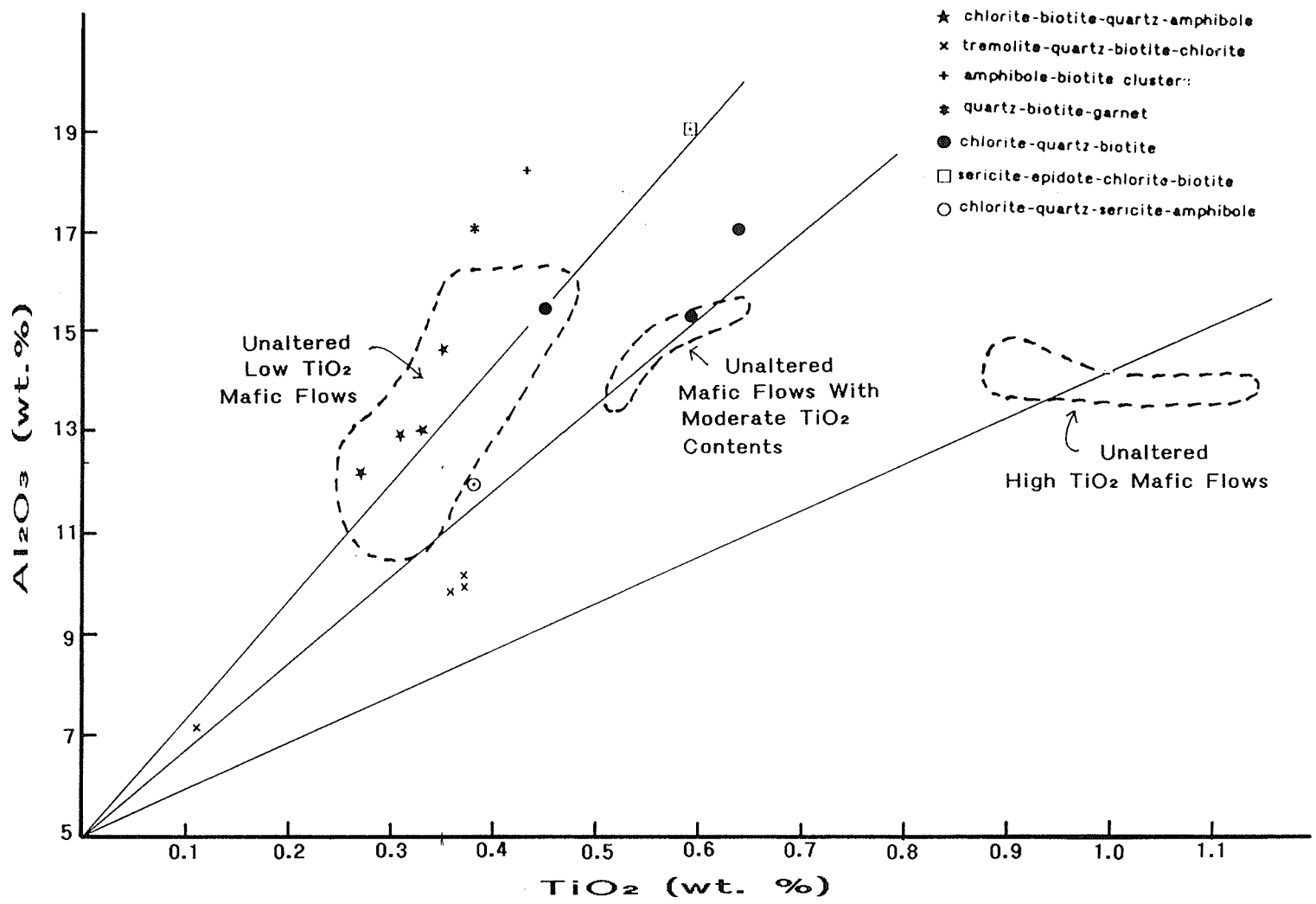


Figure 53: Al₂O₃/TiO₂ ratios of alteration assemblages possibly derived from mafic precursors, compared to characteristic values for the various sub-groups defined in Figure 40. Lines drawn through each field and the origin show possible positions of altered samples derived from each sub-group; altered samples may plot along these lines if TiO₂ and Al₂O₃ were immobile and the rock was subject to a mass gain or loss during alteration.

samples plot on or close to both low TiO_2 and moderate TiO_2 trend lines, or between the two. The chlorite-quartz-sericite-amphibole assemblage plots between the low TiO_2 and moderate TiO_2 trend lines and may have been derived from either. Most samples of the tremolite-quartz-biotite-chlorite assemblage plot between the moderate and high TiO_2 trend lines.

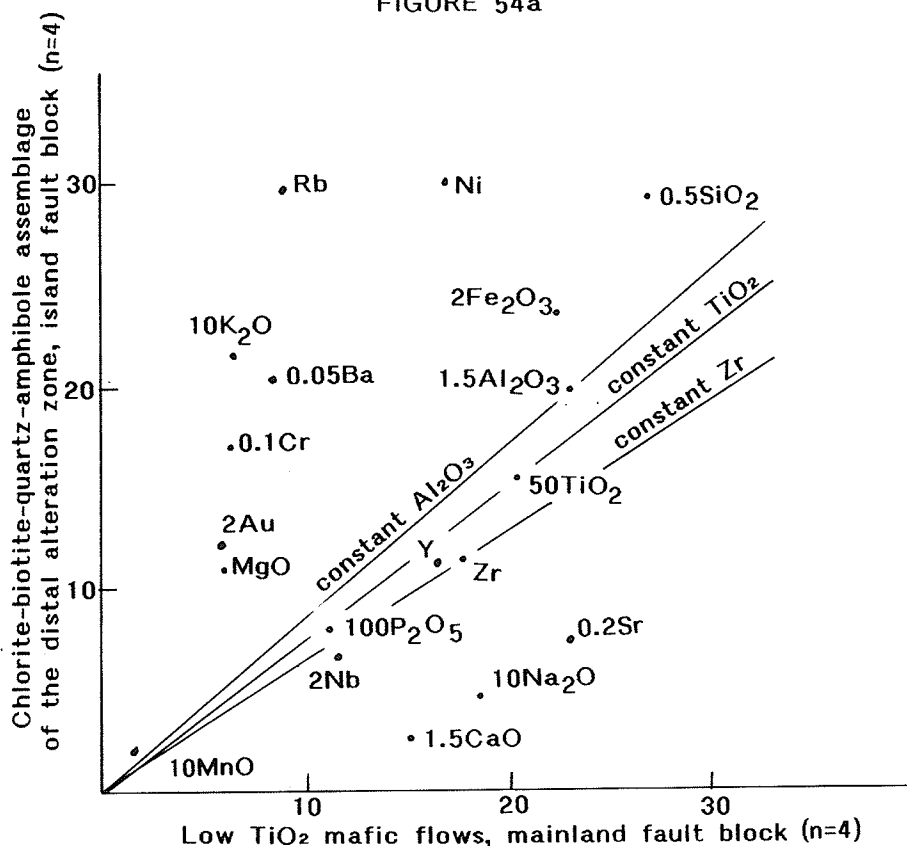
Most mass balance tests were made using averages for each subgroup based only on data from formation 3 of the mainland fault block; data from the island fault block were generally not used because of the greater pervasive alteration there. The chemical data base for primary intermediate rocks is limited, and only one intermediate sample, a plagioclase-phyric flow, was analyzed from formation 3. This sample is from the island fault block, but was used as a control sample because no comparable data are available from the mainland fault block. Because the single moderate TiO_2 mafic flow sample analyzed from formation 3L lacks trace element data, a comparison is also made to moderate TiO_2 mafic samples from formation 3I in order to observe possible changes in trace element values; the behavior of all major elements was determined from the comparison to the mainland sample, due to the pervasive alteration present in the island rock suite. For comparisons to moderate TiO_2 mafic flows from the island fault block, the rocks adjacent to and possibly altered by the intrusion of the gabbro have been excluded from the calculation of the mean; these include all porphyroblastic units listed in Table 5.

There are two methods of mass balancing that are widely used

to determine the chemical effects of alteration: a computational method outlined by Gresens (1967), and a graphical method outlined by Grant (1986). Gresens' method uses an equation relating compositional variation to volume changes. Metasomatic effects can then be determined by calculation of gains and losses of specific chemical components. The method requires that one variable be fixed or known. The usual practice is to assume that either the volume of the rock has remained constant during metasomatism, or that one major element, generally Al_2O_3 , was immobile during the chemical transfer.

In Grant's method, Gresens' equation is re-arranged into a linear relationship between the concentration of a component in the altered rock and that in the original. Simultaneous solution of such equations for all components that show no relative gain or loss of mass defines an isocon, which is a reference line corresponding to a zero concentration change. The choice of isocon fixes the volume and compositional changes. In general, the reference line is determined by a best fit to the data. The isocon may also be based on constant mass, volume, or concentration of some component. The relative gains and losses of mobile components are given by the displacement of data points for all other components from the reference isocon (Figure 54). Components plotting above the isocon have been added; those below the reference line have been lost. Because the inherent assumption that certain elements are immobile during alteration is uncertain, these plots should be used with caution; they are only a general

FIGURE 54a

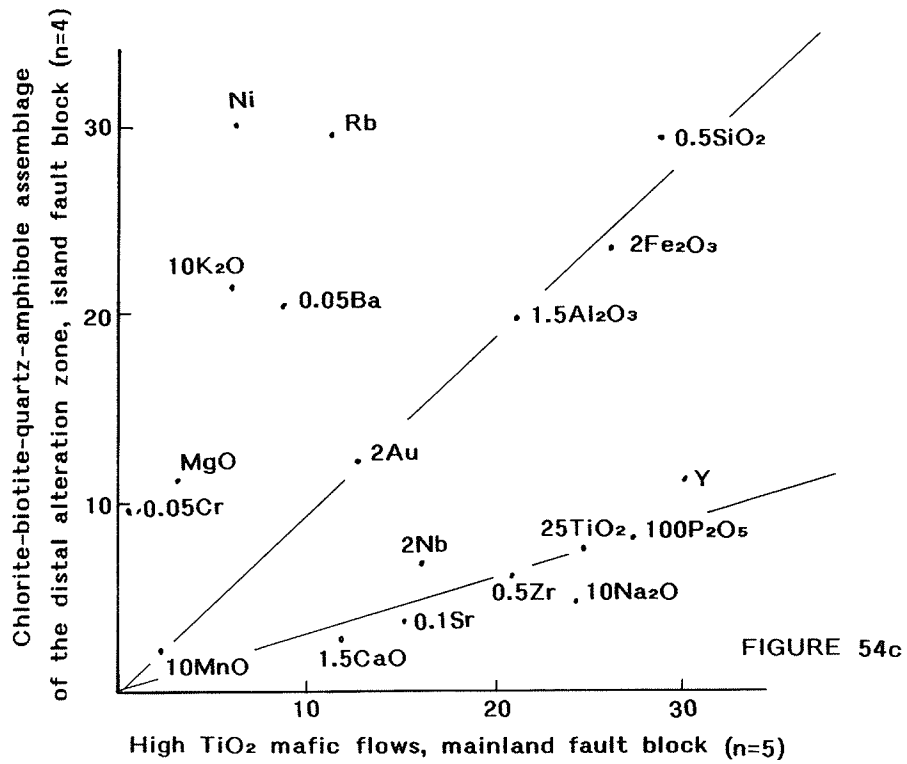
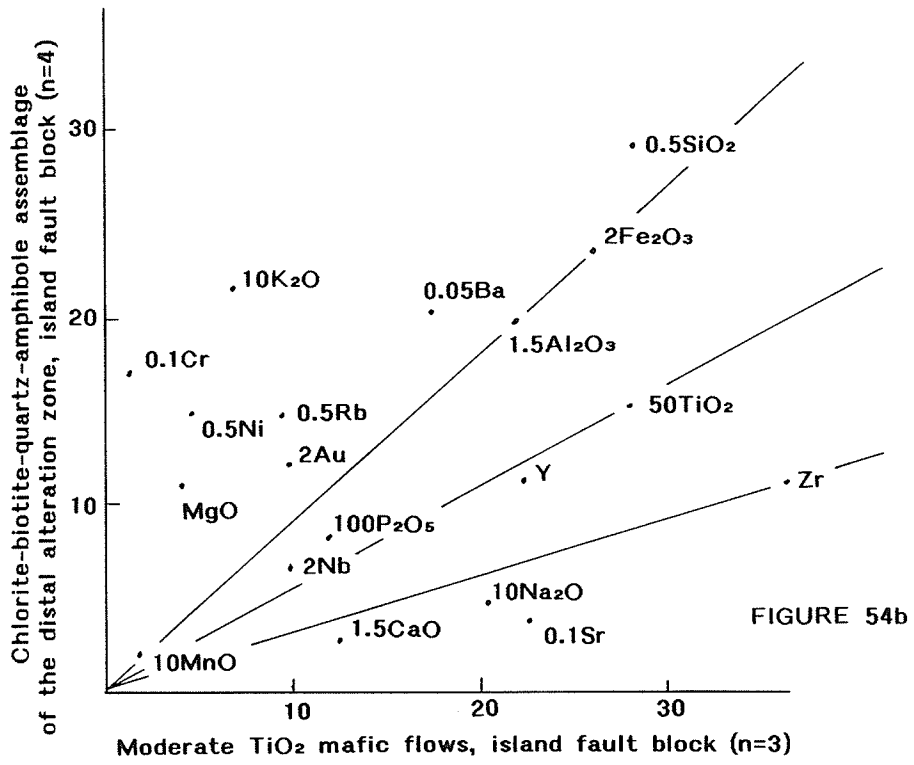


Figures 54 to 63 are isocon diagrams, a graphical procedure to demonstrate gains and losses of elements during alteration. The lines through the origin are isocons, based on the immobility of TiO₂, Zr, or Al₂O₃. Provided the element which defines the isocon is immobile, elements that plot above each isocon are gained during alteration, those plotting below the line are lost. The units used are as follows: wt % for all oxides; ppm for Sr, Rb, Nb, Y, Ni, Cr, and Ba; and ppb for Au. The value of each element or oxide, multiplied by the prefix indicated, corresponds to the number on the x-axis for the assumed precursor, and y-axis for the alteration assemblage interpreted to be derived from it.

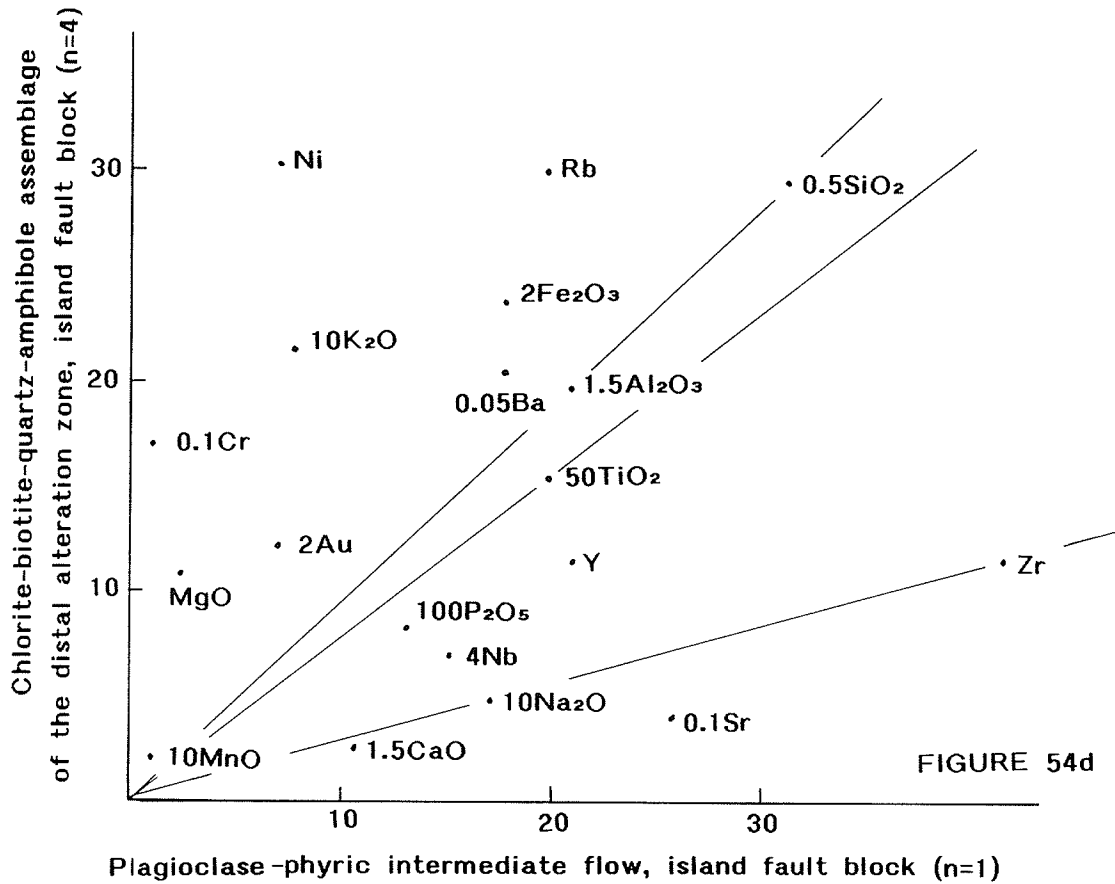
indicator of alteration patterns.

For the purpose of the present study, Grants' isocon method was employed to establish general alteration trends; calculations to determine actual quantitative values of elemental fluxes were not attempted due to the uncertainties mentioned above. On each isocon plot, (Figures 54-63), TiO_2 , Al_2O_3 , and Zr should ideally all lie along a linear trend from the origin, defining an isocon, provided that they are immobile and the correct precursor composition is being compared. In many plots Zr, TiO_2 , and Al_2O_3 do not lie along a linear trend. The Zr data base is smaller than that of TiO_2 and Al_2O_3 and may not be as accurate a representation of changes. Therefore, on each diagram, three different isocons are indicated, each independantly based on TiO_2 , Al_2O_3 , and Zr immobility. The area between the isocons represents the area of uncertainty; the true isocon may lie anywhere within the area, provided that the true precursor has been chosen and at least one of the fore-mentioned elements is immobile. Components that plot outside the area of uncertainty are considered to be mobile.

Samples of each major alteration assemblage described in Chapter 6 have been independently compared to best possible precursor lithologies using the procedures described above. Due to the uncertainty in precursor lithologies for several alteration assemblages, the isocon diagrams themselves were used to further constrain the choice of most likely precursor. For assemblages in which precursors were uncertain, this also provides verification that the most appropriate precursor composition is being compared.



Refer to Figure 54a for explanation of diagrams



Refer to Figure 54a for explanation of diagram

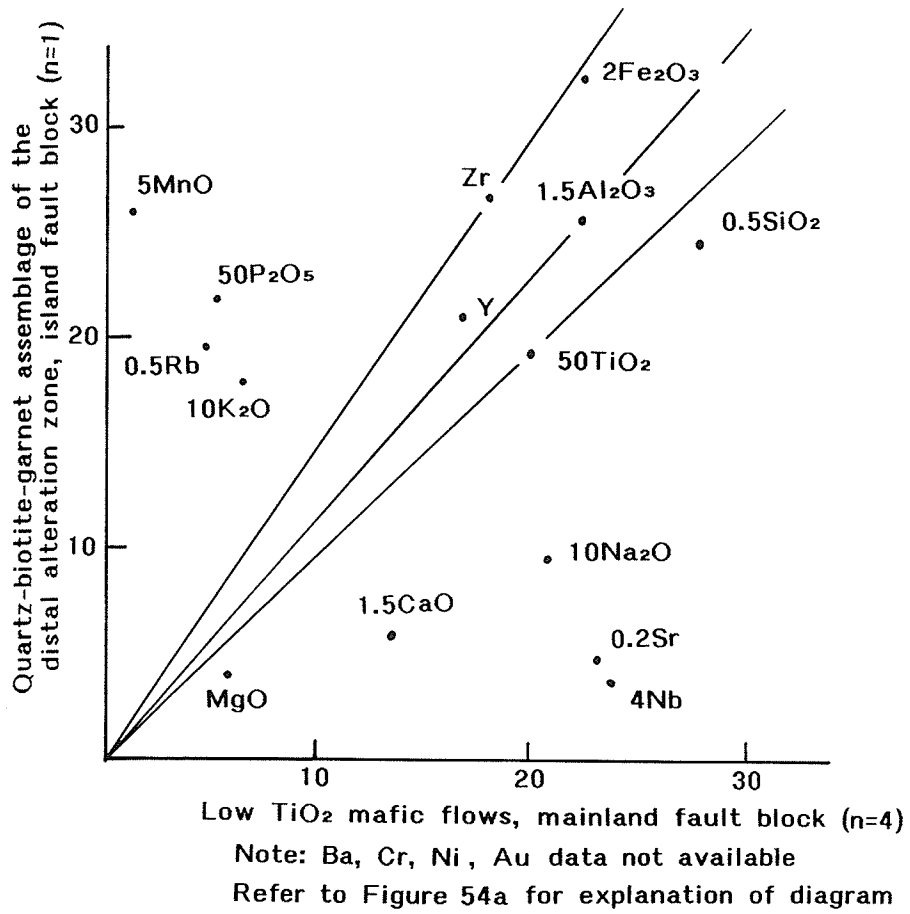
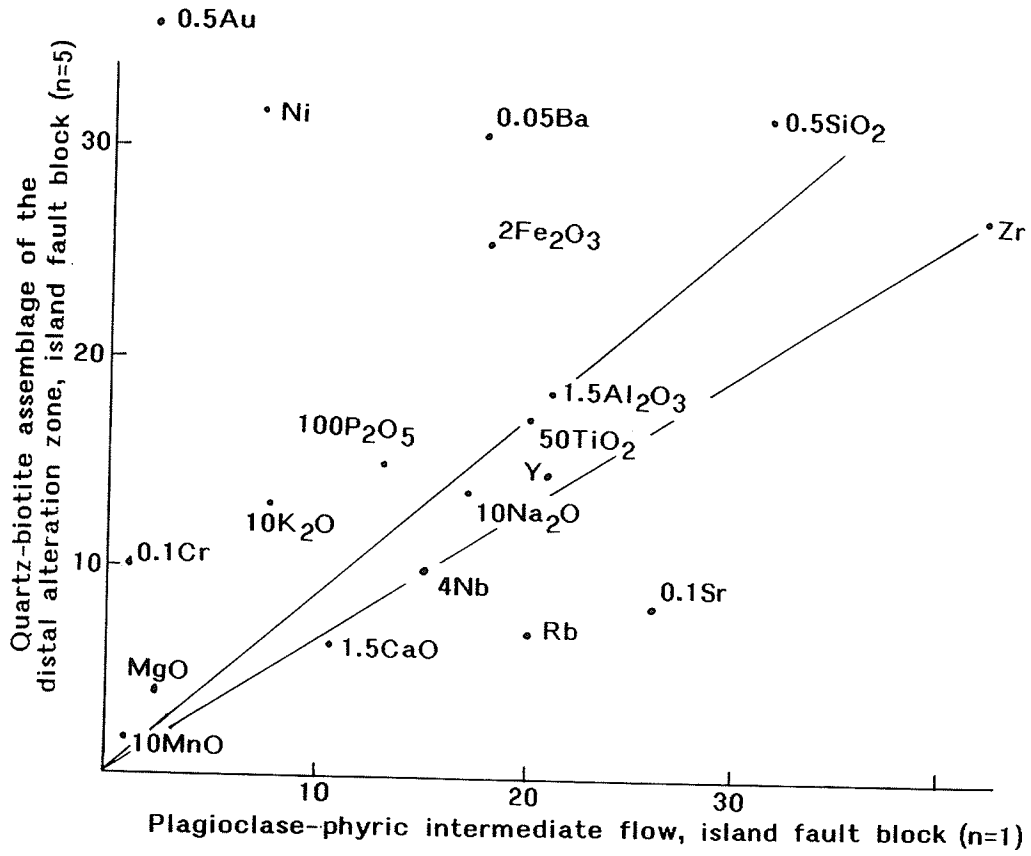


FIGURE 55



Refer to Figure 54a for explanation of diagram

FIGURE 56

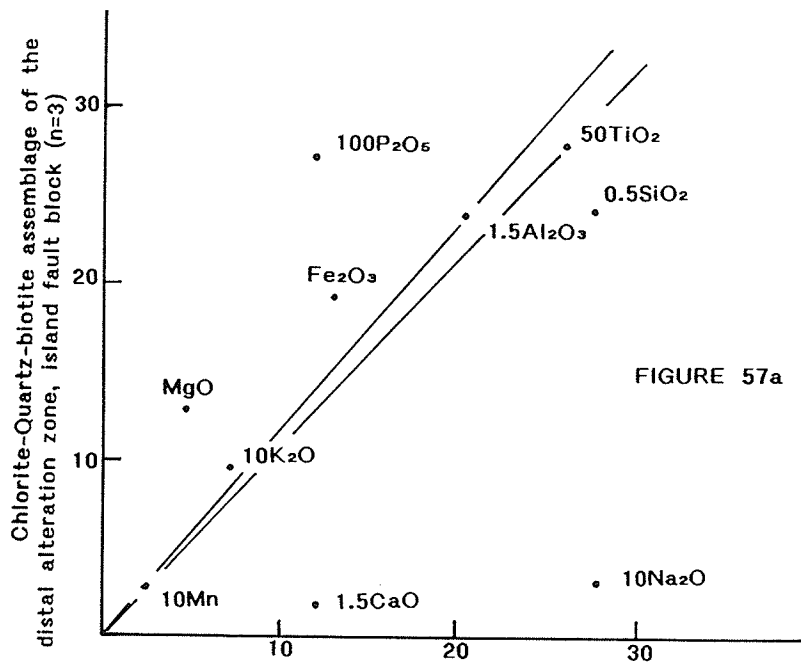


FIGURE 57a

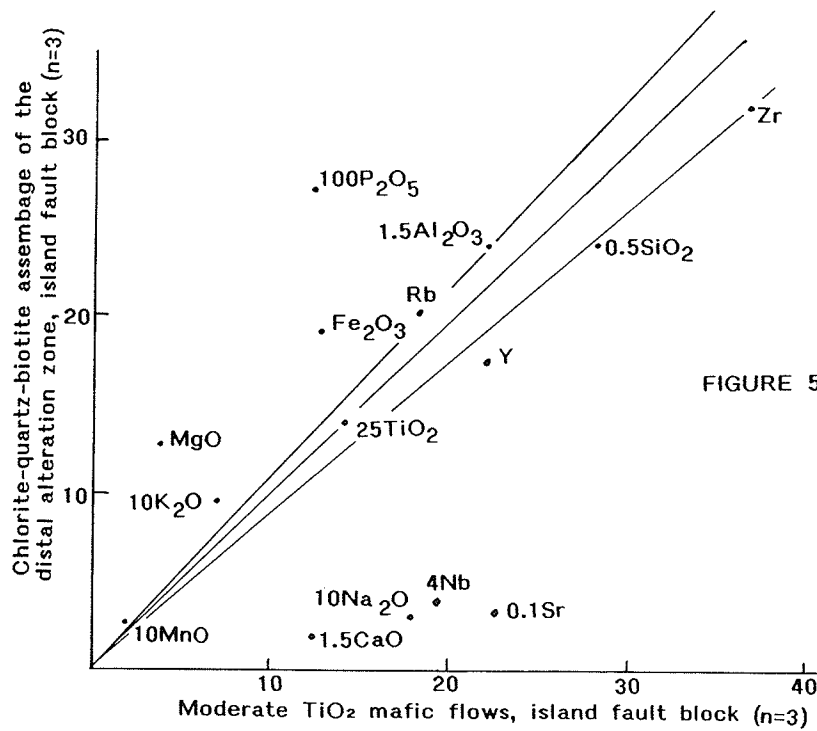


FIGURE 57b

Refer to Figure 54a for explanation of diagrams

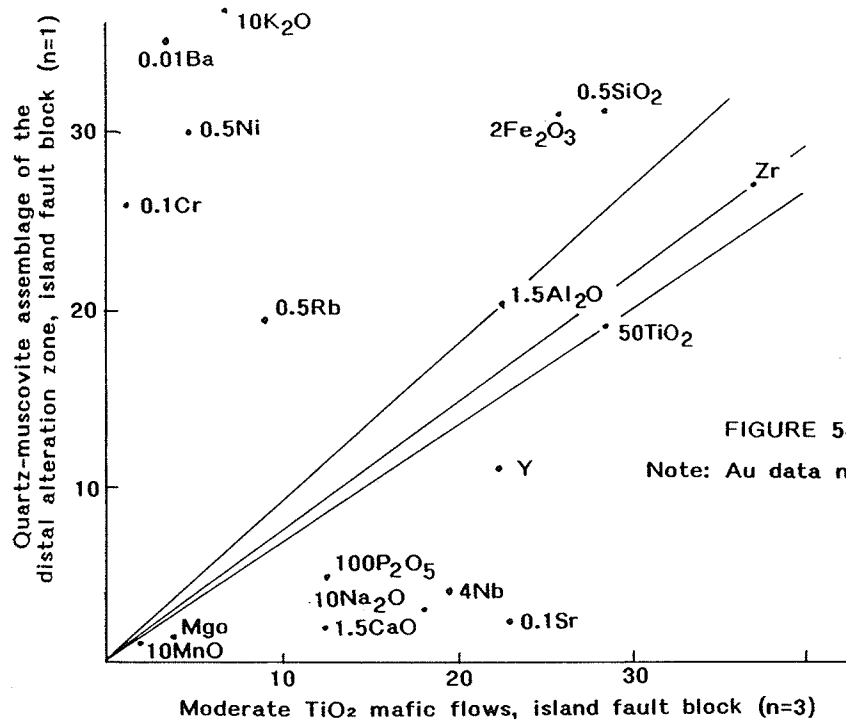


FIGURE 58a

Note: Au data not available

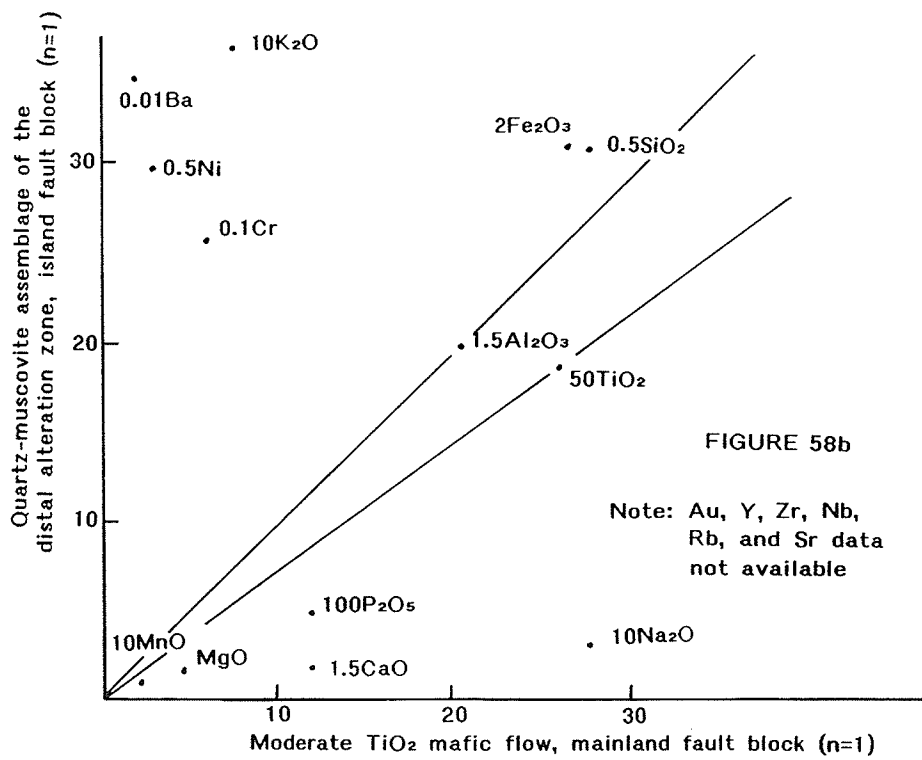
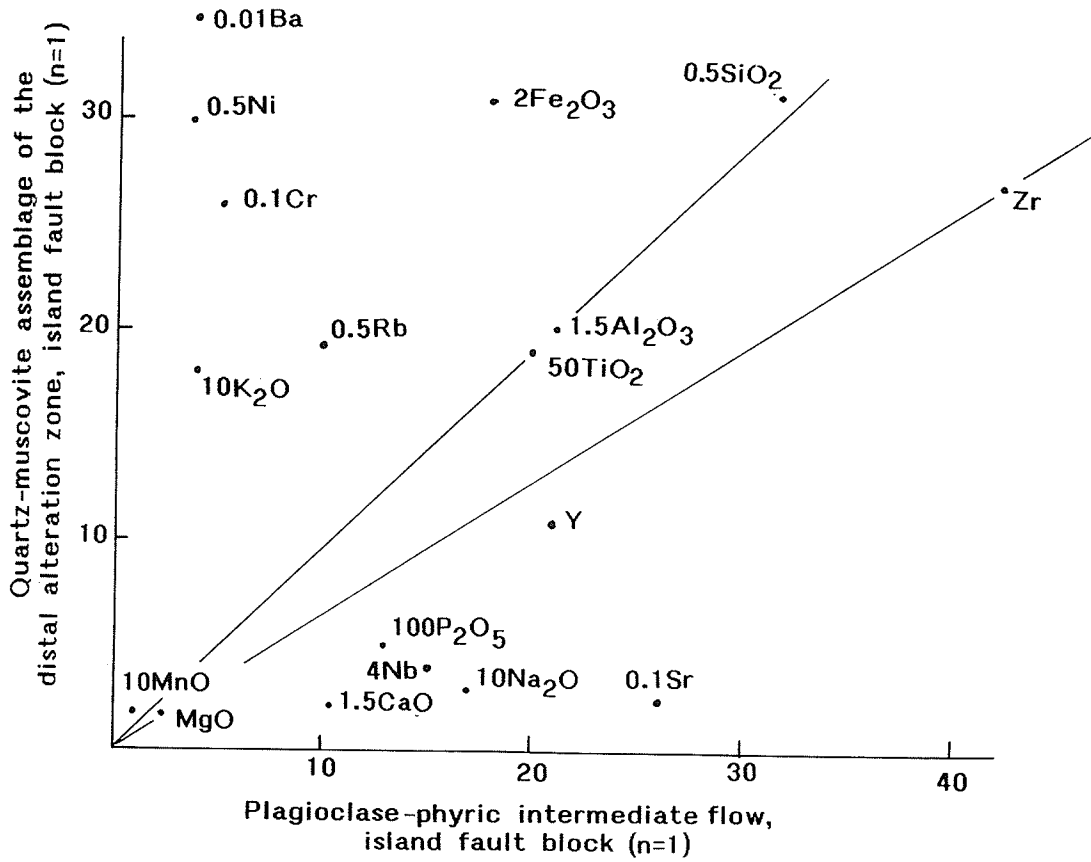


FIGURE 58b

Note: Au, Y, Zr, Nb, Rb, and Sr data not available

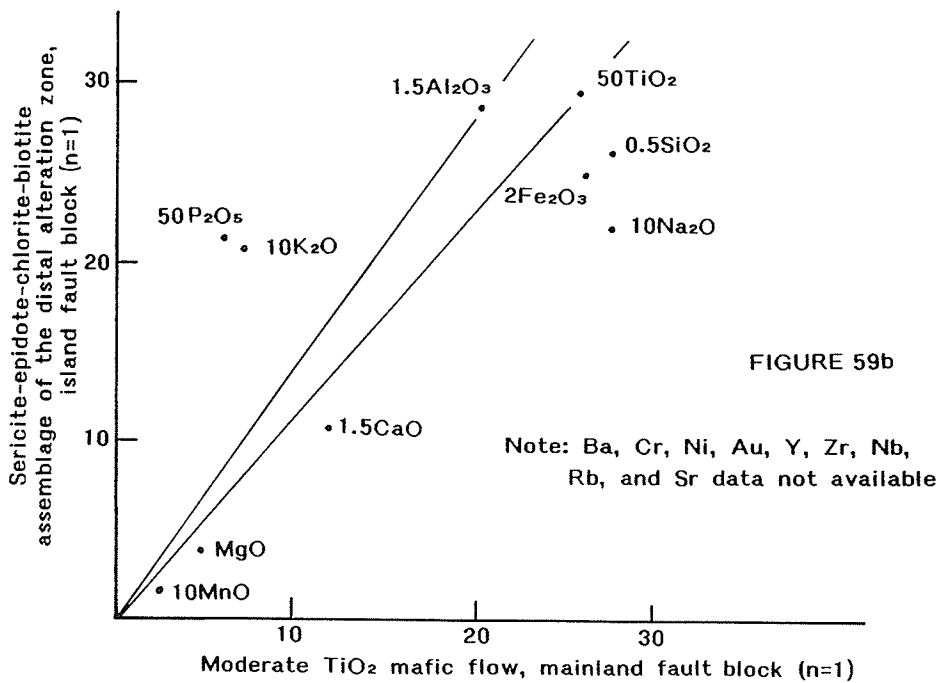
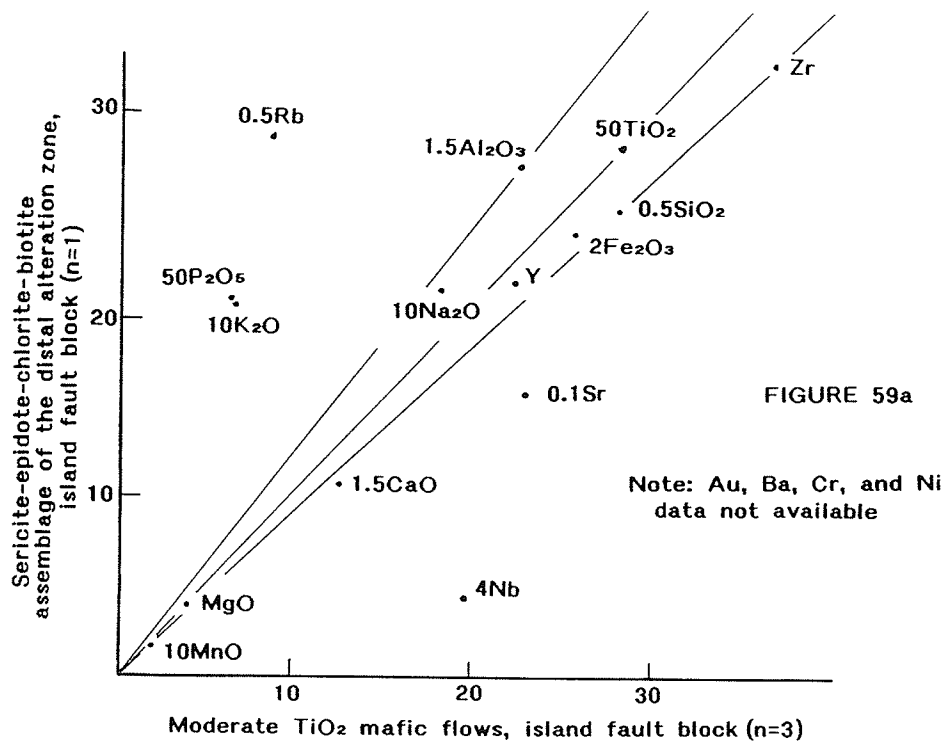
Refer to Figure 54a for explanation of diagrams

FIGURE 58c

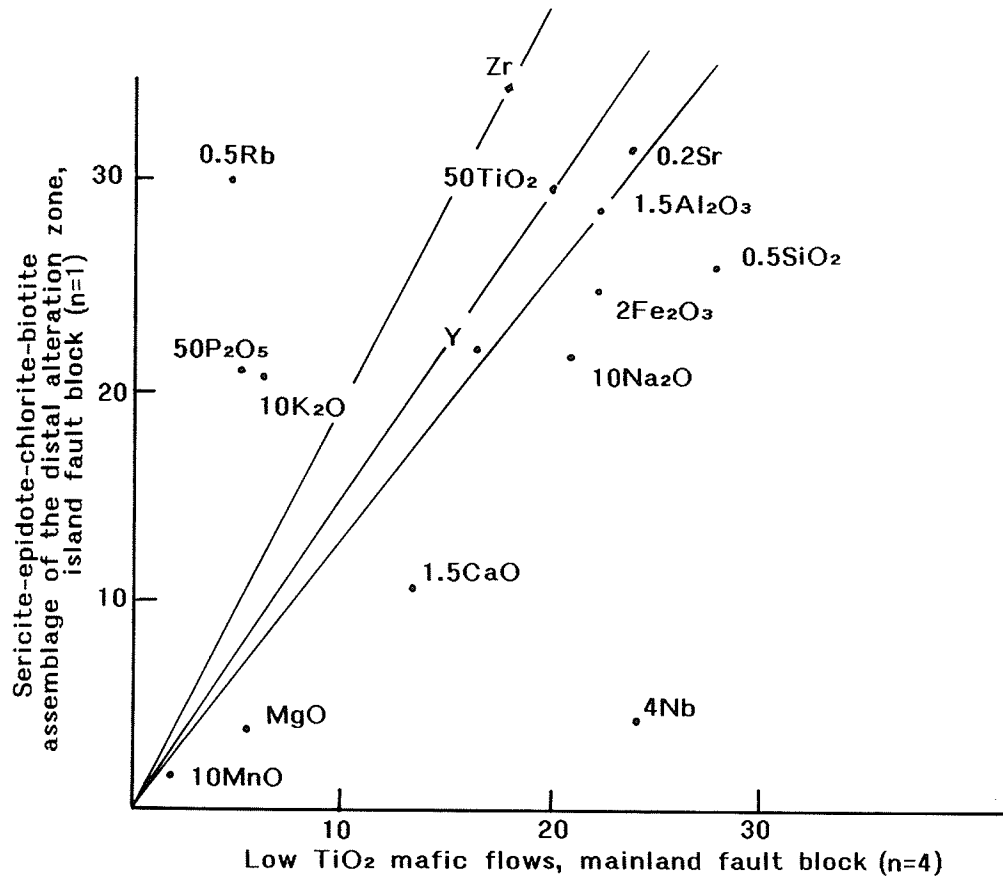


Note: Au data not available

Refer to Figure 54a for explanation of diagram

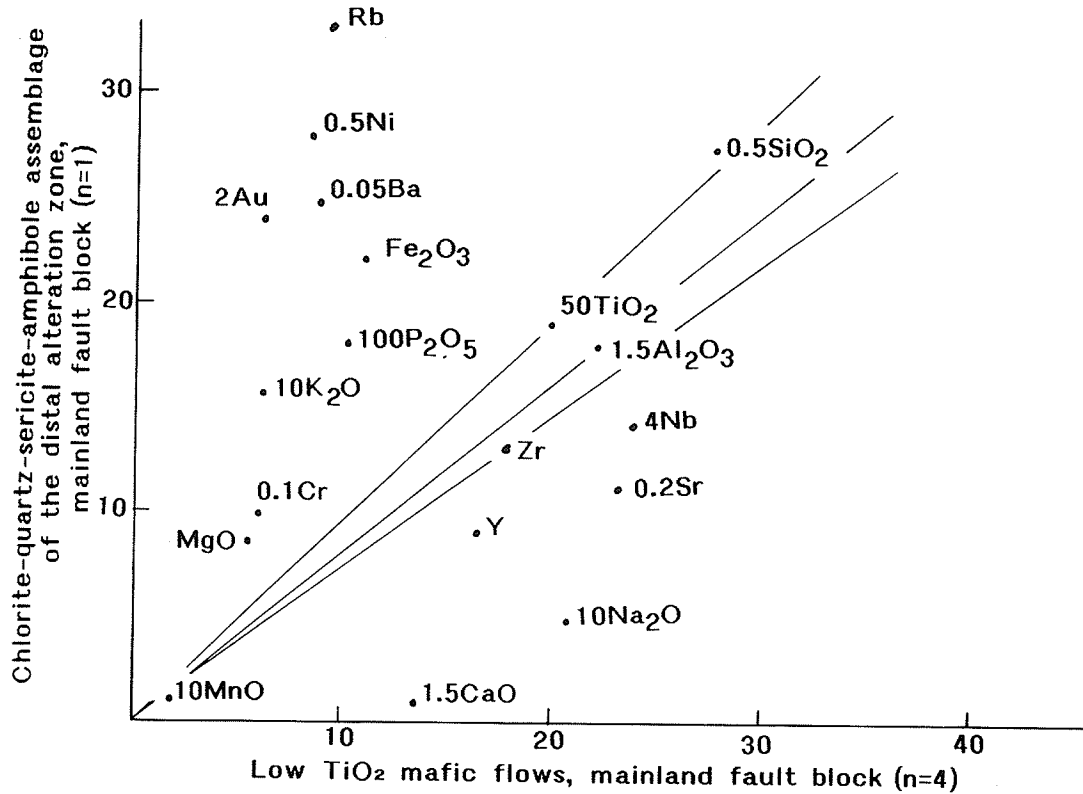


Refer to Figure 54a for explanation of diagrams



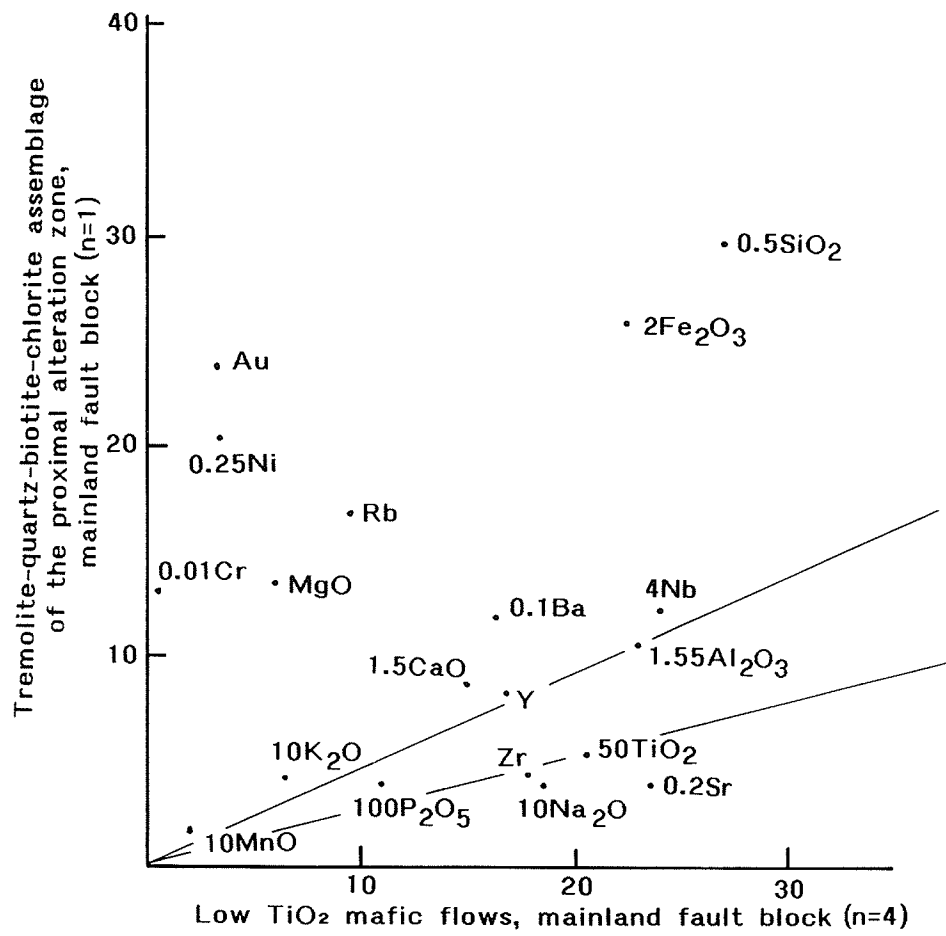
Note: Ba, Cr, Ni, and Au data not available
 Refer to Figure 54a for explanation of diagram

FIGURE 59c



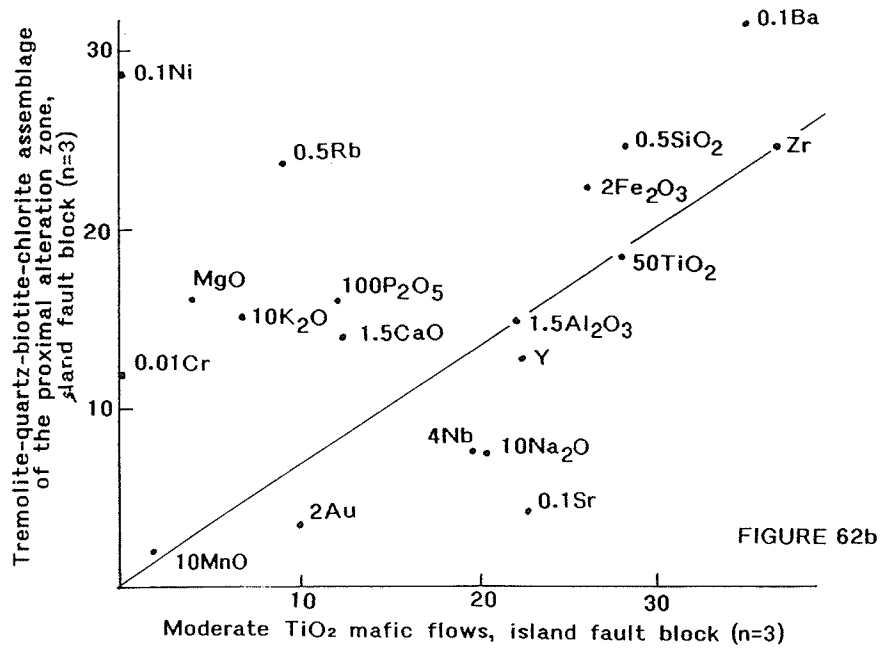
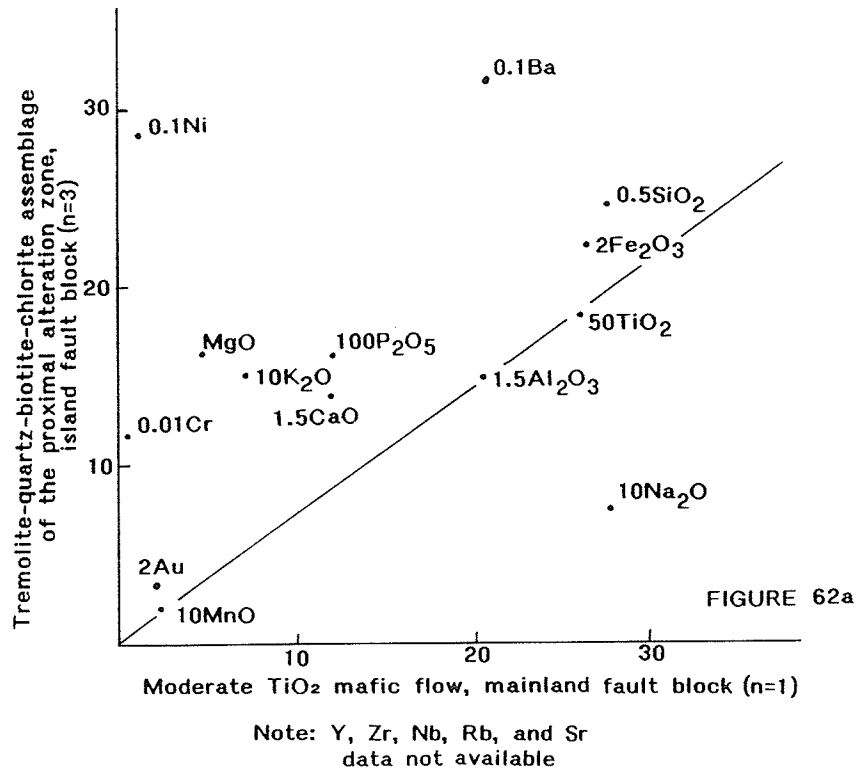
Refer to Figure 54a for explanation of diagram

Figure 60

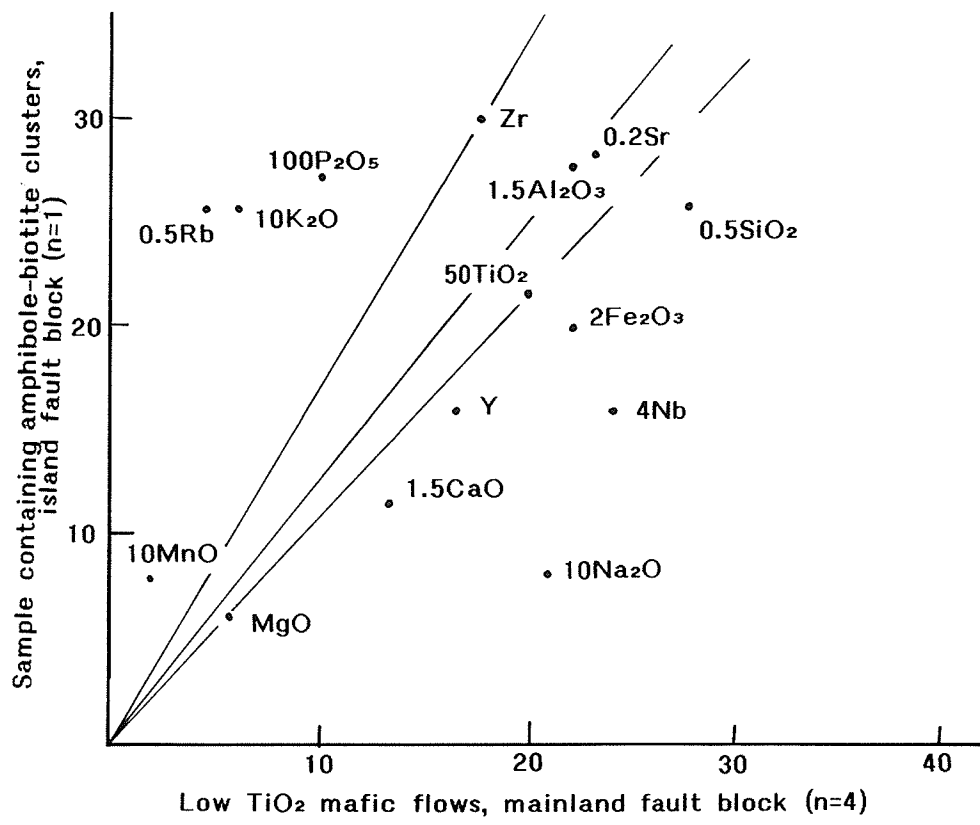


Refer to Figure 54a for explanation of diagram

FIGURE 61



Refer to Figure 54a for explanation of diagrams



Note: Ba, Cr, Ni, and Au data not available

Refer to Figure 54a for explanation of diagram

FIGURE 63

All rock lithologies have been tested as a potential precursor for each alteration assemblage; this data are summarized in Table 8 which indicates the degree to which each control group fits. The data provided in Figure 53 support the precursors chosen on the basis of petrographic and spatial evidence. Comparisons to various felsic lithologies are also indicated to demonstrate how inappropriate these are as potential precursors. For each alteration assemblage, the control group in which the three isocons are most coincident was taken to be the most likely precursor rock type for the assemblage in question and these diagrams are the basis of Figures 54 to 64. Isocon diagrams comparing the chlorite-biotite-quartz-amphibole assemblage to the various mafic sub-groups and the intermediate flow are also provided to illustrate the compatibility of the best fit precursor, relative to other lithologic matches. With the exception of Figures 54b-d, isocon plots for discarded lithologies are not presented. For assemblages quartz-muscovite and sericite-epidote-chlorite-biotite, two precursor types are equally possible for each, and both possibilities are shown (Figures 58a-d, 59a-c). All analyses used were re-calculated on a volatile-free basis. The results have been tabulated in Table 9.

Table 8: Measure of the coincidence of isocons independently based on constant Zr, TiO₂, and Al₂O₃ for each alteration assemblage using various lithologies as a control group. Numbers given are the angle in degrees between the widest spaced isocons; the lowest value for each alteration assemblage represents the most likely precursor lithology based on Ti, Zr, and Al immobility.

	Low TiO ₂ Mafic Flow (3L)	Moderate TiO ₂ Mafic Flow (3I)	High TiO ₂ Mafic Flow (3L)	Plagioclase-phyric Intermediate Flow (3I)	Felsic flow (2L)	Felsic tuff (4L)	Felsic crystal tuff (4L)
Chlorite-biotite- quartz-amphibole	8	25	26	28	39	34	34
Quartz-biotite- garnet	12	15	30	18	38	33	24
Quartz-biotite	21	12	15	8	29	24	25
Chlorite-quartz- biotite	14	6	20	12	35	28	35
Quartz-muscovite	13	8	24	11	31	26	28
Sericite-epidote- chlorite-biotite	11	9	23	16	37	31	32
Chlorite-quartz- sericite-amphibole	8	19	15	26	36	32	37
Tremolite-quartz- biotite-chlorite (mainland fault block)	11	18	21	21	27	24	18
Tremolite-quartz- biotite-chlorite (island fault block)	10	1	15	11	26	20	35
Amphibole-biotite clusters	12	15	29	17	39	33	25

TABLE 9: SUMMARY OF THE VARIOUS ALTERATION TYPES, AND THE CHEMICAL CHANGES INVOLVED IN THE FORMATION OF THE ASSEMBLAGES

DISTAL ALTERATION (ISLAND FAULT BLOCK, UNLESS OTHERWISE SPECIFIED)

ALTERATION ASSEMBLAGE	GAINS	LOSSES	IMMOBILE, UNCERTAIN OR VARIABLE	POSSIBLE PRECURSOR
Chlorite-biotite-quartz-amphibole (Figure 54a)	Mg, Fe, Si, K, Mn? Rb, Ni, Ba, Cr, Au	Ca, Na, Sr, Nb?	Y, P	Low TiO ₂ mafic flow
Quartz-biotite-garnet* (Figure 55)	K, Mn, P, Rb	Ca, Na, Si, Mg, Sr, Nb	Y, Fe	Low TiO ₂ mafic flow
Quartz-biotite (Figure 56)	Mg, Fe, Si, K, P, Ni, Ba, Cr, Au, Mn?	Ca? Sr, Rb	Na, Y, Nb	Plagioclase-phyric intermediate flow
Chlorite-quartz-biotite* (Figure 57a,b)	Mg, Fe, K? P	Ca, Na, Si, Sr, Nb, Y	Mn, Rb	Moderate TiO ₂ mafic flow
Quartz-muscovite +/-biotite* (Figure 58a,b,c)	K, Rb, Ni, Ba, Fe, Si, Cr	Ca, Na, P, Sr, Nb, Y	Mn, Mg, Fe, Si	Plagioclase-phyric intermediate flow, or moderate TiO ₂ mafic flow
Sericite-epidote-chlorite-biotite* (Figure 59a,b,c)	K, P, Rb	Ca, Na, Si, Mg, Fe, Nb, Mn?	Y, Sr	Low or moderate TiO ₂ mafic flow
Chlorite-quartz-sericite-amphibole (Figure 60) Mainland fault block	Mg, Fe, K, P, Rb, Ni, Ba, Cr, Au Si?	Ca, Na, Sr, Nb, Y, Mn?		Low TiO ₂ mafic flow

PROXIMAL ALTERATION

Tremolite-quartz-biotite-chlorite Mainland fault block (Figure 61)	Ca, Mg, Fe, Si, K, Mn? Rb, Ni, Ba, Nb, Cr, Au, Y?	Na, Sr,	P	Low TiO ₂ mafic flow
Tremolite-quartz-biotite-chlorite Island fault block (Figure 62a,b)	Ca, Mg, Fe, Si, K, P, Rb, Ni, Ba, Cr, Au,	Na, Sr, Nb, Y	Mn	Moderate TiO ₂ mafic flow

PERIPHERAL TYPE (ISLAND FAULT BLOCK)

Biotite-amphibole clusters* (Figure 63)	K, P, Mn, Rb	Ca, Na, Si, Fe, Nb, Y	Sr, Mg	Low TiO ₂ mafic flow
--	--------------	--------------------------	--------	------------------------------------

* Y, Zr, Nb, Sr, Rb, &/or Ba, Cr, Ni, Au data not available

7.4 CHANGES IN WHOLE ROCK CHEMISTRY - RESULTS

7.4.1 Distal Alteration Zones

The central part of the distal alteration zone in the island fault block, sub-zone 1 in Figure 26, is dominated by the alteration assemblage chlorite-biotite-quartz-amphibole; a single sample of the quartz-biotite-garnet assemblage was also obtained from this sub-zone. Figures 54a, 55, and Table 8, verify the conclusion drawn from Figure 53 that both assemblages appear to have been derived from low TiO_2 mafic flows. In the chlorite-biotite-quartz-amphibole assemblage, the dominant component of sub-zone 1, the central part of the distal zone, is characterized by the following trends: (1) addition of Mg, Fe, Si, Rb, Ni, Ba, Cr, K, and Au (Table 9); (2) loss of Sr, Na, Nb, and Ca (Table 9); (3) and no change in P and Y. In the less common quartz-biotite-garnet assemblage, Mg and Si show losses, P shows a gain, and Fe is immobile.

Sub-zone 2 of the distal alteration zone in the island fault block is characterized by assemblages quartz-biotite, quartz-muscovite+/-biotite, and chlorite-quartz-biotite. Based on petrographic data, the quartz-biotite assemblage is interpreted to be derived from plagioclase-phyric intermediate flows; petrographic and spatial relations also indicate that the quartz-muscovite+/-biotite assemblage may have been derived from an intermediate or felsic precursor. The parental lithology of the chlorite-quartz-

biotite assemblage could not be determined from petrographic data, but based on stratigraphic position both mafic and intermediate precursors would be possible. A comparison of TiO_2 and Zr contents to potential precursor lithologies indicates that assemblages proposed to have mafic precursors predominantly lie close to the mafic trend line; the assemblages proposed to have intermediate precursor straddle the boundary between intermediate and mafic fields (Figure 52). Consequently, assemblages proposed to have been derived from intermediate precursors were compared to the intermediate plagioclase-phyric flow as well as the various mafic lithologies. The isocon diagrams indicate that the quartz-muscovite+/-biotite assemblage could have been derived equally well from moderate TiO_2 mafic flows or plagioclase-phyric intermediate flows; both possibilities are provided (Figures 58a,b,c). The isocon plots indicate that the chlorite-quartz-biotite assemblage is most likely derived from moderate TiO_2 mafic flows (Table 8). Although trace element data are not available for all assemblages, the isocon plots indicate that similar chemical changes took place in all alteration assemblages of sub-zone 2, regardless of precursor types (Figures 56, 57, 58; Table 9). These changes include (1) addition of K, Fe, and for assemblages with trace element data, addition also of Au, Ni, Ba, and Cr (Table 9); (2) loss of Ca and Sr (Table 9); (3) no change or loss of Y, Na, and Nb (Table 9); (4) movement of Si, Mg, P, and Rb is variable and varies from gains to losses to no change depending on the assemblage; and 5) no change or addition of Mn.

Sub-zone 3, which forms the northwest and southeast margins of the distal alteration zone of the island fault block, is characterized by the assemblages chlorite-quartz-sericite-amphibole and sericite-epidote-chlorite-biotite. Based on the best fit isocons, the chlorite-quartz-sericite-amphibole assemblages appear to have been derived from low TiO_2 mafic flows; the sericite-epidote-chlorite-biotite assemblage may have had a low TiO_2 or moderate TiO_2 mafic precursor. Trace element data are not available for all assemblages, but the isocon diagrams indicate that similar chemical changes took place in both alteration assemblages, regardless of precursor types (Figures 59, 60; Table 9). The alteration in sub-zone 3 is characterized by the following chemical trends: (1) addition of K, P, and Rb, and for assemblages with trace element data, addition also of Cr, Au, Ni, and Ba (Table 9); (2) loss of Ca, Na, and Nb (Table 9); (3) variable change of Fe, Si, and Mg with either gains or losses, depending on the assemblage (Table 9); (4) no change or loss of Sr and Y, depending on the assemblage (Table 9); and 50 slight loss of Mn, but Mn lies close to an isocon making this conclusion tenuous.

7.4.2 Proximal Alteration Zones

Geochemical data are only available for a single assemblage of the proximal alteration zone, the tremolite-quartz-biotite-chlorite

assemblage. This assemblage in the island fault block appears to have been derived from moderate TiO_2 mafic flows, whereas the single sample from the mainland fault block for which chemistry is available seems to have been derived from a low TiO_2 mafic flow (Figure 53: Table 8). Isocon diagrams indicate the following chemical trends in proximal alteration zones of both island and mainland fault blocks: Ni, Rb, Mg, K, Ca, Ba, Si, Au and Fe are gained; Na and Sr are lost; and depending on fault block, Y and Nb may show gains or losses, and P and Mn may be immobile or gained.

Visual examination of the chemical analyses shows that the tremolite-quartz-biotite-chlorite assemblage is notable for extremely high elemental abundances of Mg, Cr, and Ni, much greater than any other altered or unaltered rock types (Tables 5, 6, 7). Similar high Mg-Cr-Ni rocks are associated with other sulfide deposits, and opinion on the genesis of these rocks varies. High Mg-Cr-Ni wallrocks in the Pyriton district of Alabama (Stow and Tull, 1982) are interpreted to represent a primary lithology rather than the product of metasomatic addition of Mg, Cr and Ni. Another occurrence of high Mg-Cr-Ni rocks is found at the MacLellan Mine in the Lynn Lake greenstone belt of Manitoba. Fedikow (1986) has proposed a primary origin for the unit, although others have proposed that the rock type is an alteration product. At Vamp Lake, the high Mg-Cr-Ni rocks that are represented by the tremolite-quartz-biotite-chlorite assemblage have similar chemical trends as other alteration types. This feature, plus the association of the assemblage with mineralization and the thinness of the unit

suggests that it is the result of alteration.

7.4.3 Peripheral Alteration

The only forms of peripheral alteration for which chemical data are available are samples containing biotite-amphibole clusters and chlorite-epidote veining (Table 7). The chlorite-epidote veining has not been tested for element mobility because the alteration forms a very minor amount of the rock in which it is contained. The sample containing biotite-amphibole alteration was compared to the most probable precursor for this particular sample, low TiO₂ mafic flows (Figure 62). The diagram indicates that the alteration resulted in the following chemical changes: (1) an increase in Rb, K, P, and Mn; and (2) a decrease in Ca, Y, Fe, Si, Nb, and Na. Sr and Mg appear to be virtually immobile.

7.5 Summary of the chemical features of alteration

It would appear that elemental fluxes during alteration were generally similar in all assemblages examined from both distal and peripheral alteration zones. The result was a consistent gain in K, Ni, Cr, Ba, and Au; and a gain in Rb, Fe, Mg, P, and Si in most assemblages. Ca is inevitably lost; Na, Sr, and Nb are usually lost. The movement of Y and Mn is variable, depending on alteration

assemblage: Y is either immobile, or lost; and Mn may show gains or losses. In the case of uncertain precursors, similar elemental trends are evident regardless of which primary sub-group was used as control.

The tremolite-quartz-biotite-chlorite assemblage of the proximal alteration zones show similar trends as distal and peripheral alteration zones for most elements, with one major exception; Ca is gained rather than lost. Without additional chemical data on other assemblages of the proximal alteration zones, it cannot be established whether this difference is ubiquitous to all alteration assemblages proximal to the mineralization.

7.6 MINERAL CHEMISTRY

7.6.1 Chemical variations of chlorite

Changes in the chemical composition of chlorite, with its extensive solid-solution series, can be a useful indicator of metasomatic alteration. Variation in Al/Al+Si and/or Fe/Fe+Mg values reflect the extent of alteration (Zhong et al, 1985). A total of 35 chlorite crystals from various locations in each alteration zone were chemically analyzed by electron microprobe to

determine chlorite composition changes as a function of alteration assemblage, type of alteration zone, or position in alteration zone. The complete analyses for all samples are listed in Appendix C.

The results have been plotted on a chlorite discrimination diagram (Figure 64), which indicates that three types of chlorite are present. According to this classification, most of the chlorites are ripidolites, although there is some overlap into the pynochlorite and sheridanite fields.

On an Fe/Fe+Mg vs Al/Al+Si diagram (Figure 65) it can be seen that, at Vamp Lake, the observed interference colors of chlorites are related to chemical composition, and can be used as a general compositional indicator. The general correlation between interference color and chlorite composition has been noted in previous studies (Frater, 1983). This figure also shows that there is a wide range of chlorite compositions in the altered rocks, and a large variation in chlorite composition in some samples.

In Figures 66 and 67, the analyses are differentiated by type of alteration zone, hosting fault block, alteration assemblage, and amount of chlorite present in the sample as a general indicator of degree of chlorite alteration. Several trends are evident from these diagrams. Generally, chlorites from the marginal and peripheral regions of the distal alteration zone in the island fault block are chemically more variable in character, both among and within samples, than central regions. This may be indicative of the presence of chlorite unrelated to the alteration in peripheral

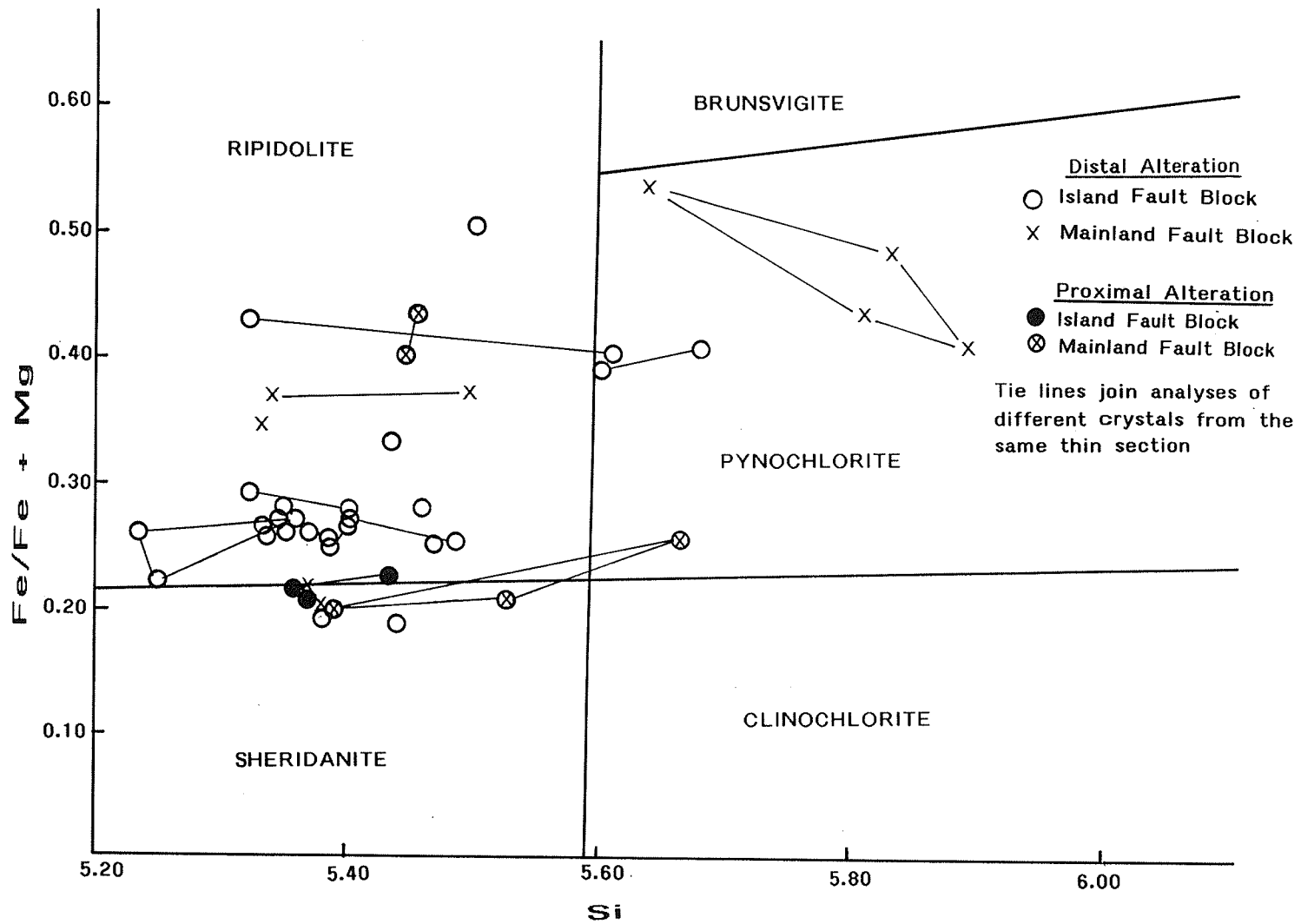


FIGURE 64: CLASSIFICATION OF CHLORITES ACCORDING TO HEY (1954)

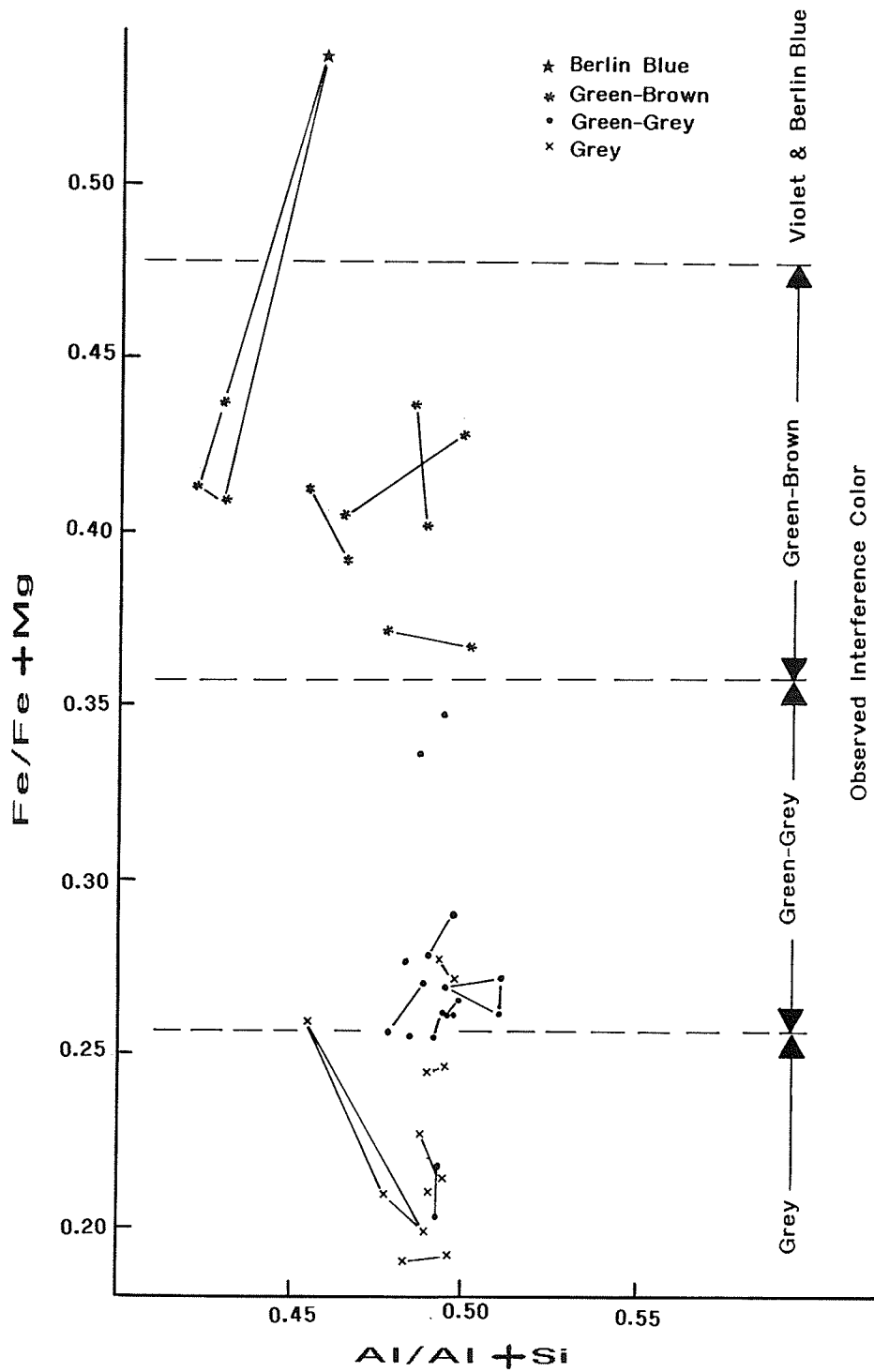


FIGURE 65: COMPOSITION OF CHLORITE; RELATIONSHIP TO OBSERVED INTERFERENCE COLOR

Note: tie lines join analyses of different crystals from the same thin section

DISTAL ALTERATION ZONES

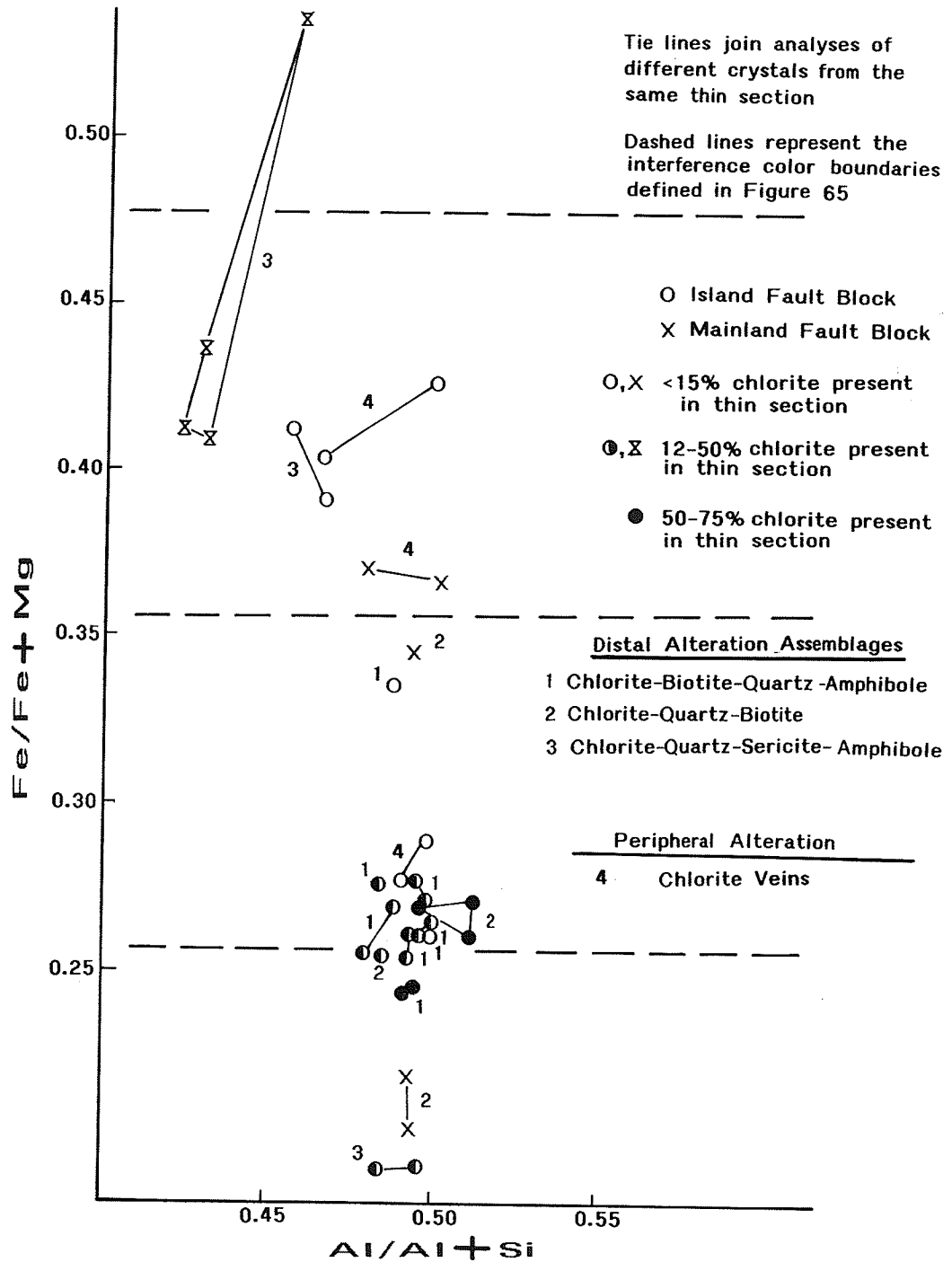


FIGURE 66: RELATIONSHIP BETWEEN ALTERATION ASSEMBLAGE TYPE AND CHLORITE COMPOSITION WITHIN DISTAL ALTERATION ZONES

PROXIMAL ALTERATION ZONES

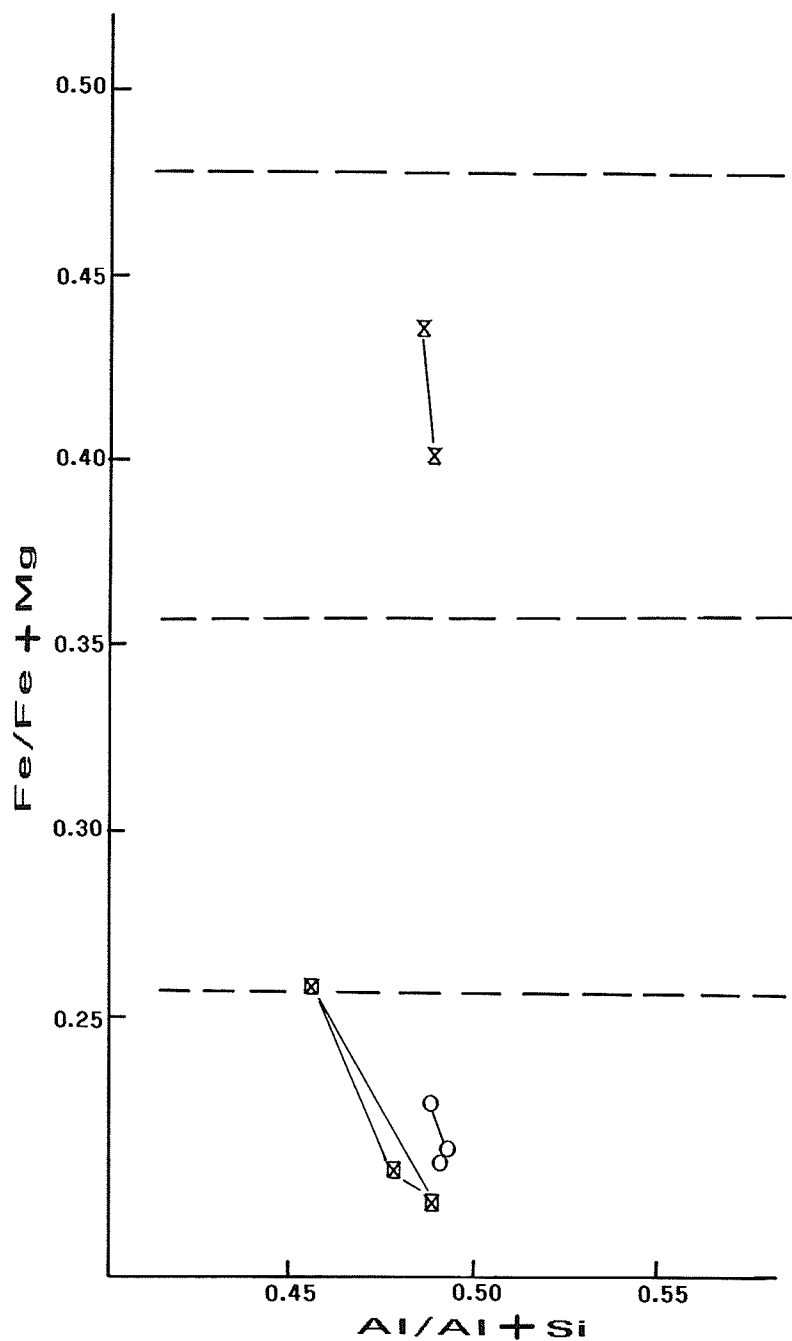


FIGURE 67: COMPOSITION OF CHLORITE FROM THE TREMOLITE-QUARTZ-BIOTITE-CHLORITE ALTERATION ASSEMBLAGE OF PROXIMAL ALTERATION ZONES

Refer to Figure 66 for explanation of symbols used

and marginal samples. Chlorite from the chlorite-biotite-quartz-amphibole alteration assemblage from the central part of the island distal alteration zone are concentrated in one area of the plot and show the least variation in composition. In two of three samples, chlorite from proximal alteration zones are slightly more Mg-rich than chlorite from the central part of the distal alteration zone (Figures 66, 67). In general, chlorite from similar alteration assemblages from each fault block are characterized by similar compositions.

7.6.2 Biotite-Chlorite Intergrowths

As discussed in section 6.3, proximal alteration assemblages contain crystals that optically resemble green biotite. Several of these crystals were analyzed with the electron microprobe to determine their composition. The results indicate a wide range in composition between samples and even within individual crystals. The resultant analyses (see Appendix C) indicate that these crystals are a mixture of chlorite and biotite. Although Mg, Fe and Al are relatively constant in all analyses, the chlorite-like parts contain more H₂O and less Si, K and Ti than the biotite-like parts; all intermediate states between the two end members occur. These results indicate that these crystals are actually composed of intimately intergrown chlorite and biotite, probably the result of the chloritization of biotite.

Similar crystals have been the focus of other studies that

have tried to determine the mechanism of the biotite-chlorite transformation. Banos and Amouric (1984) have proposed that the process is a solid-state reaction produced by the brucitization of the interlayer levels (K planes) of biotite. Alternatively, Veblen and Ferry (1983) have proposed that chloritization occurs by the replacement of tetrahedral-octahedral-tetrahedral mica layers in biotite by brucite-like layers. The transformation has been proposed to involve the introduction of H₂O, H⁺, Mg and Fe, and major losses of K and Si (Veblen & Ferry, 1983).

Chapter 8

MINERALIZATION

There are two mineralization occurrences or zones in the Vamp Lake area. The largest zone is partly exposed on the large island of the island fault block, whereas the smaller, less economically important second zone occurs under the lake in the mainland fault block, about 400 m west of, and along strike from the island zone (Figure 5). These will be referred to as the island zone and the lake zone respectively. Both zones are concordant with host strata.

The island zone has been traced from the surface outcrops on the island to a depth of 350 m, and has been traced for a strike length of 190 m (Figures 8-12). The island zone has a maximum thickness of 18 m. At the present erosion surface, a second sulfide zone occurs 20 m above the main mineralization zone; the distance between the two zones decreases with depth, and the 2 mineralized zones appear to merge at a depth of 90 m (Figures 8, 9). Mineralization in this upper zone has been traced for a strike length of 60 m. Mineralization in the island ore zone is composed of 2 distinct ore types based on economic components and their characteristics; an auriferous Cu-Zn rich ore, and a Zn-rich ore.

Although sulfide mineralization remains open at depth, most of the economic ore grade material occurs as a 1.5-14.7 m thick auriferous Cu-Zn ore lens between 200 and 275 m depth in the lower ore unit; this lens has been traced for a strike length of 120 m and plunges approximately 75 degrees northeast. A second economic grade massive sulfide lens, 15 m thick, forms the upper ore unit;

it outcrops at the surface of the ore discovery island, and has been traced to a depth of 90 m along a strike length of 60 m. Ore intersections of this second zone were unavailable for examination, and therefore the mineralogical and textural characteristics of the body are unknown. As such, the subsequent descriptions of the island ore zone refer only to the lower unit. Assay results indicate that this upper ore zone contains both Cu-Zn and Zn-rich ore; neither is gold-rich. The remainder of the island ore zone consists of disseminated sulfide minerals that contain only minor Cu and Zn, locally grading into thin lenses of high sulfide mineral content. These types are described in detail in sections 8.1 to 8.1.2.2.

The lake ore zone is a high sulfide content Zn-Cu ore body that intersects the lake bottom 250 m west of the ore discovery island. The tabular-shaped body has a strike length of 134 m, is 12 m thick at its widest point, and can be traced from the 4 m deep lake bottom to a depth of 95 m. In the lake zone, disseminated sulfides only occur in the proximal alteration zone.

Total tonnage of proven ore reserves of the Vamp Lake deposit is reported to be 422,422 tonnes (Walker, 1985). This is a combination of the island ore zone (218,904 tonnes) and the lake zone (203,518 tonnes). Ore grade estimates for the island ore zone were given as 6.07 g/t Au (values cut to 34.28g/t); 17.14 g/t Ag; 2.13% Cu; and 2.2% Zn. The lake zone has significantly lower grades of 2.36 g/t Au; 12.0 g/t Ag; 1.16% Cu; and 2.3% Zn.

8.1 CHARACTERISTICS OF THE ISLAND ORE ZONE

Sulfide mineralization in the island fault block can be subdivided into three general types based on mineralogy, textures, economic components, and location. Two economic and subeconomic ore types have been differentiated; the third sulfide type is non-economic. The spatial relationships of the various sulfide types and host rocks, and typical ore grades for each sulfide type, are illustrated in several representative drill hole sections provided in Figures 68-72. For the purpose of this discussion, the terms economic and subeconomic are relative, and are not necessarily meant to imply actual mineable ores for monetary profit.

The Cu-Zn sulfide ore is generally restricted to a stratiform 1.5-14.7 m thick lens at a depth of 200 to 275 m below surface and at the extreme eastern end of the island ore zone. The lens has a strike length of 120 m. In this location it forms the base of the island ore zone, in contact with altered mafic footwall rocks. This ore type is commonly overlain by a concordant, economic to subeconomic Zn-rich ore, 0.45 to 3.0 m thick, which extends laterally outward forming the remainder of the island ore zone. The contact between the Cu-Zn and Zn-rich ore is relatively sharp.

Disseminated mineralization is found 1.5-7.6 m above, and up to 1.2 m below, the main ore lens. In outer margins of the island ore zone, and where the Cu-Zn ore is absent, the disseminated sulfide zones are more diffuse and occur in a zone up to 4.5 m thick immediately below the Zn-rich ore (Figure 68), and extend up

FIGURE 68: ORE ZONE INTERSECTION OF DRILL HOLE CON 7

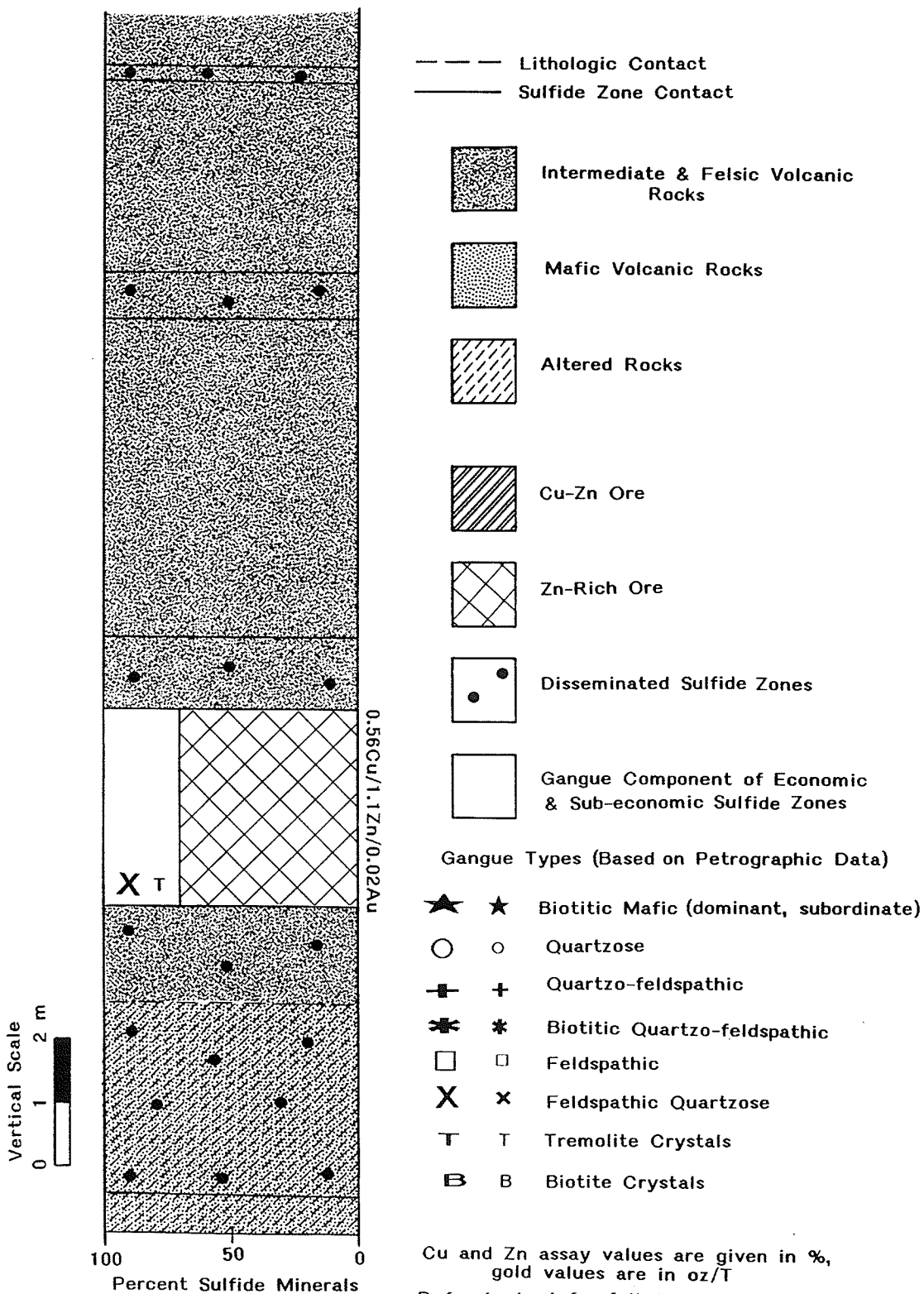
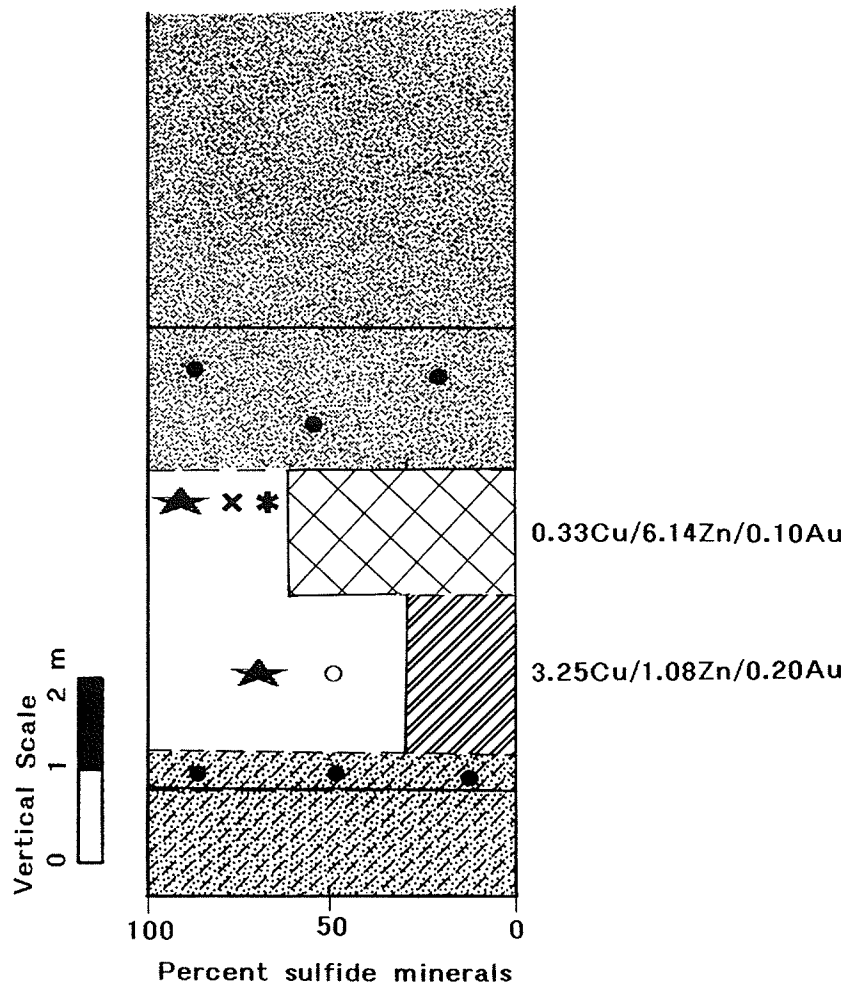
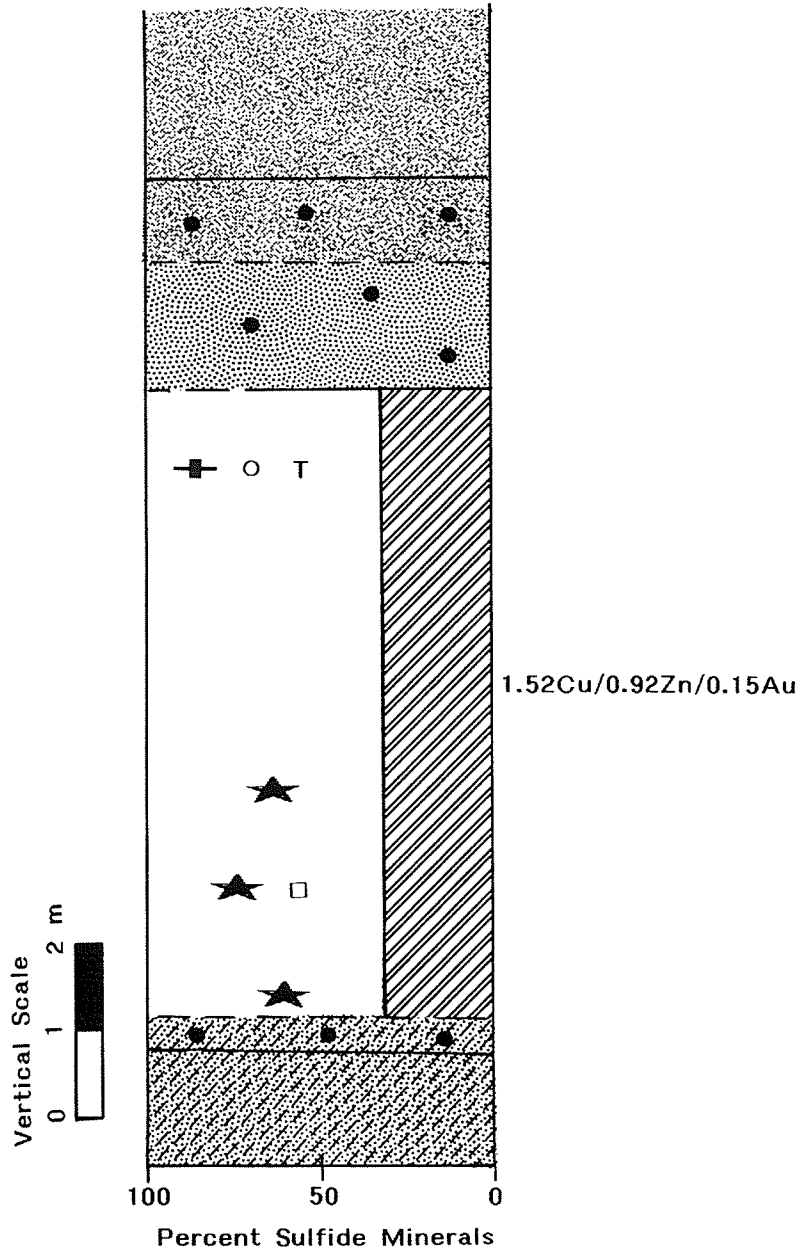


FIGURE 69: ORE ZONE INTERSECTION OF DRILL HOLE CON 57



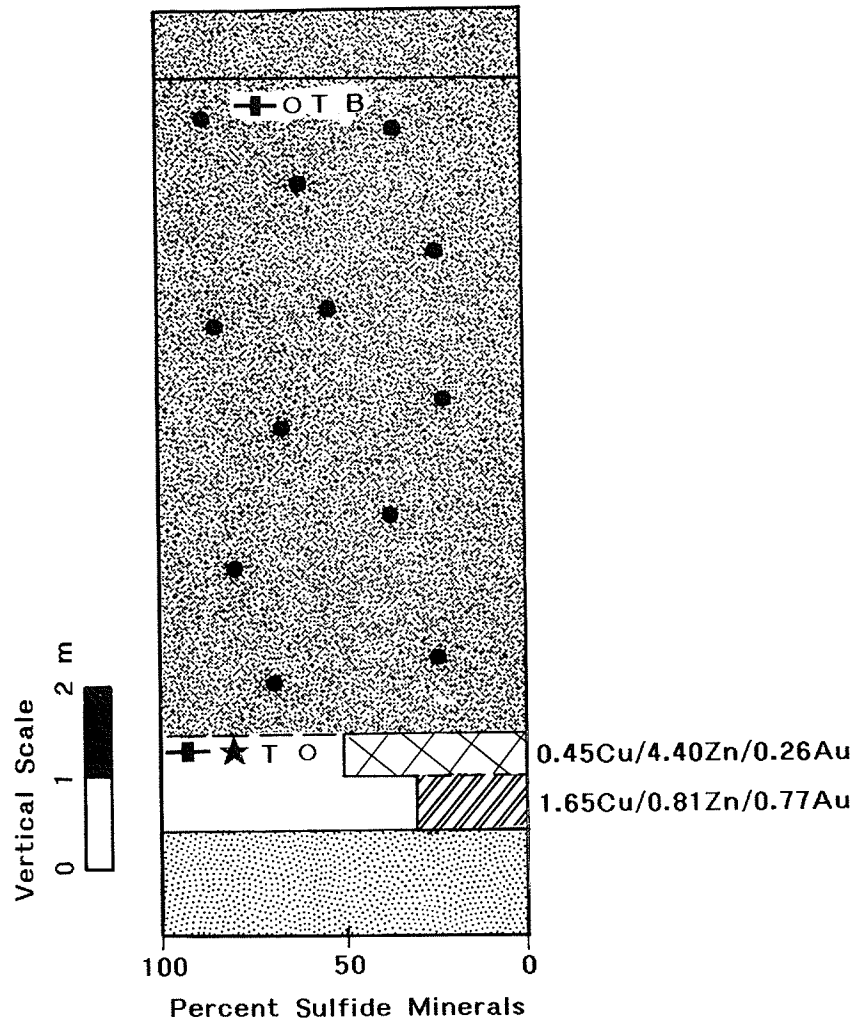
Refer to Figure 68 for explanation of symbols and patterns

FIGURE 70: ORE ZONE INTERSECTION OF DRILL HOLE CON 44W2



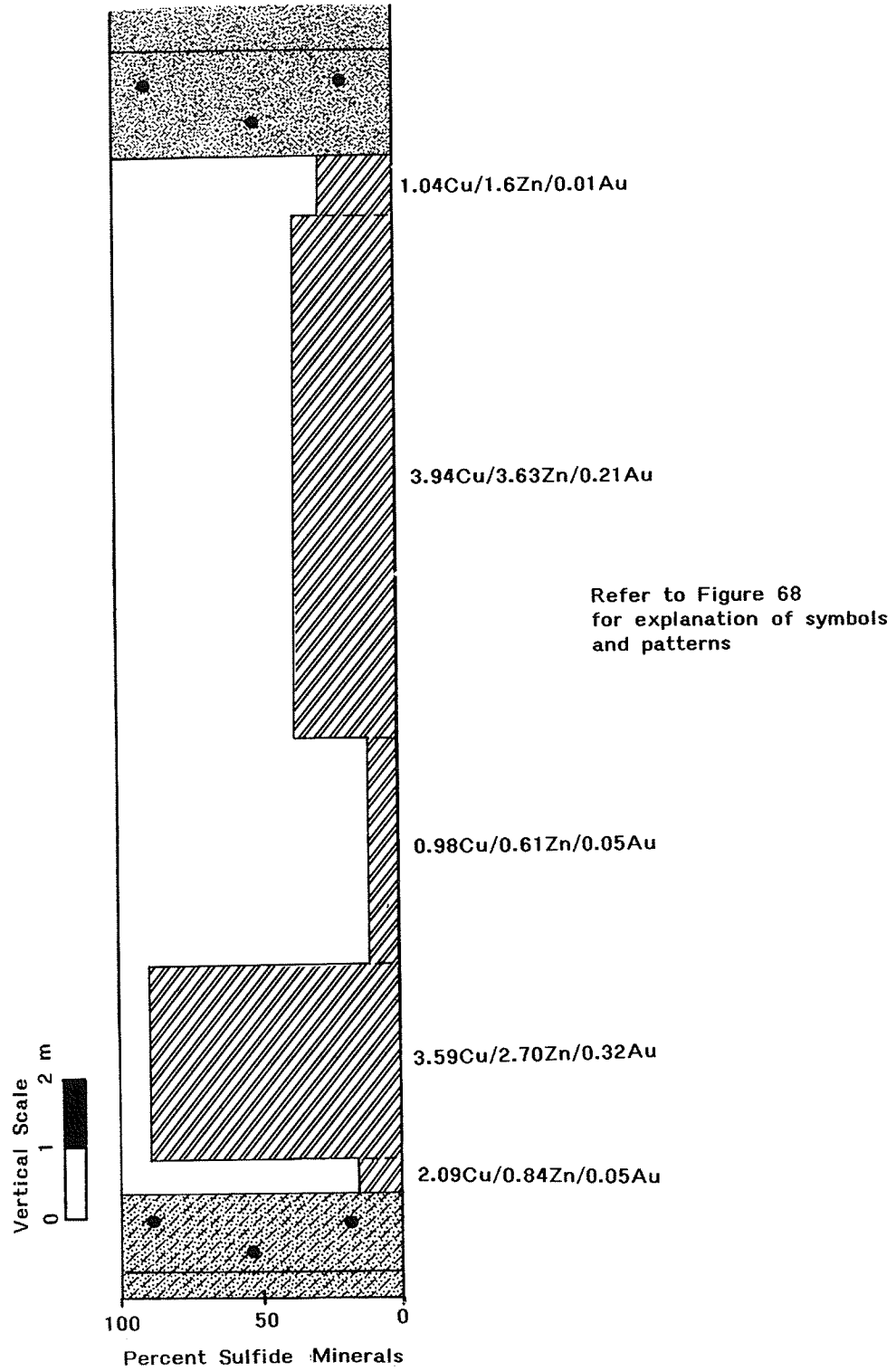
Refer to Figure 68 for explanation of symbols and patterns

FIGURE 71: ORE ZONE INTERSECTION OF
DRILL HOLE CON 5



Refer to Figure 68 for explanation of symbols
and patterns

FIGURE 72: ORE ZONE INTERSECTION OF
DRILL HOLE CON 39



to 50 m above the Zn-rich ore. Disseminated sulfides above the Cu-Zn or Zn-rich ore occur in felsic volcanic hangingwall rocks. In the stratigraphic hangingwall of the island ore zone, disseminated sulfides below the Cu-Zn ore generally occur in proximally altered mafic rocks. Disseminated sulfides locally grade into 3-75 cm thick lenses of high sulfide mineral content. The large number of intersections of such lenses within and among widely spaced drill holes make correlation of individual lenses impossible, and therefore the orientation and dimensions of individual lenses could not be established. Where Zn-rich ore is absent, the Cu-Zn ore grades directly into the disseminated sulfide.

Both Cu-Zn and Zn-rich types of ore are mineralogically simple and contain similar sulfide components - pyrite, pyrrhotite, sphalerite, and chalcopyrite - although in different proportions and with different textural characteristics. The disseminated sulfide and the thin lenses of high sulfide mineral content within it are composed of pyrite and pyrrhotite, with trace amounts of sphalerite and chalcopyrite.

8.1.1 Cu-Zn Ore

8.1.1.1 Sulfide Mineralogy

Sulfide minerals generally comprise 20-70% of the Cu-Zn ore of the island ore zone; in order of decreasing abundance, they are

pyrrhotite plus pyrite, chalcopyrite, and sphalerite. The pyrite and pyrrhotite abundances are highly variable. In places, pyrite is the dominant sulfide component and pyrrhotite is the least abundant sulfide mineral, but in other places this relationship is reversed with pyrrhotite being the dominant sulfide mineral and pyrite the least abundant. This variation appears to have a patchy distribution. Chalcopyrite is almost invariably more abundant than sphalerite.

Pyrite occurs dominantly as irregular 0.07->0.8 mm grains that are fractured and brecciated, and locally poikilitic (Figures 73 and 74); as 0.03-0.1 mm euhedral crystals (Figure 73); and rarely, as >0.8 mm wide veins exhibiting minor brecciation and segmentation. The euhedral crystals occasionally exhibit rounded embayments of the caries type, may contain gangue inclusions, and rarely, were found as overgrowths on irregular pyrite grains. Locally, the irregular pyrite grains coalesce to form large masses several millimeters in size. The euhedral pyrite crystals, the inclusions, and the caries type of embayments, are commonly cited as features of metamorphosed ores (Vokes, 1969). As a result, the euhedral pyrite crystals are interpreted to have formed as a result of crystal growth under metamorphic conditions.

Pyrrhotite is commonly poikilitic and generally occurs in the following forms: <0.01-0.4 mm interstitial grains between other sulfides and gangue (Figure 75); aggregates composed of irregularly shaped 0.01->0.8 mm grains of mixed chalcopyrite, sphalerite and pyrrhotite; and irregularly shaped 0.01->0.8 mm grains in gangue.

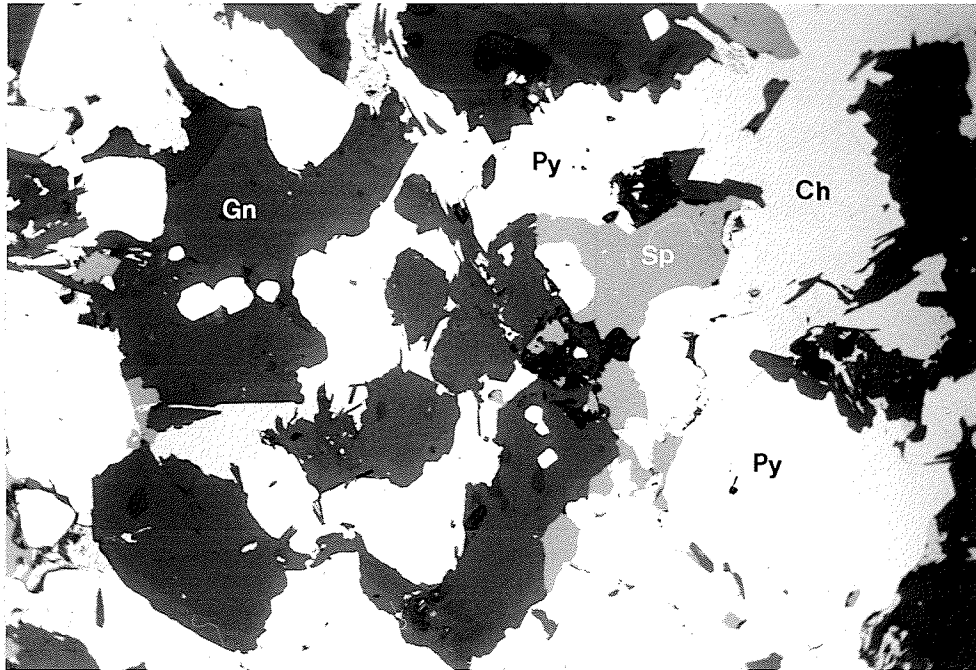


Figure 73: CON 44W2-775.5; Island Ore Zone; Cu-Zn ore. Irregular masses of chalcopyrite and sphalerite partly surrounding anhedral, brecciated pyrite grains and silicate fragments. Euhedral pyrite crystals (top center) that cross-cut the boundary between chalcopyrite and gangue are evidence of metablastic growth (recrystallization). The caries type of rounded embayments on lower left corner of the euhedral pyrite crystal is also a typical fabric of metablastic growth. Gangue consists of the biotitic mafic type aggregates described in the text.

In Figures 73 to 85, the width of each photomicrograph is approximately equivalent to 1.2 mm. Sample numbers correspond to diamond drill hole numbers and depth in feet. Abbreviations used are as follows: Py=pyrite; Po=pyrrhotite; Sp=sphalerite; Ch=chalcopyrite; Gn=gangue. See text for descriptions of gangue types.

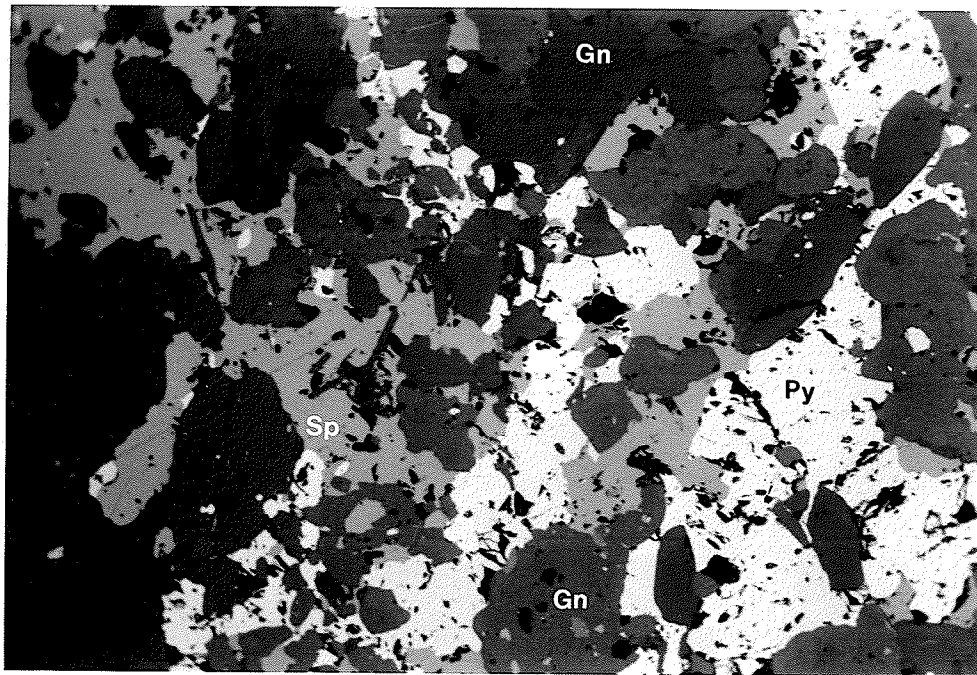


Figure 74: CON 45A-896.5; Island Ore Zone; Cu-Zn ore. Irregular to rounded silicate gangue areas and poikilitic, brecciated pyrite in a sphalerite matrix. The smaller, darker colored inclusions in pyrite and sphalerite are aggregates of quartz. Quartz is more abundant in the sulfide part of the ore than it is in the gangue. Larger, lighter colored non-sulfide gangue is biotitic mafic type gangue and subordinate biotitic feldspathic type. The gangue cross-cut sulfide-sulfide contacts; quartz inclusions within the sulfides terminate at these contacts.

Refer to Figure 73 for explanation of scale, location, and abbreviations.

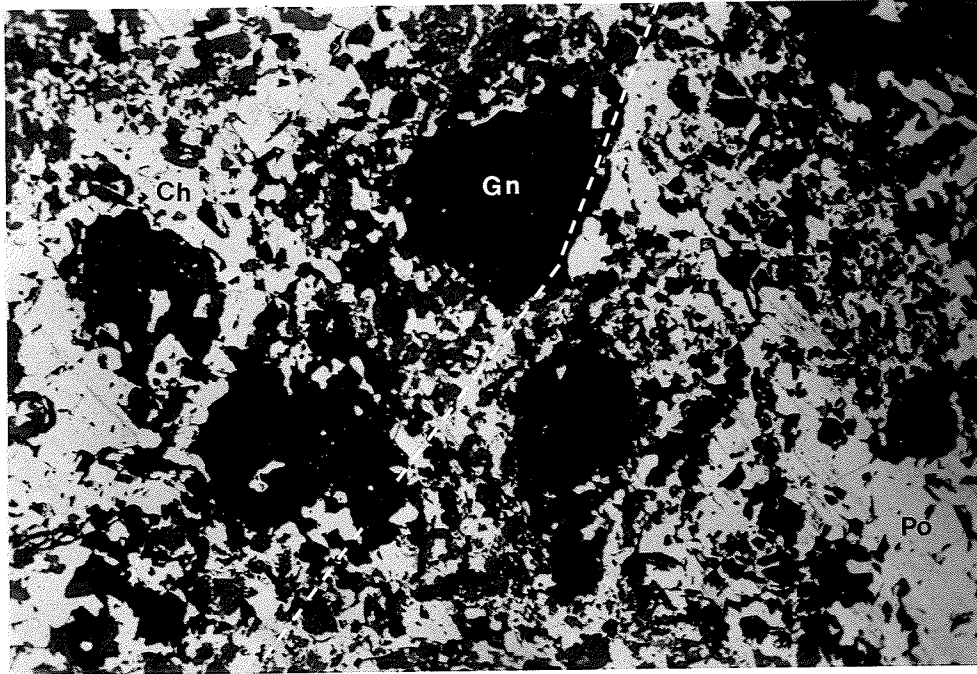


Figure 75: CON 44W2-787; Island Ore Zone; Cu-Zn type ore. Poikilitic chalcopyrite and pyrrhotite matrix to large, rounded gangue areas. Approximate contact between pyrrhotite and chalcopyrite is indicated by the dashed line. This sample is slightly different from other Cu-Zn ore specimens in terms of gangue mineralogy. In addition to being more rounded than usual, the dominant gangue is the normally subordinate quartzo-feldspathic type; the inclusions in the sulfide matrix are mainly quartzose gangue, and lesser pale green amphibole crystals, some of which have pyrrhotite cores.

Refer to Figure 73 for explanation of scale, location, and abbreviations.

Chalcopyrite occurs in several forms: 0.2->0.8 mm interstitial grains among brecciated pyrite, pyrrhotite, and gangue (Figure 73); irregularly shaped 0.01->0.8 mm grains in mixed aggregates of commonly poikilitic, chalcopyrite, sphalerite and pyrrhotite; <0.01 mm irregular blebs in gangue (Figure 75); <0.01 mm veins filling fractures in pyrite; and narrow, 0.02-0.07 mm rims, partly enclosing pyrite grains.

Sphalerite commonly occurs as: <0.8 mm irregular grains mixed with chalcopyrite and/or pyrrhotite (Figure 73); 0.06-0.3 mm interstitial grains between pyrite grains (Figures 73 and 74); <0.2-0.3 mm inclusions in pyrite, chalcopyrite, or pyrrhotite; <0.01 mm veins filling fractures in pyrite; and <0.01-0.3 mm inclusions within gangue (Figure 74). Most textural forms of sphalerite are poikilitic.

8.1.1.2 Gold Content

Assay results from diamond drill core have shown that gold values of >0.15 oz/T are found only in the island ore zone and are almost exclusively in the main Cu-Zn sulfide lens (Figures 8-12); values range from 0.01 to 3.0 oz/T, with a mean Au content of 0.18 oz/T. In places, elevated gold values are present through the entire thickness of the Cu-Zn lens (Figures 68, 71), but in other places high gold values are restricted to zones within the lens

(Figure 72).

Gold was not identified in this study nor in an independent scanning electron microprobe study completed at the Institute of Mineral Research, Michigan Technological University (Hwang, 1984). As a result, the phase in which the gold occurs is presently unknown.

8.1.2 Zn-Rich Ore

8.1.2.1 Sulfide Mineralogy

The sulfide components of the Zn-rich ore of the island ore zone, in order of decreasing abundance, are pyrrhotite, pyrite, sphalerite, and chalcopyrite. In Zn-rich ore, each sulfide mineral has a more restricted range of abundances and morphological forms than in Cu-Zn ore. Sulfide components generally comprise 60-70% of this type of ore.

Pyrite occurs in the following forms: irregular 0.07->0.8 mm grains that in places coalesce to form large masses (Figure 76); and 0.3-8.0 mm euhedral to subhedral crystals (Figure 77) similar to, although larger than, those of Cu-Zn ore. Pyrrhotite commonly forms poikilitic, brecciated masses of irregularly shaped 0.01->0.8 mm grains mixed with sphalerite, and possibly chalcopyrite (Figures 76 and 78), or interstitial matrix to pyrite crystals. Rarely, it

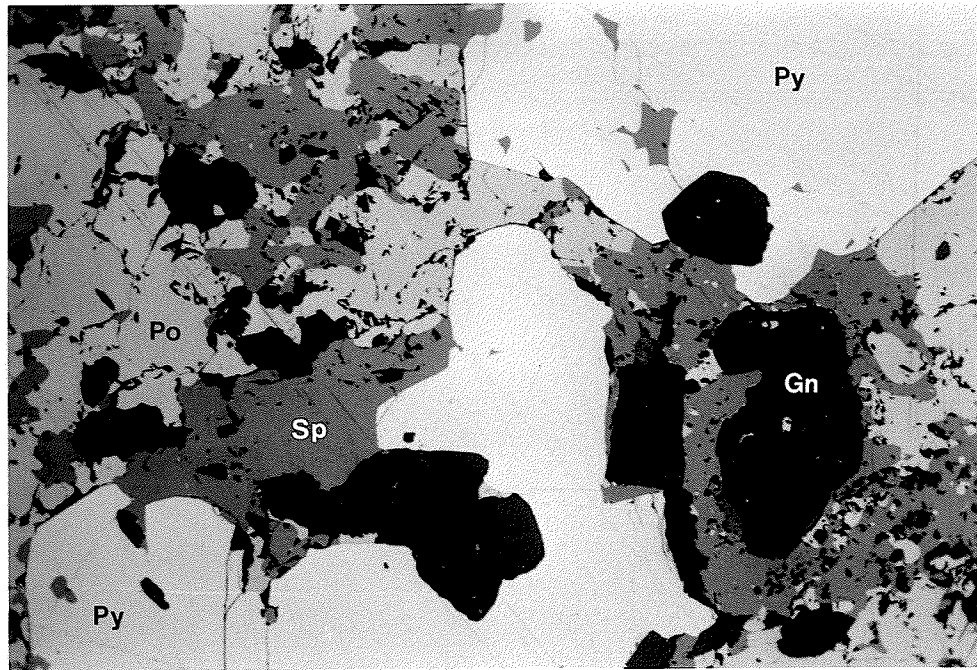


Figure 76: CON 7-788.5; Island Ore Zone; Zn-rich ore. Large subhedral pyrite in poikilitic pyrrhotite plus sphalerite matrix. Silicate inclusions in the matrix are <0.1-0.15 mm non-pleochroic amphibole crystals. Larger non-sulfide gangue aggregates are feldspathic quartzose type.

Refer to Figure 73 for explanation of scale, location, and abbreviations.

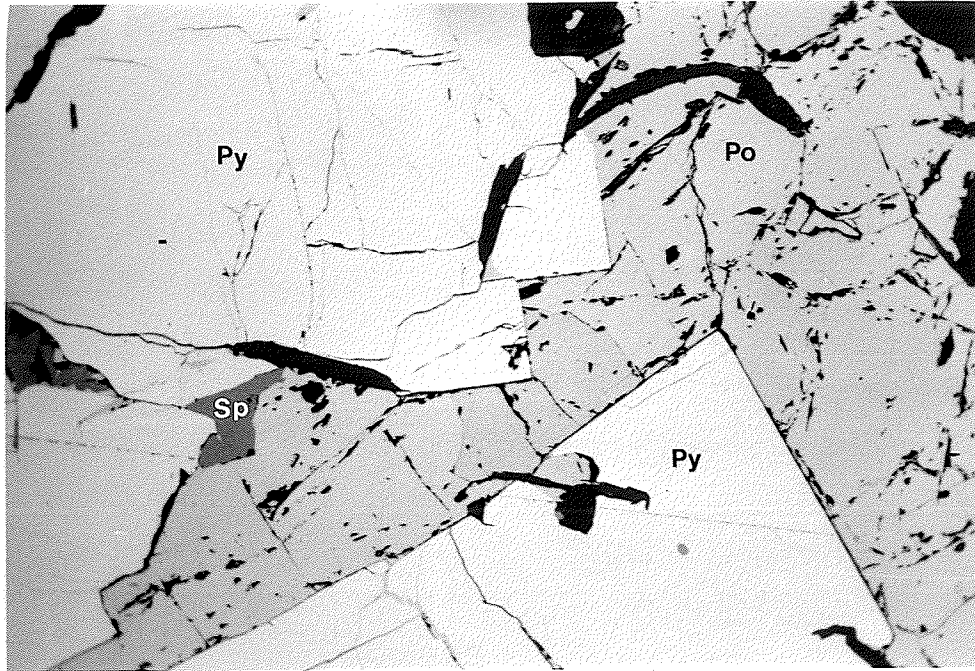


Figure 77: CON 6-632; Island Ore Zone; Zn-rich ore. Large euhedral crystals of pyrite and inter-granular pyrrhotite, which has also filled fractures in pyrite. Gangue shown consists mainly of biotite.

Refer to Figure 73 for explanation of scale, location and abbreviations.

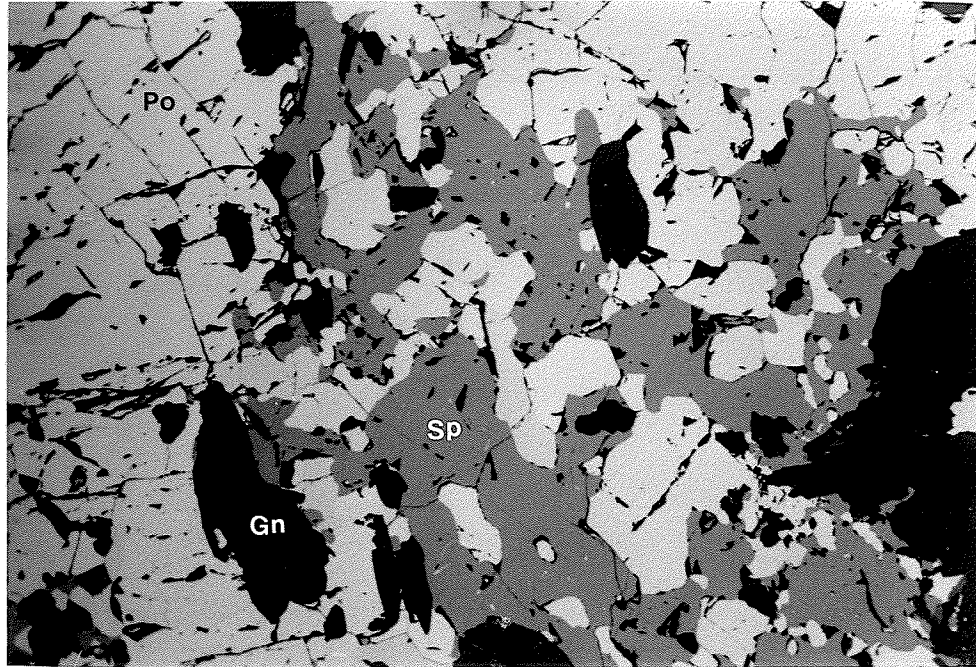


Figure 78: CON 7-788.5; Island Ore Zone; Zn-rich ore. Large irregular masses of fractured, poikilitic pyrrhotite in a sphalerite matrix. Larger non-sulfide areas are feldspathic quartzose gangue; smaller silicate inclusions in the sulfides are pale, non-pleochroic amphibole crystals.

Refer to Figure 73 for explanation of scale, location, and abbreviation.

fills <0.01 mm fractures in pyrite (Figure 77). The pyrrhotite-filled fractures in pyrite metacrysts are interpreted to be tension fractures, which are defined as veinlets within nodules and metacrysts that terminate in the parent rock and are filled by mobile sulfides such as pyrrhotite, chalcopyrite, and sphalerite (Vokes, 1971). Sphalerite most commonly occurs as poikilitic, <0.8 mm irregular grains intermixed with pyrrhotite, and interstitial to pyrite grains (Figure 76 and 78); and as <0.2-0.3 mm non-poikilitic blebs in pyrite (Figure 76). Two generations of sphalerite may be present: poikilitic sphalerite is locally overgrown by non-poikilitic grains. Chalcopyrite occurs as irregular <0.01-0.4 mm grains intergrown with sphalerite and interstitial to pyrite and pyrrhotite (Figure 79); 0.07 mm wide rims, partly enclosing pyrite grains (Figures 80 and 81); and <0.01 mm fracture fillings in pyrite. Where this ore type overlies the Cu-Zn ore, chalcopyrite abundance is slightly higher than where the Cu-Zn ore is absent.

8.1.3 Disseminated (Non-economic) Sulfide Zones

Disseminated sulfides zones are characterized by the presence of 1-6% (locally increasing to 20%) evenly disseminated pyrite and/or pyrrhotite, with trace amounts of sphalerite and chalcopyrite. Minor (<0.5%) Cu and Zn values are found in this type of mineralization in both hangingwall and footwall positions. Disseminated sulfides also occur within the distal alteration zones

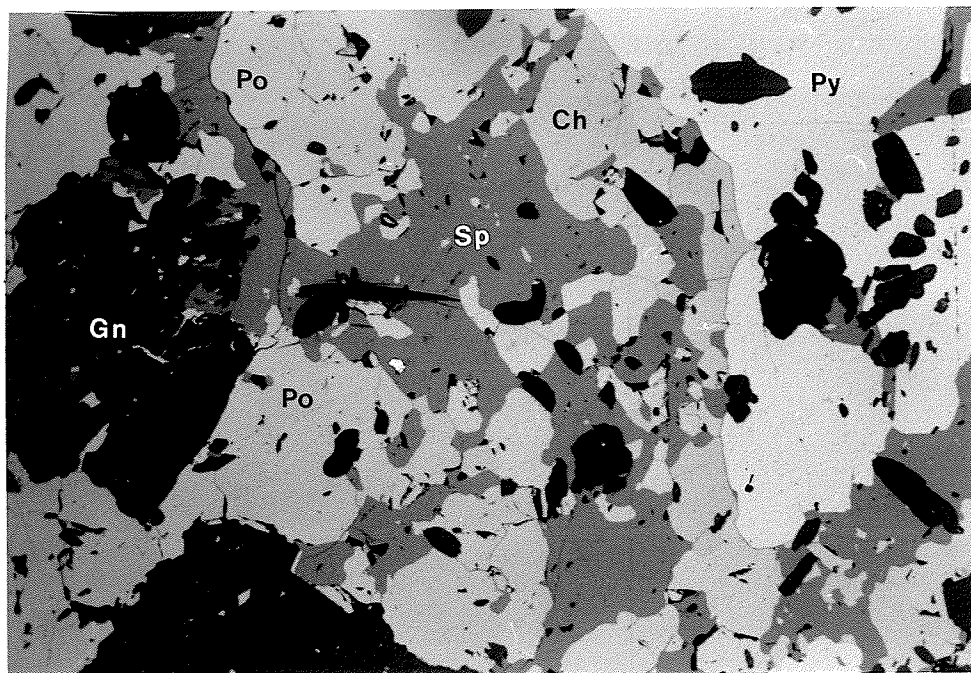


Figure 79: CON 57-763; Island Ore Zone; Zn-rich ore, overlying the Cu-Zn ore. Intergrown grains of poikilitic pyrrhotite, sphalerite and chalcopyrite interstitial to anhedral pyrite grains. The dominant gangue resembles the mafic type aggregates, but lacks biotite, and there is lesser feldspathic quartzose and biotitic quartzo-feldspathic gangue.

Refer to Figure 73 for explanation of scale, location and abbreviations.

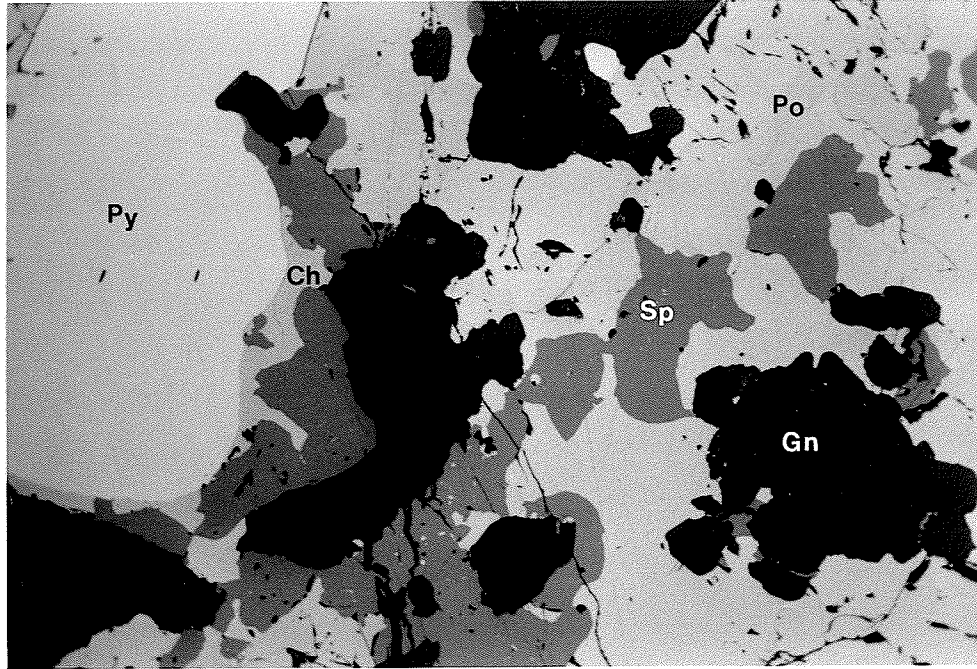


Figure 80: CON 5-401; Island Ore Zone; Zn-rich ore, overlying the Cu-Zn zone. Large rounded pyrite grain; chalcopyrite and sphalerite rims pyrite and also form irregular blebs in the pyrrhotite matrix. Gangue consists of quartzo-feldspathic type aggregates, and isolated <0.1-0.45 mm crystals of quartz and amphibole.

Refer to Figure 73 for explanation of scale, location, and abbreviations.

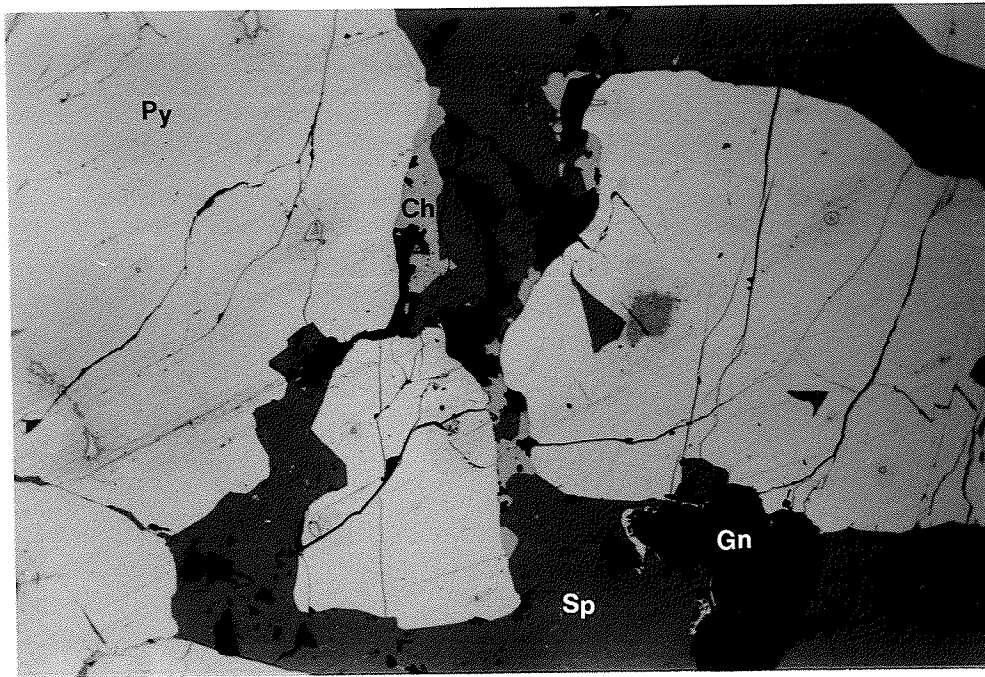


Figure 81: CON 5-401; Island Ore Zone; Zn-rich ore, overlying the Cu-Zn zone. Anhedral pyrite grains with intergranular sphalerite. Tension fractures within pyrite also contain sphalerite. Minor chalcopyrite occurs around the edges of the pyrite grains. Gangue consists of individual quartz crystals, and larger gangue aggregates consist of amphibole crystals.

Refer to Figure 73 for explanation of scale, location and abbreviations.

which generally contain minor Zn (<0.5%), although this may locally increase (Figure 8).

Sulfides generally comprise 50-75% of lenses of high sulfide mineral content. The sulfide component of the lenses consist of 70-83% pyrrhotite matrix, and 17-30%, 0.04-0.18 mm rounded pyrite grains (Figures 82, 83). Such rounded pyrite crystals in metamorphosed ore are commonly interpreted to be the result of rounding from plastic flowage within more ductile intergranular minerals (Nold, 1983). These are commonly referred to as rolled pyrite metacrysts. Some pyrite grains are also cracked or shattered (Figure 82), a feature typical of deformation accompanying metamorphic recrystallization.

8.1.4 Gangue Mineralogy

The Cu-Zn ore typically contains 30-80% gangue, dominated by 2 main types of silicate aggregates, biotitic mafic and quartzose (Figure 69, 70); quartzo-feldspathic and feldspathic types of gangue aggregate are usually subordinate, but are locally dominant in the upper part of the Cu-Zn ore (Figure 70). The Zn-rich ore typically contains 30-40% gangue; 70-90% of the total gangue consists of biotitic mafic, feldspathic quartzose, biotitic quartzo-feldspathic, quartzose, and quartzo-feldspathic types (Figures 68, 69, 71). The remaining gangue of the Zn-rich ore consists of individual crystals or monomineralic aggregates of

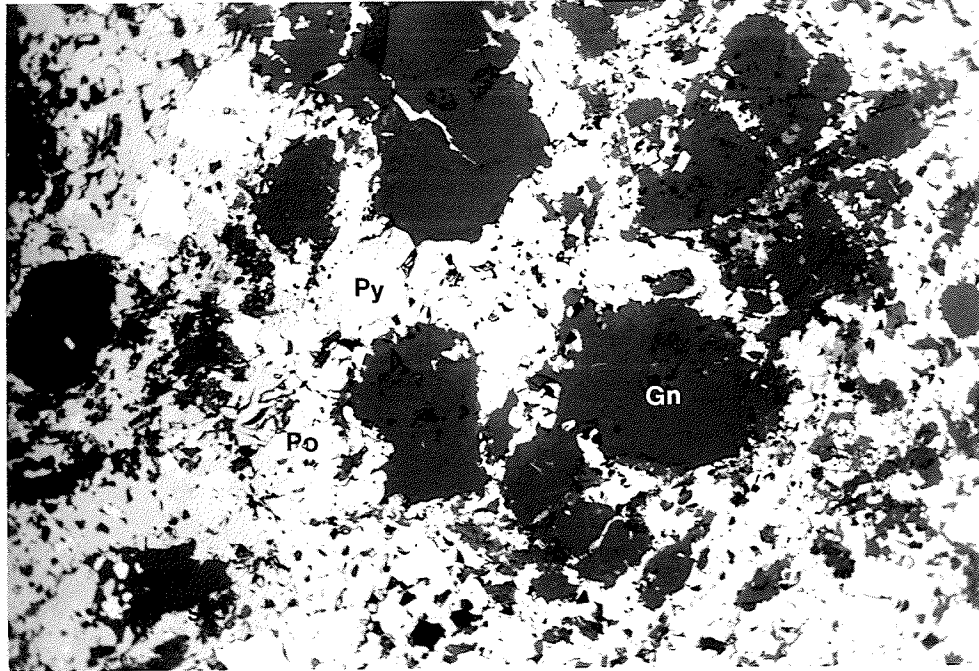


Figure 82: CON 5-424.5; Cu- and Zn-poor, high sulfide mineral lens in disseminated sulfide zone. Rounded pyrite grains and rounded gangue material in a poikilitic pyrrhotite matrix. Cracked or shattered pyrite grains also occur locally (top left). The non-sulfide areas consist of quartzo-feldspathic type gangue. Also present are quartzose aggregates, and large pale, non-pleochroic amphibole and biotite crystals.

Refer to Figure 73 for explanation of scale, location, and abbreviations.

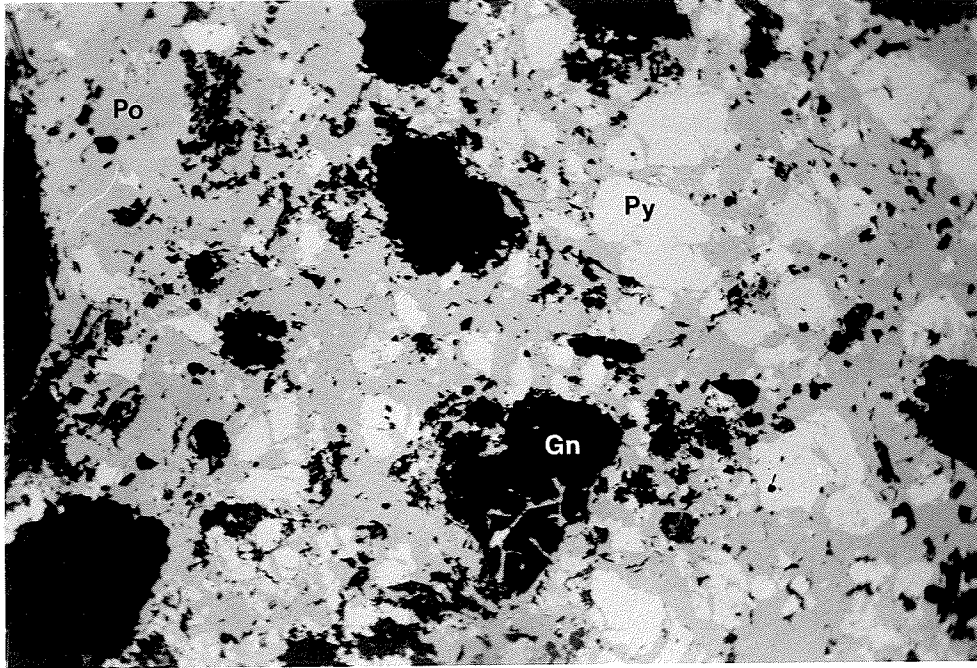


Figure 83: CON 5-424.5; Cu- and Zn-poor, high sulfide mineral lens in disseminated sulfide zone. Rounded pyrite grains and gangue areas in a pyrrhotite matrix. The larger non-sulfide gangue is the quartzo-feldspathic type; remaining gangue consists of quartzose aggregates and individual pale green amphibole and biotite crystals.

Refer to Figure 73 for explanation of scale, location, and abbreviations.

tremolite, and biotite. In high sulfide mineral content lenses within disseminated sulfide zones, two types of gangue aggregates were recognized, quartzo-feldspathic and quartzose; subordinate tremolite and biotite crystals are also present.

Biotitic mafic gangue in both the Cu-Zn and Zn-rich ore consists of 0.6-7.0 mm irregular to rounded aggregates (Figure 73) composed of: 45-90%, 0.15-1.2 mm amphibole; 10-20%, <0.1-0.7 mm biotite; and 5-20%, 0.9-1.7 mm aggregates of <0.1 mm plagioclase. Locally, there is up to 15%, <0.1-0.34 mm quartz. In the Zn-rich ore, the biotitic mafic gangue aggregates contain 7-15%, <0.1-0.9 mm sulfide grains (pyrrhotite & sphalerite) which are interstitial to, and form inclusions within, amphibole. In some aggregates, the amphibole is similar to the pale, non-pleochroic variety found in the tremolite-quartz-biotite-chlorite assemblage of proximal alteration zone. Mica associated with this amphibole is typically the green biotite-chlorite intergrowths rather than pure biotite; rarely the biotite-chlorite intergrowths form 1.8 mm wide veins comprising 0.25 mm laths.

Quartzose gangue in both the Cu-Zn and Zn-rich ore consists of irregular to rounded 0.1-2.7 mm aggregates of <0.1-0.48 mm quartz (Figure 74) or 1.7-3.0 mm wide veins of <0.1-0.48 mm quartz that also contain 10-15% sulfide and locally 5% amphibole or biotite-chlorite intergrowths. In lenses of high sulfide mineral content within disseminated sulfide zones, quartzose gangue forms rounded aggregates, 0.1-1.8 mm in size.

The quartzo-feldspathic gangue comprises 1.8-5.1 mm aggregates

consisting of 40-55%, <0.1 mm plagioclase, and 25-45%, <0.1-0.7 mm quartz in 0.8-1.6 mm aggregates. Feldspathic gangue comprises 1.35-3.4 mm rounded aggregates consisting of 60-88%, <0.1-0.22 mm plagioclase; 10-40%, <0.1-0.33 mm biotite; and trace-2% amphibole. Both gangue types may also contain 5%, 0.45-1.35 mm patches consisting of 30-60% sulfide and 40-70% epidote. Although generally subordinate to the mafic and quartzose gangue types in the Cu-Zn zone, the quartzo-feldspathic type is locally the dominant gangue material in the upper part of the Cu-Zn ore (Figure 70).

The biotitic quartzo-feldspathic gangue is a minor component of Zn-rich ore and comprises 0.45-3.5 mm aggregates composed of 40-80%, <0.1 mm plagioclase, with rare 0.24-0.33 mm grains; 10-60%, <0.1-0.6 mm quartz; and 5-10%, <0.1-0.15 mm biotite laths and 0.45 mm anhedral patches. Where the underlying Cu-Zn lens is absent, the gangue in Zn-rich ore is dominated by feldspathic quartzose material (Figure 68) in 0.2-5.0 mm rounded to irregularly shaped aggregates composed of 40-80%, 0.1-0.72 mm quartz; 18-30%, <0.1 mm plagioclase; 5-20% sulfide; and trace-10%, 0.1-0.9 mm biotite. Locally these aggregates contain up to 40% epidote.

8.2 CHARACTERISTICS OF THE LAKE ORE ZONE

The lake ore zone consists of a single concordant lens that subcrops beneath the lake on the mainland fault block. Original size (i.e. tonnage) and pre-erosional dimensions of the lens are

unknown. The lake ore zone contains slightly less tonnage than the combined economic lenses of the island ore zone. The zone is mineralogically and texturally simple, consisting exclusively of Zn-Cu-rich ore, that is texturally and mineralogically similar to the Zn-rich ore of the island ore zone, although the lake ore zone contains substantially less pyrrhotite and more chalcopyrite. Boundaries of the ore zone with the host rocks are usually sharp and well defined with the exception of the lateral peripheries, where the sulfide is less abundant, and forms 1.7-7.0 mm thick layers containing 20-85% sulfide minerals within sulfide-free rock.

8.2.1 Sulfide Mineralogy

Sulfide minerals comprise 20-75% of the lake ore zone; in order of decreasing abundance these minerals are: pyrite, sphalerite, chalcopyrite, and pyrrhotite. No layering or zonation of ore minerals have been noted; the ore zone appears to be relatively homogeneous in texture and composition.

Pyrite generally occurs as 0.05-0.8 mm euhedral to subhedral crystals that in places are brecciated (Figures 84, 85), and it locally forms 0.8 mm thick veins. Sphalerite occurs as 0.25->0.8 mm poikilitic grains interstitial to pyrite, and as 0.01-0.06 mm blebs within gangue, or less commonly, within pyrite. Chalcopyrite occurs as fracture fillings within pyrite, as narrow rims partly enclosing pyrite grains, and as 0.01-0.4 mm irregular patches intergrown with

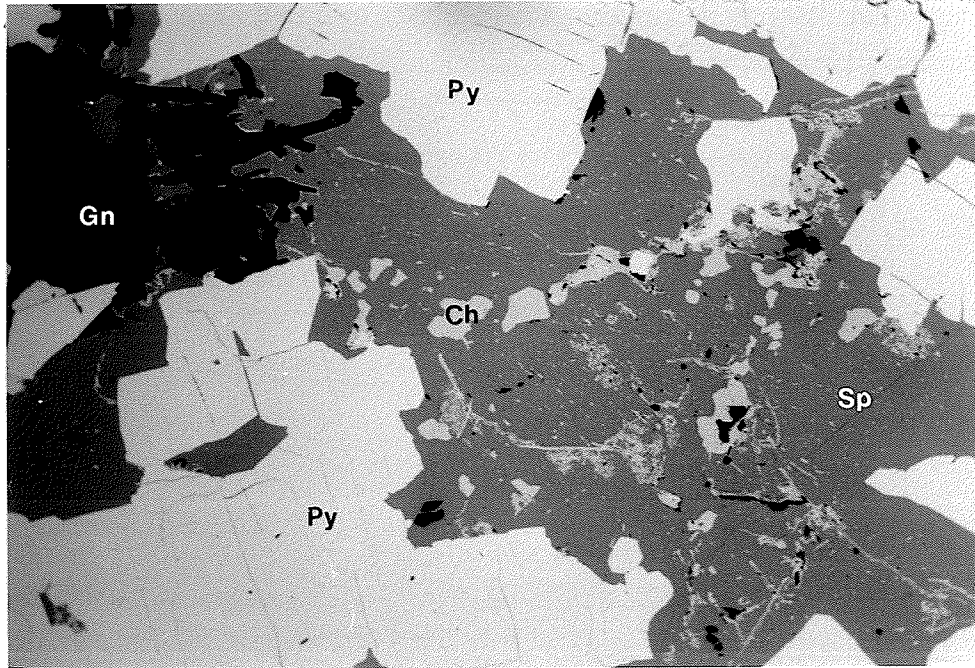


Figure 84: CON 20-115; Lake Ore Zone. Subhedral pyrite crystals in a sphalerite matrix. Chalcopyrite occurs as a vermicular exsolution in the sphalerite. Gangue consists of irregular aggregates of quartz and chlorite, and minor amphibole crystals.

Refer to Figure 73 for explanation of scale, location and abbreviations.

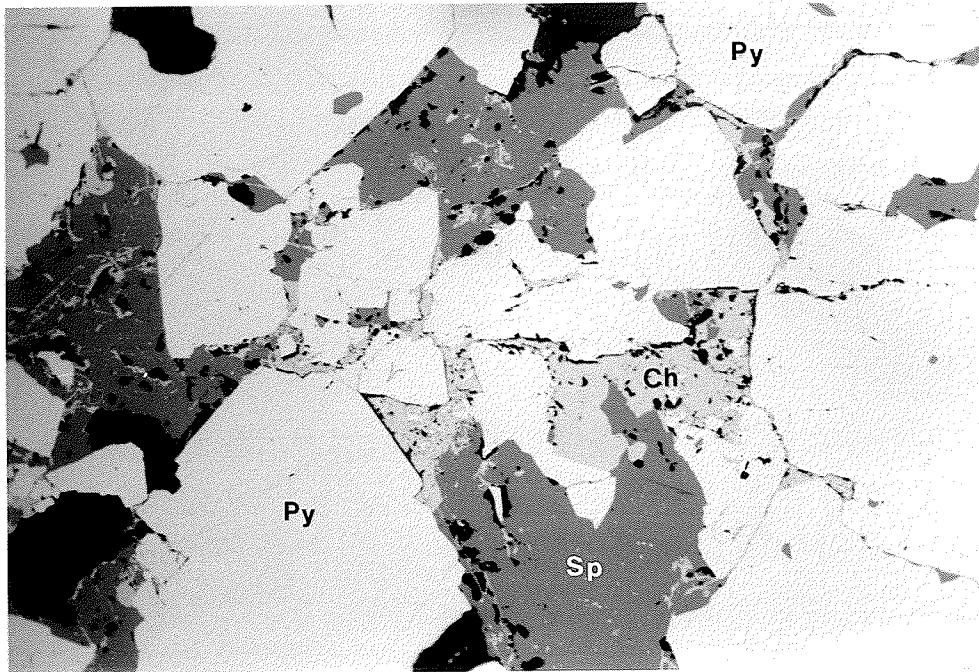


Figure 85: CON 20-115; Lake Ore Zone. Subhedral, brecciated pyrite crystals with interstitial sphalerite and chalcopyrite. Chalcopyrite also occurs as vermicular exsolutions within sphalerite, and fills fractures in pyrite grains.

Refer to Figure 73 for explanation of scale, location, and abbreviations.

sphalerite. It also occurs as small blebs or vermicular inclusions within sphalerite (Figures 84, 85); these are interpreted to be the result of exsolution of chalcopyrite from sphalerite, a common texture of this particular pair of minerals in high grade metamorphic terrains (Vokes, 1969). Pyrrhotite forms 0.01-0.25 mm poikilitic grains intergrown with chalcopyrite and sphalerite; and as 0.01-0.06 mm poikilitic, irregular grains in gangue.

8.2.2 Gangue Mineralogy

Gangue comprises 25-45% of the lake ore zone. The dominant gangue component is 0.23-1.36 mm quartz crystals that form irregularly shaped patches up to 4.5 mm in size. The remainder of the gangue is 0.1-1.35 mm aligned chlorite laths, which are characterized by green-brown to grey birefringence and form 0.22-3.2 mm wide veins or aggregates, and scattered 0.5 mm amphibole crystals with resorbed rims.

Quartz is the only gangue component in the sulfide-rich layers at the lateral boundaries of the zone. Sulfide-free interlayers are composed of: 55%, <0.1 mm plagioclase; 19%, <0.1-0.22 mm quartz; 13%, 0.26-0.6 mm sub-poikilitic, anhedral to subhedral amphibole; and 13%, 0.17 mm biotite laths. The quartz in the sulfide-free interlayers is much finer grained than the quartz of the sulfide-rich layers.

Chapter 9

Discussion

9.1 INTRODUCTION

The petrographic, textural, and chemical characteristics of the host rocks and ores of the Vamp Lake deposit have been described in the previous chapters. These characteristics and implications regarding the genesis of the deposit will be discussed in the present chapter in order to address the following points:

1. Classification of the Vamp Lake deposit based on lithologic associations and physical characteristics, and comparison of the physical and chemical features of the Vamp Lake deposit with other deposits of comparable type, in order to determine similarities and differences, and their possible significance for genetic implication.
2. Examination of the chemical and mineralogical changes that occurred during alteration, and their significance.
2. The relationship between alteration and mineralization.
3. Genesis of the Vamp Lake deposit

9.2 TYPE OF DEPOSIT - CLASSIFICATION

The Vamp Lake deposit is similar in many respects to other massive sulfide deposits in the Flin-Flon-Snow Lake greenstone belt, but there are some differences that may reflect slight variations in genesis. The characteristics of the Vamp Lake deposit

are discussed below.

9.2.1 External characteristics of the ore zones

Vamp Lake deposit is a stratabound accumulation of >50% sulfide minerals, hosted by volcanic rocks; underlying pillowed mafic flows indicate a subaqueous environment. These characteristics classify this ore body as a volcanogenic massive sulfide deposit according to Lydon, 1984.

Although the typical economic massive sulfide deposit contains 1-10 million tonnes of ore (Lydon, 1984), the smaller size of the Vamp Lake deposit is not unusual when compared to similar deposits in the Flin Flon-Snow Lake greenstone belt (Table 1). There are, however, some physical characteristics of the Vamp Lake deposit that distinguish it from many massive sulfide deposits. Most massive sulfide deposits have a gradational lower contact, with an underlying Cu-stringer zone (Franklin et al, 1981); a Cu-stringer zone is absent at Vamp Lake and the lower contact of the ore is sharp. Upper contacts of most massive sulfide deposits are described as sharp (Franklin et al, 1981), but in the island ore zone at Vamp Lake, the ore lens grades upward into a disseminated sulfide zone locally up to 50 m thick.

Traditionally there has been a strong emphasis in the literature on the association of massive sulfide deposits and fragmental footwall rocks (Sangster & Scott, 1976). However, according to a relatively new classification outlined by Morton &

Franklin (1987), there is a second category of massive sulfide deposits, Noranda-type, which are associated with mafic and felsic flows, rather than fragmental rock types. Vamp Lake would fit this category of massive sulfide deposits.

9.2.2 Internal characteristics of the Vamp Lake deposit

Archean and Proterozoic massive sulfide deposits usually consist of pyrite, pyrrhotite, chalcopyrite and sphalerite (Franklin et al, 1981; Sangster & Scott, 1976). The Vamp Lake deposit is also characterized by these minerals, and it is thus a typical massive sulfide deposit in terms of sulfide mineralogy. The Cu and Zn grades of the deposit are also comparable to other deposits in the Flin Flon area (Table 2). The Au content of the Vamp Lake deposit, however, is unusual for this area; this difference will be addressed later.

The island ore zone of the Vamp Lake deposit is characterized by an upward and outward zonation of Cu-Zn-Au ore to Zn-rich ore, but no zoning was observed in the lake ore zone. Distinctive metal zonation, similar to that found in the island ore zone, is one of the most diagnostic features of volcanogenic massive sulfide deposits (Lydon, 1984). This zonation is usually ascribed to the effects of physiochemical gradients on mineral precipitation from hydrothermal fluids (Lydon, 1988).

9.2.3 Deformation and metamorphism of ores

Volcanogenic ore deposits are an integral part of the stratigraphic sequence and thus should have been subjected to the same deformation and metamorphic events that affected the host rocks. A number of textural features indicative of both metamorphism and deformation can be observed in metamorphosed sulfide deposits. Only the more brittle sulfides such as pyrite record evidence of deformation (Vokes, 1969; Craig & Vokes, 1993). The fractures in the brittle mineral pyrite, and cracked, shattered and brecciated pyrite grains are evidence of deformed ores (Vokes, 1971; Vokes, 1993), as are the rounded pyrite grains and rounded gangue areas (Vokes, 1969; Gair & Slack, 1984; Klemd et al, 1987; Marshall & Gilligan, 1989, Vokes, 1993).

Metamorphic fabrics are those attributed to recrystallization and metablastic growth during progressive metamorphism. Minerals of high form energy such as pyrite grow as metacrysts with well developed crystal faces (Vokes, 1969); inclusions and carries type embayments are common metamorphic features of these crystals (Vokes, 1969). At high metamorphic grades some sulfide minerals become ductile and tend to flow around gangue minerals and less ductile sulfide grains (Vokes, 1969). The remobilized nature of sphalerite, chalcopyrite, and pyrrhotite is indicated by their matrix forming and fracture filling occurrences (Vokes, 1971; Pederson, 1980). Healing of cataclastically deformed pyrite by infilling with relatively ductile pyrrhotite or chalcopyrite, is typical, as is the infilling of fractures in brittle sulfides by

more ductile sulfides (Vokes, 1993). The exsolution of chalcopyrite in sphalerite is evidence that the ore attained a medium amphibolite metamorphic grade. The presence of large euhedral pyrite crystals that show no evidence of deformation, and are rarely found overgrowing irregular pyrite grains are evidence that metamorphism continued after the termination of deformational stresses (Vokes, 1969).

9.3 SPATIAL ASSOCIATION OF ALTERATION ZONES WITH MINERALIZATION

9.3.1 Distal alteration zones

The sulfide and silicate mineralogy of the distal alteration zones, and chemical and spatial evidence suggest a relationship between the processes responsible for alteration and those responsible for mineralization. As indicated earlier, distal zones are found in footwall positions, immediately below both ore zones. The alteration assemblages in both distal zones contain 6-20% sulfide minerals. Comparable sulfide contents do not occur in unaltered rock units between the alteration and ore zones. Although most of the contained sulfide is pyrite, minor sphalerite is present, as indicated by anomalous Zn values throughout the alteration zone (section 8.1.3), which locally increase to economic grades (Figures 8-12), indicating that the alteration process was capable of deposition of sulfide minerals, some of which was Zn-

bearing. The local presence of the silicate component gahnite in the chlorite-quartz-biotite assemblage of the mainland fault block is indirect evidence of this. It has been proposed that such Zn-rich spinels form by desulfurization reactions involving a member of the Fe-S-O system and sphalerite with either garnet or an aluminosilicate (Spry & Scott, 1986a,b). Gahnite is an accessory mineral in alteration zones at most massive sulfide deposits that attained amphibolite grade metamorphism (Franklin et al, 1981).

9.3.2 Proximal Alteration Zones

Proximal alteration zones at Vamp Lake are stratiform, thin, and spatially associated with the ore zones. The Vamp Lake deposit differs somewhat from the norm because this alteration is equally developed both below and above the lake ore zone; in the island fault block, as in most other ore deposits of this type, the alteration is most highly developed beneath the ore body. The proximal alteration zones contain low grade Cu-Zn values generally in the form of disseminated sulfides (section 8.1.3). In the mainland fault block, disseminated sulfides are restricted to the alteration envelope, but in the island block, disseminated type sulfides extent as much as 50 m into the hangingwall, well past the locally developed proximal alteration of hangingwall felsic rocks.

9.4 GENESIS OF ALTERATION

The mineralogical characteristics of the distal alteration zones at Vamp Lake are comparable to hydrothermal alteration zones commonly associated with proximal volcanogenic massive sulfide deposits. Although the assemblages themselves are variable among deposits, the individual components are similar; chlorite, biotite, muscovite, quartz, sericite, and tremolite are among the components reported in alteration zones associated with other metamorphosed massive sulfide deposits (Larson, 1984; Walford & Franklin, 1982; Knuckey et al, 1982).

Whole rock chemical data indicate that Na and Ca depletion, and K and Mg enrichment are common in hydrothermal alteration zones associated with massive sulfide deposits (Franklin et al., 1981; Riverin & Hodgson, 1980; Vivaldo, 1985; Lydon 1984). These trends are evident in most of the alteration assemblages of the distal island alteration zone. Data in the literature are limited regarding possible trace element changes in alteration zones. Therefore, it is not known whether the Rb, Cr, Ni, and Ba enrichment, and Sr and Nb depletion observed at Vamp Lake are typical of hydrothermal alteration associated with the generation of massive sulfide deposits.

Although there are less data on the the alteration zones in the mainland fault block, the chemistry and mineralogy of the zones are similar to those of the island fault block and they are interpreted to have formed by similar processes. As indicated

above, the chemical and mineralogical characteristics of the zones is consistent with hydrothermal alteration processes typically associated with massive sulfide deposits. Based on the mineralogical, and possible chemical similarity between alteration zones in both fault blocks, a similar hydrothermal process may have formed both zones.

9.4.1 Distal zones

At Vamp Lake, there are morphological and spatial differences in the distal alteration zones in each fault block. The alteration zone in the island fault block is a relatively thick, pod-like body, with a length to width ratio of approximately 3. It is concordant and widens towards the present erosional surface (Figures 5a-5d). The mainland distal zone is extremely narrow by comparison; length to width ratio is uncertain, because the eastern end of the alteration zone is truncated by the east-trending fault, but the existing part has a ratio of 22, which is a minimum value for the zone. The differences in distal zones between fault blocks may indicate a separate genesis for the two bodies, and the zones are discussed separately in the following section.

As indicated earlier, the distal zones in each fault block are the product of hydrothermal activity. The zones may represent: 1) a hydrothermal alteration pipe; 2) a hydrothermal reservoir; 3) a secondary hydrothermal feeder zone or offshoot from a main pipe or conduit, or 4) hydrothermal alteration associated with a shear

zone.

9.4.1.1 Island Fault Block

The distal alteration zone contains many mineralogical and chemical similarities to hydrothermal alteration pipes described in the literature. A mineralogical zonation of alteration minerals is frequently reported in hydrothermal alteration pipes of massive sulfide deposits (Larson, 1984; Walford & Franklin, 1982; Knuckey et al, 1982); deposits in the Flin Flon-Snow Lake belt are characterized by alteration pipes with MgO-enriched chloritic cores, and sericitic peripheral zones (Franklin et al, 1981). The Vamp Lake distal island zone display two types of mineralogical variation: 1) an upward and downward change in assemblage due to the alteration of mafic flows, and 2) localized changes in sub-zone 2 that represent a change in precursor lithology. Sub-zone 2 contain both mafic precursor rocks and intermediate rocks; the altered mafic flows are characterized by the alteration assemblage chlorite-quartz-biotite, and the rocks interpreted to have been derived from intermediate flows are now characterized by the assemblages quartz-biotite and quartz-muscovite. The lateral continuity of the quartz-muscovite and quartz-biotite assemblages within sub-zone 2 parallel regional stratigraphy, supporting a stratigraphic control. The mafic rocks show systematic changes in alteration assemblages as a function of position within the alteration zone. The central part of the zone is characterized by the assemblages chlorite-biotite-quartz-amphibole and quartz-

biotite-garnet, derived from low TiO_2 mafic flows. Northward to sub-zone 2, mafic flows are characterized by the assemblage chlorite-quartz-biotite, whereas in the outer margins of the zone they are characterized by chlorite-quartz-sericite-amphibole and sericite-epidote-chlorite-biotite assemblages.

Variations in mineral chemistry are well documented within hydrothermal alteration pipes beneath volcanogenic massive sulfide deposits. This variation is most evident in chlorites which show a progressive decrease in $\text{Mg}/\text{Mg}+\text{Fe}$ outward from the core of the alteration pipe (Larson, 1984; Hall, 1982; Henley & Thornley, 1981). Walford and Franklin (1982) have proposed that Fe-rich chlorite forms in the low temperature (outer) part of the alteration zone whereas Mg-rich chlorite is produced in the higher temperatures cores. At Vamp Lake, a similar relationship could not be established with the available data; chlorite from altered mafic rocks in the central part of the island distal zone has a more restricted compositional range than chlorite from altered mafic rocks in the outer margins of the zone, which encompasses the composition of chlorites from the core as well as chlorites which are more Mg-rich and Mg-poor. As noted in section 7.6.1, the variability of some of the chlorite from samples in the outer margin may indicate the presence of chlorite unrelated to the alteration.

Morphological features of the distal alteration zone are not compatible with a hydrothermal alteration pipe model. Typical hydrothermal alteration pipes cross-cut stratigraphy, and are

generally connected to the massive sulfide body (Lydon, 1984; Franklin et al, 1981). The distal island zone appears concordant, and is separated from the mineralization by unaltered units. The alteration assemblages are characterized by phyllosilicate minerals that display a well developed schistosity parallel to regional foliation, and the local development of axial planar and crenulation cleavage, indicating that the alteration zone pre-dates regional deformation. Therefore, the original morphology of the zone could have been changed by deformation, flattening an original cross-cutting body, and making it nearly parallel to stratigraphy. Most Canadian massive sulfide deposits have undergone penetrative deformation, and in many of these, the alteration zone has been transposed to a position of apparent lateral conformity with the massive sulfide body (Lydon, 1984; Franklin et al, 1981). The Flin Flin, Stall Lake, Anderson Lake and Normetal orebodies of the Flin Flon-Snow Lake belt are examples of deposits that are interpreted to be laterally transposed from their alteration pipes. Several features of the distal alteration zone at Vamp Lake, however, are not compatible with such an explanation; the alteration zone is a uniform distance far below, but directly underneath the ore zone with no lateral separation of distal alteration and ore zone, and the deformed three-dimensional shape of the zone does not appear to indicate a high degree of flattening. Thus spatial and morphological characteristics of the zone are consistent to some degree with a hydrothermal alteration pipe.

A different interpretation is the secondary feeder model, in

which the distal island alteration zone would represent a stratigraphically or structurally controlled off-shoot from a main conduit. Although this model could account for its spatial position and stratiform nature of the alteration zone, the pod-like morphology of the zone is difficult to reconcile as a stratigraphically or structurally controlled off-shoot which would presumably be more thinner and laterally continuous in nature.

A third, and more likely interpretation is the hydrothermal reservoir model. Hydrothermal reservoir properties are consistent with the conformable nature and position of the distal island alteration zone. The decreasing size with depth of the alteration zone could indicate that the main part of the reservoir was above the present day erosion surface. The actual feeder to the massive sulfide body may have been removed by erosion, along with most of the reservoir, or it may be present below the alteration zone, but was not intersected because drilling would be parallel to such a zone. The former alternative is more likely, because the density of drill holes would severely limit the size of such an undiscovered zone.

In conclusion, the internal characteristics, the morphology, and the spatial position of the distal alteration zone is consistent with a hydrothermal reservoir model, and most likely represents the remnants of a hydrothermal reservoir, the main body of which has been eroded away.

9.4.1.2 Mainland Fault Block

The present morphology of the mainland distal zone, particularly the high aspect ratio and stratiform nature of the zone, is much different from the the typical cross-cutting hydrothermal alteration pipe described in the literature (Franklin et al, 1981). The present morphology appears to preclude a hydrothermal alteration pipe model because it is highly unlikely that deformation could have produced such a morphology from a typical hydrothermal conduit pipe. The alteration zone in the mainland fault block may represent: 1) shear related hydrothermal alteration, or 2) a stratigraphically or structurally controlled secondary feeder zone. Both models are compatible with the extremely thin and continuous nature of the alteration zone. However, the chemistry and mineralogy of the zone is comparable to the distal island zone, suggesting that a comparable hydrothermal process was responsible for both; the shear model has therefore been ruled out. Since the mainland distal zone terminates at the fault, it is possible that it represents a lateral feeder off the hydrothermal reservoir (the distal island zone).

9.4.2 Proximal Alteration Zones

The proximal alteration zones may be 1) the result of alteration at the seawater-rock interface by the expulsion of ore-bearing hydrothermal fluids from a nearby vent, or 2) a metasomatic zone produced during metamorphism of the ore body.

9.4.2.1 Island Fault block

The metamorphic model for alteration is based on the premise that the metamorphic degradation of pyrite to pyrrhotite releases S to the environment (Vokes, 1962; Vokes, 1969; McDonald, 1967; Craig & Vokes, 1993); reactions of silicates with sulfur possibly derived from this source will lead to relatively iron-poor silicates within and adjacent to orebodies, and may be responsible for aureoles of Mg-metasomatism around some ore bodies (Vokes, 1969). Evidence against such a model in the island fault block is the asymmetric development of the alteration zone; alteration produced in this manner should have been equally well developed above and below the ore body, although the different lithologies above and below the ore body could have played a role in asymmetrical development of alteration. The spatial characteristics of the island ore zone are also not consistent with this model. As described in earlier sections, the proximal alteration zone extends past the ore zone, along an apparently stratigraphically controlled horizon.

The model most consistent with the data for the island fault block is alteration at the seawater-rock interface by the expulsion of ore-bearing hydrothermal fluids from a nearby vent. Such an alteration model is consistent with the thin, stratigraphically controlled, continuous nature of the zone, and its footwall position to the ore. The chemical changes in mafic rock of the proximal alteration zone are somewhat similar to those found in the distal zones, but there are some differences in the proximal zone

such as higher Mg, Cr, and Ni contents, and addition of Ca. The chlorite contained in this zone tend to be more Mg-rich as well (section 7.6.1). The different chemical characteristics of the proximal zone may reflect seawater-hydrothermal fluid mixing near the water-rock interface. Similar data on the behavior of Cr and Ni at the seawater-interface are not available.

9.4.2.2 Mainland Fault Block

The lake ore zone, in contrast to the island ore ore, has well developed proximal alteration in both hangingwall and footwall positions. The thickness of the alteration is less than 11 m, but the thickness is similar on all sides of the ore body. Proximal alteration of the mainland fault block therefore appears to be more spatially associated with the ore zone, and does not appear to have the same stratigraphic control evident in the proximal alteration zone of the island fault block. The alteration assemblages are identical above and below the lake ore zone, suggesting a similar genesis for altered rocks in both positions. Hangingwall alteration is present at a few other volcanogenic deposits elsewhere in the Churchill Province, although it is generally weakly developed (Franklin & Thorpe, 1982). The presence of hangingwall alteration has been noted also at the Amulet Lower A deposit at Noranda, and at many of the Kuroko deposits (Franklin et al, 1981). Alteration immediately above an ore zone is best developed where a second ore zone occurs stratigraphically above the first. In Kuroko deposits,

and other deposits where there are no overlying ore zones, hangingwall alteration is relatively subtle, and little chemical change occurred (Franklin et al, 1981). The hangingwall alteration above the island ore zone is weakly developed and thus does not appear to be unusual. The proximal alteration of the Lake Ore Zone is more enigmatic. The alteration is nearly as well developed above the ore as below, and contact with overlying unaltered rock is relatively sharp. Therefore its presence cannot be attributed to an overlying deposit.

The metamorphic model outlined in section 9.4.2.1 is consistent with the well developed alteration on all sides of the ore body. However, the island ore zone was subjected to the same metamorphic regime as the lake zone, and therefore should also have developed a pronounced hangingwall alteration in the same manner as the lake zone. Thus, although this model may be responsible for part of the alteration, it cannot account for all the features of the proximal alteration of both fault blocks.

The seawater-rock alteration interface model proposed for the proximal island zone could also account for the footwall proximal alteration of the mainland zone, although the more restricted occurrence of the mainland proximal alteration zone would suggest a different fluid regime in this locality. The hangingwall alteration of the lake zone is more enigmatic. Although the hangingwall alteration may indicate that the zone was buried while still hot and still reacting with the surrounding medium, there are insufficient data on the alteration in this locality to ascertain

the genesis with certainty.

9.5 GENESIS OF MINERALIZATION

The ore zones of the Vamp Lake deposit are stratabound, occurring at the contact between underlying mafic flows, and overlying felsic to intermediate volcanoclastic rocks. This setting is disturbed only on the ore discovery island, where a mafic sill has been intruded after deposition of mineralization and overlying lithologies splitting the mineralization into two ore zones. Based on the stratigraphic correlation the lake ore zone is interpreted to have been deposited at the same time as the island ore zone, and simply represents the emplacement of a more distal form of deposit from the same hydrothermal system.

9.5.1 Island Ore Zone

9.5.1.1 Economic to Sub-Economic Ore

The proximal alteration zone represents hydrothermal alteration of rocks at the seawater-rock interface (section 9.4.2.1). This implies that the source of the ore-bearing hydrothermal fluid, the vent area, was nearby. The higher Cu/Zn ratios suggested by the ore grades of the island ore zone relative to the lake ore zone would also suggest closer proximity to the

vent area (Lydon, 1984). Part of the hydrothermal reservoir apparently underlies the island ore zone as the distal alteration zone, suggesting that the feeder pipe was close, although not directly beneath the present ore zone. The Cu-Zn ore is therefore interpreted to have been deposited close to the hydrothermal vent, from ore-bearing hydrothermal fluids. The quartzose gangue common in this ore type is dissimilar to adjacent wall rocks suggesting that this gangue may be of hydrothermal origin (Lydon, 1984), indirectly supporting the hydrothermal deposition model.

9.5.1.2 Disseminated sulfide Zone

The disseminated sulfide zone in the hangingwall of the island ore zone may have been generated in one of two manners: 1) it may reflect renewed or continued hydrothermal activity, during the deposition of the overlying felsic units, or 2) it may be the result of metamorphic degradation of pyrite to pyrrhotite, and the subsequent release and reaction of sulfur with silicate minerals in the wall rocks to produce disseminated sulfides. Metamorphic development is consistent with the disseminated nature of the zone, but does not agree with the more extensive nature of the disseminated sulfides in the hangingwall relative to the footwall of the zone, extending up to 50 m above the zone, the lack of disseminated sulfides above the lake zone, or the breaks between disseminated zones evident in Figure 73. Renewed or continued hydrothermal activity during the deposition of the intermediate and

felsic volcanoclastic hangingwall sequence is consistent with the hangingwall position of the disseminated sulfide zone, and the local breaks in the zone. As such, this is the more likely model.

9.5.1.4 Gold Mineralization

Gold content in the Vamp Lake deposit is highly variable, ranging from 2.37 g/t in the lake ore zone, to 6.07 g/t in the island ore zone. The abundance of gold in the lake zone is comparable to other sulfide deposits in the Flin-Flon Snow Lake greenstone belt. Gold content of these deposits range from 0.10 to 3.39 g/t, and the 1.32 g/t average is well above the 0.7 g/t average for similar deposits from the Superior Province, with the exception of the Horne, Quemont, Lenoire, and Tache Lake deposits, each of which contain 6.2 g/t Au (Franklin & Thorpe, 1982). The higher gold content of the island ore zone is similar to that of the few gold-rich volcanogenic massive sulfide deposits in the Superior Province. The anomalous gold content of the island ore zone may reflect the chemical conditions at the time of mineralization or may represent a secondary enrichment. The spatial association between the Cu-Zn ore and the high gold contents seen in Figures 69 to 72 suggest that the gold is related to the deposition of the Cu-Zn sulfide ore. A copper-gold association, similar to that of the Cu-Zn ore of the island ore zone, has been documented in other deposits, particularly those with high Cu/Zn ratios such as Mt. Lyell and Mt. Chalmers in eastern Australia (Large et al., 1988), and the Millenbach mine at Noranda (Knuckey

et al, 1982).

This association may be due to the chemical characteristics of the hydrothermal fluids responsible for the transport and deposition of the associated metals. Studies from modern seafloor deposits indicate that the gold content of volcanogenic massive deposits is a function of the chemistry of the hydrothermal system (Hannington & Scott, 1988). The higher average gold content of sulfide deposits in the Churchill Province relative to the Superior Province may simply reflect chemical differences in the hydrothermal systems that operated in these separate regions.

Studies have shown that temperature, pH, salinity, dissolved S, and O or S activity control the chemistry of the hydrothermal fluid by the following relationship:

$$a\text{AuCl}_2^- / a\text{Au}(\text{HS})_2^- = (K_1/K_2) [(a\text{H}^+)^2(a\text{Cl}^-)^2 / (a\text{H}_2\text{S})^2] \quad (\text{Large et al, 1988})$$

Calculations based on this relationship indicate that gold transportation as AuCl_2^- complexes is favored by high temperature fluids ($>300^\circ\text{C}$), with high salinity ($>$ seawater), low pH (4.5), low $a\text{H}_2\text{S}$ ($<10^{-2.5}\text{M}$), and moderate to high $f\text{O}_2$. Such conditions favor the mutual transport and precipitation of gold and copper (Large et al., 1988). The transport of gold as a bisulfide complex ($\text{Au}(\text{HS})_2^-$) is favored by lower temperature fluids ($150\text{--}300^\circ\text{C}$), low salinity ($<$ seawater), moderate to alkaline pH (>4.5), high $a\text{H}_2\text{S}$ ($>10^{-2.5}\text{M}$), and moderate $f\text{O}_2$. These conditions favour the mutual transport and deposition of gold, lead and zinc. It has been suggested that most hydrothermal fluids responsible for the formation of volcanogenic massive sulfide deposits transport gold in solution as a gold

bisulfide complex ($\text{Au}(\text{HS})_2$), accounting for the fewer deposits with gold-copper associations.

Evidence from fluid density, geothermometry and S isotopes indicates that mixing of hydrothermal fluids with cold seawater is also an important control for localization of gold in massive sulfide deposits near the vent fluid-seawater interface (Hannington & Scott, 1988). This is primarily a function of decreasing temperature and increasing pH, resulting in the deposition of gold and copper from the hydrothermal fluid, particularly if the gold was being transported as a chloride complex which is stable at higher temperature and lower pH conditions. The Cu-Zn-Au ore of the island ore zone at Vamp Lake is interpreted to have been deposited from hydrothermal fluids that transported the metals as a chloride complex. The mixing of the hydrothermal fluids with seawater and subsequent deposition of the Cu-Zn-Au ore near the vent fluid-seawater interface is consistent with the proposed genesis of the underlying proximal alteration of this particular ore zone.

9.5.2 Lake Ore Zone

The Zn-rich nature of the lake ore zone, the pod-like morphology of the zone, and the lack of directly associated hydrothermal vent type alteration in the mainland fault block may imply that the lake ore zone is a more distal type of deposit that accumulated at least 400 m or more from the expulsion point of the hydrothermal exhalations, based on the relative position of the

more proximal island ore zone. Distal deposits may represent brine pools formed by high density ore solutions that accumulated in a topographic depression. Deposits generated in such a way typically have a tabular or sheet-like morphology, and higher Zn-Cu ratios, possibly the result of lower ore solution temperatures (Lydon, 1988). The lower Cu/Zn ratio of the lake zone supports such an origin for this ore body. Distal deposits do not have associated alteration zones (Bailes & Syme, 1989), and the lack of a hydrothermal vent in this area indirectly supports the model. Although the lake ore zone is not associated with fine-grained cherts and graphitic mudstones that typically overlie and host other distal deposits in the Flin Flon area (Bailes & Syme, 1989), the absence of such units could merely reflect a shorter hiatus in volcanic activity.

9.6 TIMING OF MINERALIZATION AND ALTERATION

As indicated by the metamorphic and cataclastic textures of the ores, the Vamp Lake deposit has been metamorphosed and deformed. This, in conjunction with the plunge of the island ore zone, which is consistent with regional lineations observed in the country rocks, supports a pre-deformational and pre-metamorphic origin for the deposit. The presence of chalcopyrite exsolutions in sphalerite (as seen in Figure 84) indicates that temperatures of at least 350-400 degrees celsius were reached during metamorphism (Vokes, 1969). This is consistent with the amphibolite metamorphic

grade indicated by the mineralogy of the host rocks. This interpretation is consistent with the inferred pre-metamorphic origin of the alteration zones associated with the ore zones, as suggested by the schistosity of the alteration assemblages which parallel regional foliation.

The proposed hydrothermal model for the alteration and emplacement of the island ore zone and the associated proximal alteration implies that the ore was deposited after the emplacement of the mafic units of formation 3, and prior to the deposition of the intermediate and felsic dominated formation 4. The presence of sulfide-bearing fragments in hangingwall intermediate units (Figure 20) is consistent with the interpretation that some mineralization occurred prior to the deposition of the overlying units. The disseminated nature of the upper part of the island zone probably reflects a more diffuse and less focussed hydrothermal activity. The lake zone was deposited prior to the generation of the overlying disseminated sulfide zone in the island fault block.

CONCLUSIONS

1. The Vamp Lake deposit is interpreted to be a synvolcanic massive sulfide deposit in a tholeiitic island arc setting.
2. Stratigraphic correlation across the east-trending fault indicates that both the island and lake zones were deposited at the same time. The island ore zone is interpreted to be a proximal type of deposit; the hydrothermal vent was nearby, although not directly beneath it. The lake zone is interpreted to be a more distal deposit, produced from the same hydrothermal system as that responsible for the island ore zone.
3. Remnants of the hydrothermal system are reflected in the presence of the distal and proximal alteration zones. The island distal alteration zone is interpreted to represent a hydrothermal reservoir, the main part of which has been eroded away; the distal lake zone may be a stratigraphically controlled off-shoot from the reservoir. Proximal alteration zones show slight variations from distal zones in mineralogy and chemistry. These features may reflect alteration at the seawater-rock interface by hydrothermal fluid that was mixing with seawater.
4. The hydrothermal vent has not been found, and may have been above the present day erosion surface. Most of the ore produced by this hydrothermal system would presumably have been located above the vent area, suggesting that it has been eroded as well.

REFERENCES

- Bailes, A.H., 1970, Geology: Snow Lake, Flin Flon, Sherridon Area. Manitoba Dept. of Mines, Resource & Environmental Management (1:350,000 map).
- Bailes, A.H., 1971, Preliminary Compilation of the Geology of the Snow Lake-Flin Flon Sherridon Area. Man. Dept. of Energy & Mines, Mines Branch Geological Paper 1, 23 p.
- Bailes, A.H., Syme, E.C., Galley, A., Price, D.P., Skirrow, R. and Ziehlke, D.J., 1987, Early Proterozoic volcanism, hydrothermal activity, and associated ore deposits at Flin Flon and Snow Lake, Manitoba. Geological Association of Canada and Mineralogical Association of Canada Joint Annual Meeting, Saskatoon, Saskatchewan, May 20-24, 95 p.
- Bailes, A.H., and Syme, E.C., 1989, Geology of the Flin Flon-White Lake Area. Man. Dept. of Energy & Mines, Geological Report GR 87-1, 313 p.
- Banos, Juan Olives, and Amouric, Marc, 1984, Biotite chloritization by interlayer brucitization as seen by HRTEM. American Mineralogist, v. 69, p. 869-871.
- Barker, A.J., 1990, Introduction to Metamorphic Textures and Microstructures. 162 p.
- Beccaluva, L., Ohnenstetler, D., Ohnenstetler, M., 1979, Geochemical discrimination between ocean floor and island arc tholeiite - application to some ophiolites. Can. J. Earth Sci. v. 16, p. 1874-1882.
- Bruce, E.L., 1918, Amisk - Athapapuskow Lakes district. Geological Survey of Canada, Memoir 105, 91 p.
- Campbell, I.H., Coad, P., Franklin, J.M., Gorton, M.P., Scott, S.D., Sowa, J., and Thurston, P.C., 1982, Rare earth elements in volcanic rocks associated with Cu-Zn massive sulphide mineralization: a preliminary report. Can J. or Earth Sci, v. 19, p. 619-623.
- Canadian Mines Handbook 1989-1990, 1989, (edited by C.D. Gardiner), Northern Miner Press Limited, 608 p.
- Craig, J.R., and Vokes, F.M., 1993, The metamorphism of pyrite and pyritic ores: an overview. Mineralogical Magazine, v. 57, p. 3-18.
- Fedikow, M.A.F., 1986, Geology of the Agassiz stratabound Au-Ag deposit, Lynn Lake, Manitoba. Manitoba Energy & Mines

Geological Services. Open File Report OF85-5. 80 p.

- Finlow-Bates, T., Stumpfl, E.F., 1981, The behavior of so-called immobile elements in hydrothermally altered rocks associated with volcanogenic submarine-exhalative ore deposits. *Mineral. Deposita*, v. 16, p. 319-328.
- Fisher, R.V., 1966, Rocks composed of volcanic fragments. *Earth Sci. Rev.* v. 1, p.287-298.
- Franklin, J.M. and Thorpe, R.I., 1982, A Comparative Metallogeny of the Superior, Slave and Churchill Provinces. In: H.S. Robinson Memorial Volume, Precambrian Sulfide Deposits (edited by R.W. Hutchinson, C.D. Spence, and J.M. Franklin). *Geol. Assoc. of Canada Special Paper 25*, p. 3-90.
- Franklin, J.M., Lydon, J.W., Sangster, D.F., 1981, Volcanic associated massive sulfide deposits. *Econ. Geol.* 75th Anniversary volume, p. 485-627.
- Frater K.M., 1983, Geology of the Golden Grove prospect, western Australia: A volcanogenic massive sulfide-magnetite deposit. *Econ. Geol.* v. 78, p. 875-919.
- Froese, E., & Moore, J.M., 1980, Metamorphism in the Snow Lake area, Manitoba. *Geol. Surv. of Canada Paper 78-27*
- Gair, J.E., & Vokes, F.M., 1984, A special issue devoted to massive sulfide deposits of the Appalachian-Caledonian Orogen. *Econ. Geol.* v. 79, p.1425-1427.
- Gair, J.E., & Slack, J.F., 1984, Deformation, geochemistry and origin of massive sulfide deposits, Gossan lead district, Virginia. *Econ. Geol.* v. 79, p. 1483-1520.
- Gale, G.H., Somerville, R.C., Chornoby, J., Haystead, B., Provins, N., Braun, D., Munday, D., Walker, A., 1982, Geological setting of mineral deposits at Ruttan Thompson, Snow Lake and Flin Flon, Manitoba. *Geological Assoc. of Canada & Mineralogical Assoc. of Canada Joint Annual Meeting, Wpg., Man., May 19-23*, 59 p.
- Gale, G.H., 1983, Proterozoic exhalative massive sulfide deposits. *Geol. Soc. of America. Memoir 161*, p.191-207.
- Gass, I.G., 1982, Upper Proterozoic (Pan-African) calc-alkaline magmatism in NE Africa & Arabia. In: *Andesites: Orogenic Andesites and related rocks.* (R.S. Thorpe, ed.). John Wiley & Sons, New York. pp. 591-609.
- Gibson, H.L., Watkinson, D.H., and Comba, C.D.A., 1983, Silicification: Hydrothermal Alteration in an Archean

- Geothermal System within the Amulet Rhyolite Formation, Noranda, Quebec. *Econ. Geol.* v. 78, p. 954-971.
- Grant, James A., 1986, The Isocon Diagram - a Simple Solution to Gresens' Equation for Metasomatic Alteration. *Econ. Geol.* v. 81, p. 1976-1982.
- Gresens, Randall L. 1967, Composition - volume relationship of metasomatism. *Chem. Geol.* v. 2, p. 47-65.
- Hall, B.V., 1982, Geochemistry of the alteration pipe at the Amulet upper A deposit, Noranda, Quebec. *Can J. Earth Sci.* v. 19, p. 2060-2084.
- Hannington, M.D., & Scott, S.D., 1988, Gold mineralisation in volcanogenic massive sulfides; modern and ancient. In: Goode, A.D.T., Smyth, E.L., Birch, W.D., & Bosma, L.I. (eds), *Bicentennial Gold '88; Extended Abstracts; Oral Programme.* *Geol. Soc. of Australia, Abstracts v 22*, p. 353-358.
- Henley, R.W., and Thornley, P., 1981, Low grade metamorphism and the geothermal environment of massive sulphide ore from Buchans, Newfoundland. In: *The Buchans orebodies: Fifty years of geology and mining* (ed. by E.A. Swanson, D.F. Strong, J.G. Thurlow). *Geol. Assoc. of Canada Special Paper 22*, p. 205-228.
- Hey, M.H., 1954, A new review of the chlorites. *Min. Mag.*, v. 30, p. 277.
- Hughes, C.J., 1973. Spilites, Keratophyres, and the Igneous Spectrum. *Geol. Mag.*, v. 6, p. 513-527.
- Hwang, Jiann-yang, 1984, Mineralogical study of Hudvam mine drill cores, 29 p. unpublished. Institute of Mineral Research, Michigan Technological University; Houghton, Michigan.
- Irvine, T.N., and Baragar, W.R.A., 1971, A guide to the chemical classification of the common volcanic rocks. *Can. J. of Earth Sci.*, v. 8, p. 521-548.
- Jensen, L. S., 1976, A New Cation Plot for Classifying Subalkalic Volcanic Rocks. Ontario Div. Mines, Misc. Paper 66, 22p.
- Klemm, R., Maiden, K.J., & Okrusch, M., 1987, The Matchless copper deposit, SW Africa/Namibia: a deformed and metamorphosed massive sulfide deposit. *Econ. Geol.*, v. 82, p. 587-599.
- Knuckey, M.J., Comba, C.D.A., Riverin, G., 1982, Structure, metal zoning and alteration at the Millenbach deposit, Noranda, Quebec. In: *Precambrian sulphide deposits* (edited by R.W. Hutchinson, C.D. Spence and J.M. Franklin). *Geol. Assoc. of Canada Special Paper 25*, p. 255-295.

- Koo, Jahak, and Mossman, David J., 1975, Origin and metamorphism of the Flin Flon stratabound Cu-Zn sulfide deposit, Saskatchewan and Manitoba. *Econ. Geol.* v. 70, p. 48-62.
- Kranidiotis, P., and MacLean, W.H., 1987, Systematics of the Chlorite Alteration at the Phelps Dodge Massive Sulfide Deposit, Matagami, Quebec. *Econ. Geol.*, v. 82. p. 1898-1911.
- Large, R., Huston, D., McGoldrick, P.J., McArthur, G., & Ruxton, P., 1988, Gold distribution and genesis in Palaeozoic volcanogenic massive sulfide systems, Eastern Australia. In: Goode, A.D.T., Smyth, E.L., Birch, W.D., & Bosma, L.I. (eds), *Bicentennial Gold '88; Extended Abstracts; Oral Programme.* *Geol. Soc. of Australia, Abstracts v 22*, p. 121-126.
- Larson, Peter B., 1984, Geochemistry of the alteration pipe at the Bruce Cu-Zn volcanogenic massive sulfide deposit, Arizona. *Econ. Geol.* v. 70, p. 1880-1896.
- Lydon, John W., 1984, Ore deposit models - 8. Volcanogenic massive sulphide deposits part 1: a descriptive model. *Geoscience Canada* v. 11, No. 4, p. 195-202.
- Lydon, John W., 1988, Ore deposit models #14. Volcanogenic massive sulphide deposits part 2: genetic models. *Geoscience Canada*, v. 15, no. 1, p. 43-65.
- Marshall, B., & Gilligan, L.B., 1989, Durchbewegung Structure, Piercement Cusps, and Piercement Veins in Massive Sulfide Deposits: Formation and Interpretation. *Econ. Geol.*, v. 84, p. 2311-2319.
- McDonald, J.A., 1967, Metamorphism and its effects on sulphide assemblages. *Mineralium deposita*, v. 2, p. 200-220.
- McGlynn, I.C., 1959, Elbow-Heming lakes area, Manitoba. *Geol. Surv. Can. Memoir* 305, 305 p.
- Morton, R.L., Franklin, J.M., 1987, Two-Fold Classification of Archean Volcanic-Associated Massive Sulfide Deposits. *Econ. Geol.* v. 82, p. 1057-1063.
- Nold, John L., 1983, The Holden Mine, a metamorphosed volcanogenic deposit in the Cascade Range of Washington. *Econ. Geol.* v. 78, p. 944-953.
- Parliment A., 1966, Report on the property of Vamp Lake Mines Ltd., Athapapuskow Mining Division Manitoba (unpublished report).
- Pearce, J.A., 1975, Basalt Geochemistry used to Investigate Post-tectonic Environments on Cyprus: *Tectonophysics*, v. 25, p. 61-67.

- Pearce, J.A. and Cann, J.R., 1973, Tectonic setting of basic volcanic rocks determined using trace element analyses. *Earth & Planetary Sci. Letters*, v. 19, p. 290-300.
- Pearce, J.A., and Gale, G.H. 1977, Identification of ore deposit environment from trace element geochemistry of associated igneous host, p. 14-24. In: *Volcanic processes in ore genesis* (anonymous), Inst, Mining & Metallurgy, 188 p.
- Pederson, F.D., 1980, Remobilization of the massive sulfide ore of the Black Angel Mine, Central West Greenland. *Econ. Geol.* v. 75. p. 1022-1041.
- Prouse, D.E., and Esposito, B., 1989, Mineral exploration/development in Manitoba - 1989. Exploration Services Section, Mines Branch, Manitoba Dept. of Energy & Mines, 5 p.
- Riverin, Gerald, and Hodgson, C.Jay, 1980, Wall-rock alteration at the Millenbach Cu-Zn mine, Noranda, Quebec. *Econ. Geol.* v. 75, p. 424-444.
- Roberts, R. Gwilym, and Reardon, Eric J., 1978, Alteration and ore forming processes at Mattagami Lake Mine, Quebec. *Can. J. of Earth Sci.* v. 15, p. 1-21.
- Sangster, D.F., 1972, Precambrian volcanogenic massive sulfide deposits in Canada - a review. *Geol. Surv. Can. Paper* 72-22.
- Sangster, D.F., and Scott, S.D., 1976, Precambrian strata-bound, massive Cu-Zn-Pb sulfide ores of North America. In Wolf, K.H., *Handbook of strata-bound and stratiform ore deposits*; Amsterdam, Elsevier, p. 129-222.
- Spry, Paul G., and Scott, Steven D., 1986a, The stability of zincian spinels in sulfide systems and their potential as exploration guides for metamorphosed massive sulfide deposits. *Econ. Geol.* v. 81, p. 1446-1463.
- Spry, Paul G., and Scott, Steven D., 1986b, Zincian spinel and staurolite as guides to ore in the Appalachians and Scandinavian Caledonides. *Canadian Minerologist* v. 4, p. 147-163.
- Stauffer, M.R. and Mukherjee, A.C., 1971, Superimposed deformations in the Missi Metasedimentary rocks near Flin Flon, Manitoba. *Canadian J. of Earth Sci.*, v. 8, p. 217-242.
- Stauffer, M.R., Mukherjee, A.C., Koo, J., 1975, The Amisk Group: An Aphebian (?) island arc deposit. *Can. J. of Earth Sci.*, v. 12, p. 2021-2035.
- Stephen, Michael B., Swinden, H. Scott, Slack, John F., 1984,

- Correlation of massive sulphide deposits in the Appalachian-Caledonian Orogen on the basis of paleotectonic setting. *Econ. Geol.*, v. 79, p. 1442-1478.
- Stow, Stephen H., and Tull, James F., 1982, Geology and geochemistry of the stratabound sulfide deposits of the Pyriton district, Alabama. *Econ. Geol.* v. 77, p. 322-334.
- Syme, E.C., Bailes, A.H., Price, D.P., Ziehlke, D.V., 1982, Flin Flon volcanic belt: geology and ore deposits at Flin Flon-Snow Lake, Manitoba. *Geol. Assoc. of Canada and Min. Assoc. of Canada, Joint Annual Meeting, Winnipeg, Man., May 20-24, 91 p.*
- Veblen, David R., Ferry, John M., 1983, A TEM study of the biotite-chlorite reaction and comparison with petrologic observations. *American Mineralogist*, v. 68, p. 1160-1168.
- Vivaldo, Waldo, 1985, The geology and genesis of the Proterozoic massive sulfide deposit at Garpenberg, Central Sweden. *Econ. Geol.* v. 80, p. 17-32.
- Vokes, F.M., 1962, Mineral Paragenesis of the massive ore bodies of the Caledonides of Norway. *Econ. Geol.*, v. 57, p. 890-903.
- Vokes, F.M., 1969, A review of the metamorphism of sulfide deposits. *Earth Sci. Rev.* v. 5, p. 99-143.
- Vokes, F.M., 1971, Some aspects of the regional metamorphic mobilization of preexisting sulphide deposits. *Mineral. Deposita* v. 6, p. 122-129.
- Vokes, F.M., 1993, Post-recrystallisation mobilisation phenomena in metamorphosed stratabound sulphide ores. *Mineralogical Magazine*, v. 57, p. 19-28.
- Walford, P.C., Franklin, J.M., 1982, The Anderson Lake Mine, Snow Lake Manitoba. In: *Precambrian sulphide deposits* (edited by R.W. Hutchinson, C.D. Spence and J.M. Franklin). *Geol. Assoc. of Canada Special Paper 25*, p. 481-523.
- Walker, A.A., 1982, Hudson Mines Ltd. Geological Report, (unpublished), 5 p.
- Walker, A.A., 1985, Hudvam proven ore reserves (unpublished report), 4 p
- Winchester, J.A. and Floyd. P.A., 1977, Geochemical discrimination of different magma series and their differentiation products using immobile elements. *Chem. Geol.*, v. 20, p. 325-343.
- Wynne, P.J. and Strong, D.F., 1984, The Strickland prospect of southwestern Newfoundland: a lithogeochemical study of

metamorphosed and deformed volcanogenic massive sulfides.
Econ. Geol., v. 79, p. 1620-1642.

Zhong, William J.S., Hughes, John M., Scotford, David M., 1985, The response of chlorite to metasomatic alteration in Appalachian ultramafic rocks. Canadian Mineralogist, v. 23, p. 443-446.

APPENDIX A

Silicate Mineralogy of Whole Rock Samples

		Mineralogy (%)																		
Sample Number	Location	Qu	Pl	Hbl	T	E	Z	Cz	Bi	Cl	M	St	Ga	Gah	P	Ca	S	BC	Sh	Opagues
GR 6	L-3	36	28			12			12	<1	6		<1							6
GR 8	L-2	43	35	2		3			12	2										3
GR 12	L-4	47	40			2			7		<1		2			1				1
GR 13	L-3	6	43	49																2
GR 14	L-3	13	27	60																2
GR 19	L-4	41	35	7		7			8	<1			2							2
GR 25	L-4	35	36	12		5			8				2							2
GR 26	L-3	28	14	56																2
GR 32	L-4	32	40	25				1												2
GR 33	L-5	29	34	35																2
GR 35	L-7	35	53	2					10		<1									2
GR 36	L-3	23	13	50		10			2											2
GR 39	L-4	64	18	9		4			3											2
GR 40	L-4	15	35	45		3										<1	<1			2
GR 48	L-4	20	46	17		16										<1	<1			2
GR 49	L-3	27	23	45		5										<1				1
GR 59	L-4	41	25	24		4			<1					2						4
TR 21	L-3	3	26			17			9	11							26			8
52-350	L-4	29	31			15	2		20	<1										3
52-374	L-4	26	7	61					1								<1			5
53-474	L-4	49	13	20		8			10											3
59-47	L-3	38	27	30		<1														5
59-81.5	L-3	23	17	30		30														8
59-214.5	L-3	33	24		3					25							7			5
67-117	L-3	3	44	50		<1			3	<1										1
67-291	L-3	25	30	40					4											1
67-787	L-4	26	44	30																1
67-889	L-7	70	20							10										1
139-260.5	L-3	12	4						18	58		2	<1							6
139-325	L-3	25							3	66									1	6
139-502	L-3	37	36			2			15											10
140-176.5	L-3	20	19	55					5											1
140-264	L-3	32	42	5					15				<1							6
140-298	L-3	36	10			12					13		2			<1	17			10
Con 9-121	L-3	22	31	41					1											5
Con 9-312	L-3	32	23	10					20	15										5
Con 20-124	L-4	36	30	20																2
Con 24-158	L-3	30			44	12												20		6
Con 24-167.5	L-3	51	8	30					8											3
Con 44-123	L-3	29	35	29																7
Con 44-154	L-3	40		4					25	30										1
Con 44-248	L-3	43	3	7					15	25										7
Con 44-432	L-3	26	22	50					1											1
Con 45A-479	L-3	7	19	71		2														1
Con 45A-491	L-3	1	5	90		4	<1	<1	<1											1
Con 45A-835.5	L-3	32	43	15		8			<1											2
Con 45A-860	L-3	1			85				2											2
Con 51-171	L-3	52	7	35					6											2
Con 51-584	L-3	3	1	96																2
Con 51-682	L-3	20	39	40																1
Con 52-96.5	L-2	27	33	30					4				1							5
Con 52-614.5	L-2	47	29	7		3			10				1				3			3
Con 57-172	L-3	18	30	45		3														4
Con 57-188	L-3	8	13	75		2														2
Con 57-343.5	L-3	7	15	71		3														3
Con 57-551.5	L-3	18	36	40		3				<1						<1				3
Con 57-674.5	L-3	18	2	65		9														6
Con 57-753	L-3	3			88				7	1										1
Con 57-779	L-4	49	35			9			1											6
Con 62-477	L-3	19	25						15				38							3
Con 62-522	L-3	8	31	10		15			14	4			4				12			2
Con 63-171	L-3	13	57			3			14	2										11
Con 63-188.5	L-3	32		9					11	46									1	1
Con 63-253.5	L-3		13	71		10				1										5
Con 63-446.5	L-3	36	19						19	1										25
Con 63-590	L-7	39	39			6			14											2
Con 63-898.5	L-3	43	5	49		1														2
Con 63-1035	L-3	6			79				10	4										1
Con 63-1116	L-4	58	17			10										2				7
Con 64-122	L-2	25	33	25		16			5	1										7

Abbreviations Used:

Qu - Quartz	M - Muscovite
Pl - Plagioclase	St - Staurolite
Hbl - Hornblende	Gar - Garnet
Tr - Tremolitic Amphibole	Gah - Gahnite
E - Epidote	Ca - Calcite
Z - Zoisite	S - Sericite
Cz - Clinzoisite	BC - Biotite-Chlorite Intergrowths
Bi - Biotite	Pr - Prehnite
Cl - Chlorite	Sh - Sphene

APPENDIX B

Electron microprobe analyses of chlorite from various assemblages and locations, as tabulated below. In the following pages, the number in brackets following the sample number refer to analyses from different crystals from the same sample; those with letter designations refer to different analyses from the same crystal.

<u>Sample</u>	<u>Assemblage</u>	<u>Location</u>
59-214	chlorite-quartz-sericite-amphibole	Mainland distal zone
139-325	chlorite-quartz-biotite	Island distal zone
CON 7-130	chlorite-biotite-quartz-amphibole	Island distal zone
CON 7-165	chlorite-biotite-quartz-amphibole	Island distal zone
CON 7-246.5	chlorite veins	Island peripheral
CON 20-115	tremolite-quartz-biotite-chlorite	Mainland proximal zone
CON 24-121	tremolite-quartz-biotite-chlorite	Mainland proximal zone
CON 24-160	biotite-chlorite intergrowths	Mainland proximal zone
CON 26-92	chlorite-quartz-biotite	Mainland distal zone
CON 26-102	chlorite-quartz-biotite	Mainland distal zone
CON 26-129	chlorite veins	Mainland peripheral
CON 39-732.5	tremolite-quartz-biotite-chlorite	Island proximal zone
CON 44-154	chlorite-biotite-quartz-amphibole	Island distal zone
CON 44-228	chlorite-biotite-quartz-amphibole	Island distal zone
CON 44-248	chlorite-biotite-quartz-amphibole	Island distal zone
CON 44-317.5	chlorite-biotite-quartz-amphibole	Island distal zone
CON 44-767	biotite-chlorite intergrowths	Island proximal zone
CON 44-775	biotite-chlorite intergrowths	Island proximal zone
CON 62-367.5	chlorite-biotite-quartz-amphibole	Island distal zone
CON 62-392	chlorite-biotite-quartz-amphibole	Island distal zone
CON 63-67.5	chlorite-quartz-sericite-amphibole	Island distal zone
CON 63-188	chlorite-biotite-quartz-amphibole	Island distal zone
CON 63-449.5	chlorite-quartz-biotite	Island distal zone
CON 63-549.5	chlorite-quartz-sericite-amphibole	Island distal zone
CON 63-1035	tremolite-quartz-biotite-chlorite	Island proximal zone
CON 64-470.5	chlorite veing	Island peripheral

Sample 59-214 (1)

QUANTITATIVE EDS RESULTS
(ZAF CORRECTIONS VIA MAGIC V)

ELEMENT & LINE	K-RATIO	WEIGHT PERCENT	PRECISION 2 SIGMA	OXIDE FORMULA	OXIDE PERCENT	NO. OF CATIONS IN FORMULA
HG KA	0.0484	8.35	0.17	HGO	13.84	4.3727
AL KA	0.0645	10.18	0.13	AL2O3	19.23	4.8040
SI KA	0.0870	12.44	0.13	SI02	26.61	5.6402
K KA	0.0002	0.02	0.01	K2O	0.02	0.0065
CA KA	0.0004	0.05	0.01	CAO	0.06	0.0143
MN KA	0.0019	0.21	0.03	MNO	0.27	0.0486
FE KA	0.2008	22.25	0.27	FE0	28.63	5.0749
O *		35.17				
TOTAL					88.66	19.9611

NUMBER OF CATIONS CALCULATED ON BASIS OF 28 OXYGEN ATOMS.

* DETERMINED BY STOICHIOMETRY

Sample 59-214 (2)

ELEMENT & LINE	K-RATIO	WEIGHT PERCENT	PRECISION 2 SIGMA	OXIDE FORMULA	OXIDE PERCENT	NO. OF CATIONS IN FORMULA
HG KA	0.0632	10.58	0.17	HGO	17.54	5.5078
AL KA	0.0592	9.37	0.14	AL2O3	17.70	4.3946
SI KA	0.0904	12.89	0.13	SI02	27.57	5.8088
FE KA	0.1696	18.90	0.27	FE0	24.31	4.2828
O *		35.39				
TOTAL					87.13	19.9939

Sample 59-214 (3)

ELEMENT & LINE	K-RATIO	WEIGHT PERCENT	PRECISION 2 SIGMA	OXIDE FORMULA	OXIDE PERCENT	NO. OF CATIONS IN FORMULA
HG KA	0.0685	11.33	0.19	HGO	18.78	5.7510
AL KA	0.0608	9.61	0.14	AL2O3	18.16	4.3978
SI KA	0.0929	13.27	0.14	SI02	28.40	5.8341
K KA	0.0005	0.05	0.01	K2O	0.06	0.0168
FE KA	0.1613	17.99	0.25	FE0	23.14	3.9756
O *		36.29				
TOTAL					88.55	19.9754

Sample 59-214 (4)

QUANTITATIVE EDS RESULTS
(ZAF CORRECTIONS VIA MAGIC V)

ELEMENT & LINE	K-RATIO	WEIGHT PERCENT	PRECISION 2 SIGMA	OXIDE FORMULA	OXIDE PERCENT	NO. OF CATIONS IN FORMULA
HG KA	0.0666	11.04	0.18	HG ₀	18.30	5.7030
AL KA	0.0588	9.30	0.14	AL ₂ O ₃	17.57	4.3295
SI KA	0.0925	13.18	0.13	SI ₀₂	28.19	5.8928
FE KA	0.1600	17.86	0.25	FE ₀	22.98	4.0170
O *		35.66				
TOTAL					87.03	19.9424

NUMBER OF CATIONS CALCULATED ON BASIS OF 28 OXYGEN ATOMS.

* DETERMINED BY STOICHIOMETRY

Sample 139-325 (1)

QUANTITATIVE EDS RESULTS
(ZAF CORRECTIONS VIA MAGIC V)

ELEMENT & LINE	K-RATIO	WEIGHT PERCENT	PRECISION 2 SIGMA	OXIDE FORMULA	OXIDE PERCENT	NO. OF CATIONS IN FORMULA
MG KA	0.0871	13.54	0.20	MGO	22.45	6.6630
AL KA	0.0798	12.45	0.16	AL2O3	23.52	5.5192
SI KA	0.0849	12.32	0.13	SI02	26.37	5.2498
K KA	0.0006	0.06	0.01	K2O	0.08	0.0197
MN KA	0.0025	0.28	0.03	MNO	0.37	0.0620
FE KA	0.1033	11.61	0.21	FE0	14.93	2.4868
O *		37.45				
TOTAL					87.72	20.0004

NUMBER OF CATIONS CALCULATED ON BASIS OF 28 OXYGEN ATOMS.

* DETERMINED BY STOICHIOMETRY

Sample 139-325 (2)

ELEMENT & LINE	K-RATIO	WEIGHT PERCENT	PRECISION 2 SIGMA	OXIDE FORMULA	OXIDE PERCENT	NO. OF CATIONS IN FORMULA
MG KA	0.0888	13.77	0.20	MGO	22.84	6.8247
AL KA	0.0786	12.27	0.16	AL2O3	23.19	5.4799
SI KA	0.0841	12.20	0.12	SI02	26.11	5.2344
MN KA	0.0024	0.28	0.03	MNO	0.36	0.0604
FE KA	0.1001	11.25	0.20	FE0	14.47	2.4261
O *		37.19				
TOTAL					86.96	20.0256

Sample 139-325 (3)

ELEMENT & LINE	K-RATIO	WEIGHT PERCENT	PRECISION 2 SIGMA	OXIDE FORMULA	OXIDE PERCENT	NO. OF CATIONS IN FORMULA
MG KA	0.0873	13.62	0.20	MGO	22.58	6.7972
AL KA	0.0750	11.73	0.15	AL2O3	22.15	5.2734
SI KA	0.0857	12.40	0.13	SI02	26.53	5.3580
TI KA	0.0002	0.03	0.01	TIO2	0.04	0.0067
MN KA	0.0021	0.24	0.03	MNO	0.31	0.0530
FE KA	0.1028	11.55	0.21	FE0	14.86	2.5102
O *		36.92				
TOTAL					86.48	19.9986

Sample CON 7-130

QUANTITATIVE EDS RESULTS
(ZAF CORRECTIONS VIA MAGIC V)

ELEMENT & LINE	K-RATIO	WEIGHT PERCENT	PRECISION 2 SIGMA	OXIDE FORMULA	OXIDE PERCENT	NO. OF CATIONS IN FORMULA
HG KA	0.0873	13.64	0.20	HGO	22.62	6.8003
AL KA	0.0728	11.39	0.14	AL ₂ O ₃	21.53	5.1179
SI KA	0.0876	12.65	0.13	SiO ₂	27.06	5.4583
FE KA	0.1068	12.01	0.22	FeO	15.45	2.6062
O *		36.96				
TOTAL					86.65	19.9827

NUMBER OF CATIONS CALCULATED ON BASIS OF 28 OXYGEN ATOMS.

* DETERMINED BY STOICHIOMETRY

Sample CON 7-165 (1)

QUANTITATIVE EDS RESULTS
(ZAF CORRECTIONS VIA MAGIC V)

ELEMENT & LINE	K-RATIO	WEIGHT PERCENT	PRECISION 2 SIGMA	OXIDE FORMULA	OXIDE PERCENT	NO. OF CATIONS IN FORMULA
MG KA	0.0922	14.19	0.21	MGO	23.52	6.9708
AL KA	0.0766	11.93	0.15	AL2O3	22.54	5.2828
SI KA	0.0878	12.69	0.13	SI02	27.15	5.3988
K KA	0.0016	0.18	0.02	K2O	0.22	0.0552
FE KA	0.0951	10.66	0.21	FE0	13.71	2.2799
O *		37.50				
TOTAL					87.15	19.9874

NUMBER OF CATIONS CALCULATED ON BASIS OF 28 OXYGEN ATOMS.

* DETERMINED BY STOICHIOMETRY

Sample CON 7-165 (2)

ELEMENT & LINE	K-RATIO	WEIGHT PERCENT	PRECISION 2 SIGMA	OXIDE FORMULA	OXIDE PERCENT	NO. OF CATIONS IN FORMULA
MG KA	0.0942	14.50	0.21	MGO	24.04	7.1153
AL KA	0.0752	11.77	0.15	AL2O3	22.24	5.2031
SI KA	0.0876	12.68	0.13	SI02	27.13	5.3861
CR KA	0.0000	0.00	0.00	CR2O3	0.00	0.0000
FE KA	0.0964	10.80	0.22	FE0	13.90	2.3078
O *		37.56				
TOTAL					87.31	20.0123

Sample CON 7-246.5

QUANTITATIVE EDS RESULTS
(ZAF CORRECTIONS VIA MAGIC V)

ELEMENT & LINE	K-RATIO	WEIGHT PERCENT	PRECISION 2 SIGMA	OXIDE FORMULA	OXIDE PERCENT	NO. OF CATIONS IN FORMULA
MG KA	0.0512	8.68	0.18	MGO	14.38	4.5354
AL KA	0.0700	10.94	0.14	AL2O3	20.67	5.1523
SI KA	0.0851	12.16	0.12	SI02	26.01	5.5031
MN KA	0.0034	0.37	0.04	MNO	0.48	0.0861
FE KA	0.1864	20.40	0.29	FEO	26.25	4.6439
O *		35.25				
TOTAL					87.80	19.9208

NUMBER OF CATIONS CALCULATED ON BASIS OF 28 OXYGEN ATOMS.

* DETERMINED BY STOICHIOMETRY

Sample CON 20-115 (1)

QUANTITATIVE EDS RESULTS
(ZAF CORRECTIONS VIA MAGIC V)

ELEMENT & LINE	K-RATIO	WEIGHT PERCENT	PRECISION 2 SIGMA	OXIDE FORMULA	OXIDE PERCENT	NO. OF CATIONS IN FORMULA
HG KA	0.0611	10.15	0.19	HGO	16.83	5.2199
AL KA	0.0712	11.17	0.14	AL2O3	21.10	5.1750
SI KA	0.0851	12.25	0.12	SI02	26.22	5.4542
K KA	0.0006	0.06	0.01	K2O	0.08	0.0199
MN KA	0.0020	0.23	0.03	MNO	0.29	0.0513
FE KA	0.1613	18.08	0.26	FE0	23.27	4.0480
O *		35.84				
TOTAL					87.78	19.9683

NUMBER OF CATIONS CALCULATED ON BASIS OF 28 OXYGEN ATOMS.

* DETERMINED BY STOICHIOMETRY

Sample CON 20-115 (2)

ELEMENT & LINE	K-RATIO	WEIGHT PERCENT	PRECISION 2 SIGMA	OXIDE FORMULA	OXIDE PERCENT	NO. OF CATIONS IN FORMULA
HG KA	0.0663	10.88	0.18	HGO	18.04	5.5130
AL KA	0.0729	11.43	0.14	AL2O3	21.61	5.2214
SI KA	0.0858	12.39	0.13	SI02	26.50	5.4337
K KA	0.0007	0.08	0.01	K2O	0.09	0.0237
MN KA	0.0024	0.28	0.03	MNO	0.36	0.0617
FE KA	0.1499	16.84	0.24	FE0	21.66	3.7140
O *		36.36				
TOTAL					88.25	19.9675

Sample CON 24-121 (1)

QUANTITATIVE EDS RESULTS
(ZAF CORRECTIONS VIA MAGIC V)

ELEMENT & LINE	K-RATIO	WEIGHT PERCENT	PRECISION 2 SIGMA	OXIDE FORMULA	OXIDE PERCENT	NO. OF CATIONS IN FORMULA
HG KA	0.0915	14.26	0.21	HGO	23.65	7.0470
AL KA	0.0677	10.66	0.13	AL2O3	20.14	4.7439
SI KA	0.0919	13.25	0.14	SiO2	28.34	5.6662
MN KA	0.0017	0.19	0.03	MNO	0.25	0.0418
FE KA	0.1008	11.45	0.21	FeO	14.73	2.4628
O *		37.30				
TOTAL					87.11	19.9618

NUMBER OF CATIONS CALCULATED ON BASIS OF 28 OXYGEN ATOMS.

* DETERMINED BY STOICHIOMETRY

Sample CON 24-121 (2)

ELEMENT & LINE	K-RATIO	WEIGHT PERCENT	PRECISION 2 SIGMA	OXIDE FORMULA	OXIDE PERCENT	NO. OF CATIONS IN FORMULA
HG KA	0.1045	15.76	0.20	HGO	26.13	7.5721
AL KA	0.0764	11.96	0.15	AL2O3	22.60	5.1785
SI KA	0.0892	12.95	0.13	SiO2	27.71	5.3871
FE KA	0.0799	9.02	0.18	FeO	11.60	1.8858
O *		38.35				
TOTAL					88.03	20.0236

Sample CON 24-121 (3)

ELEMENT & LINE	K-RATIO	WEIGHT PERCENT	PRECISION 2 SIGMA	OXIDE FORMULA	OXIDE PERCENT	NO. OF CATIONS IN FORMULA
HG KA	0.1027	15.53	0.20	HGO	25.74	7.3797
AL KA	0.0756	11.83	0.15	AL2O3	22.36	5.0685
SI KA	0.0927	13.43	0.14	SiO2	28.74	5.5272
FE KA	0.0842	9.49	0.19	FeO	12.20	1.9631
O *		38.77				
TOTAL					89.04	19.9385

Sample CON 24-160 (1A)

QUANTITATIVE EDS RESULTS
(ZAF CORRECTIONS VIA MAGIC V)

ELEMENT & LINE	K-RATIO	WEIGHT PERCENT	PRECISION 2 SIGMA	OXIDE FORMULA	OXIDE PERCENT	NO. OF CATIONS IN FORMULA
MG KA	0.0802	12.79	0.19	MGO	21.20	6.4371
AL KA	0.0545	8.56	0.12	AL2O3	16.17	3.8824
SI KA	0.1021	14.45	0.12	SI02	30.91	6.2951
K KA	0.0081	0.90	0.03	K2O	1.09	0.2831
CR KA	0.0021	0.23	0.02	CR2O3	0.34	0.0543
MN KA	0.0013	0.15	0.02	MNO	0.19	0.0329
FE KA	0.1164	13.20	0.21	FEO	16.99	2.8932
O *		36.61				
TOTAL					86.89	19.8781

NUMBER OF CATIONS CALCULATED ON BASIS OF 28 OXYGEN ATOMS.

* DETERMINED BY STOICHIOMETRY

Sample CON 24-160 (1B)

ELEMENT & LINE	K-RATIO	WEIGHT PERCENT	PRECISION 2 SIGMA	OXIDE FORMULA	OXIDE PERCENT	NO. OF CATIONS IN FORMULA
MG KA	0.0817	12.76	0.19	MGO	21.15	6.1526
AL KA	0.0580	8.95	0.13	AL2O3	16.92	3.8914
SI KA	0.1109	15.49	0.13	SI02	33.14	6.4684
K KA	0.0210	2.30	0.06	K2O	2.77	0.6898
CA KA	0.0012	0.12	0.01	CAO	0.17	0.0356
CR KA	0.0033	0.35	0.03	CR2O3	0.51	0.0783
MN KA	0.0025	0.27	0.04	MNO	0.35	0.0582
FE KA	0.1088	11.99	0.22	FEO	15.42	2.5173
O *		38.20				
TOTAL					90.44	19.8916

Sample CON 24-160 (2A)

QUANTITATIVE EDS RESULTS
(ZAF CORRECTIONS VIA MAGIC V)

ELEMENT & LINE	K-RATIO	WEIGHT PERCENT	PRECISION 2 SIGMA	OXIDE FORMULA	OXIDE PERCENT	NO. OF CATIONS IN FORMULA
HG KA	0.0846	13.26	0.19	HGO	21.99	6.5100
AL KA	0.0570	8.90	0.13	AL2O3	16.81	3.9347
SI KA	0.1055	14.91	0.12	SI02	31.90	6.3363
K KA	0.0166	1.85	0.05	K2O	2.23	0.5638
CA KA	0.0006	0.07	0.01	CAO	0.09	0.0201
CR KA	0.0020	0.22	0.02	CR2O3	0.32	0.0501
MN KA	0.0010	0.12	0.02	MNO	0.15	0.0260
FE KA	0.1035	11.76	0.21	FE0	15.12	2.5122
O *		37.54				
TOTAL					88.62	19.9532

NUMBER OF CATIONS CALCULATED ON BASIS OF 28 OXYGEN ATOMS.

* DETERMINED BY STOICHIOMETRY

Sample CON 24-160 (2B)

ELEMENT & LINE	K-RATIO	WEIGHT PERCENT	PRECISION 2 SIGMA	OXIDE FORMULA	OXIDE PERCENT	NO. OF CATIONS IN FORMULA
HG KA	0.0785	12.53	0.21	HGO	20.78	6.1708
AL KA	0.0535	8.36	0.12	AL2O3	15.80	3.7106
SI KA	0.1081	15.15	0.12	SI02	32.40	6.4565
K KA	0.0103	1.13	0.04	K2O	1.36	0.3467
CA KA	0.0008	0.09	0.01	CAO	0.12	0.0261
CR KA	0.0015	0.16	0.02	CR2O3	0.23	0.0357
MN KA	0.0014	0.16	0.02	MNO	0.20	0.0344
FE KA	0.1299	14.29	0.23	FE0	18.38	3.0630
O *		37.42				
TOTAL					89.28	19.8437

Sample CON 24-160 (3)

QUANTITATIVE EDS RESULTS
(ZAF CORRECTIONS VIA MAGIC V)

ELEMENT & LINE	K-RATIO	WEIGHT PERCENT	PRECISION 2 SIGMA	OXIDE FORMULA	OXIDE PERCENT	NO. OF CATIONS IN FORMULA
HG KA	0.0803	12.40	0.18	HGO	20.56	5.9104
AL KA	0.0568	8.67	0.13	AL ₂ O ₃	16.39	3.7252
SI KA	0.1183	16.37	0.14	SIO ₂	35.03	6.7559
K KA	0.0347	3.81	0.07	K ₂ O	4.58	1.1279
CA KA	0.0009	0.10	0.01	CAO	0.13	0.0276
TI KA	0.0008	0.09	0.01	TIO ₂	0.15	0.0216
CR KA	0.0017	0.18	0.02	CR ₂ O ₃	0.27	0.0412
FE KA	0.1001	11.05	0.20	FE ₂ O ₃	14.22	2.2933
O *		38.66				
TOTAL					91.34	19.9032

NUMBER OF CATIONS CALCULATED ON BASIS OF 28 OXYGEN ATOMS.

* DETERMINED BY STOICHIOMETRY

Sample CON 26-92 (1)

QUANTITATIVE EDS RESULTS
(ZAF CORRECTIONS VIA MAGIC V)

ELEMENT & LINE	K-RATIO	WEIGHT PERCENT	PRECISION 2 SIGMA	OXIDE FORMULA	OXIDE PERCENT	NO. OF CATIONS IN FORMULA
HG KA	0.1039	15.67	0.23	HGO	25.98	7.5032
AL KA	0.0773	12.10	0.15	AL2O3	22.86	5.2205
SI KA	0.0893	12.97	0.13	SiO2	27.76	5.3775
FE KA	0.0813	9.17	0.18	FeO	11.79	1.9110
O *		38.49				
TOTAL					88.40	20.0122

NUMBER OF CATIONS CALCULATED ON BASIS OF 28 OXYGEN ATOMS.

* DETERMINED BY STOICHIOMETRY

Sample CON 26-92 (2)

ELEMENT & LINE	K-RATIO	WEIGHT PERCENT	PRECISION 2 SIGMA	OXIDE FORMULA	OXIDE PERCENT	NO. OF CATIONS IN FORMULA
HG KA	0.0988	15.05	0.22	HGO	24.95	7.3730
AL KA	0.0757	11.84	0.15	AL2O3	22.37	5.2263
SI KA	0.0873	12.65	0.13	SiO2	27.07	5.3676
FE KA	0.0854	9.62	0.19	FeO	12.38	2.0524
O *		37.60				
TOTAL					86.76	20.0193

Sample CON 26-102

QUANTITATIVE EDS RESULTS
(ZAF CORRECTIONS VIA MAGIC V)

ELEMENT & LINE	K-RATIO	WEIGHT PERCENT	PRECISION 2 SIGMA	OXIDE FORMULA	OXIDE PERCENT	NO. OF CATIONS IN FORMULA
HG KA	0.0749	12.06	0.20	HGO	19.99	6.0925
AL KA	0.0734	11.50	0.15	AL2O3	21.74	5.2382
SI KA	0.0844	12.19	0.12	SI02	26.07	5.3310
CA KA	0.0002	0.02	0.01	CAO	0.03	0.0068
TI KA	0.0005	0.06	0.01	TIO2	0.10	0.0153
CR KA	0.0019	0.20	0.02	CR2O3	0.29	0.0466
MN KA	0.0011	0.12	0.02	MNO	0.15	0.0266
FE KA	0.1322	14.79	0.24	FEO	19.03	3.2544
O *		36.47				
TOTAL					87.41	20.0113

NUMBER OF CATIONS CALCULATED ON BASIS OF 28 OXYGEN ATOMS.

* DETERMINED BY STOICHIOMETRY

Sample CON 26-129 (1)

QUANTITATIVE EDS RESULTS
(ZAF CORRECTIONS VIA MAGIC V)

ELEMENT & LINE	K-RATIO	WEIGHT PERCENT	PRECISION 2 SIGMA	OXIDE FORMULA	OXIDE PERCENT	NO. OF CATIONS IN FORMULA
HG KA	0.0717	11.64	0.19	HGO	19.30	5.8722
AL KA	0.0710	11.14	0.14	AL2O3	21.04	5.0635
SI KA	0.0875	12.58	0.13	SI02	26.92	5.4955
MN KA	0.0023	0.26	0.03	MNO	0.33	0.0579
FE KA	0.1425	15.86	0.26	FE0	20.40	3.4836
O *		36.52				
TOTAL					88.00	19.9728

NUMBER OF CATIONS CALCULATED ON BASIS OF 28 OXYGEN ATOMS.

* DETERMINED BY STOICHIOMETRY

Sample CON 26-129 (2)

ELEMENT & LINE	K-RATIO	WEIGHT PERCENT	PRECISION 2 SIGMA	OXIDE FORMULA	OXIDE PERCENT	NO. OF CATIONS IN FORMULA
HG KA	0.0711	11.48	0.19	HGO	19.03	5.8072
AL KA	0.0757	11.82	0.15	AL2O3	22.33	5.3877
SI KA	0.0845	12.19	0.12	SI02	26.07	5.3387
K KA	0.0002	0.03	0.01	K2O	0.03	0.0080
CA KA	0.0008	0.08	0.01	CAO	0.12	0.0254
MN KA	0.0012	0.14	0.02	MNO	0.18	0.0310
FE KA	0.1375	15.31	0.25	FE0	19.70	3.3735
O *		36.41				
TOTAL					87.45	19.9715

Sample CON 39-732.5 (1)

QUANTITATIVE EDS RESULTS
(ZAF CORRECTIONS VIA MAGIC V)

ELEMENT & LINE	K-RATIO	WEIGHT PERCENT	PRECISION 2 SIGMA	OXIDE FORMULA	OXIDE PERCENT	NO. OF CATIONS IN FORMULA
HG KA	0.0995	15.10	0.22	HGO	25.03	7.3503
AL KA	0.0764	11.91	0.15	AL2O3	22.51	5.2256
SI KA	0.0881	12.73	0.13	SI02	27.23	5.3649
CA KA	0.0001	0.01	0.00	CAO	0.02	0.0032
CR KA	0.0020	0.21	0.02	CR2O3	0.31	0.0485
FE KA	0.0852	9.46	0.19	FE0	12.17	2.0057
O *		37.85				
TOTAL					87.28	19.9981

NUMBER OF CATIONS CALCULATED ON BASIS OF 28 OXYGEN ATOMS.

* DETERMINED BY STOICHIOMETRY

Sample CON 39-732.5 (2)

ELEMENT & LINE	K-RATIO	WEIGHT PERCENT	PRECISION 2 SIGMA	OXIDE FORMULA	OXIDE PERCENT	NO. OF CATIONS IN FORMULA
HG KA	0.0961	14.65	0.21	HGO	24.29	7.1483
AL KA	0.0759	11.81	0.15	AL2O3	22.32	5.1942
SI KA	0.0892	12.86	0.13	SI02	27.52	5.4344
CR KA	0.0026	0.28	0.03	CR2O3	0.41	0.0643
FE KA	0.0888	9.86	0.20	FE0	12.69	2.0951
O *		37.76				
TOTAL					87.23	19.9363

Sample CON 44-154

QUANTITATIVE EDS RESULTS
(ZAF CORRECTIONS VIA MAGIC V)

ELEMENT & LINE	K-RATIO	WEIGHT PERCENT	PRECISION 2 SIGMA	OXIDE FORMULA	OXIDE PERCENT	NO. OF CATIONS IN FORMULA
HG KA	0.0764	12.22	0.20	HGO	20.27	6.1497
AL KA	0.0731	11.43	0.14	AL2O3	21.60	5.1826
SI KA	0.0867	12.48	0.13	SI02	26.69	5.4338
CR KA	0.0007	0.08	0.01	CR2O3	0.11	0.0182
MN KA	0.0025	0.28	0.03	MNO	0.36	0.0629
FE KA	0.1279	14.24	0.23	FEO	18.32	3.1188
O *		36.63				
TOTAL					87.36	19.9659

NUMBER OF CATIONS CALCULATED ON BASIS OF 28 OXYGEN ATOMS.

* DETERMINED BY STOICHIOMETRY

Sample CON 44-228 (1)

QUANTITATIVE EDS RESULTS
(ZAF CORRECTIONS VIA MAGIC V)

ELEMENT & LINE	K-RATIO	WEIGHT PERCENT	PRECISION 2 SIGMA	OXIDE FORMULA	OXIDE PERCENT	NO. OF CATIONS IN FORMULA
HG KA	0.0898	13.97	0.20	HGO	23.16	6.9417
AL KA	0.0749	11.74	0.15	AL ₂ O ₃	22.19	5.2582
SI KA	0.0855	12.41	0.13	SI ₂ O ₂	26.54	5.3367
MN KA	0.0019	0.22	0.03	MNO	0.28	0.0479
FE KA	0.0997	11.32	0.21	FE ₂ O ₃	14.57	2.4497
O *		37.08				
TOTAL					86.74	20.0342

NUMBER OF CATIONS CALCULATED ON BASIS OF 28 OXYGEN ATOMS.

* DETERMINED BY STOICHIOMETRY

Sample CON 44-228 (2)

ELEMENT & LINE	K-RATIO	WEIGHT PERCENT	PRECISION 2 SIGMA	OXIDE FORMULA	OXIDE PERCENT	NO. OF CATIONS IN FORMULA
HG KA	0.0885	13.77	0.20	HGO	22.83	6.8167
AL KA	0.0764	11.96	0.15	AL ₂ O ₃	22.59	5.3331
SI KA	0.0857	12.45	0.13	SI ₂ O ₂	26.63	5.3338
K KA	0.0007	0.08	0.01	K ₂ O	0.10	0.0244
MN KA	0.0014	0.16	0.02	MNO	0.20	0.0341
FE KA	0.1009	11.46	0.21	FE ₂ O ₃	14.74	2.4698
O *		37.22				
TOTAL					87.09	20.0118

Sample CON 44-248 (1)

QUANTITATIVE EDS RESULTS
(ZAF CORRECTIONS VIA MAGIC V)

ELEMENT & LINE	K-RATIO	WEIGHT PERCENT	PRECISION 2 SIGMA	OXIDE FORMULA	OXIDE PERCENT	NO. OF CATIONS IN FORMULA
HG KA	0.0898	13.98	0.20	HGO	23.18	6.8157
AL KA	0.0755	11.82	0.15	AL2O3	22.33	5.1911
SI KA	0.0884	12.81	0.13	SI02	27.41	5.4074
K KA	0.0007	0.08	0.01	K2O	0.10	0.0251
MN KA	0.0016	0.19	0.02	MNO	0.24	0.0400
FE KA	0.1062	11.92	0.22	FE0	15.34	2.5304
O *		37.79				
TOTAL					88.59	20.0096

NUMBER OF CATIONS CALCULATED ON BASIS OF 28 OXYGEN ATOMS.

* DETERMINED BY STOICHIOMETRY

Sample CON 44-248 (2)

ELEMENT & LINE	K-RATIO	WEIGHT PERCENT	PRECISION 2 SIGMA	OXIDE FORMULA	OXIDE PERCENT	NO. OF CATIONS IN FORMULA
HG KA	0.0934	14.44	0.21	HGO	23.95	7.0084
AL KA	0.0739	11.59	0.15	AL2O3	21.89	5.0662
SI KA	0.0902	13.06	0.13	SI02	27.94	5.4857
FE KA	0.1020	11.46	0.21	FE0	14.74	2.4209
O *		37.98				
TOTAL					88.53	19.9812

Sample CON 44-317.5 (1)

QUANTITATIVE EDS RESULTS
(ZAF CORRECTIONS VIA MAGIC V)

ELEMENT & LINE	K-RATIO	WEIGHT PERCENT	PRECISION 2 SIGMA	OXIDE FORMULA	OXIDE PERCENT	NO. OF CATIONS IN FORMULA
HG KA	0.0650	10.70	0.20	HGO	17.74	5.5270
AL KA	0.0671	10.51	0.13	AL2O3	19.85	4.8918
SI KA	0.0878	12.55	0.13	SI02	26.85	5.6140
K KA	0.0006	0.07	0.01	K2O	0.08	0.0224
CA KA	0.0011	0.12	0.01	CAO	0.13	0.0351
MN KA	0.0037	0.41	0.04	MNO	0.53	0.0940
FE KA	0.1509	16.74	0.27	FEO	21.54	3.7657
O *		35.66				
TOTAL					86.76	19.9513

NUMBER OF CATIONS CALCULATED ON BASIS OF 28 OXYGEN ATOMS.

* DETERMINED BY STOICHIOMETRY

Sample CON 44-317.5 (2)

ELEMENT & LINE	K-RATIO	WEIGHT PERCENT	PRECISION 2 SIGMA	OXIDE FORMULA	OXIDE PERCENT	NO. OF CATIONS IN FORMULA
HG KA	0.0612	10.12	0.19	HGO	16.78	5.2748
AL KA	0.0726	11.35	0.14	AL2O3	21.45	5.3311
SI KA	0.0821	11.79	0.12	SI02	25.22	5.3194
K KA	0.0009	0.10	0.01	K2O	0.12	0.0324
CA KA	0.0008	0.09	0.01	CAO	0.12	0.0277
MN KA	0.0035	0.39	0.04	MNO	0.51	0.0903
FE KA	0.1573	17.43	0.25	FEO	22.43	3.9556
O *		35.36				
TOTAL					86.63	20.0313

Sample CON 44-767 (1A)

QUANTITATIVE EDS RESULTS
(ZAF CORRECTIONS VIA MAGIC V)

ELEMENT & LINE	K-RATIO	WEIGHT PERCENT	PRECISION 2 SIGMA	OXIDE FORMULA	OXIDE PERCENT	NO. OF CATIONS IN FORMULA
HG KA	0.0413	7.03	0.16	HGO	11.65	3.6697
AL KA	0.0462	7.11	0.12	AL2O3	13.43	3.3453
SI KA	0.1117	15.29	0.13	SI02	32.70	6.9116
K KA	0.0400	4.33	0.08	K2O	5.22	1.4062
CA KA	0.0011	0.11	0.01	CAO	0.16	0.0361
TI KA	0.0013	0.14	0.02	TI02	0.23	0.0373
CR KA	0.0012	0.12	0.02	CR2O3	0.18	0.0294
FE KA	0.1860	20.37	0.29	FE0	26.20	4.6313
O *		35.28				
TOTAL					89.77	20.0668

NUMBER OF CATIONS CALCULATED ON BASIS OF 28 OXYGEN ATOMS.

* DETERMINED BY STOICHIOMETRY

Sample CON 44-767 (1B)

ELEMENT & LINE	K-RATIO	WEIGHT PERCENT	PRECISION 2 SIGMA	OXIDE FORMULA	OXIDE PERCENT	NO. OF CATIONS IN FORMULA
HG KA	0.0422	7.08	0.16	HGO	11.73	3.6127
AL KA	0.0494	7.53	0.12	AL2O3	14.23	3.4635
SI KA	0.1158	15.80	0.13	SI02	33.79	6.9803
K KA	0.0498	5.40	0.09	K2O	6.50	1.7135
TI KA	0.0016	0.18	0.02	TI02	0.30	0.0468
CR KA	0.0015	0.15	0.02	CR2O3	0.22	0.0364
FE KA	0.1735	19.02	0.27	FE0	24.47	4.2266
O *		36.10				
TOTAL					91.25	20.0798

NUMBER OF CATIONS CALCULATED ON BASIS OF 28 OXYGEN ATOMS.

* DETERMINED BY STOICHIOMETRY

Sample CON 44-767 (1C)

ELEMENT & LINE	K-RATIO	WEIGHT PERCENT	PRECISION 2 SIGMA	OXIDE FORMULA	OXIDE PERCENT	NO. OF CATIONS IN FORMULA
HG KA	0.0444	7.51	0.17	HGO	12.45	3.8813
AL KA	0.0499	7.69	0.13	AL2O3	14.53	3.5796
SI KA	0.1092	15.02	0.12	SI02	32.14	6.7194
K KA	0.0385	4.17	0.08	K2O	5.02	1.3401
TI KA	0.0017	0.19	0.02	TI02	0.31	0.0494
CR KA	0.0012	0.12	0.02	CR2O3	0.18	0.0302
FE KA	0.1825	19.99	0.28	FE0	25.71	4.4964
O *		35.66				
TOTAL					90.35	20.0964

Sample CON 44-767 (1D)

ELEMENT & LINE	K-RATIO	WEIGHT PERCENT	PRECISION 2 SIGMA	OXIDE FORMULA	OXIDE PERCENT	NO. OF CATIONS IN FORMULA
HG KA	0.0406	7.20	0.16	HGO	11.94	4.0332
AL KA	0.0466	7.39	0.12	AL2O3	13.96	3.7290
SI KA	0.0894	12.51	0.13	SI02	26.76	6.0652
K KA	0.0058	0.62	0.03	K2O	0.75	0.2164
CA KA	0.0008	0.08	0.01	CAO	0.12	0.0287
TI KA	0.0013	0.14	0.02	TI02	0.23	0.0390
CR KA	0.0016	0.16	0.02	CR2O3	0.23	0.0418
FE KA	0.2243	24.47	0.30	FE0	31.48	5.9653
O *		32.90				
TOTAL					85.47	20.1186

Sample CON 44-767 (2A)

QUANTITATIVE EDS RESULTS
(ZAF CORRECTIONS VIA MAGIC V)

ELEMENT & LINE	K-RATIO	WEIGHT PERCENT	PRECISION 2 SIGMA	OXIDE FORMULA	OXIDE PERCENT	NO. OF CATIONS IN FORMULA
HG KA	0.0490	8.09	0.16	HGO	13.41	3.9968
AL KA	0.0531	8.10	0.12	AL2O3	15.30	3.6045
SI KA	0.1170	16.09	0.13	SI02	34.43	6.8830
K KA	0.0536	5.89	0.09	K2O	7.09	1.8086
TI KA	0.0024	0.27	0.02	TI02	0.45	0.0680
CR KA	0.0021	0.22	0.02	CR2O3	0.33	0.0515
MN KA	0.0017	0.19	0.03	MNO	0.24	0.0412
FE KA	0.1526	17.07	0.24	FE0	21.96	3.6717
O *		37.29				
TOTAL					93.21	20.1252

NUMBER OF CATIONS CALCULATED ON BASIS OF 28 OXYGEN ATOMS.

* DETERMINED BY STOICHIOMETRY

Sample CON 44-767 (2B)

ELEMENT & LINE	K-RATIO	WEIGHT PERCENT	PRECISION 2 SIGMA	OXIDE FORMULA	OXIDE PERCENT	NO. OF CATIONS IN FORMULA
HG KA	0.0489	8.16	0.17	HGO	13.54	4.0887
AL KA	0.0535	8.22	0.12	AL2O3	15.53	3.7090
SI KA	0.1114	15.35	0.13	SI02	32.84	6.6543
K KA	0.0409	4.43	0.07	K2O	5.34	1.3791
TI KA	0.0024	0.26	0.02	TI02	0.44	0.0671
CR KA	0.0019	0.20	0.02	CR2O3	0.29	0.0462
MN KA	0.0006	0.07	0.02	MNO	0.09	0.0150
FE KA	0.1736	18.95	0.27	FE0	24.38	4.1314
O *		36.79				
TOTAL					92.43	20.0906

Sample CON 44-767 (3A)

QUANTITATIVE EDS RESULTS
(ZAF CORRECTIONS VIA MAGIC V)

ELEMENT & LINE	K-RATIO	WEIGHT PERCENT	PRECISION 2 SIGMA	OXIDE FORMULA	OXIDE PERCENT	NO. OF CATIONS IN FORMULA
HG KA	0.0452	7.75	0.16	MGO	12.84	4.0402
AL KA	0.0514	8.02	0.12	AL2O3	15.16	3.7703
SI KA	0.1022	14.26	0.12	SI02	30.51	6.4397
K KA	0.0250	2.73	0.06	K2O	3.29	0.8866
TI KA	0.0013	0.14	0.02	TI02	0.24	0.0379
CR KA	0.0017	0.18	0.02	CR2O3	0.26	0.0438
MN KA	0.0016	0.18	0.02	MNO	0.23	0.0419
FE KA	0.1896	21.13	0.26	FEO	27.18	4.7983
O *		35.32				
TOTAL					89.72	20.0587

NUMBER OF CATIONS CALCULATED ON BASIS OF 28 OXYGEN ATOMS.

* DETERMINED BY STOICHIOMETRY

Sample CON 44-767 (3B)

ELEMENT & LINE	K-RATIO	WEIGHT PERCENT	PRECISION 2 SIGMA	OXIDE FORMULA	OXIDE PERCENT	NO. OF CATIONS IN FORMULA
HG KA	0.0463	7.89	0.16	MGO	13.09	4.1248
AL KA	0.0510	7.92	0.12	AL2O3	14.96	3.7270
SI KA	0.1034	14.32	0.12	SI02	30.64	6.4792
K KA	0.0256	2.77	0.06	K2O	3.33	0.8987
TI KA	0.0015	0.17	0.02	TI02	0.28	0.0444
CR KA	0.0018	0.19	0.02	CR2O3	0.27	0.0455
FE KA	0.1903	20.75	0.29	FEO	26.69	4.7201
O *		35.26				
TOTAL					89.26	20.0396

Sample CON 44-767 (4)

QUANTITATIVE EDS RESULTS
(ZAF CORRECTIONS VIA MAGIC V)

ELEMENT & LINE	K-RATIO	WEIGHT PERCENT	PRECISION 2 SIGMA	OXIDE FORMULA	OXIDE PERCENT	NO. OF CATIONS IN FORMULA
HG KA	0.0428	7.17	0.16	HGO	11.89	3.6786
AL KA	0.0484	7.38	0.12	AL2O3	13.94	3.4100
SI KA	0.1163	15.81	0.13	SI02	33.82	7.0212
K KA	0.0433	4.66	0.08	K2O	5.61	1.4869
CA KA	0.0014	0.15	0.02	CAO	0.21	0.0471
TI KA	0.0017	0.19	0.02	TIO2	0.32	0.0492
CR KA	0.0015	0.16	0.02	CR2O3	0.23	0.0377
FE KA	0.1746	18.89	0.27	FE0	24.30	4.2186
O *		35.92				
TOTAL					90.32	19.9492

NUMBER OF CATIONS CALCULATED ON BASIS OF 28 OXYGEN ATOMS.

* DETERMINED BY STOICHIOMETRY

Sample CON 44-767 (5)

QUANTITATIVE EDS RESULTS
(ZAF CORRECTIONS VIA MAGIC V)

ELEMENT & LINE	K-RATIO	WEIGHT PERCENT	PRECISION 2 SIGMA	OXIDE FORMULA	OXIDE PERCENT	NO. OF CATIONS IN FORMULA
HG KA	0.0445	7.43	0.17	HGO	12.32	3.7846
AL KA	0.0523	7.96	0.13	AL2O3	15.04	3.6539
SI KA	0.1130	15.44	0.13	SI02	33.03	6.8088
K KA	0.0440	4.74	0.08	K2O	5.71	1.5006
CA KA	0.0011	0.11	0.01	CAO	0.16	0.0354
TI KA	0.0021	0.23	0.02	TIO2	0.39	0.0598
CR KA	0.0016	0.17	0.02	CR2O3	0.25	0.0400
MN KA	0.0019	0.21	0.03	MNO	0.27	0.0479
FE KA	0.1711	18.50	0.26	FE0	23.80	4.1038
O *		36.17				
TOTAL					90.95	20.0348

NUMBER OF CATIONS CALCULATED ON BASIS OF 28 OXYGEN ATOMS.

* DETERMINED BY STOICHIOMETRY

Sample CON 44-767 (6)

QUANTITATIVE EDS RESULTS
(ZAF CORRECTIONS VIA MAGIC V)

ELEMENT & LINE	K-RATIO	WEIGHT PERCENT	PRECISION 2 SIGMA	OXIDE FORMULA	OXIDE PERCENT	NO. OF CATIONS IN FORMULA
HG KA	0.0448	7.54	0.15	HG0	12.50	3.8389
AL KA	0.0536	8.23	0.12	AL2O3	15.54	3.7753
SI KA	0.1094	15.08	0.12	SI02	32.27	6.6491
K KA	0.0376	4.07	0.08	K2O	4.90	1.2884
CA KA	0.0008	0.08	0.01	CAO	0.12	0.0263
TI KA	0.0016	0.18	0.02	TIO2	0.30	0.0460
CR KA	0.0021	0.21	0.02	CR2O3	0.31	0.0506
MN KA	0.0010	0.11	0.02	MNO	0.14	0.0240
FE KA	0.1793	19.56	0.28	FEO	25.17	4.3376
O *		36.18				
TOTAL					91.24	20.0361

NUMBER OF CATIONS CALCULATED ON BASIS OF 28 OXYGEN ATOMS.

* DETERMINED BY STOICHIOMETRY

Sample CON 44-775 (1A)

QUANTITATIVE EDS RESULTS
(ZAF CORRECTIONS VIA MAGIC V)

ELEMENT & LINE	K-RATIO	WEIGHT PERCENT	PRECISION 2 SIGMA	OXIDE FORMULA	OXIDE PERCENT	NO. OF CATIONS IN FORMULA
HG KA	0.0703	10.68	0.18	HGO	17.72	5.0242
AL KA	0.0565	8.41	0.12	AL2O3	15.89	3.5632
SI KA	0.1312	17.83	0.15	SI02	38.16	7.2594
K KA	0.0702	7.79	0.10	K2O	9.38	2.2770
TI KA	0.0027	0.31	0.03	TI02	0.52	0.0747
CR KA	0.0016	0.18	0.02	CR2O3	0.26	0.0387
FE KA	0.0763	8.63	0.19	FE0	11.10	1.7661
O *		39.19				
TOTAL					93.02	20.0034

NUMBER OF CATIONS CALCULATED ON BASIS OF 28 OXYGEN ATOMS.

* DETERMINED BY STOICHIOMETRY

Sample CON 44-775 (1B)

ELEMENT & LINE	K-RATIO	WEIGHT PERCENT	PRECISION 2 SIGMA	OXIDE FORMULA	OXIDE PERCENT	NO. OF CATIONS IN FORMULA
HG KA	0.0684	10.39	0.18	HGO	17.23	4.1614
AL KA	0.0565	8.38	0.12	AL2O3	15.84	3.0245
SI KA	0.1343	18.25	0.16	SI02	39.04	6.3255
K KA	0.0702	7.79	0.10	K2O	9.39	1.9399
TI KA	0.0027	0.31	0.03	TI02	0.52	0.0637
CR KA	0.0016	0.18	0.02	CR2O3	0.26	0.0330
FE KA	0.0763	8.63	0.19	FE0	11.10	1.5041
O *		39.44				
TOTAL					93.37	17.0521

Sample CON 44-775 (1C)

ELEMENT & LINE	K-RATIO	WEIGHT PERCENT	PRECISION 2 SIGMA	OXIDE FORMULA	OXIDE PERCENT	NO. OF CATIONS IN FORMULA
HG KA	0.0674	10.31	0.17	HGO	17.09	4.9117
AL KA	0.0567	8.42	0.12	AL2O3	15.91	3.6165
SI KA	0.1292	17.50	0.14	SI02	37.44	7.2213
K KA	0.0673	7.40	0.11	K2O	8.91	2.1918
CA KA	0.0003	0.03	0.01	CA0	0.05	0.0096
TI KA	0.0025	0.28	0.02	TI02	0.47	0.0680
CR KA	0.0013	0.14	0.02	CR2O3	0.21	0.0323
FE KA	0.0837	9.31	0.19	FE0	11.97	1.9309
O *		38.66				
TOTAL					92.05	19.9822

Sample CON 44-775 (2)

QUANTITATIVE EDS RESULTS
(ZAF CORRECTIONS VIA MAGIC V)

ELEMENT & LINE	K-RATIO	WEIGHT PERCENT	PRECISION 2 SIGMA	OXIDE FORMULA	OXIDE PERCENT	NO. OF CATIONS IN FORMULA
HG KA	0.0675	10.24	0.17	HGO	16.98	4.8338
AL KA	0.0580	8.55	0.12	AL2O3	16.16	3.6371
SI KA	0.1321	17.85	0.15	SiO2	38.19	7.2943
K KA	0.0720	7.92	0.10	K2O	9.54	2.3232
TI KA	0.0026	0.29	0.02	TiO2	0.48	0.0692
CR KA	0.0020	0.22	0.03	CR2O3	0.33	0.0494
FE KA	0.0764	8.51	0.19	FeO	10.94	1.7479
O *		39.04				
TOTAL					92.62	19.9549

NUMBER OF CATIONS CALCULATED ON BASIS OF 28 OXYGEN ATOMS.

* DETERMINED BY STOICHIOMETRY

Sample CON 44-775 (3)

QUANTITATIVE EDS RESULTS
(ZAF CORRECTIONS VIA MAGIC V)

ELEMENT & LINE	K-RATIO	WEIGHT PERCENT	PRECISION 2 SIGMA	OXIDE FORMULA	OXIDE PERCENT	NO. OF CATIONS IN FORMULA
HG KA	0.0685	10.40	0.17	HGO	17.25	4.9086
AL KA	0.0558	8.25	0.12	AL2O3	15.59	3.5088
SI KA	0.1335	18.03	0.15	SiO2	38.57	7.3638
K KA	0.0710	7.80	0.10	K2O	9.40	2.2897
TI KA	0.0020	0.22	0.02	TiO2	0.37	0.0531
CR KA	0.0019	0.21	0.02	CR2O3	0.31	0.0466
FE KA	0.0778	8.66	0.19	FeO	11.14	1.7796
O *		39.05				
TOTAL					92.63	19.9502

NUMBER OF CATIONS CALCULATED ON BASIS OF 28 OXYGEN ATOMS.

* DETERMINED BY STOICHIOMETRY

Sample CON 62-367.5 (1)

QUANTITATIVE EDS RESULTS
(ZAF CORRECTIONS VIA MAGIC V)

ELEMENT & LINE	K-RATIO	WEIGHT PERCENT	PRECISION 2 SIGMA	OXIDE FORMULA	OXIDE PERCENT	NO. OF CATIONS IN FORMULA
HG KA	0.0910	14.06	0.20	HGO	23.32	6.9001
AL KA	0.0765	11.92	0.15	AL2O3	22.53	5.2714
SI KA	0.0876	12.65	0.13	SI02	27.07	5.3733
FE KA	0.1034	11.45	0.21	FE0	14.74	2.4462
O *		37.56				
TOTAL					87.65	19.9910

NUMBER OF CATIONS CALCULATED ON BASIS OF 28 OXYGEN ATOMS.

* DETERMINED BY STOICHIOMETRY

Sample CON 62-367.5 (2)

QUANTITATIVE EDS RESULTS
(ZAF CORRECTIONS VIA MAGIC V)

ELEMENT & LINE	K-RATIO	WEIGHT PERCENT	PRECISION 2 SIGMA	OXIDE FORMULA	OXIDE PERCENT	NO. OF CATIONS IN FORMULA
HG KA	0.0930	14.33	0.21	HGO	23.76	6.9722
AL KA	0.0764	11.91	0.15	AL2O3	22.51	5.2235
SI KA	0.0885	12.79	0.13	SI02	27.35	5.3856
CR KA	0.0011	0.11	0.02	CR2O3	0.16	0.0253
FE KA	0.1015	11.25	0.20	FE0	14.47	2.3830
O *		37.87				
TOTAL					88.26	19.9899

NUMBER OF CATIONS CALCULATED ON BASIS OF 28 OXYGEN ATOMS.

* DETERMINED BY STOICHIOMETRY

Sample 62-392

QUANTITATIVE EDS RESULTS
(ZAF CORRECTIONS VIA MAGIC V)

ELEMENT & LINE	K-RATIO	WEIGHT PERCENT	PRECISION 2 SIGMA	OXIDE FORMULA	OXIDE PERCENT	NO. OF CATIONS IN FORMULA
MG KA	0.0889	13.81	0.20	MGO	22.89	6.8573
AL KA	0.0759	11.85	0.15	AL ₂ O ₃	22.39	5.3038
SI KA	0.0860	12.44	0.13	SI ₂ O ₂	26.62	5.3505
K KA	0.0002	0.02	0.01	K ₂ O	0.03	0.0076
TI KA	0.0001	0.02	0.01	TI ₂ O ₂	0.03	0.0040
MN KA	0.0018	0.20	0.03	MNO	0.26	0.0445
FE KA	0.0999	11.24	0.20	FE ₂ O ₃	14.46	2.4297
O *		37.10				
TOTAL					86.68	19.9974

NUMBER OF CATIONS CALCULATED ON BASIS OF 28 OXYGEN ATOMS.

* DETERMINED BY STOICHIOMETRY

Sample CON 63-67.5 (1)

QUANTITATIVE EDS RESULTS
(ZAF CORRECTIONS VIA MAGIC V)

ELEMENT & LINE	K-RATIO	WEIGHT PERCENT	PRECISION 2 SIGMA	OXIDE FORMULA	OXIDE PERCENT	NO. OF CATIONS IN FORMULA
HG KA	0.1032	15.54	0.23	HGO	25.77	7.5080
AL KA	0.0776	12.13	0.15	AL2O3	22.91	5.2785
SI KA	0.0884	12.86	0.13	SiO2	27.51	5.3780
K KA	0.0008	0.09	0.01	K2O	0.11	0.0269
MN KA	0.0006	0.07	0.02	MNO	0.09	0.0151
FE KA	0.0748	8.51	0.19	FeO	10.95	1.7897
O *		38.14				
TOTAL					87.34	19.9962

NUMBER OF CATIONS CALCULATED ON BASIS OF 28 OXYGEN ATOMS.

* DETERMINED BY STOICHIOMETRY

Sample CON 63-67.5 (2)

QUANTITATIVE EDS RESULTS
(ZAF CORRECTIONS VIA MAGIC V)

ELEMENT & LINE	K-RATIO	WEIGHT PERCENT	PRECISION 2 SIGMA	OXIDE FORMULA	OXIDE PERCENT	NO. OF CATIONS IN FORMULA
HG KA	0.1048	15.78	0.23	HGO	26.17	7.6622
AL KA	0.0745	11.68	0.15	AL2O3	22.07	5.1093
SI KA	0.0891	12.95	0.13	SiO2	27.70	5.4407
FE KA	0.0745	8.48	0.19	FeO	10.91	1.7926
O *		37.95				
TOTAL					86.84	20.0047

NUMBER OF CATIONS CALCULATED ON BASIS OF 28 OXYGEN ATOMS.

* DETERMINED BY STOICHIOMETRY

Sample CON 63-188 (1)

QUANTITATIVE EDS RESULTS
(ZAF CORRECTIONS VIA MAGIC V)

ELEMENT & LINE	K-RATIO	WEIGHT PERCENT	PRECISION 2 SIGMA	OXIDE FORMULA	OXIDE PERCENT	NO. OF CATIONS IN FORMULA
HG KA	0.0881	13.72	0.20	HGO	22.75	6.7811
AL KA	0.0763	11.92	0.15	AL2O3	22.53	5.3101
SI KA	0.0862	12.49	0.13	SI02	26.73	5.3453
MN KA	0.0013	0.15	0.02	MNO	0.19	0.0320
FE KA	0.1047	11.76	0.21	FE0	15.13	2.5311
O *		37.28				
TOTAL					87.32	19.9996

NUMBER OF CATIONS CALCULATED ON BASIS OF 28 OXYGEN ATOMS.

* DETERMINED BY STOICHIOMETRY

Sample CON 63-188 (2)

ELEMENT & LINE	K-RATIO	WEIGHT PERCENT	PRECISION 2 SIGMA	OXIDE FORMULA	OXIDE PERCENT	NO. OF CATIONS IN FORMULA
HG KA	0.0876	13.69	0.20	HGO	22.70	6.7957
AL KA	0.0746	11.68	0.15	AL2O3	22.08	5.2257
SI KA	0.0861	12.46	0.13	SI02	26.65	5.3532
K KA	0.0009	0.10	0.01	K2O	0.12	0.0320
MN KA	0.0013	0.15	0.02	MNO	0.19	0.0325
FE KA	0.1076	12.08	0.22	FE0	15.55	2.6110
O *		37.12				
TOTAL					87.29	20.0500

Sample CON 63-449.5

QUANTITATIVE EDS RESULTS
(ZAF CORRECTIONS VIA MAGIC V)

ELEMENT & LINE	K-RATIO	WEIGHT PERCENT	PRECISION 2 SIGMA	OXIDE FORMULA	OXIDE PERCENT	NO. OF CATIONS IN FORMULA
Mg KA	0.0906	14.03	0.20	MgO	23.26	6.9252
Al KA	0.0739	11.57	0.15	Al ₂ O ₃	21.86	5.1468
Si KA	0.0884	12.80	0.13	SiO ₂	27.38	5.1684
K KA	0.0009	0.10	0.01	K ₂ O	0.12	0.0304
Ca KA	0.0011	0.12	0.01	CaO	0.16	0.0347
Fe KA	0.0969	11.02	0.22	FeO	14.18	2.3678
O *		37.33				
TOTAL					86.96	19.9734

NUMBER OF CATIONS CALCULATED ON BASIS OF 28 OXYGEN ATOMS.

* DETERMINED BY STOICHIOMETRY

Sample CON 63-549.5 (1)

QUANTITATIVE EDS RESULTS
(ZAF CORRECTIONS VIA MAGIC V)

ELEMENT & LINE	K-RATIO	WEIGHT PERCENT	PRECISION 2 SIGMA	OXIDE FORMULA	OXIDE PERCENT	NO. OF CATIONS IN FORMULA
HG KA	0.0675	11.09	0.18	HGO	18.38	5.6721
AL KA	0.0675	10.61	0.13	AL ₂ O ₃	20.05	4.8920
SI KA	0.0880	12.64	0.13	SiO ₂	27.04	5.5979
CA KA	0.0004	0.04	0.01	CaO	0.06	0.0126
TI KA	0.0002	0.02	0.01	TiO ₂	0.03	0.0048
MN KA	0.0043	0.48	0.04	MNO	0.62	0.1087
FE KA	0.1461	16.45	0.27	FeO	21.16	3.6633
O *		36.02				
TOTAL					87.35	19.9513

NUMBER OF CATIONS CALCULATED ON BASIS OF 28 OXYGEN ATOMS.

* DETERMINED BY STOICHIOMETRY

Sample CON 63-549.5 (2)

ELEMENT & LINE	K-RATIO	WEIGHT PERCENT	PRECISION 2 SIGMA	OXIDE FORMULA	OXIDE PERCENT	NO. OF CATIONS IN FORMULA
HG KA	0.0649	10.73	0.20	HGO	17.80	5.5155
AL KA	0.0651	10.26	0.15	AL ₂ O ₃	19.39	4.7499
SI KA	0.0890	12.77	0.13	SiO ₂	27.31	5.6788
CA KA	0.0009	0.10	0.02	CaO	0.14	0.0303
MN KA	0.0034	0.38	0.04	MNO	0.49	0.0871
FE KA	0.1544	17.37	0.25	FeO	22.34	3.8845
O *		35.86				
TOTAL					87.47	19.9462

Sample CON 63-1035

QUANTITATIVE EDS RESULTS
(ZAF CORRECTIONS VIA MAGIC V)

ELEMENT & LINE	K-RATIO	WEIGHT PERCENT	PRECISION 2 SIGMA	OXIDE FORMULA	OXIDE PERCENT	NO. OF CATIONS IN FORMULA
HG KA	0.0998	15.19	0.22	HG0	25.19	7.4474
AL KA	0.0749	11.74	0.15	AL2O3	22.19	5.1862
SI KA	0.0872	12.66	0.13	SI02	27.08	5.3711
CR KA	0.0010	0.11	0.02	CR2O3	0.16	0.0256
FE KA	0.0823	9.34	0.19	FE0	12.01	1.9927
O *		37.59				
TOTAL					86.63	20.0230

Sample CON 64-470.5 (1)

QUANTITATIVE EDS RESULTS
(ZAF CORRECTIONS VIA MAGIC V)

ELEMENT & LINE	K-RATIO	WEIGHT PERCENT	PRECISION 2 SIGMA	OXIDE FORMULA	OXIDE PERCENT	NO. OF CATIONS IN FORMULA
HG KA	0.0869	13.60	0.20	HGO	22.54	6.8041
AL KA	0.0736	11.53	0.15	AL2O3	21.79	5.1992
SI KA	0.0860	12.44	0.13	SiO2	26.62	5.3900
FE KA	0.1067	12.01	0.22	FeO	15.45	2.6171
O *		36.82				
TOTAL					86.40	20.0104

NUMBER OF CATIONS CALCULATED ON BASIS OF 28 OXYGEN ATOMS.

* DETERMINED BY STOICHIOMETRY

Sample CON 64-470.5 (2)

ELEMENT & LINE	K-RATIO	WEIGHT PERCENT	PRECISION 2 SIGMA	OXIDE FORMULA	OXIDE PERCENT	NO. OF CATIONS IN FORMULA
HG KA	0.0862	13.52	0.20	HGO	22.41	6.6658
AL KA	0.0759	11.87	0.15	AL2O3	22.43	5.2750
SI KA	0.0862	12.47	0.13	SiO2	26.68	5.3239
MN KA	0.0021	0.23	0.03	MNO	0.30	0.0504
FE KA	0.1140	12.69	0.23	FeO	16.32	2.7235
O *		37.37				
TOTAL					88.15	20.0586

APPENDIX C

Major and trace element analyses of all geochemical samples are given in the following pages. All samples are listed in order of sample number. Refer to Tables 5-7 for information regarding rock type and location. Mineralogical components of each sample are given in Appendix A.

	62-660	62-674	62-674	63-47	69-615	69-214.6	67-117	67-291	67-787	67-689	109-625	109-602	140-178.6	140-284	140-288
SiO ₂	60.70	59.20	66.30	58.20	53.20	50.80	52.30	54.90	67.10	68.40	46.80	63.60	55.60	59.10	57.50
TiO ₂	1.09	0.33	0.42	0.90	0.39	0.31	0.36	0.52	0.51	0.33	0.42	0.35	0.55	0.36	0.35
Al ₂ O ₃	15.60	11.60	13.40	13.70	16.00	10.90	15.80	13.50	10.50	15.30	14.40	15.30	14.90	14.40	12.40
Fe ₂ O ₃	6.62	11.10	8.35	12.00	9.87	19.80	11.70	13.00	10.60	3.11	15.60	7.09	11.90	10.10	14.30
MnO	0.09	0.20	0.16	0.23	0.17	0.09	0.22	0.23	0.18	0.06	0.28	0.16	0.21	0.07	0.11
HgO	2.56	5.65	1.28	3.22	5.97	7.37	6.42	4.73	1.53	1.11	13.50	2.33	4.49	3.94	1.46
CaO	5.35	7.94	6.17	5.29	10.50	0.54	8.84	7.96	5.64	3.24	0.74	4.22	8.02	5.17	1.32
Na ₂ O	3.20	1.65	2.41	2.95	1.81	0.37	2.26	2.76	1.64	4.62	0.03	2.93	1.50	1.06	0.28
K ₂ O	2.11	0.72	0.65	0.80	0.53	1.46	0.91	0.71	1.18	1.40	0.33	1.71	1.01	2.07	3.42
P ₂ O ₅	0.57	0.14	0.17	0.17	0.07	0.04	0.07	0.12	0.20	0.11	0.10	0.07	0.12	0.06	0.05
H ₂ O+	1.16	1.62	0.85	1.70	0.85	8.31	1.08	1.00	1.00	1.39	6.93	1.70	1.16	2.85	7.85
Total	99.05	100.15	100.16	99.16	99.36	99.99	99.96	99.43	100.08	99.07	99.13	99.46	99.46	99.18	99.04
Rb	30	10	10	30	20	10	30	20	20	40	10	40	20	50	30
Ba	1150	170	200	270	90	500	240	210	220	390	190	850	930	640	3520
Sr	1180	70	130	190	160	50	150	170	90	440	10	220	170	150	20
Cr	20	340	10	10	40	100	40	50	10	10	180	20	10	70	260
Ni	17	90	4	6	14	56	16	12	3	6	24	16	11	22	60
Zr	210	10	30	40	20	30	10	10	30	100	10	30	20	10	20
Cu	27	1200	100	130	96	640	33	29	45	4	15	190	110	320	150
AN	45	61	54	47	69	44	61	49	56	28	92	45	71	74	72
Q	19	19	32	17	8	18	4	9	36	27	14	25	15	23	29
or	12	4	4	5	3	9	5	4	7	8	2	10	6	12	20
ab	27	14	20	25	15	3	19	23	14	39	0	25	13	9	2
an	22	22	24	22	34	2	30	22	18	15	3	20	31	25	6
C	0	0	0	0	0	8	0	0	0	1	13	1	0	1	6
di	1	14	5	3	14	0	11	14	8	0	0	0	7	0	0
hy	9	21	9	19	19	46	25	21	12	5	54	13	22	21	22
et	4	3	3	3	3	3	3	3	3	2	3	3	3	3	3
il	2	1	1	2	1	1	1	1	1	1	1	1	1	1	1
ap	1	0	0	0	0	0	0	0	0	0	0	0	0	0	0
FeO*	5.96	9.99	7.52	10.80	8.88	17.82	10.53	11.70	9.54	2.80	14.04	6.38	10.71	9.09	12.87
F/F+M	0.703	0.643	0.857	0.774	0.603	0.768	0.626	0.716	0.864	0.720	0.515	0.737	0.709	0.699	0.899
Rb/Sr	0.025	0.143	0.077	0.158	0.125	0.200	0.200	0.118	0.222	0.091	1.000	0.182	0.118	0.333	1.500
K/Rb	584	598	540	221	220	1212	252	295	490	291	274	355	419	344	946
K/Ba	15.2	35.2	27.0	24.6	48.9	24.2	31.5	28.1	44.5	29.8	14.4	16.7	9.0	26.8	8.1
den	2.44	2.50	2.43	2.48	2.54	2.53	2.54	2.52	2.43	2.37	2.59	2.42	2.52	2.46	2.43

	CON9-121	CON9-312	CON20-124	CON24-158	CON24-167.6	CON44-123	CON44-164	CON44-248	CON44W2-432	CON45A-836.6	CON45A-860	CON51-171	CON51-584	CON51-882	CON5296.6
SiO ₂	56.90	56.90	66.10	57.50	59.90	56.30	60.20	52.30	56.60	62.70	48.50	59.70	53.50	57.80	58.80
TiO ₂	0.26	0.30	0.64	0.11	0.38	0.55	0.30	0.33	0.55	0.40	0.36	0.89	0.19	0.28	0.32
Al ₂ O ₃	12.50	12.50	13.60	6.75	13.10	14.80	12.60	13.80	14.70	13.90	9.70	14.00	8.53	12.80	15.10
Fe ₂ O ₃	11.00	10.00	6.67	12.60	10.30	12.90	9.06	12.80	12.80	8.84	11.00	11.90	12.20	11.90	9.90
MnO	0.18	0.11	0.12	0.17	0.18	0.19	0.11	0.08	0.19	0.11	0.18	0.18	0.23	0.20	0.18
HgO	6.77	10.50	1.33	12.90	4.26	3.90	8.70	9.85	3.62	2.43	15.70	2.84	11.30	4.99	3.37
CaO	7.81	2.24	6.32	5.56	6.15	7.75	0.97	1.53	8.54	7.01	9.30	6.86	11.10	9.00	8.08
H ₂ O	1.65	0.33	2.70	0.36	2.75	1.51	0.70	0.63	1.76	1.69	0.76	2.58	0.95	1.27	1.80
K ₂ O	0.69	2.72	0.60	0.42	0.56	0.54	2.60	2.62	0.64	0.74	1.27	0.67	0.24	0.36	1.38
P ₂ O ₅	0.06	0.04	0.16	0.03	0.07	0.14	0.04	0.05	0.13	0.13	0.16	0.17	0.04	0.05	0.15
H ₂ O+	1.54	3.31	1.16	3.54	1.62	1.00	4.08	5.39	0.70	1.16	2.23	0.47	0.93	0.54	0.85
Total	99.36	98.95	99.40	99.94	99.27	99.58	99.36	99.38	100.23	99.11	99.16	100.26	99.21	99.19	99.93
Rb	10	80	10	20	20	20	70	40	30	30	40	10	10	10	30
Ba	180	530	170	120	220	370	440	490	270	360	280	240	70	150	320
Sr	150	40	330	10	320	240	50	50	210	290	40	150	30	100	370
Cr	280	210	10	1320	90	10	70	90	10	10	1160	10	710	50	30
Ni	21	27	6	82	27	9	27	33	7	7	240	4	8	6	9
Zr	10	10	80	10	10	20	10	10	10	10	10	40	10	10	10
Cu	130	61	93	190	300	94	61	140	48	170	48	160	2	18	13
AN	64	80	50	84	48	71	43	58	67	66	75	53	69	72	66
Q	15	19	32	18	19	17	27	13	16	29	0	20	7	19	18
cr	4	16	4	2	3	3	15	15	4	4	8	4	1	2	8
ab	14	3	23	3	23	13	6	5	15	14	6	22	8	11	15
an	25	11	23	16	22	32	5	7	30	28	19	25	18	28	29
C	0	5	0	0	0	0	7	7	0	0	0	0	0	0	0
di	11	0	6	10	7	5	0	0	9	5	21	7	30	13	8
hy	25	38	5	44	19	23	32	41	20	13	28	16	30	21	16
cl	0	0	0	0	0	0	0	0	0	0	11	0	0	0	0
at	3	3	3	2	3	3	3	3	3	3	3	3	2	3	3
il	0	1	1	0	1	1	1	1	1	1	1	2	0	1	1
ap	0	0	0	0	0	0	0	0	0	0	0	0	0	0	0
FeO†	9.90	9.00	6.00	11.34	9.27	11.61	8.15	11.52	11.52	7.96	9.90	10.71	10.98	10.71	8.91
F/F+H	0.598	0.465	0.822	0.472	0.689	0.752	0.487	0.541	0.764	0.768	0.391	0.793	0.498	0.686	0.730
Rb/Sr	0.067	2.000	0.030	2.000	0.063	0.093	1.400	0.800	0.143	0.103	1.000	0.067	0.333	0.100	0.081
K/Rb	573	282	498	174	232	224	308	544	177	205	264	556	199	299	382
K/Ba	31.8	42.6	29.3	29.1	21.1	12.1	49.0	44.4	19.7	17.1	37.6	23.2	28.5	19.9	35.8
den	2.52	2.50	2.42	2.55	2.47	2.51	2.46	2.51	2.51	2.45	2.63	2.48	2.59	2.52	2.48

	CON52-614.5	CON57-172	CON57-343.5	CON57-551.5	CON57-674.5	CON57-753	CON57-779	CON63-171	CON63-188.5	CON63-253.5	CON63-446.5	CON63-590	CON63-1035	CON63-1116	CON64-122
SiO ₂	73.00	55.89	53.70	58.00	54.10	48.90	68.90	61.30	53.80	56.40	56.00	69.20	47.80	68.30	67.80
TiO ₂	0.31	0.56	0.34	0.33	0.35	0.35	0.37	1.11	0.25	0.29	0.24	0.30	0.36	0.37	0.53
Al ₂ O ₃	11.80	14.80	14.30	14.00	12.50	9.67	12.40	15.70	11.50	11.00	7.49	16.10	9.95	14.20	13.00
Fe ₂ O ₃	5.37	12.60	11.80	12.70	12.00	11.10	6.86	6.73	12.90	11.90	19.80	2.66	10.90	6.37	7.06
MnO	0.11	0.18	0.20	0.19	0.21	0.24	0.09	0.08	0.16	0.16	0.07	0.06	0.19	0.05	0.10
MgO	0.76	3.66	5.75	3.32	6.99	15.80	0.68	2.90	12.10	8.27	6.05	0.96	16.00	0.54	1.00
CaO	3.22	8.38	9.03	9.29	10.80	9.22	4.49	4.90	1.84	9.24	0.38	4.24	8.93	4.21	3.91
Na ₂ O	3.88	2.00	1.71	1.15	0.76	0.72	2.81	3.44	0.11	0.81	0.11	4.26	0.73	2.96	3.66
K ₂ O	0.86	0.82	0.49	0.52	0.32	1.40	1.22	2.01	0.44	0.27	1.67	1.01	1.80	1.43	1.17
P ₂ O ₅	0.07	0.14	0.05	0.12	0.05	0.16	0.21	0.58	0.05	0.05	0.03	0.10	0.17	0.14	0.16
H ₂ O+	0.62	1.23	1.62	0.47	1.08	1.62	1.70	1.08	6.00	1.16	7.77	0.85	1.93	1.39	0.70
Total	100.00	100.17	98.99	100.09	99.16	99.18	99.73	99.83	99.15	99.55	99.61	99.74	98.76	99.96	99.09
Rb	20	20	10	10	10	30	20	40	10	20	10	30	50	40	30
Ba	450	420	160	270	120	310	390	1170	180	80	370	530	350	660	530
Sr	160	230	100	230	100	10	110	1040	16	40	20	380	20	140	190
Cr	10	10	30	20	290	1190	10	30	320	160	210	10	1180	10	10
Ni	3	11	17	5	42	360	31	19	33	29	57	4	260	45	6
Zr	90	10	10	10	10	10	50	210	10	10	10	110	20	40	80
Cu	28	150	110	72	110	290	440	8	180	41	860	19	30	540	27
AN	27	63	67	76	82	76	43	41	90	79	64	36	75	44	33
Q	38	14	11	20	13	0	36	19	22	16	26	29	0	34	31
or	5	5	3	3	2	8	7	12	3	2	19	6	11	8	7
ab	33	17	14	10	6	6	24	29	1	7	1	36	6	25	31
an	12	29	30	32	30	19	18	21	9	26	2	20	19	20	16
C	0	0	0	0	0	0	0	0	8	0	5	1	0	0	0
di	3	10	12	12	19	21	3	0	0	16	0	0	20	0	2
hy	5	19	23	19	23	28	6	10	47	28	43	4	20	7	7
ol	0	0	0	0	0	11	0	0	0	0	0	0	17	0	0
at	3	3	3	3	3	3	3	4	3	3	3	1	3	3	3
il	1	1	1	1	1	1	1	2	0	1	0	1	1	1	1
ap	0	0	0	0	0	0	0	1	0	0	0	0	0	0	0
FeO*	4.83	11.34	10.62	11.43	10.80	9.99	6.17	6.06	11.61	10.71	17.82	2.39	9.81	5.73	6.35
F/F+M	0.867	0.759	0.653	0.778	0.612	0.393	0.902	0.679	0.493	0.568	0.747	0.719	0.385	0.915	0.866
Rb/Sr	0.125	0.087	0.100	0.043	0.100	3.000	0.182	0.038	1.000	0.500	0.500	0.079	2.500	0.286	0.158
K/Rb	357	340	407	432	266	387	506	417	365	112	1386	279	299	297	324
K/Ba	15.9	16.2	25.4	16.0	22.1	37.5	26.0	14.3	20.3	28.0	37.5	15.8	42.7	18.0	18.3
den	2.36	2.51	2.54	2.51	2.56	2.62	2.39	2.43	2.54	2.55	2.49	2.37	2.63	2.39	2.39

	CON64-470.5	GR-6	GR-8	GR-12	GR-13	GR-14	GR-19	GR-25	GR-28	GR-32	GR-33	GR-35	GR-36	GR-39	GR-40
SiO ₂	55.00	72.10	71.00	73.00	59.00	55.20	72.00	72.50	54.40	65.50	55.30	71.30	60.80	70.60	55.60
TiO ₂	0.32	0.35	0.36	0.25	0.82	0.39	0.25	0.31	0.89	0.60	0.64	0.30	0.32	0.37	0.65
Al ₂ O ₃	1.70	12.50	11.90	12.50	13.80	13.90	12.50	12.10	14.50	12.80	15.40	15.20	12.10	14.10	15.60
Fe ₂ O ₃	11.40	5.07	5.72	4.85	11.50	11.90	5.45	5.59	13.10	8.33	11.60	2.65	11.00	3.51	10.50
MnO	0.09	0.11	0.10	0.12	0.29	0.22	0.10	0.10	0.23	0.18	0.18	0.05	0.18	0.07	0.18
MgO	6.76	0.64	0.48	0.48	3.16	4.95	0.67	0.66	4.30	1.86	4.69	0.90	4.44	0.58	4.31
CaO	5.60	4.31	4.31	3.27	7.41	9.99	3.93	3.49	9.28	5.51	8.57	3.51	8.54	4.88	9.01
Na ₂ O	2.44	2.64	3.55	3.63	2.48	1.25	3.08	2.60	1.73	3.10	2.08	4.46	1.43	3.54	1.98
K ₂ O	1.23	1.34	0.74	1.07	0.87	0.48	1.09	1.80	0.36	0.70	0.53	1.27	0.36	0.68	0.53
P ₂ O ₅	0.06	0.09	0.10	0.06	0.15	0.06	0.06	0.07	0.12	0.14	0.11	0.09	0.06	0.14	0.12
H ₂ O+	3.39	1.08	0.47	0.39	0.70	0.85	0.54	0.77	0.62	0.54	0.47	0.31	0.77	0.47	0.54
Total	98.99	100.23	98.73	99.62	100.18	99.19	99.67	99.99	99.53	99.26	99.57	100.04	100.00	98.94	99.02
Rb	30	20	20	20	20	20	20	30	10	10	20	30	30	10	40
Ba	300	390	290	360	160	160	330	470	120	200	180	620	170	290	190
Sr	140	170	160	120	160	90	140	180	130	170	130	480	110	180	140
Cr	90	10	10	10	10	70	10	10	10	10	20	10	50	10	20
Ni	20	4	3	3	8	10	3	5	8	5	10	6	18	4	14
Zr	10	90	90	70	50	10	70	100	20	60	10	110	10	30	30
Cu	35	43	9	6	87	74	5	24	94	49	90	4	73	92	33
AN	49	45	32	32	53	75	40	42	68	42	64	31	68	41	66
Q	9	40	37	39	18	15	39	40	13	29	12	31	24	36	14
or	7	8	4	6	5	3	6	11	2	4	3	8	2	4	3
ab	21	22	30	31	21	11	26	22	15	26	18	38	12	30	17
an	20	18	14	15	24	31	17	16	31	19	31	17	26	21	32
C	0	0	0	0	0	0	0	0	0	0	0	0	0	0	0
di	6	2	6	1	10	15	2	1	12	6	9	0	14	2	10
hy	28	4	3	5	15	19	5	6	19	9	20	4	18	3	17
at	3	2	3	2	3	3	3	3	3	3	3	1	3	2	3
il	1	1	1	0	2	1	0	1	2	1	1	1	1	1	1
ap	0	0	0	0	0	0	0	0	0	0	0	0	0	0	0
FeO*	10.26	4.56	5.15	4.37	10.35	10.71	4.90	5.03	11.79	7.50	10.44	2.39	9.90	3.16	9.45
F/F+K	0.605	0.880	0.916	0.903	0.771	0.688	0.882	0.886	0.737	0.805	0.694	0.730	0.694	0.848	0.691
Rb/Sr	0.214	0.118	0.125	0.167	0.125	0.222	0.143	0.167	0.077	0.059	0.154	0.063	0.273	0.056	0.286
K/Rb	340	556	307	444	361	199	452	498	299	581	220	351	100	564	110
K/Ba	34.0	28.5	21.2	23.4	45.1	24.9	27.4	31.8	24.9	29.1	24.4	17.0	17.6	19.5	23.2
den	2.50	2.37	2.38	2.36	2.49	2.53	2.37	2.37	2.54	2.43	2.52	2.36	2.49	2.38	2.52

	GR48	GR49	GR59
SiO ₂	62.90	56.40	62.30
TiO ₂	0.62	0.31	0.52
Al ₂ O ₃	14.90	13.40	12.90
Fe ₂ O ₃	8.32	11.60	11.60
MnO	0.16	0.19	0.20
MgO	1.72	5.08	1.13
CaO	7.97	9.69	6.09
Na ₂ O	2.12	1.32	2.42
K ₂ O	0.38	0.37	0.73
P ₂ O ₅	0.24	0.05	0.38
H ₂ O+	0.39	0.77	0.85
Total	99.72	99.18	99.12
Rb	10	10	20
Ba	180	140	350
Sr	110	110	100
Cr	10	30	10
Ni	4	10	13
Zr	20	10	40
Cu	28	64	110
AN	63	73	52
Q	28	16	27
cr	2	2	4
ab	18	11	20
an	30	30	22
di	7	15	5
hy	9	20	14
at	3	3	3
il	1	1	1
ap	1	0	1
FeO*	7.49	10.44	10.44
F/F+M	0.816	0.677	0.904
Rb/Sr	0.091	0.091	0.200
K/Rb	315	307	303
K/Ba	17.5	21.9	17.3
den	2.46	2.53	2.45



REPORT: 017-1079

PROJECT: NONE

PAGE 1A

SAMPLE NUMBER	ELEMENT UNITS	SiO2 PCT	TiO2 PCT	Al2O3 PCT	Fe2O3a PCT	MnO PCT	MgO PCT	CaO PCT	Na2O PCT	K2O PCT	P2O5 PCT	LOI PCT
GR-3		56.80	1.05	13.80	13.30	0.22	3.62	8.37	2.43	0.58	0.28	0.60
DUPLICATE		57.00	0.97	14.00	13.00	0.21	3.34	8.60	2.44	0.61	0.36	0.45
GR-7		54.70	1.14	14.00	14.20	0.24	3.49	8.99	2.25	0.56	0.46	0.40
GR-15		71.90	0.26	11.40	4.92	0.11	0.58	4.57	2.29	1.15	0.21	0.75
GR-52		68.40	0.36	11.30	7.35	0.24	2.60	3.04	1.34	1.74	0.49	1.50
TR-21		50.00	0.57	18.40	11.90	0.14	3.63	6.81	2.07	1.98	0.40	3.95
139-280.5		45.20	0.56	14.50	18.80	0.21	11.50	1.02	0.55	1.72	0.33	5.55
139-365		42.50	0.60	16.00	19.90	0.28	11.12	1.83	0.29	0.67	0.34	6.20
139-442.5		62.84	0.41	12.30	12.80	0.14	1.32	5.28	1.73	0.44	0.39	2.30
139-481		64.12	0.31	9.68	11.30	0.46	5.19	5.46	0.87	0.33	0.19	2.80
CON45A-479		52.30	0.29	10.70	12.70	0.23	10.40	10.90	1.23	0.30	0.31	0.70
DUPLICATE		53.30	0.33	10.90	12.70	0.27	10.30	11.00	1.17	0.29	0.32	0.80
DUPLICATE												
CON45A-491		52.40	0.29	10.80	13.60	0.24	10.10	11.50	0.93	0.27	0.27	0.70
CON57-188		50.38	0.32	12.20	12.60	0.26	10.70	11.80	1.13	0.51	0.37	0.60
CON62-477		49.10	0.38	16.90	16.10	5.14	4.21	3.97	0.95	1.77	0.43	1.35
CON62-522		51.40	0.42	18.20	9.95	0.77	6.10	7.64	0.79	2.51	0.27	1.60
CON63-898.5		52.40	0.32	12.00	12.70	0.27	10.20	11.80	1.15	0.33	0.31	0.50

Bondar-Clegg & Company Ltd.
 130 Pemberton Ave.
 North Vancouver, B.C.
 Canada V7P 1R3
 Phone: (604) 983-0681
 Telex: 04-332657



BONDAR-CLEGG

Geochemical
 Lab Report

REPORT: 017-1079

PROJECT: NONE

PAGE 18

SAMPLE NUMBER	ELEMENT UNITS	Total PCT	S PCT
GR-3		101.05	<0.01
DUPLICATE		100.98	
GR-7		100.43	<0.01
GR-45		98.15	0.06
GR-52		98.36	0.31
TR-21		99.85	4.26
139-280.5		99.94	2.63
139-365		99.73	1.05
139-442.5		99.95	4.55
139-481		100.71	3.51
CON45A-479		100.07	<0.01
DUPLICATE		101.38	
DUPLICATE			
CON45A-491		101.11	0.05
CON57-188		100.87	0.16
CON62-477		100.30	3.27
CON62-522		99.65	0.57
CON63-898.5		101.97	0.09

RAY ASSAY LABORATORIES

SAMPLE	FE PPM	CO PPM	NI PPM	CU PPM	ZN PPM
52-350	>10000	21	17	27.0	100.
52-374	>10000	22	90	1200.	180.
52-474	>10000	14	4	100.	71.0
59-47	>10000	26	6	130.	110.
59-81.5	8400	9	14	96.0	14.0
59-214.5	>10000	59	56	640.	78.0
67-117	>10000	14	16	33.0	57.0
67-291	>10000	15	12	29.0	34.0
67-787	>10000	11	3	45.0	41.0
67-889	>10000	10	6	4.0	79.0
139-325	>10000	22	24	15.0	350.
139-502	>10000	18	16	190.	890.
140-176.5	>10000	23	11	110.	36.0
140-264	>10000	30	22	320.	330.
140-298	>10000	43	60	150.	3800.
CON9-121	>10000	28	21	130.	25.0
CON9-312	>10000	29	27	61.0	140.
CON20-124	>10000	11	6	93.0	41.0
CON24-158	>10000	61	82	190.	63.0
CON24-167.5	>10000	26	27	300.	360.
CON44-123	>10000	19	9	94.0	45.0
CON44-154	>10000	40	27	61.0	320.
CON44-248	>10000	44	33	140.	140.
CON44W2-432	>10000	12	7	48.0	27.0
CON45A-835.5	>10000	39	7	170.	32.0
CON45A-860	>10000	33	240	48.0	33.0
CON51-171	>10000	13	4	160.	33.0
CON51-584	5700	5	8	1.5	41.0
CON51-682	>10000	8	6	18.0	14.0
CON52-96.5	>10000	16	9	13.0	60.0
CON52-614.5	>10000	5	3	28.0	110.
CON57-172	>10000	22	11	150.	28.0
CON57-343.5	>10000	22	17	110.	30.0
CON57-551.5	>10000	9	5	72.0	17.0
CON57-674.5	>10000	27	42	110.	14.0
CON57-753	>10000	43	360	290.	310.
CON57-779	>10000	15	31	440.	1100.
CON63-171	>10000	20	19	8.0	82.0
CON63-188.5	>10000	41	33	180.	150.
CON63-253.5	>10000	23	29	41.0	24.0
CON63-446.5	>10000	72	57	860.	380.
CON63-590	>10000	8	4	19.0	110.
CON63-1035	>10000	30	260	30.0	52.0
CON63-1116	>10000	20	45	540.	1200.
CON64-122	>10000	10	6	27.0	98.0
CON64-470.5	>10000	40	20	35.0	23.0
GR-6	>10000	7	4	43.0	270.
GR-8	>10000	5	3	8.5	54.0
GR-12	>10000	4	3	5.5	82.0
GR-13	>10000	11	8	87.0	51.0

> - CONCENTRATION TOO HIGH FOR TREATMENT BY GEOCHEMICAL METHOD

RAY ASSAY LABORATORIES

SAMPLE	FE PPM	CO PPM	NI PPM	CU PPM	ZN PPM
GR-14	>10000	10	10	74.0	23.0
GR-19	>10000	5	3	5.0	64.0
GR-25	>10000	8	5	24.0	92.0
GR-26	>10000	9	8	94.0	23.0
GR-32	>10000	8	5	49.0	28.0
GR-33	>10000	9	10	90.0	18.0
GR-35	>10000	8	6	4.0	51.0
GR-36	>10000	22	18	73.0	14.0
GR-39	>10000	8	4	92.0	34.0
GR-40	>10000	11	14	33.0	19.0
GR-48	>10000	7	4	28.0	23.0
GR-49	>10000	10	10	64.0	11.0
GR-59	>10000	16	13	110.	260.

> - CONCENTRATION TOO HIGH FOR TREATMENT BY GEOCHEMICAL METHOD

RAY ASSAY LABORATORIES

SAMPLE	AU PPB	HG PPM	P PPM	CA PPM	HN PPM
52-350	<2	>10000	2300	7100	420
52-374	50	7800	560	7300	320
52-474	24	2700	620	4300	240
59-47	<2	8300	690	4300	490
59-81.5	3	3900	250	7200	110
59-214.5	12	>10000	160	1000	440
67-117	<2	8600	230	3400	260
67-291	<2	5600	460	4300	260
67-787	<2	3600	790	6900	410
67-889	<2	6200	440	3800	300
139-325	18	>10000	420	2500	940
139-502	3900	>10000	280	1300	590
140-176.5	49	6100	460	9800	200
140-264	120	>10000	280	>10000	330
140-298	480	7500	180	2100	200
CON9-121	12	8100	180	3500	150
CON9-312	7	>10000	160	2500	370
CON20-124	29	4300	630	3200	170
CON24-158	24	>10000	100	1500	280
CON24-167.5	110	6900	280	3100	230
CON44-123	5	5900	560	>10000	180
CON44-154	5	>10000	170	700	560
CON44-248	7	>10000	190	1100	330
CON44W2-432	5	5600	510	6800	240
CON45A-835.5	4	5900	540	6300	190
CON45A-860	<2	>10000	740	3200	150
CON51-171	4	4100	690	4500	180
CON51-584	<2	3600	110	2700	96
CON51-682	<2	3400	150	8100	150
CON52-96.5	4	8500	630	5500	350
CON52-614.5	2	2700	270	2500	290
CON57-172	5	6500	540	5500	250
CON57-343.5	3	>10000	200	9900	390
CON57-551.5	3	3100	430	>10000	210
CON57-674.5	3	4100	180	10000	130
CON57-753	3	>10000	700	2700	210
CON57-779	74	3200	830	4800	190
CON63-171	<2	>10000	2400	6800	270
CON63-188.5	6	>10000	200	1000	390
CON63-253.5	14	5300	160	7500	120
CON63-446.5	24	>10000	90	900	380
CON63-590	6	4700	380	1700	230
CON63-1035	<2	>10000	720	2500	190
CON63-1116	87	2800	540	2400	150
CON64-122	<2	4200	610	2900	380
CON64-470.5	<2	>10000	230	3300	200
GR-6	<2	3700	350	1900	330
GR-8	<2	2700	360	3400	260
GR-12	<2	2000	220	1700	200
GR-13	3	4400	580	5100	340

> - CONCENTRATION TOO HIGH FOR TREATMENT BY GEOCHEMICAL METHOD

RAY ASSAY LABORATORIES

SAMPLE	AU PPH	MG PPM	P PPM	CA PPM	MN PPM
GR-14	6	3700	230	8500	180
GR-19	<2	2500	230	2400	230
GR-25	<2	3300	280	2300	300
GR-26	9	3500	490	7500	190
GR-32	<2	3000	570	3700	230
GR-33	<2	4700	420	4400	160
GR-35	4	4200	330	1200	220
GR-36	3	4100	190	6000	180
GR-39	3	2000	550	3500	140
GR-40	<2	3900	420	6500	150
GR-48	<2	2400	900	7600	190
GR-49	<2	3500	170	6200	130
GR-59	27	3100	1600	6000	260

KAY ASSAY LABORATORIES

SAMPLE	MO PPM	AG PPM	CD PPM	PB PPM
52-350	4	<0.5	<1	<2
52-374	4	0.5	<1	<2
52-474	3	<0.5	<1	<2
59-47	4	<0.5	<1	<2
59-81.5	2	<0.5	<1	<2
59-214.5	7	<0.5	<1	<2
67-117	3	<0.5	<1	<2
67-291	3	<0.5	<1	<2
67-787	3	<0.5	<1	<2
67-889	3	<0.5	<1	6
139-325	4	<0.5	<1	<2
139-502	4	1.0	3	74
140-176.5	3	<0.5	<1	4
140-264	5	1.5	1	86
140-298	5	1.5	5	1000
CON9-121	2	<0.5	<1	2
CON9-312	5	<0.5	<1	2
CON20-124	2	0.5	<1	<2
CON24-158	5	<0.5	<1	8
CON24-167.5	4	0.5	2	18
CON44-123	5	<0.5	<1	<2
CON44-154	6	<0.5	<1	<2
CON44-248	7	<0.5	<1	<2
CON44W2-432	3	<0.5	<1	<2
CON45A-835.5	3	<0.5	<1	<2
CON45A-860	3	<0.5	<1	<2
CON51-171	3	<0.5	<1	<2
CON51-584	1	<0.5	<1	6
CON51-682	2	<0.5	<1	4
CON52-96.5	3	<0.5	1	2
CON52-614.5	3	<0.5	<1	<2
CON57-172	3	<0.5	<1	<2
CON57-343.5	4	<0.5	<1	<2
CON57-551.5	3	<0.5	<1	<2
CON57-674.5	3	<0.5	<1	<2
CON57-753	4	<0.5	<1	2
CON57-779	6	0.5	4	4
CON63-171	8	<0.5	<1	2
CON63-188.5	5	<0.5	<1	<2
CON63-253.5	2	<0.5	<1	<2
CON63-446.5	10	1.5	<1	8
CON63-590	2	<0.5	<1	12
CON63-1035	4	<0.5	<1	<2
CON63-1116	16	0.5	4	<2
CON64-122	5	<0.5	<1	<2
CON64-470.5	4	<0.5	<1	<2
GR-6	4	<0.5	1	<2
GR-8	3	<0.5	<1	<2
GR-12	3	<0.5	<1	<2
GR-13	3	<0.5	1	<2

JAY ASSAY LABORATORIES

SAMPLE	MO PPM	AG PPM	CD PPM	PB PPM
GR-14	2	<0.5	<1	<2
GR-19	3	<0.5	<1	<2
GR-25	4	<0.5	<1	<2
GR-26	2	<0.5	<1	<2
GR-32	2	<0.5	<1	<2
GR-33	2	<0.5	<1	<2
GR-35	3	<0.5	<1	<2
GR-36	2	<0.5	1	<2
GR-39	2	<0.5	<1	<2
GR-40	2	<0.5	<1	<2
GR-48	2	<0.5	<1	<2
GR-49	2	<0.5	<1	<2
GR-59	4	<0.5	1	<2



REPORT: 017-1078

PROJECT: NONE

PAGE 1B

SAMPLE NUMBER	ELEMENT UNITS	Total PCT	S PCT
GR-6		98.13	0.23
DUPLICATE			
DUPLICATE		98.53	
GR-8			<0.01
GR-12			0.02
GR-13			<0.01
GR-14			0.03
GR-19			<0.01
GR-25			0.06
GR-26			<0.01
GK-32			<0.01
GK-33			<0.01
DUPLICATE			
GR-35			
GR-36		100.09	0.28
GR-39			<0.01
GE-40		101.41	0.01
GK-48		98.05	<0.01
GE-49			0.06
GR-59			1.17
CON9-121			0.61
DUPLICATE			
CON9-312			0.46
CON20-124			0.31
CON24-158		101.32	0.91
CON24-167.5			0.73
CON44-123		101.50	0.10
CON44-154		101.39	0.54
CON44-248			2.03
CON44-432			<0.01
CON45A-835.5			0.28
CON45A-860			0.07
CONS1-171			0.04
CONS1-584			<0.01
CONS1-682			<0.01
CON52-98.5			<0.01
CON52-614.5			0.03
CON57-172			0.33
CON57-343.5			0.08
DUPLICATE			



REPORT: 017-1078

PROJECT: NONE

PAGE 2R

SAMPLE NUMBER	ELEMENT UNITS	Total PCT	S PCT
CONS7-551.5			0.05
CONS7-674.5			0.51
CONS7-753			0.38
CONS7-779			2.26
CON63-171			0.05
CON63-188.5			1.33
CON63-253.5			0.26
CON63-466.5			7.55
CON63-590			0.10
DUPLICATE			
CON63-1035			0.06
CON63-1116			1.97
CON64-122			0.04
CON64-470.5			1.52
52-350			<0.01
52-374			1.46
52-474			0.52
59-47	101.87		0.41
DUPLICATE			
59-81.5	101.20		0.03
59-214.5	101.13		5.16
DUPLICATE	99.97		
67-117			0.10
67-291			0.11
67-787			0.04
67-889			0.01
139-325			0.41
139-502			1.28
140-176.5			1.02
140-264			2.17
140-298			6.66
TK-14	100.70		0.04
TK-15	100.89		0.02
TK-16	100.74		0.21



REPORT: 417-1078

PROJECT: NONE.

PAGE 1

SAMPLE NUMBER	ELEMENT UNITS	CO2 PCT	SAMPLE NUMBER	ELEMENT UNITS	CO2 PCT
GR-6		0.05	CON63-188.5		0.01
GR-8		0.18	CON63-253.5		0.08
GR-12		0.05	CON63-466.5		0.02
GR-13		0.01	CON63-590		0.02
GR-14		0.10	CON63-1035		0.02
GR-19		0.09	CON63-1116		0.07
GR-25		0.08	CON64-122		0.16
GR-26		0.07	CON64-470.5		0.03
GR-32		0.02	52-356		0.16
GR-33		0.01	52-374		0.00
GR-35			52-474		0.04
GR-36		<0.01	59-47		0.08
GR-39		0.18	59-81.5		0.02
GR-40		0.04	59-214.5		<0.01
GR-48		0.04	67-117		0.01
GR-49		<0.01	67-291		0.02
GR-59		<0.01	67-787		0.25
CON9-121		0.03	67-889		0.21
CON9-312		0.03	139-325		0.04
CON20-124		0.02	139-502		0.01
CON24-158		0.08	140-176.5		0.01
CON24-167.5		0.06	140-264		0.01
CON44-123		0.02	140-298		<0.01
CON44-154		0.02	TR-14		0.05
CON44-248		0.01	TR-15		0.02
CON44W2-432		0.02	TR-16		0.05
CON45A-835.5		0.05			
CON45A-960		0.03			
CON51-171		0.01			
CON51-584		0.04			
CON51-682		0.07			
CON52-96.5		0.03			
CON52-614.5		0.16			
CON57-172		0.01			
CON57-343.5		0.34			
CON57-551.5		0.03			
CON57-674.5		0.02			
CON57-753		0.02			
CON57-779		0.19			
CON63-171		0.03			

Bondar-Clegg & Company Ltd.
5420 Canosa Rd.
Ottawa, Ontario,
Canada K1J 8X3
Phone: (613) 749-2220
Telex: 053-3233



Certificate
of Analysis

REPORT: 417-1079

PROJECT: HOME

PAGE 1

SAMPLE NUMBER	ELEMENT UNITS	CO2 PCT
GR-3		0.18
GR-7		0.12
GR-45		0.33
GR-52		0.04
TR-21		0.02
139-280.5		0.15
139-365		0.02
139-442.5		0.01
139-481		0.04
CON45A-479		0.09
CPN45A-491		0.12
CON57-188		0.03
CON62-477		0.05
CON62-522		0.03
CON63-898.5		0.03

A55

Chief Chemist

XRF analyses performed at the University of Manitoba

(in ppm)

Sample number	Y	Zr	Nb	Rb	Sr	Rh
1. 52-350	24.74	243.46	17.67	38.21	966.25	2.54
2. 52-374	15.59	20.31	3.02	13.06	88.46	2.20
3. 59-214.5	8.90	13.14	3.51	33.34	55.18	1.89
4. 140-264	9.49	26.56	2.84	41.30	157.41	2.32
5. CON 20-124	36.21	80.53	4.24	10.06	273.75	2.63
6. CON 24-158	8.44	4.65	3.09	16.80	20.80	2.23
7. CON 44-154	8.98	11.67	0	46.47	63.62	2.61
8. CON 45A-835.5	21.10	42.10	3.82	19.80	263.25	2.42
9. CON 45A-860						
10. CON 51-171	32.92	55.31	7.75	16.89	152.59	2.19
11. CON 51-682	13.22	13.64	3.16	5.71	117.75	2.16
12. CON 52-96.5	17.95	26.56	5.01	22.72	334.21	2.29
13. CON 52-614.5	45.72	107.36	7.72	12.15	143.53	2.90
14. CON 57-172	22.45	37.02	4.93	18.53	229.61	2.11

Sample number	Y	Zr	Nb	Rb	Sr	Rh
15. CON57-551.5	15.06	23.30	1.32	6.52	226.68	2.09
16. CON 57-674.5	13.85	16.12	5.16	6.42	124.27	2.09
17. CON 563-171	24.50	240.55	16.49	41.66	855.64	2.56
18. CON 63-188.5	13.73	10.93	3.38	12.37	11.04	2.34
19. CON 63-1035	12.75	24.65	1.88	47.59	44.01	2.19
20. CON64-122	39.07	90.89	10.35	18.43	174.49	2.69
21. CON 64-470.5	32.13	171.28	22.76	12.51	391.17	1.97
22. GR 12	34.15	80.45	8.51	14.85	114.36	2.95
23. GR 13	30.64	51.20	4.83	15.86	157.75	2.21
24. GR 14	16.73	17.71	6.03	9.43	117.31	2.12
25. GR 26	26.61	39.16	7.87	5.68	145.88	2.04
26. GR 35	11.15	123.60	4.40	25.22	353.17	3.18
27. GR 36	14.84	15.75	3.60	6.50	120.34	2.22
28. GR 39	22.27	47.21	3.10	11.55	145.28	3.07
29. GR 48	25.63	38.43	4.10	6.05	121.03	2.44
30. GR 49	14.67	17.01	2.61	4.95	103.19	2.16

X-RAY ASSAY LABORATORIES 15-MAY-92 REPORT 18880 REF. 12134 PAGE

SAMPLE	RB PPM	SR PPM	Y PPM	ZR PPM	NB PPM
TR21	60	158	7	35	<2
139-280.5	28	38	5	33	<2
139-365	13	28	<2	29	<2
139-442.5	8	116	<2	28	2
139-481	6	52	<2	26	3
140-298	39	25	<2	27	<2
CON62-477	39	98	6	27	<2
CON62-522	51	142	<2	30	4

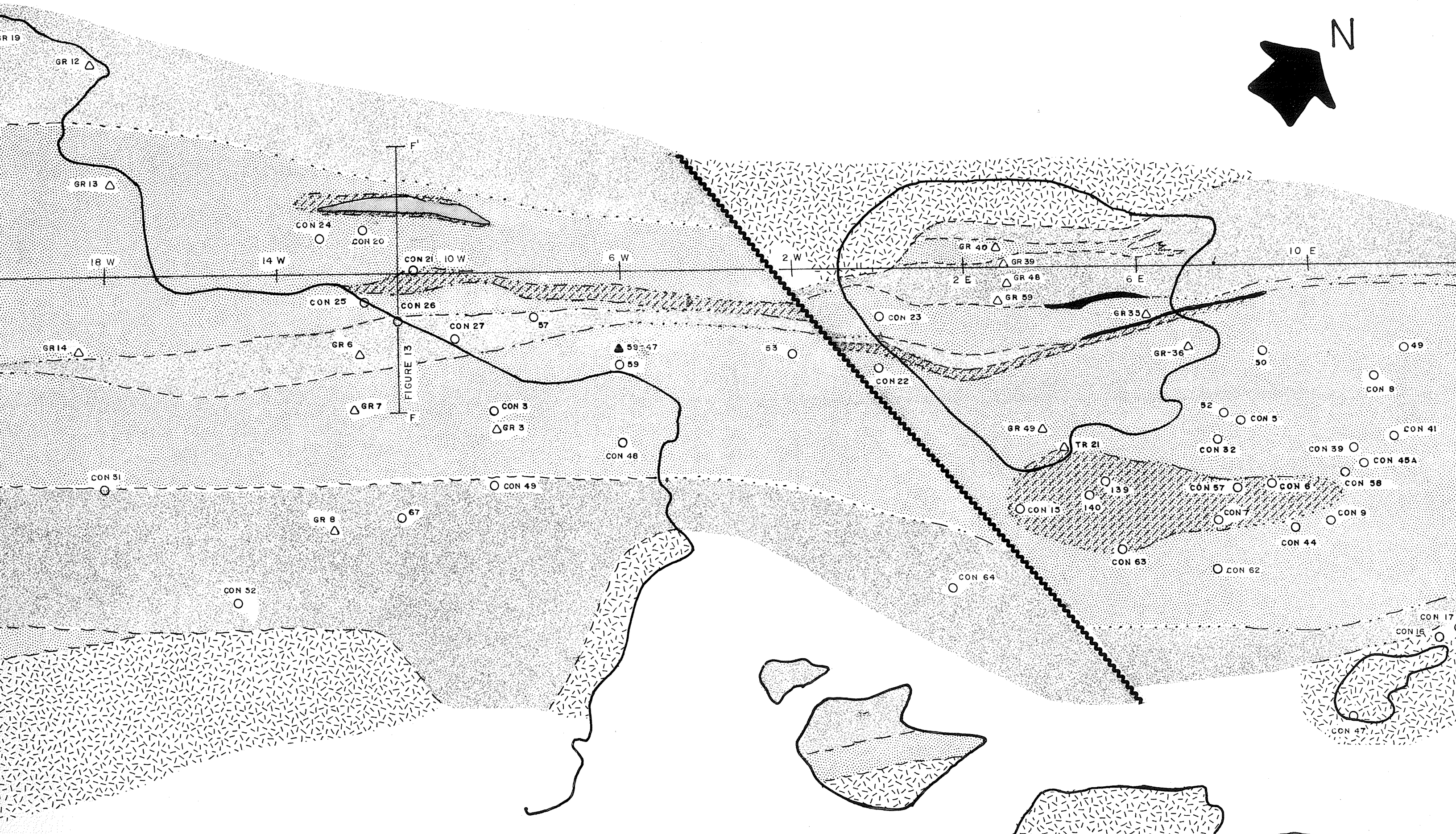
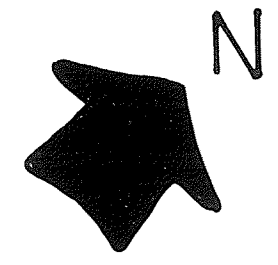


FIGURE 5A: SURFACE PLAN

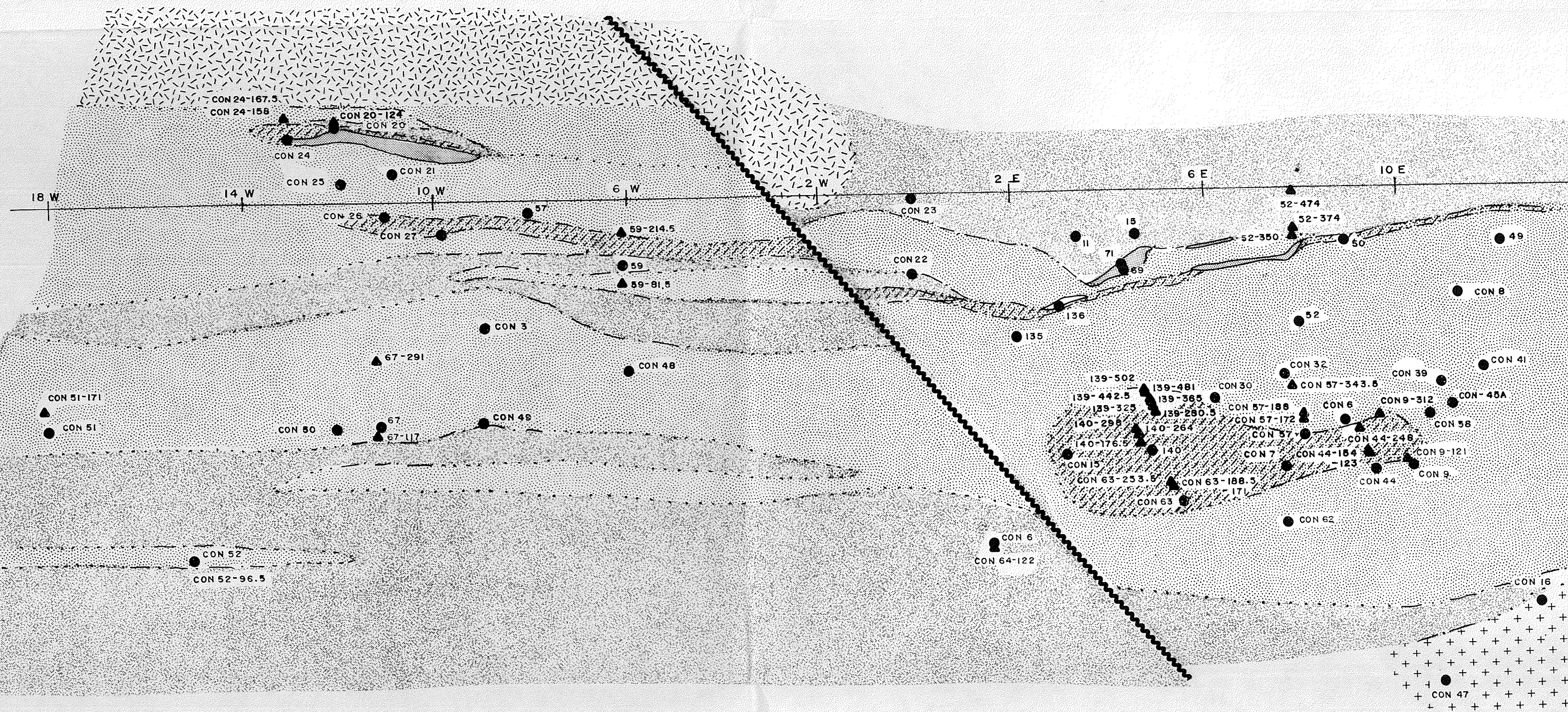


FIGURE 5B: 30 m PLAN

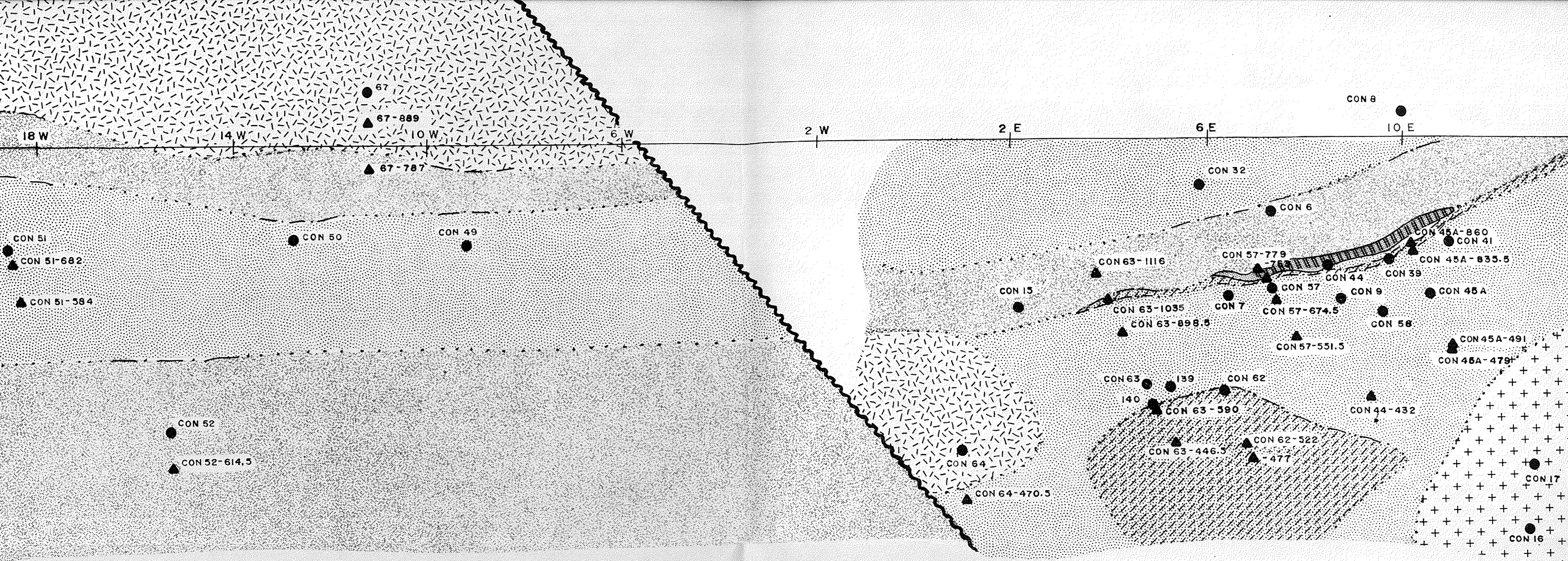


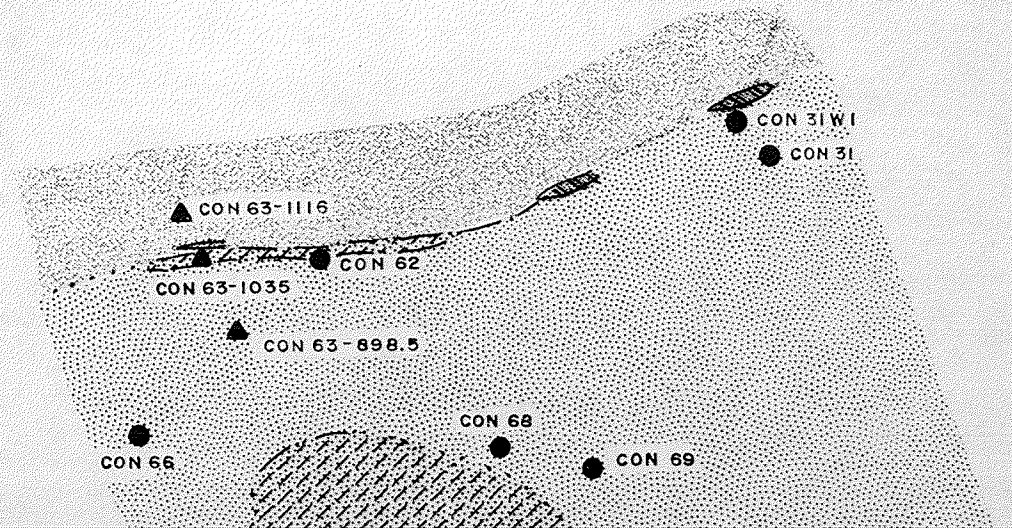
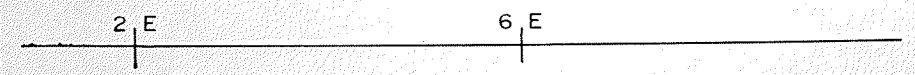
FIGURE 5B: 200 m PLAN

Individual contact symbols refer to the degree of certainty regarding the position of the contact in question:

SURFACE GEOLOGY

- High degree of confidence
- Low degree of certainty (inferred)

CONTACTS INFERRED FROM SUBSURFACE DATA




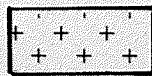
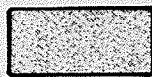




Individual contact symbols refer to the degree of certainty regarding the position of the contact in question:

SURFACE GEOLOGY

- — — High degree of confidence
- Low degree of certainty (inferred)

CONTACTS INFERRED FROM SUBSURFACE DATA

- . - . Moderate degree of certainty (projected from distances of <60 m along dip, or strong correlation between diamond drill holes)
- Low degree of certainty (projected from distances of >60 m along dip)
- Position or configuration uncertain

-  GRANODIORITE
-  GABBRO
-  INTERMEDIATE AND FELSIC VOLCANIC ROCKS
-  MAFIC VOLCANIC ROCKS
-  ALTERATION ZONE
-  ORE ZONE (Cu &/or Zn)
-  ANOMALOUS GOLD

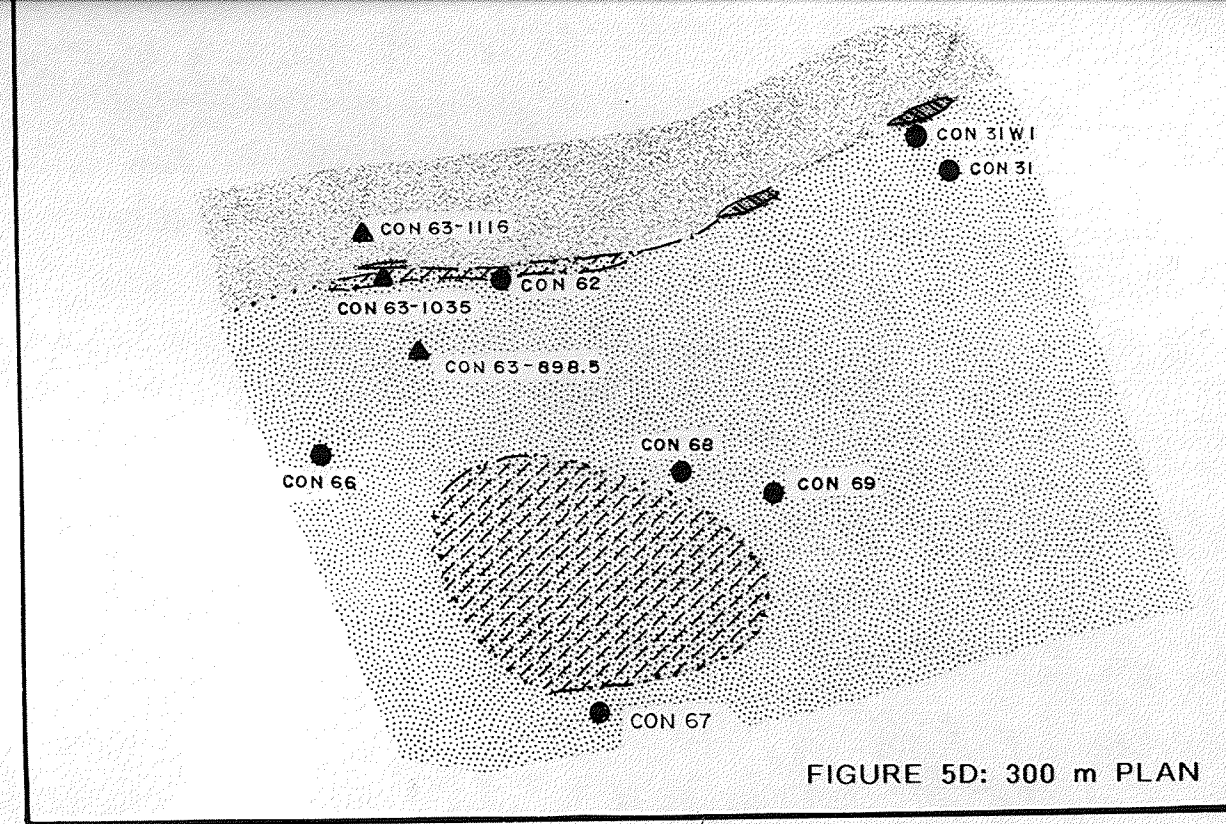


FIGURE 5D: 300 m PLAN

- Diamond Drill Hole Collars (Surface Plan)
- Location where diamond drill hole intersects the horizontal plane at depths of 30 m, 200 m, and 300 m (figures B, C, and D respectively)
- △ Geochemical sample site (surface plane)
- ▲ Geochemical sample site (projected onto the nearest corresponding plan section)
- ~~~~~ Trace of fault
- Surface expression of ore zone

